UNIVERSITY OF LJUBLJANA
Faculty of Mechanical Engineering

VALIDATION OF NUMERICAL SIMULATIONS BY DIGITAL SCANNING OF 3D SHEET METAL OBJECTS

PhD thesis

Submitted to Faculty of Mechanical Engineering, University of Ljubljana
in partial fulfilment of the requirements for the degree of Doctor of Philosophy

Samir Lemeš

Supervisor:
prof. dr. Karl Kuzman

Ljubljana, 2010

UNIVERZA V LJUBLJANI

Fakulteta za Strojništvo

VALIDACIJA NUMERIČNIH SIMULACIJ Z DIGITALIZIRANIMI POSNETKI PLOČEVINASTIH OBJEKTOV

Doktorsko delo

Predložil Fakulteti za strojništvo Univerze v Ljubljani
za pridobitev znanstvenega naslova doktor znanosti

Samir Lemeš

Mentor:

prof. dr. Karl Kuzman, univ.dipl.inž.

Ljubljana, 2010

Univerza v Ljubljani
Fakulteta za strojništvo

Aškerčeva cesta 6
1000 Ljubljana, Slovenija
telefon (01) 47 71 200
faks (01) 25 18 567
dekanat@fs.uni-lj.si

Tekoča številka: Dr/342

Datum: 15.5.2006

Na osnovi sklepa 6. seje Senata Univerze v Ljubljani z dne 9. maja 2006 izdajam naslednjo

O D L O Č B O

Senat Univerze v Ljubljani je na svoji seji dne 9.5.2006

kandidatu **mag.Samiru Lemešu**

1. sprejel temo doktorske disertacije z naslovom:

   Validacija numeričnih simulacij z digitaliziranimi posnetki 3D pločevinastih objektov

2. imenoval mentorja: prof.dr. Karl Kuzman

3. odobril pisanje disertacije v angleškem jeziku

V skladu s členom 169 Statuta Univerze v Ljubljani z dne 21.12.2004 mora kandidat najpozneje v štirih letih od dneva, ko je bila sprejeta tema disertacije, predložiti izdelano doktorsko disertacijo.

Prof.dr. Karl Kuzman,
dekan

Pravni pouk:
Zoper to odločbo je dopusten ugovor na Senat Univerze v Ljubljajni v roku 15 dni od prejema odločbe.

Dostavljeno:
mag.S.Lemeš
dr.K.Kuzman

Acknowledgments

I would like to express my deepest gratitude to my supervisor, Prof.Dr. Karl Kuzman, for his patience, guidance and helping me refine my research. Thanks to Prof.Dr.-Ing.Dr.-Ing.E.h.Dr.h.c.mult. Albert Weckenmann, for innovative idea for this research. Thanks to Prof.Dr. Nermina Zaimović-Uzunović, for continuous support and numerous projects from which this research was performed.

Thanks to my friends and colleagues: E. Baručija-Hodžić, E. Berberović, L. Botolin, D. Ćurić, N. Drvar, J. Duhovnik, S. Galijašević, G. Gantar, S. Gazvoda, M. Huseinspahić, A. Karač, B. Nardin, T. Pepelnjak, D. Spahić, D. Švetak, B. Trogrlić, A. Uzunović, N. Vukašinovič, B. Žagar, for unselfish support in providing up-to-date literature, product samples and assembly for experiments, and for sharing their research experience with me.

Thanks to Slovenian Tool and Die Center Tecos Celje and Faculty of Mechanical Engineering in Ljubljana for providing their laboratory resources. Thanks to Slovenian Science and Education Foundation Ad-futura and ARRS Slovenia for their financial support.

Thanks to CAD/CAE software vendors: Materialise, Simpleware, Rapidform, UGS, Solidworks, for providing educational and evaluation licences of their software.

And last but not least, thanks to my beloved wife Igda, daughter Lamija and son Tarik, for their patience, support and permanent inspiration.

DR/342 UDC 519.6:531.7

Samir Lemeš

Validation of Numerical Simulations by Digital Scanning of 3D Sheet Metal Objects

Ključne besede:

- Numerical simulations,
- 3D scanning,
- Springback,
- Measurement uncertainty

Abstract:

Validation is the subjective process that determines the accuracy with which the mathematical model describes the actual physical phenomenon. This research was conducted in order to validate the use of finite element analysis for springback compensation in 3D scanning of sheet metal objects. The measurement uncertainty analysis was used to compare the digitized 3D model of deformed sheet metal product with the 3D model obtained by simulated deformation. The influence factors onto 3D scanning and numerical simulation processes are identified and analysed. It is shown that major contribution to measurement uncertainty comes from scanning method and deviations of parts due to manufacturing technology. The analysis results showed that numerical methods, such as finite element method, can successfully be used in computer-aided quality control and automated inspection of manufactured parts.

DR/342 UDK 519.6:531.7

Samir Lemeš

Validacija numeričnih simulacij z digitaliziranimi posnetki pločevinastih objektov

Ključne besede:

- Numerične simulacije,
- 3D skeniranje,
- Elastično izravnavanje,
- Merilna negotovost

Izvleček:

Validacija je subjektiven proces, ki določa natančnost, s katero matematični model opisuje dejanski fizični pojav. Ta raziskava je bila izvedena z namenom, da bi preverili uporabo metode končnih elementov za kompenzacijo elastične izravnave v 3D skeniranju pločevinastih objektov. Analiza merilne negotovosti je bila uporabljena za primerjavo digitaliziranega 3D modela deformiranega pločevinastega izdelka z 3D modelom, pridobljenim z simulirano deformacijo. Faktorji vpliva na 3D skeniranje in na numerično simulacijo procesov so opredeljeni in analizirani. Raziskava je pokazala, da velik prispevek k merilno negotovosti prihaja iz metode skeniranja in odstopanja delov zaradi proizvodne tehnologije. Analiza rezultatov je pokazala, da lahko numerične metode, kot je metoda končnih elementov, uspešno uporabljamo v računalniško podprto kontrolo kakovosti in v avtomatiziranih pregledih izdelanih delov.

Table of contents

1. Introduction 1
1.1. Description of the general research areas 1
1.2. Problem definition 2
1.3. Dissertation structure 3

2. Literature review 5
2.1. Springback 5
2.2. Tolerances 7
2.3. Process optimization for sheet-metal production 7
2.4. Reverse engineering 9
2.5. Optical 3D measuring for quality control of sheet metal products 9
2.6. Measurement uncertainty 11
2.7. Use of FEM in quality control of sheet metal products 13
2.8. Conclusion 14

3. Motivation 15
3.1. Proposed procedure 19

4. Determination of product characteristics 21
4.1. Product description 21
4.2. Material properties 22
4.3. Clamping assembly 24

5. 3D scanning 27
5.1. 3D file formats 34
5.2. Converting scanned data into FEA models 35
5.3. Estimation of errors induced by data conversion 37

6. Deformation analysis 41
6.1. 2D contour deformation analysis 41
6.2. Circular cross-section perimeters 44
6.3. Deviations between unclamped, clamped and nominal CAD part 46

7. 3D finite element analysis 55
7.1. 2D contour FEM analysis 55
7.1.1. Boundary conditions 56
7.1.2. Analysis results 57
7.2. 3D model FEM analysis 62
7.2.1. Meshing 62
7.2.2. Boundary conditions 64
7.2.3. Analysis results 68

8. Measurement uncertainty 73
8.1. Influence factors 78
8.2. Mathematical model of measurement system 88
8.3. GUM-based uncertainty analysis 94

9. Statistical analysis 101

10. Algorithm for automated measurement process 105

11. Conclusions 111
11.1. Main results 113
11.2. Scientific contribution 114
11.3. Suggestions for future researches 115
11.4. Assessment of the thesis 115

12. References 117

13. Povzetek v slovenščini 125
13.1. Uvod 125
13.1.1. Opis splošnega področja raziskovanja 125
13.1.2. Opredelitev problema 127
13.1.3. Struktura disertacije 127
13.2. Zaključki 131
13.2.1. Glavni rezultati 133
13.2.2. Znanstveni prispevek 134
13.2.3. Predloge za nadaljnja raziskovanja 134
13.2..4. Ocena teze 135

Annexes
Annex A: Material properties i
Annex B: Graphical representation of cross-section deviations v
Annex C: Listings of Fortran programs xv
Annex D: Summary data for all scanned points in toleranced crosssection xix

About the author xxi

Izjava xxiii

List of symbols

$\overline{q}$	Arithmetic mean of the *n* results
A80	Strain
C	Hardening coefficient
c_i	Sensitivity coefficient
E	Comparison error
E	Modulus of elasticity
G	Shear modulus
H	Hausdorff distance
k	Coverage factor
l	Length
L	Length
l_0	Initial length
MPE_E	Maximum Permissible Indication Error
MPE_P	Maximum Permissible Probing Error
n	Deformation Strengthening Exponent; Number of measurements
P	Perimeter
P_0	Initial perimeter
q_k	Result of the k^{th} measurement
r	Normal Anisotropy Factor; Radius
R_m	Ultimate Strength
$R_{p0,2}$	Yield Stress
U	Expanded uncertainty

u_0	Uncertainty from physical clamping deformation
u_1	Uncertainty from temperature variations
u_2	Uncertainty from material properties
u_3	Uncertainty from scanning errors
$u_{3\text{-}1}$	Uncertainty from manufacturing errors
$u_{3\text{-}2}$	Uncertainty from declared 3D CMM accurracy
$u_{3\text{-}3}$	Uncertainty from 3D scanning method
u_4	Uncertainty from declared 3D scanner accurracy
u_5	Uncertainty from digitized data conversion
u_6	Uncertainty from simulated deformation
u_7	Uncertainty from numerical computation
u_{comb}	Combined standard uncertainty
U_D	Uncertainty from experimental data
U_{DA}	Uncertainty from data aproximations
U_{DEXP}	Uncertainty from experiment
u_i	Standard uncertainties of components
U_S	Uncertainty from simulation result
U_V	Validation uncertainty
U_{SMA}	Uncertainty from simulation modelling assumptions
U_{SN}	Uncertainty from numerical solution of equations
U_{SPD}	Uncertainty from previous data
α	Thermal expansion coefficient
δ_D	Error from experimental data
δ_{DA}	Error from data aproximations
δ_{DEXP}	Error from experiment
Δr	Displacement
δ_{SMA}	Error from simulation modelling assumptions
δ_{SN}	Error from numerical solution of equations
δ_{SPD}	Error from previous data
ΔT	Temperature deviation
θ	Angle
ν	Poissons ratio; Degrees of freedom
ν_{eff}	Effective degrees of freedom
σ	Stress

List of figures

3.1. Measuring chain with a tactile and an optical measurement system 15
3.2. Tools used for FEA in 1970's: paper-based mesh, punched cards 16
3.3. Moore's Law: "The number of transistors on a chip doubles about every two years" 16
3.4. Medieval 3D scanning (source: "Der Zeichner der Laute", Albrecht Dürer, 1525) 17
3.5. Typical 3D scanners commercially available in 2009 17
3.6. The AFI Micro intra-oral 3D scanner for dentists - still under development 18
3.7. Automotive body at the optical measurement station 18
4.1. Replacement lubricating oil filter LI 9144/25 21
4.2. Detail from technical documentation 22
4.3. Tensile testing machine at the Forming Laboratory 23
4.4. Specimens used for anisotropy tests 23
4.5. Clamping assembly 24
4.6. Clamping assembly used for 3D scanning 25
5.1. 3D digitizer ATOS II 27
5.2. Filter housings prepared for scanning 28
5.3. Fitting scans in 3D scanning software GOM 28
5.4. Correction of surface errors in GOM software 29
5.5. Errors that can be corrected automatically (reference point stickers) 30
5.6. Alignment with reference coordinate system using transformations 30
5.7. Colour laser 3D scanner NextEngine 31
5.8. The saddle bracket used for simplified 2D analysis (thickness d = 0,5 mm) 32
5.9. The samples were clamped to a rigid plate with two bolts 32

5.10. Joining scans into single point cloud using virtual reference points 33
5.11. Creating cross-sections with reference planes 33
5.12. Scanned STL model (a) processed with software ScanCAD (www.simpleware.com) using (b) accurate and (c) robust method 35
5.13. Tetrahedral mesh obtained with of ScanFE software 36
5.14. Thin-shell mesh prepared with 3-matic CAE software (www.materialise.com) 36
5.15. Cross-section used for determination of equivalent diameter 37
5.16. STL-NURBS conversion: (a) Starting point cloud; (b) Surface model approximated with 100 NURBS; (c) Surface model approximated with 500 NURBS 38
5.17. Example of manual meshing after erroneous STL-NURBS conversion 39
6.1. Contours used for 2D analysis: (a) free - unclamped, (b) clamped, (c) ideal contour 42
6.2. Constructing the spline through imported points from 3D scanned contour 43
6.3. Example of measuring deviations between unclamped and clamped contour 43
6.4. Cross-section used for 3D analysis 44
6.5. Relation between deformation of a cylinder and a plate 44
6.6. Deviation between unclamped part and nominal CAD data can be calculated and visualised within GOM 3D scanning software 46
6.7. Cartesian coordinate system used to visualise radius deviations 46
6.8. Cross-section radii of unclamped (free) and clamped part 47
6.9. Rotational profile fitting 48
6.10. Vectors used to calculate RMS error between clamped and unclamped profiles 49
6.11. Interpolation of vectors defining clamped and unclamped profiles 49
6.12. Program for RMS-based profile fitting: (a) Interpolation; (b) Fitting 50
6.13. Example of rotational fitting based on RMS 51
6.14. Mapping aligned surface and force vectors 51
6.15. Finding best match between two images by minimizing Hausdorff distance 52
7.1. The erroneous simulation result due to wrong boundary conditions 56
7.2. Finite element mesh with boundary conditions 57
7.3. The influence of boundary conditions on simulation results 57
7.4. Steps required to validate FEM results by digitized data 58
7.5. Conversion of FEM results into CAD model 58
7.6. The graphical representation of 2D FEM analysis results 59
7.7. The deviation between 2D contours obtained by real and by simulated clamping 60
7.8. Dimensional deviations derived from 2D FEM simulation results 62

7.9. Common regular surfaces discretized with triangular thin-shell finite elements 62
7.10. Choosing finite element type and size 63
7.11. Using different coordinate systems to define boundary conditions: single translation 64
7.12. Displacement boundary conditions based on extracted CAD feature 65
7.13. Surface-based boundary conditions, transformed to node-based displacements 65
7.14. Surface-based boundary conditions with equivalent radius 66
7.15. Surface-based boundary conditions with interpolated cross-sections 67
7.16. The surface sections of the scanned part with forced displacements 67
7.17. Stress concentration due to different Δr between neighbouring segments 68
7.18. The scanned free part with boundary conditions applied: forced surface displacement calculated from equivalent radius 69
7.19. FEM simulation results of the whole model, with faulty stress concentration 69
7.20. FEM simulation results presented at the lower part of the model 70
7.21. Theoretical hoop stresses (calculated from 3D scanned data) compared with 3D FEM simulation results (Von-Mises equivalent stress) 71
7.22. Dimensional deviations between FEM simulation and 3D scanning 72
8.1. Measurement chain of 3D scanner used to digitize physically clamped part 78
8.2. Measurement chain of 3D scanner with numerically simulated clamping of workpiece 79
8.3. Propagation of measurement uncertainties through simulation model 85
8.4. Influences on measurement uncertainty of 3D scanner 87
8.5. Structured light 3D scanner configuration 88
8.6. Schematic of Verification and Validation of a Simulation 91
8.7. Models of measurement system: (1) Physically clamped part, (2) Simulated clamping 94
8.8. Graphical comparison of uncertainty contributions 96
8.9. Equivalent radii of cross-section with expanded uncertainties calculated in accordance with GUM requirements 96
8.10. 3D coordinate measuring machine Carl Zeiss Contura G3 97
8.11. Graphical comparison of uncertainty contributions 99
10.1. The initial algorithm for springback compensation in 3D scanning 105
10.2. Novel algorithm for springback compensation by numerical simulations 107
13.1. Odstopanja dimenzij med MKE simulacijo in 3D skeniranjem 129
13.2. Grafična primerjava prispevkov merilno negotovosti 130

List of tables

4.1. Chemical composition 22
4.2. Summary of material testing results 24
4.3. Mechanical properties (as declared by manufacturer) 24
5.1. Comparison of properties of 3D scanners used 31
5.2. Equivalent diameters (mm) in different data conversion phases 38
6.1. Endpoint deformations between clamped and free contours 42
6.2. Equivalent hoop stresses in chosen cross-section (E=210000 N/mm^2) 45
6.3. Radii derived from cross-section of 3D scanned data 47
6.4. Hausdorff distances between clamped and unclamped 3D scanned data 53
7.1. 2D FEM simulation results 61
7.2. 3D FEM simulation results 71
8.1. The definitions given in GUM 74
8.2. Determining the coverage factor (k) according to degrees of freedom (ν) 76
8.3. Uncertainty budget associated with the determination of the circular cross-section radius of the physically clamped filter housing: 94
8.4. Uncertainty budget associated with the determination of the circular cross-section radius of the filter housing with simulated clamping 95
8.5. Radii with expanded uncertainties calculated for 5 different sheet-metal rolls. 97
8.6. Equivalent radii (mm) measured on 3D coordinate measuring machine 97
8.7. Uncertainty budget associated with the scanning errors 98
9.1. The results of experiments and simulations averaged per sheet-metal rolls. 101
9.2. Pearson correlation coefficients between observed parameters. 102
9.3. Two-sample t-test for equal means of expanded uncertainties. 102

9.4. ANOVA single factor analysis for yield stress R_{p02}. 103
9.5. ANOVA single factor analysis for deformation strengthening exponent (n). 103
9.5. ANOVA single factor analysis for hardening coefficient (C). 104
9.6. ANOVA single factor analysis for anisotropy r_{10}. 104

List of acronyms

2D	Two-dimensional
3D	Three-dimensional
A/D	Analogue/Digital
ANSI	American National Standards Institute
AP	Application Protocol
ASCII	American Standard Code for Information Interchange
ASME	American Society of Mechanical Engineers
Avg	Average
B.C.	Boundary Conditions
CAD	Computer Aided Design
CAM	Computer Aided Manufacturing
CATD	Computer-Aided Tolerancing Design
CCD	Charge Coupled Device
CI	Confidence interval
CIPM	International Committee for Weights and Measures
CMM	Coordinate Measuring Machine
CMOS	Complementary Metal Oxide Semiconductor
CT	Computed Tomography
DBDS	Digital Body Development System
DOF	Degree Of Freedom
DSP	Digital Signal Processing
ENOB	Effective Number of Bits
FEA	Finite Element Analysis

FEM	Finite Element Method
GDT	Geometric Dimensioning and Tolerancing
GPS	Geometrical Product Specifications
GUM	Guide for Uncertainty of Measurements
IGES	Initial Graphics Exchange Specification
ISO	International Organization for Standardization
MKE	Metoda končnih elementov
MRI	Magnetic Resonance Imaging
NDT	Non-Destructive Testing
NURBS	Non Uniform Rational Basis Spline
OCT	Optical Coherence Tomography
PDF	Probability density function
PDM	Product Data Management
PLM	Product Life cycle Management
R.P.	Robni pogoji
RMS	Root Mean Square
St. dev.	Standard deviation
STEP	STandard for the Exchange of Product Data
STL	Surface Tesselation Language
V&V	Verification and Validation
VFB	Virtual Function Build
VI	Virtual Instruments
VIM	International Vocabulary of Basic and General Terms in Metrology

When something seems complicated,
it just isn't mature yet...

(Japanese proverb)

An idea that does not at first appear
absurd isn't worth much...

(Albert Einstein)

1. Introduction

1.1. Description of the general research areas

The main characteristic of modern manufacturing processes is increased demand for small series of various products. Simultaneously, there is a permanent demand for productivity and production as fast as those in mass-production. Another trend is use of lightweight components, especially in automotive industry, in order to reduce fuel consumption and CO_2 emission. Mass reduction is usually accomplished through use of lightweight alloys, or by design optimisation according to stress distribution. Typical manufacturing process of these lightweight products consists of three phases: (i) manufacturing, (ii) assembling and (iii) quality control. Such a process requires modern engineering methods to be applied within each phase, with cost reduction as the major objective. A number of supporting techniques was developed recently, which are focused on particular phases of manufacturing process.

Numerical methods, such as finite element method (FEM) have wide use in optimization of technology parameters within manufacturing process, in order to reduce or to eliminate faults in final product. Residual stresses are among the most common faults in thin-walled products, and they cause springback-effect in majority of cases.

However, product faults and defects cannot be avoided, and in some cases it is not cost-effective to avoid them completely. Products containing defects are not necessary unusable; their usability directly depends on prescribed tolerance limits, both individual tolerances and complex tolerance chains. Special disciplines were developed, tolerance analysis and synthesis, in order to redirect focus from individual parts towards assembly as a whole.

Demands for increased quality of sheet-metal products also induced the need for better techniques of non-destructive testing methods and contactless methods for shape and dimension control. In the chapter about the future assessment of dimensioning and tolerancing [1], mr. Don Day says: "All capital investments should be for equipment that is compatible with the requirements of the design. Often equipment and software is justified by a return on investment. The ROI (return on investment) looks better if it can be argued that more parts may be inspected per hour and minimal or no fixtures will be required. This usually leads to greater uncertainty.". To achieve such a goal, new quality control methods should be developed, and this research offers one possible solution. Major part of this research is estimation of uncertainty which arises from the use of complex combination of engineering techniques.

For the needs of reverse engineering, 3D digitisation methods were developed, which are able to create digital model of physical product to in a very short time. Simultaneously, numerical methods, such as FEA (Finite Element Analysis), enabled significant advances in design of components and assemblies. However, numerical methods are mainly used in design phase, and rarely in the phase of quality control of the product. This research proposes new field of application of numerical methods - in the quality control phase, combined with reverse engineering methods.

Special problem in digitised models to deal with is measurement uncertainty. Although there is international standard called "Guide for Uncertainty of Measurements" [2], along with "Guidelines for Evaluating and Expressing the Uncertainty" [3], the standard is too general and therefore cannot be used directly for every type of measurement. Recently, some authors investigated measurement uncertainty of digitised data [58, 59, 61, 79, 97, 103].

Clamping system can deform part being measured [4] and such introduce error that overcomes prescribed tolerances. Clamping process is time-consuming and requires design and manufacturing of fixture system for every product being tested. Therefore, it is justifiable to simulate clamping process by means of numerical methods such as FEM. The main objective of this research is to investigate usage of finite element method to simulate clamping process, in the dimensional quality control of sheet-metal products with springback. To evaluate this method, it is necessary to determine quantitative errors and uncertainty of such a hybrid technique.

1.2. Problem definition

The idea for this research came from the project at QFM institute at the University of Erlangen, Germany, named "Lernfähige Qualitätsmanagementmethoden zur Verkürzung der Prozesskette 'Prüfen'" (Cross-linked, learning Quality-Management measures for development and use of shortened Process-Chains). The project proposed use of three methods for the simulation of the process chain: nominal/actual value comparison of defined parameters from features extracted from the measured data and from the CAD; use of a neural network to determine the distortion compensated 3D data, and finally, the finite elements method [5]. This research showed that FEM can be used for this purpose, but measurement uncertainty and reliability of such a method were inappropriate.

The main objective of this research is to determine whether it is possible to measure the geometry of thin-walled products, which are deformed as a result of residual stresses, using numerical simulations of clamping process.

Another objective is to define the conditions and assumptions required to use the Finite Element Method to compensate the deformations of measured objects, and therefore to build the innovative decision algorithm.

The dissertation objective will be tested through the following hypothesis:

- H0: Numerical simulation of clamping of sheet-metal products with elastic springback has the same measurement uncertainty as 3D scanning of physically clamped products, when clamping is simulated with appropriate boundary conditions which describe accurately the behaviour of the physical clamping.
- H1: Numerical simulation of clamping of sheet-metal products with elastic springback has significantly larger measurement uncertainty than the 3D scanning of physically clamped products.

1.3. Dissertation structure

The introductory chapter of the dissertation describes the general research areas, research objective and the hypothesis. Chapter 2 gives an overview of phenomena related to this problem and literature review of previous researches conducted in the same areas. Chapter 3 explains the motivation to use numerical simulation in dimensional control, and describes phases of the procedure proposed. Chapter 4 describes the product used in experiments, gives basic facts about

production process, equipment and results of experimental determination of material properties, and construction of rigid clamping assembly for 3D scanning. Chapter 5 deals with 3D scanning, describing the equipment, samples and procedure used in experiments, processing of scanning results, converting scanned data into FEA models, and errors induced by data conversion. In Chapter 6, the results of 3D scanning are used to determine the real dimensions and shape of sample product, in order to calculate deviations between unclamped, clamped and nominal CAD part. The computer program was developed to calculate interpolated points, to perform rotational profile fitting and to calculate RMS deviation between profiles. Chapter 7 uses digitised data to perform the finite element analysis. Due to complexity of the problem, the analysis was initially performed on a simple profile, in order to clarify assumptions and conditions which are essential to obtain the accurate results. Each phase of numerical simulation process was carefully analysed, and simulation results were finally prepared for simulation validation. Chapter 8 deals with measurement uncertainty, which includes detailed analysis of influence factors, creating mathematical model of measurement system, and uncertainty analysis according to procedures described in GUM. The results of experiments and simulations performed are subjected to statistical analysis in Chapter 9, in order to test the hypothesis set in introduction. Chapter 10 finally describes the novel algorithm for automated measurement process. Chapter 11 presents the conclusions, the main research results, scientific contribution and suggestions for future researches.

2. Literature review

This chapter gives an overview of phenomena related to this research and review of previous researches conducted in the same areas. These phenomena are springback, tolerance analysis and synthesis, process optimization for sheet-metal production, reverse engineering, optical 3D measuring for quality control of sheet metal products, measurement uncertainty and finally use of FEM in quality control of sheet metal products.

2.1. Springback

Springback is the dimensional change of the formed part after the pressure of the forming tool has been released. The cause of springback is the change in strain due to elastic recovery. Some factors that increase springback are: higher material strength, thinner material, lower Young's modulus, larger die radius and greater wipe steel clearance [6]. Modern materials, such as aluminium alloys and high-strength steels tend to exhibit greater springback. To prevent or reduce springback, a variety of methods is used nowadays. These methods include changes in a design of a die, which may undergo 5-10 costly tryouts before a satisfactory geometry is obtained [7]. Springback research has been focused onto two major issues: to effectively predict springback; and to compensate for springback in tooling design. Numerical simulation of springback in complicated auto-body panels requiring multiple operations (e.g. binder wrap and deep drawing), is time-consuming and errors from each operation could be accumulated to negatively influence the simulation accuracy.

Carden et al. performed experimental tests of springback behaviour, with extensive literature survey (73 references) and their conclusions were contradictory; i.e. some results showed that tool radii sometimes decrease and sometimes increase springback [8]. Zhang and Hu investigated residual stresses as a source of springback [9]. They concluded that great differences in results of previous researches are caused by different conditions the metal were subjected: bending,

incremental bending, reverse bending, stretching. Material properties, friction conditions and tooling design have great influence on springback behaviour. Feng et al. proposed one-step implicit solution for prediction of springback [7]. Ling et al. investigated die design with a step to reduce springback in bending [6]. Buranathiti and Cao developed analytical model to predict springback for a straight flanging process [10]. Chun et al. investigated Bauschinger effect (phenomenon of softening on reverse loading) to achieve realistic simulation of the sheet metal forming process and subsequent springback prediction [11], [12]. Crisbon in [13] and Tekiner in [14] researched springback in V-bending and concluded that the bend radius has the greatest effect on springback. Lee investigated multi-directional springback phenomena in U-draw bending process [15]. Mullan concluded in [16] that analytical models of springback prediction should be replaced by numerical algorithms, because of limitations due to assumptions. Palaniswamy et al. studied the interrelationship of the blank dimensions and interface conditions on the springback for an axisymmetric conical part manufactured by flexforming [17]. They demonstrated that the magnitude of springback and the overall dimensional quality are highly influenced by the initial dimensions of the blank. Ragai et al. discussed the effect of sheet anisotropy on the springback [18], especially blank holding force, the effect of lubrication and Bauschinger effect. They concluded that increased blank holding force and lubrication decrease springback. Lingbeek et al. developed a finite elements based springback compensation tool for sheet metal products [19]. They proposed two different ways of geometric optimisation, the smooth displacement adjustment method and the surface controlled overbending method. Both methods use results from a finite elements deep drawing simulation for the optimization of the tool shape. The results are satisfactory, but it is shown that both methods still need to be improved and that the FE simulation needs to become more reliable to allow industrial application. Viswanathan et al. proposed the use of an artificial neural network and a stepped binder force trajectory to control the springback of a steel channel forming process and to effectively capture the non-linear relationships and interactions of the process parameters [20]. Punch trajectory, which reflects variations in material properties, thickness and friction condition, was used as the key control parameter in the neural network. Xu et al showed in [21] that accurate prediction of springback by finite element simulation is still not feasible, since it involves material and geometrical non-linearity, especially for cases involving large curvatures. Verma and Haldar in [22] analysed influence of normal anisotropy on springback in high strength automotive steels. The effect of anisotropy on springback is predicted using finite element analysis for the benchmark problem of Numisheet-2005, and their research showed that springback is minimum

for an isotropic material. Lee and Kim in [23] showed that the punch corner radius in flange drawing process is the most important factor influencing the springback.

None of these methods is universal and all of them have some limitations. The consequences of these limitations are costly, time-consuming calculations and strong experience in tooling, which is hard to achieve and it is often economically unaffordable.

2.2. Tolerances

In recent years, computer-aided tolerancing design (CATD) has become an important research direction in CAD systems and integrated CAD/CAM systems. Merkley presented methods for combining tolerance analysis of assemblies and finite element analysis to predict assembly force, stress, and deformation in assemblies of compliant parts, such as airframes and automotive bodies [24]. Ji et al. represented the tolerance allocation as an optimization problem [25]. They used fuzzy comprehensive evaluation to evaluate the machinability of parts, established and solved a new mathematical model using a genetic algorithm. Their results showed that such method can be used economically to design the tolerance values of parts. Ding et al. in [26] presented the state-of-the-art, the most recent developments, and the future trends in tolerancing research. The main focus of their research is to introduce new, process-oriented approach to tolerance analysis and synthesis, in order to include effects of toll wearing onto tolerances in the context of multi-station assembly processes. The proposed methodology is based on the development and integration of three models: (i) the tolerance-variation relation; (ii) variation propagation; and (iii) process degradation. Chen et al. introduced the new term: "Locating tool failures", for the purpose of increasing quality level of assemblies, in particular for automotive body [27]. Shah et al. in [28] classified and reviewed geometric tolerance analysis methods and software for two mostly used methods, 1-D Min/Max Charts and Parametric Simulation. They proposed the new, T-map method in order to overcome the problem of compatibility with standards while providing full 3D worst case and statistical analysis.

2.3. Process optimization for sheet-metal production

A number of researches were performed in order to optimize the manufacturing process of sheet-metal products. El Khaldi in [29] presented historical development of finite element simulation technology in stamping applications. He showed that the most rapid development of these techniques occurred between 1990 and 1995, when, for example, Mazda shortened development stage from 50 to 15 days. This reduction in the simulation time came from the

rapidly improving computer technology, and it was influenced by the introduction of new tools: adaptive meshing (1994), automatic discretization/meshing of CAD models (1995), easier and more standardized input (1996) and the introduction of new implicit algorithms for a rapid and qualitative forming evaluation (1998). Haepp and Rohleder presented in [30] how Daimler-Chrysler used numerically based compensation of springback deviations during the die development process. They emphasized that there is still a need for development of automated optimization and compensation of dies or for prediction of form deviatons on assemblies. Ambrogio et al. proposed an integrated numerical/experimental procedure in order to limit the shape defects between the obtained geometry and the desired one [31]. To optimize incremental deep-drawing process, they proposed the design of optimised trajectories that result in more precise profiles. Ling et al. studied how changes in die configuration parameters affect the performance of sheet-metal in a bending die [6]. They focused their interest in springback, bend allowance, pressure pad force and residual stress in the workpiece. Siebenaler and Melkote used finite element analysis to model a fixture-workpiece system and to explore the influence of compliance of the fixture body on workpiece deformation [32]. The simulation studies showed that models of the workpiece and fixture contacts based on surface-to-surface contact elements could predict workpiece deformations and reaction forces to within 5% of the experimental values. The mesh density of the workpiece was found to be more vital to model accuracy than the fixture tip density. Liu and Hu proposed an offset beam element model for prediction of assembly variation of deformable sheet metal parts joined by resistance spot welding [33]. They gave general guidelines for sheet metal assembly product and process design. Cirak et al. proposed the use of subdivision surfaces as a common foundation for modelling, simulation, and design in a unified framework [34]. Majeske and Hammet suggested manufacturers partition variation into three components: part-to-part (the short run variation about a mean), batch-to-batch (die set to die set changes in the mean), and within batch (changes in the mean during a die set) [35]. Quantifying the sources of variation and their relative magnitude also provides the manufacturer a guide when developing a variation reduction plan, and helps to isolate the location of the variations in the body panels. In [36] Kuzman presented examples from sheet metal and bulk metal forming in order to discuss a possibility to improve and stabilize the quality of products by permanent process stability control and by positioning these processes in stable parts of technological windows. Kuzman in [37] analysed impacts of different process parameters through combination of experiments and numerical evaluations. He proved that a combination of parameters where the process is stable could be found, when these parameters are not so sensitive to the fluctuations.

All these references used FEM only to simulate manufacturing process, in order to optimize it and to avoid faults such as springback, wrinkling, waviness, warps, etc. This research area is very wide and there are numerous associations and user groups formed to exchange experiences in this area, such as IDDRG (International Deep Drawing Research Group) or joint groups of automotive producers such as Auto-Steel Partnership or Stamping Simulation Development Group (Audi, BMW, DaimlerChrysler, Opel, PSA Peugeot Citroën, Renault and Volkswagen).

2.4. Reverse engineering

Reverse engineering is a process of obtaining geometric shape from discrete samples in order to create mathematical models when the CAD model does not exist. Huang et al. presented models and algorithms for 3D feature localization and quantitative comparison [38]. They developed fast and robust algorithm for comparison of two free-form surfaces. Kase et al. presented local and global evaluation methods for shape errors of free-form surfaces [39]. These methods were applied for the evaluation of sheet metal formed by using numerical simulation data and coordinate measurement data. Sansoni and Docchio described in [40] a very special and suggestive example of optical 3D acquisition, reverse engineering and rapid prototyping of a historic automobile. They demonstrated the ease of application of the optical system to the gauging and the reverse engineering of large surfaces, as automobile body press parts and full-size clays, with high accuracy and reduced processing time, for design and restyling applications. Huang and Menq proposed a novel approach to reliably reconstruct the geometric shape from an unorganized point cloud sampled from the boundary surface of a physical object [41]. These techniques are still developing, in terms of hardware (3D scanners, optical and tactile digitisers) and software (quality control, automation, feature recognition, processing speed,...).

2.5. Optical 3D measuring for quality control of sheet metal products

A number of different techniques for optical measurements are in use nowadays: shape from shading, shape from texture, time/light in flight, laser scanning, laser tracking, Moiré interferometry, photogrammetry, structured light, etc. Monchalin presented a broad panoply of light and laser-based techniques in [42]: photogrammetry, laser triangulation, fringe projection, Moiré, D-Sight, edge-of-light, optical coherence tomography (OCT) for the evaluation of shape and surface profiles, laser induced breakdown spectroscopy for composition determination, holography, electronic speckle pattern interferometry and shearography for the detection of flaws, laser-ultrasonics for the detection of flaws and microstructure characterization. OCT and another technique called Photon Density Waves can probe transparent or translucent materials.

His presentation shows a broad overview of all optics or laser-based NDT (Non-Destructive Testing) techniques, outlining their present industrial use and future perspectives. Chen, Brown and Song also provided and overview of 3D shape measurement methods, with exhaustive bibliography consisting of 226 references [43]. Their survey emphasized advantages and disadvantages of particular optical methods, such as light intensity, global and local coordinates translation, accuracy, uncertainty, precision, repeatability, resolution and sensitivity. They also proposed some future research trends: real time computing, direct shape measurement from specular surfaces, shading problem, need for standard methodology for optical measurements, large measurement range with high accuracy, system calibration and optimization. Yang et al. presented optical methods for surface distortion measurement [44]. Galanulis presented three optical measuring technologies: digitizing, forming analysis and material property determination, which became a part of sheet metal forming in many industrial applications during the past years [45]. Jyrkinen et al. studied the quality assurance of formed sheet metal parts and stated that a machine vision system could be used in automated visual quality inspection [46]. They examined angles, distances, dimensions, existence of some other features and measuring holes. Their research showed that 3D optical measuring system is appropriate for measurement of angles and distances, but measuring diameters showed some problems, since edges of a hole could not be detected accurately. They concluded that a machine vision system can be used in quality assurance with enough accuracy. The setbacks of this method are high costs of equipment and relatively long measuring times. Gordon et al. introduced laser scanning as an instrument which may be applicable to the field of deformation monitoring [47]. The Auto-Steel Partnership issued a publication about the impact of the measurement system on dimensional evaluation processes [4]. They recommended greater emphasis on improving the correlation between detail part measurements in holding fixtures, whether CMM (Coordinate Measuring Machine) or check fixture, and part positioning at time of assembly. Some manufacturers are trying to achieve this by over-constraining large, non-rigid parts.

Optical measurements and machine vision are the leading growth technologies in the field of industrial automation, especially in automotive industry. They find application in error-proofing, dimensional metrology, pattern matching and surface inspection. Coordinate measuring machines are irreplaceable in the field of precision engineering, but their slowness and high price prevent them to become the part of automated full-scale inspection systems.

2.6. Measurement uncertainty

Uncertainty is the word used to express both the quantitative parameter qualifying measurement results and the concept that a doubt always exists about how well the result of the measurement represents the value of the quantity being measured. Intensive researches were performed and published concerning measurement uncertainty. Yan et al. focused on the uncertainty analysis and variation reduction of coordinate system estimation using discrete measurement data and is associated with the applications that deal with parts produced by end-milling processes and having complex geometry [48], [49]. They developed iterative procedure for geometric error decomposition. Huang W. et al. conducted research to improve the accuracy and throughput of coordinate dimensional gages through feature-based measurement error analysis [50]. In addition to well-known measurement uncertainty of coordinate measuring machine (CMM), they analysed error that arises from specific geometric shape of measurand (thus measuring area around the selected feature). Cordero and Lira characterized the influences of environmental perturbations and compared them with other systematic effects at phase-shifting Moiré interferometry [51]. They have found that the local displacement uncertainties depended on the sample elongation and on the reference location. An equation was found for these uncertainties as a function of the total number of fringes occurring. Ceglarek and Shi investigated in [52] influence of fixture geometry onto measurement noise in diagnostic results. To avoid fixture deformation, Gopalakrishnan in his dissertation considered workholding using contacts at concavities for rigid and deformable parts [53]. In [54] Gopalakrishnan et al. used Finite Element Method (FEM) to compute part deformation and to arrange secondary contacts at part edges and interior surfaces. Chen et al. examined model validation as a primary means to evaluate accuracy and reliability of computational simulations in engineering design [55]. Their methodology is illustrated with the examination of the validity of two finite element analysis models for predicting springback angles in a sample flanging process. Kreinovich and Ferson used statistical methods for evaluation of uncertainty in risk analysis [56]. Jing et al. analysed the measurement uncertainty of virtual instruments (VIs) [57] through the main uncertainty sources of transducer, signal conditioning, A/D conversion and digital signal processing (DSP). They concluded that the uncertainties of signal conditioning and A/D conversion usually occupy a tiny percentage compared with other uncertainties of a VI so that its combined measurement uncertainty is often dominated by the uncertainties of transducers. Since reverse engineering techniques are based on exhaustive computations, VI uncertainty is comparable with uncertainty of reverse engineering methods. Lazzari and Iuculano evaluated the uncertainty of an optical machine with a vision system for

contactless three-dimensional measurement [58]. Their paper provides the basis of the expression of the uncertainty of a measurement result obtained using the optical measurement machines and it shows the necessary requirements for the numerical evaluation of such uncertainty. De Santo et al. presented and discussed the use and evaluation of measures coming from digital images in an industrial context [59].

Locci introduced a numerical approach to the evaluation of uncertainty in nonconventional measurements on power systems [60], as an alternative to the uncertainty evaluation based on the analytical solution of the uncertainty propagation law, as prescribed by the GUM [2]. Locci also investigated the uncertainty in measurement based on digital signal processing algorithms [61]. He showed that approach based on numerical simulations is the most suitable for digital instruments, since its applicability is not influenced by the complexity of the measurement algorithm and by the number of uncertainty sources affecting the input samples. Nuccio and Spattaro contributed to research of measurement uncertainty of virtual instruments [62] and they also concluded that numerical simulation overwhelms GUM approach. They also studied influence of the effective number of bits (ENOB) onto measurement uncertainty in [63], and concluded that ENOB can not be used, since it does not take into consideration all error sources, such as offset, gain and crosstalk.

Floating point arithmetic is used in numerical computations, and this always introduces small rounding errors. Each individual operation introduces only a tiny error, particularly if double precision arithmetic is being used, but when very large numbers of computations are carried out, the is the potential for these to mount up. Kahan published a number of papers dealing with roundoff errors due to floating-point arithmetic limitations [64], [65], [66]. His work even lead to introduction of international standard for floating-point computations [67]. Kalliojärwi and Astola studied roundoff errors in signal processing systems utilizing block-floating-point representation [68]. Castrup discussed key questions and concerns regarding the development of uncertainty analysis using Excel and Lotus spreadsheet applications [69]. Fang et al. analysed errors arising from fixed-point implementations of digital signal processing (DSP) algorithms [70]. Mitra proposed compromise between fixed point and floating point format due to its acceptable numerical error properties [71]. Pitas and Strintzis analysed floating point error of 2D Fast Fourier Transform algorithms in [72] and [73]. The floating-point arithmetic can be the source of uncertainty in digital measurements, and should be studied in more details.

2.7. Use of FEM in quality control of sheet metal products

FEM was not widely used in quality inspection. Shiu et al. developed a comprehensive analysis technique for the dimensional quality inspection of sheet-metal assembly with welding-induced internal stress [74]. They proposed a minimum stress criterion for the minimum dimensional variation during sheet metal assembly and gave product design guidelines for sheet metal assembly, such as step joint design, tunnel design, planar joint design, which should be followed to prevent assembly faults. However, if these principles are not followed in design process, the errors necessarily arise. The same authors developed a flexible part assembly modelling methodology for dimensional diagnostics of the automotive body assembly process [75]. They used flexible beam modelling in dimensional control. Lipshitz and Fischer used technique called Discrete Curvature Estimation for verification of scanned engineering parts [76]. They represented scanned objects by triangular meshes, which contain very dense data with noise. In order to achieve very accurate and robust verification, the proposed curvature estimations handle noisy data. Weckenmann et al. performed research named "Cross-linked, learning Quality-Management measures for development and use of shortened Process-Chains" [5], in order to develop ideas for a modern way of manufacturing using robust, shortened and low cost process sequences for sheet light weight parts [77]. Their project proposed use of three methods for the simulation of the process chain: nominal/actual value comparison of defined parameters from features extracted from the measured data and from the CAD (morphing); use of a neural network to determine the distortion compensated 3D data, and finally, the finite elements method. They used FEM only for the control of results obtained with neural network and morphing. The starting points for this research were presented in [78]. Weckenmann and Weickmann in [79] showed that the actual limitation of the method is the measurement uncertainty and uncertainty of the accuracy of the FEM simulation. The uncertainty of virtual fixation is calculated to be ±0.7 mm, as opposed to the measurement uncertainty of CMMs for the same tasks, which is up to ±0.1 to 0.2 mm. Because of this, further investigations aimed at optimizing the measurement situation and reducing the uncertainties is proposed.

Park and Mills in [80] proposed two strategies for use of digitisation of flexible parts in order to localize them in robotic fixtures; the CAD-based method where CAD model is used as a reference geometry, and the direct calibration method with best-fit mappings. Their research showed that CAD model could lead to increased measurement errors due to the high structural flexibility of sheet metal parts, parts, which allows the actual part grasped by a robot to deform under gravity and grasping forces.

The Center for Automotive Research (CAR) at Ann Arbor, Michigan, USA, sponsored a project "Building a Virtual Auto Body: The Digital Body Development System (DBDS)" [81]. The project is realized by consortium consisting of leading academic and industrial participants: Altarum, Atlas, ATC, Autodie, CAR, Cognitens, Ford, GM, Perceptron, Riviera, Sekely, UGS PLM, Wayne State Univ. The software developed through this project would enable virtual implementation of functional build through the integration of a dimensional and finite element simulation engine with an agent-based decision support system. DBDS will simulate a newly designed automobile body and link its many components and manufacturing elements virtually, allowing designers and engineers to identify and solve problems before any assembly occurs. Then design and simulation results are integrated with manufactured part data to identify problems and novel solutions during launch. Such an approach is called "Virtual Function Build (VFB)" [82], where scanned parts are assembled virtually using assembly modelling software. Finite element analysis technology is used to deform the scanned parts to the shape that they would adopt on the functional build tooling. This is expected to reduce time to market and improve quality by focusing on the assembled product rather than individual parts. The project were scheduled to be finished in September 2008, but due to global economy crisis and financial problems of automakers in late 2009, the project was delayed.

2.8. Conclusion

Exhaustive literature review showed that it is feasible to examine if numerical methods can be implemented into automated quality control techniques based on reverse engineering technology. Large-scale projects in Europe [5] and USA [81] were initiated recently and there is a lot of research areas where contribution can be made.

3. Motivation

This research is an effort to implement modern technology in an innovative way, in order to enable quality control automation and to estimate the risks and limitations of such an approach. At the first sight, one can assume that use of simulation in dimensional control is not feasible, but there is an affirmative argument against such an attitude. It is true that currently used "positioning-clamping-measurement-unclamping" procedure is faster than proposed one: "measurement-simulation-analysis", as it is presented in Fig. 3.1.

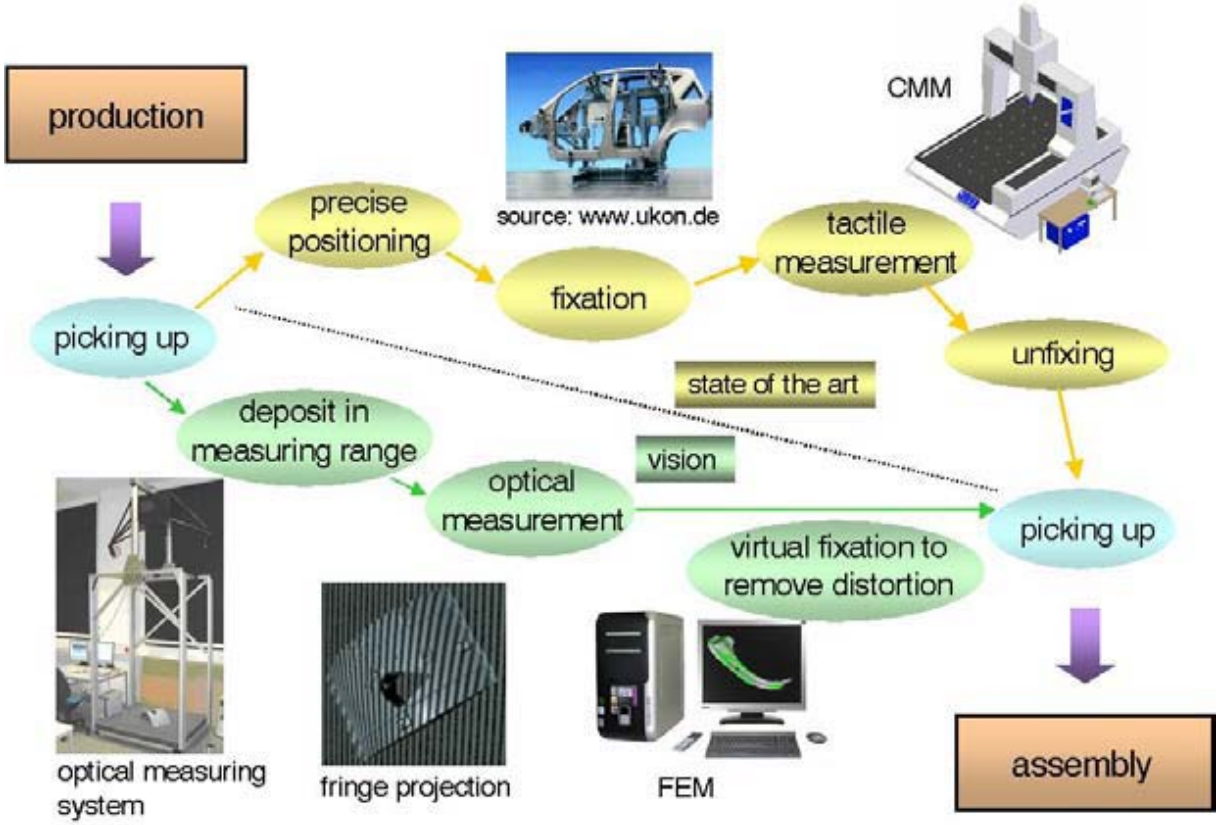

Fig. 3.1. Measuring chain with a tactile and an optical measurement system [79]

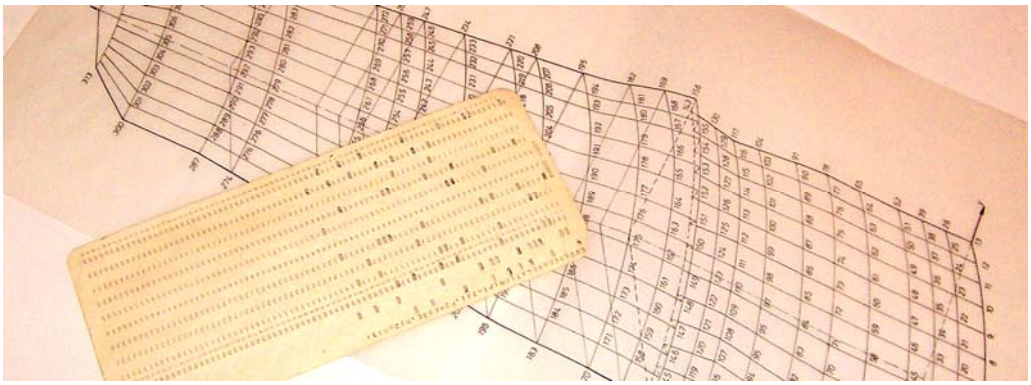

Fig. 3.2. Tools used for FEA in 1970's: paper-based mesh, punched cards

Nevertheless, the process of finite element analysis used to be extremely demanding and time-consuming. Fig. 3.2 shows the finite element tools which were used 30 years ago. Rapid development of commercial computers enabled them to perform complicated FEA tasks in a split second. Therefore, current computing speed cannot be considered as limitation, since computer processing speed and new solver algorithms tend to be increasingly fast (Fig. 3.3).

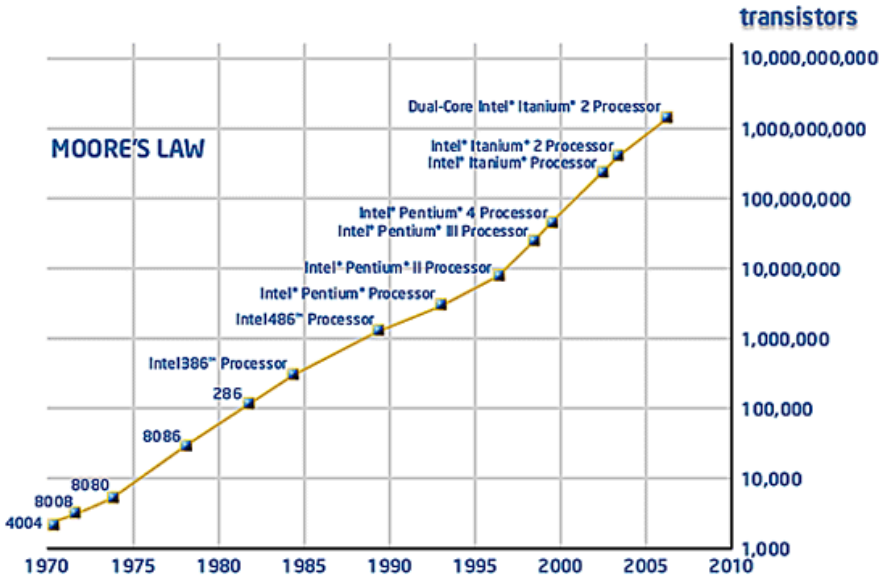

Fig. 3.3. Moore's Law: "The number of transistors on a chip doubles about every two years" (source: http://www.intel.com/technology/mooreslaw/index.htm)

Even earliest engineering tasks required reconstruction of 3D shapes (Fig. 3.4). During past decade, non-contact optical scanning proved itself as an emerging technology with evident increase in accuracy, resolution and versatility. Fig. 3.5 shows typical optical 3D scanners available in market in 2008. The prices range between 3.000 and 100.000 Euros, and it is common that accompanying software takes half the price of the system.

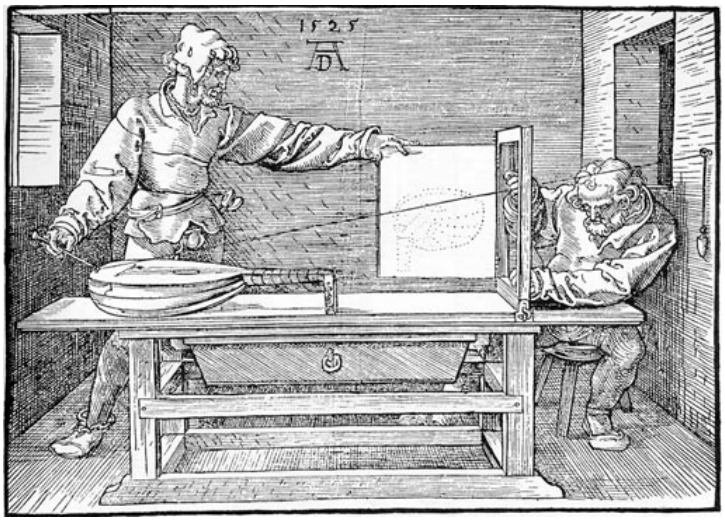

Fig. 3.4. Medieval 3D scanning (source: "Der Zeichner der Laute", Albrecht Dürer, 1525)

ZScanner 700 (www.zcorp.com)

ATOS III
(www.gom.com)

ModelMaker Z
(www.metris.com)

Desktop 3D scanner
(www.nextengine.com)

VI-9i 3D Digitizer
(www.minolta3d.com)

FastSCAN Scorpion
(www.polhemus.com)

Fig. 3.5. Typical 3D scanners commercially available in 2009

Non-contact 3D optical scanning has some advantages over other measurement techniques. Tactile coordinate measuring machines (CMM's) are extremely accurate, but they have limited speed due to inertia of mechanical components. The same limitation refers to tactile 3D digitizers. On the contrary, optical 3D scanners can acquire millions of points in second. Their

major disadvantage refers to inability to acquire "shaded" points - points and surfaces which are behind a barrier. Fig. 6 shows an example of future development of 3D scanners.

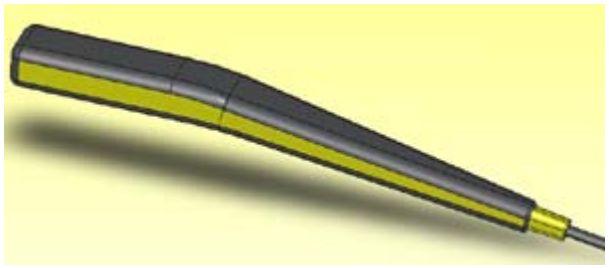

Fig. 3.6. The AFI Micro intra-oral 3D scanner for dentists - still under development (source: http://www.dphotonics.com/products/afi_micro)

Conventional measuring machines, tactile digitizers and CMM's implement a contact force between touch-probe and measured object. This force can deform measured objects, which makes optical 3D scanners unavoidable measurement tools for thin-walled products. Flexible thin-walled components are very common in automotive industry, and it is reasonable to use optical 3D scanners in an automated environment (Fig. 3.7).

Fig. 3.7. Automotive body at the optical measurement station [83]

The need for clamping/fixturing system is a disadvantage for such an automation, because it reduces flexibility and increases costs. To overcome these limitations, simulations can be used to compensate for deformation of flexible components.

3.1. Proposed procedure

In order to avoid fixtures during dimensional measurement of elastic products, it is planned to digitise products as they are (without fixture), and then to simulate clamping. To estimate if this method can be used practically, it is important to test the procedure on a real product.

This research consists of the following phases:

1. Determination of product characteristics (material properties, prescribed dimensions, tolerance limits, functional role in an assembly)
2. 3D scanning of products as they are (without clamping)
3. 3D scanning of products clamped by means of rigid fixture
4. Processing of scanning results (reverse engineering, surface clean-up, exporting to file format for finite element analysis)
5. Checking reverse engineering accuracy (estimating errors induced by consecutive computations)
6. Finite element simulation of clamping process
7. Static strain analysis based on measured deformations
8. Estimation of dominating influence factors
9. Determination of measurement uncertainty
10. Statistical analysis of results and hypothesis testing
11. Finalising algorithm for proposed procedure

The final result of this research is refined algorithm for automation-ready procedure, with well defined influence factors and measurement uncertainty.

4. Determination of product characteristics

This chapter describes the product used in experiments, gives basic facts about production process, material properties and construction of rigid clamping assembly for 3D scanning.

4.1. Product description

The product used to test the proposed procedure of virtual clamping is oil filter housing, manufactured by Mann+Hummel (Unico Filter) Tešanj, Bosnia and Herzegovina (Fig. 4.1).

Fig. 4.1. Replacement lubricating oil filter LI 9144/25

The filter consists of several parts (Fig. 4.1), whereas the housing is manufactured by deep drawing. The production rate is more than 1.100.000 pieces per year. The same product is being manufactured in Germany at the production rate above 4 millions per year. Average annual number of rejected products is around 1.600. The housing is made of mild steel grades for cold forming, manufactured by Salzgitter Flachstahl GmbH, having properties according to DIN EN 10130-02:99, quality DC04 A (DIN EN 10130-02:99 / DIN EN 10131).

The filter housing with major dimensioning is shown in fig. 4.2. The dimension which is controlled regularly is circular cross-section diameter ($Ø92^{-0,2}$) measured at 10 mm from top of the housing. This diameter will be used for control by 3D scanner and finite element analysis.

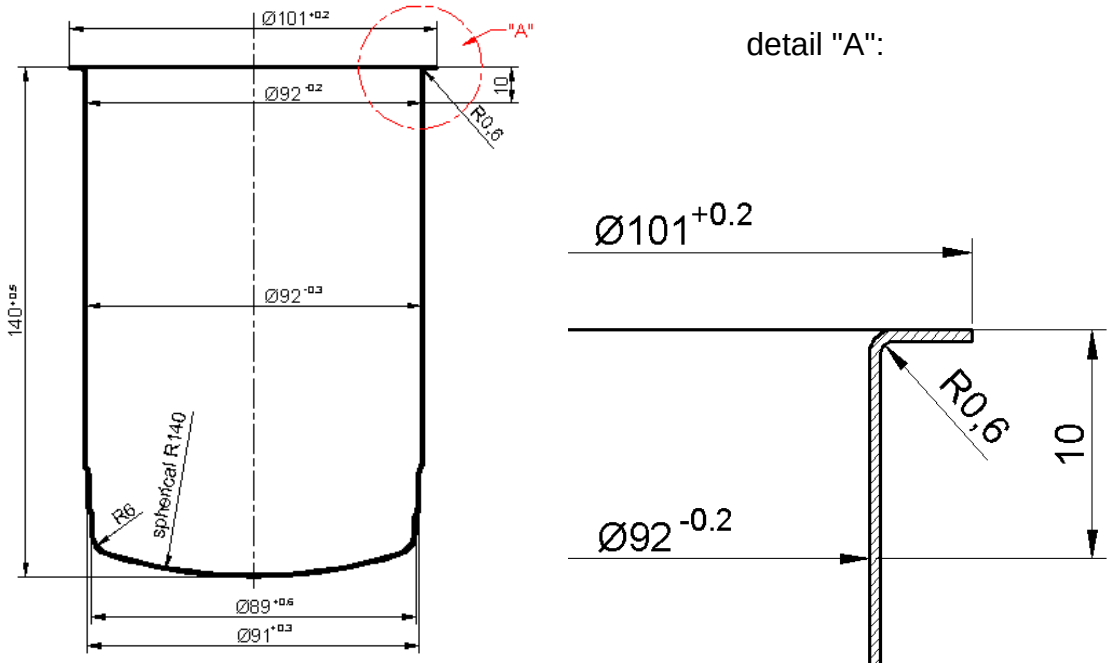

Fig. 4.2. Detail from technical documentation

4.2. Material properties

The material used has fairly uniform properties. The chemical composition rarely differs from values presented in Table 4.1.

Table 4.1. Chemical composition

Element	C (%)	Si (%)	Mn (%)	P (%)	S (%)	Al (%)
declared by manufacturer	0,03	0,01	0,19	0,006	0,005	0,054
standard requirements	0,03-0,06	max. 0,02	0,18-0,40	max. 0,02	max. 0,02	0,02-0,06

Since anisotropy is proven to be among the most influencing factors in deep drawing, the samples from all rolls were tested for anisotropy. The tests were performed at the Forming Laboratory at the Faculty of mechanical engineering in Ljubljana. Fig. 4.3 shows the uniaxial tensile testing machine Amsler, equipped with computer vision system for non-contact dimensional measurements (3 monochromatic cameras 640x480, L''' CCD, objective Cosmicar and accompanying LabView software). Claimed measurement uncertainty of the machine is ±1%.

Fig. 4.3. Tensile testing machine at the Forming Laboratory

In order to determine material properties, a set of 75 standard specimens was prepared: 5 sets of 15 specimens, each set taken from different sheet-metal roll, cut at 0°, 45° and 90° to the direction of rolling. Table 4.2 gives the brief summary of test results.

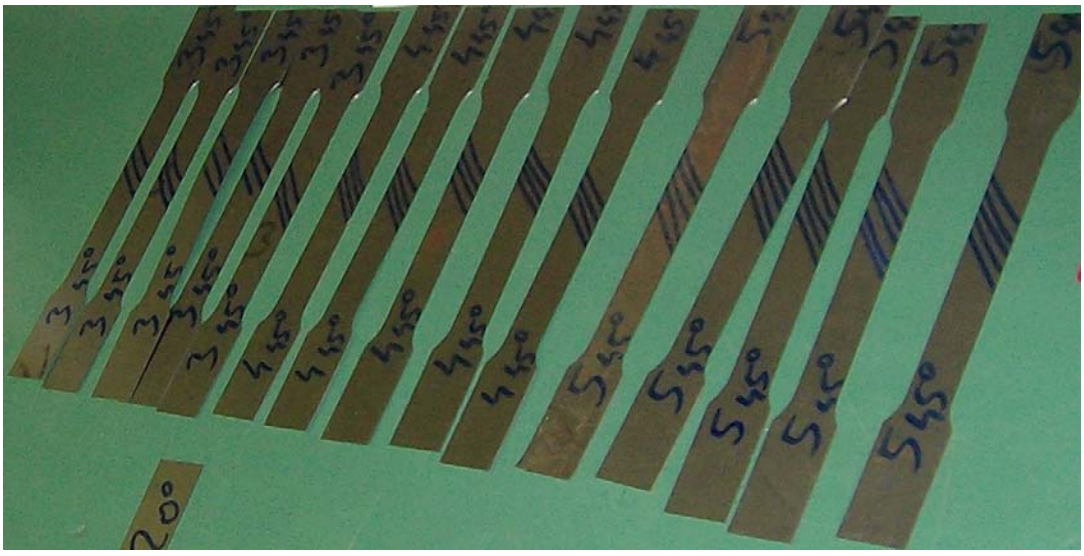

Fig. 4.4. Specimens used for anisotropy tests

Table 4.2. Summary of material testing results

Result	Roll 1	Roll 2	Roll 3	Roll 4	Roll 5	Average	St. dev.
n	0,223	0,229	0,215	0,222	0,222	0,222	0,0075

C (N/mm)	509,66	501,77	502,92	510,39	509,45	506,84	15,34
R_m (MPa)	291,50	283,81	291,74	291,94	291,73	290,15	8,06
$R_{p0,2}$ (MPa)	153,69	147,08	160,01	152,11	148,85	152,35	13,49
$R_{p0,5}$ (MPa)	175,07	165,91	180,99	175,29	173,53	174,16	7,51
A80 (%)	41,37	37,71	38,94	39,03	38,75	39,16	7,03
$r_{10}=(r_0+2r_{45}+r_{90})/4$	2,04	2,05	1,96	1,98	1,95	1,99	0,14
$r_{20}=(r_0+2r_{45}+r_{90})/4$	2,10	2,12	2,08	2,03	2,04	1,97	0,06

Results shown in Table 4.2 confirmed that material properties are mostly consistent and correspond to mechanical properties declared by manufacturer (as shown in Table 4.3). The largest differences are between declared and measured yield stresses ($R_{p0,2}$) and ultimate strengths (R_m), while average normal anisotropy factors (r), strain (A80) and deformation strengthening exponents (n) are the same, or even better than the declared ones.

Table 4.3. Mechanical properties (as declared by manufacturer)

n	R_m (MPa)	$R_{p0,2}$ (MPa)	A80 (%)	r
0,208	312,00	187,00	38	2,00

In-depth statistical analysis of measured mechanical properties will be presented in Chapter 9.

4.3. Clamping assembly

In order to simulate real conditions which occur when this housing is assembled with other filter components, a two-part rigid clamping assembly was constructed. Fig. 4.5 shows the clamping assembly. Since the thickness of sheet metal housing is 0,5 mm, the upper and the lower parts of the assembly have the 0,45 mm clearance between the coupling halves.

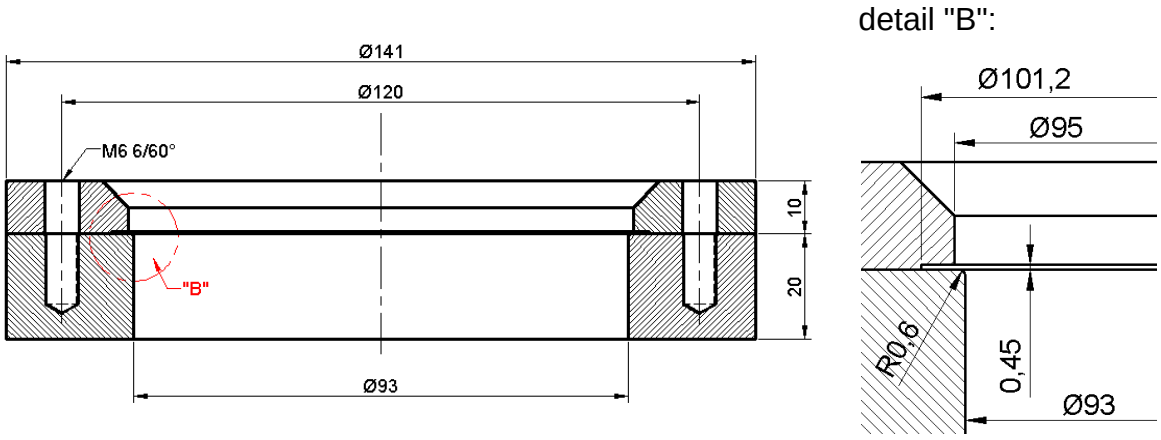

Fig. 4.5. Clamping assembly

When the housing is placed between the coupling halves, the pressure is applied by means of six M6 bolts distributed across the 120 mm circle. This pressure deforms the housing, simulating the

real filter assembly. The clamping assembly can be assumed as rigid, since its dimensions are much larger than the thickness of sheet-metal housing being measured.

The internal edge of the upper assembly component was chamfered to provide visibility of internal surface of the filter housing and to enable 3D scanning deep enough. The internal edge of the lower assembly component is filleted with radius 0.6 mm. This radius was chosen to avoid deformation induced from contact between the lower clamping assembly part and the filter housing.

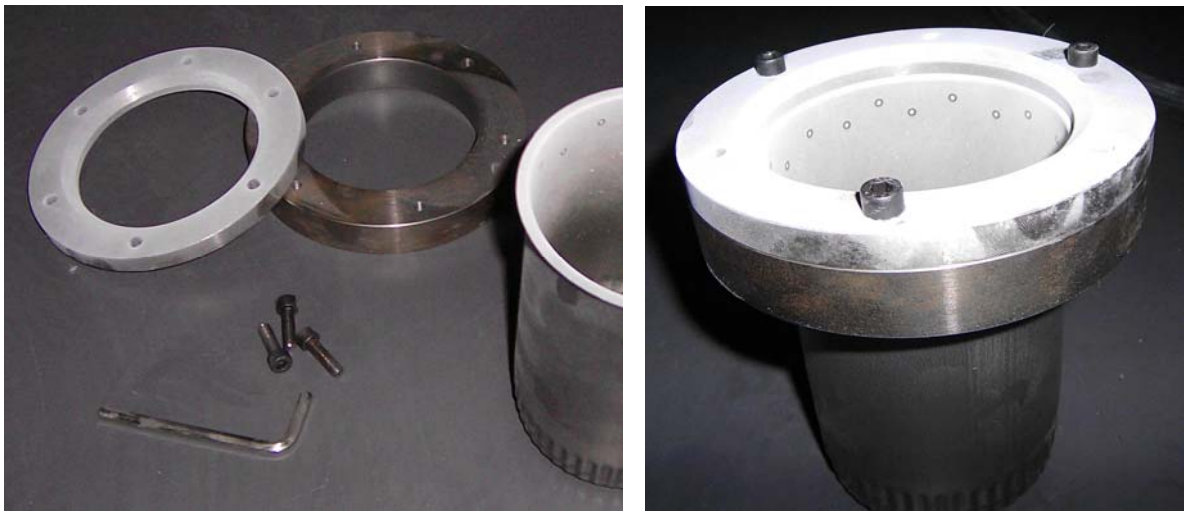

Fig. 4.6. Clamping assembly used for 3D scanning

Fig. 4.6 shows the clamping assembly used for 3D scanning of samples. First photograph shows disassembled fixture, and the photograph on the right shows the clamped filter housing.

The filter housing has thin walls (0,5 mm), and it is common to have deviation from cilindricity. This clamping assembly is rigid and it deforms the housing towards cylindrical shape, compensating deviations induced by any source: manufacturing process, material properties, anisotropy, residual stresses and other defects.

5. 3D scanning

The deformation of the filter housing is considerably small, therefore the 3D scanner should have high measuring quality. For that purpose, the high-end 3D optical measurement system ATOS II, manufactured by GOM mbH Germany, was used (Fig. 5.1).

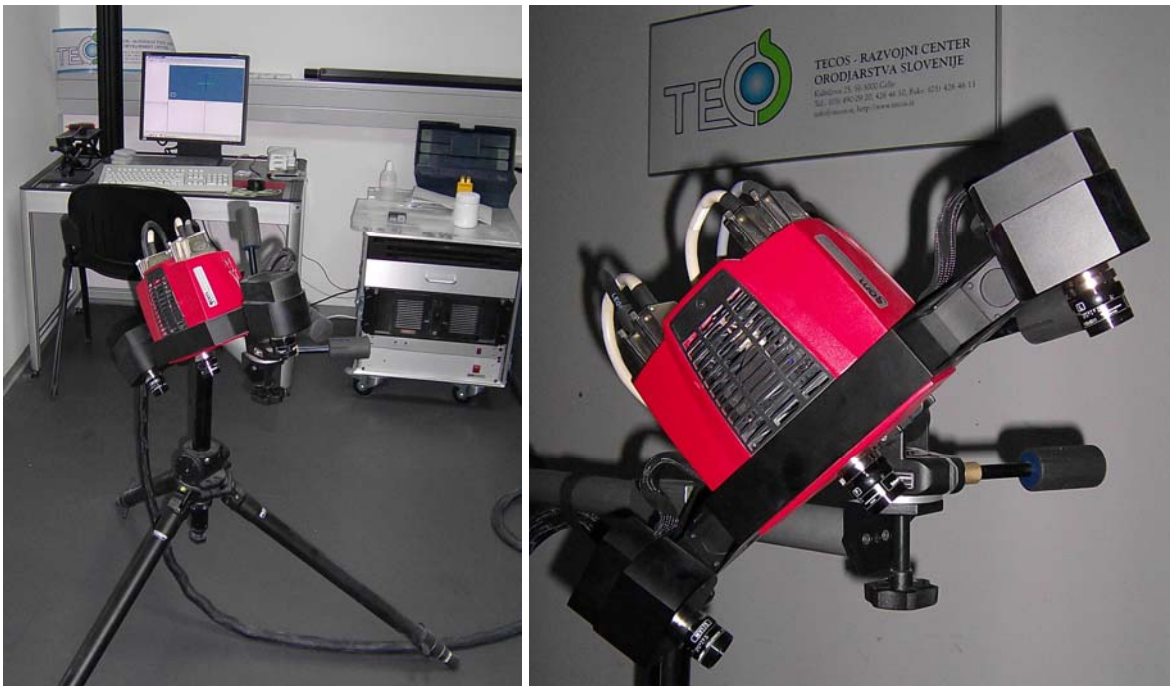

Fig. 5.1. 3D digitizer ATOS II

This flexible optical measuring machine is based on the principle of triangulation. Projected fringe patterns are observed with two cameras. 3D coordinates for each camera pixel are calculated with high precision, a polygon mesh of the object's surface is generated. The scanning was performed at the Slovenian Tool & Die Development Centre TECOS, Celje.

A total of 25 filter housings were prepared for 3D scanning: 5 sets of 5 samples, each set manufactured from different sheet-metal roll (these sets correspond to sets used for anisotropy and tensile tests). Each sample was scanned with and without clamping.

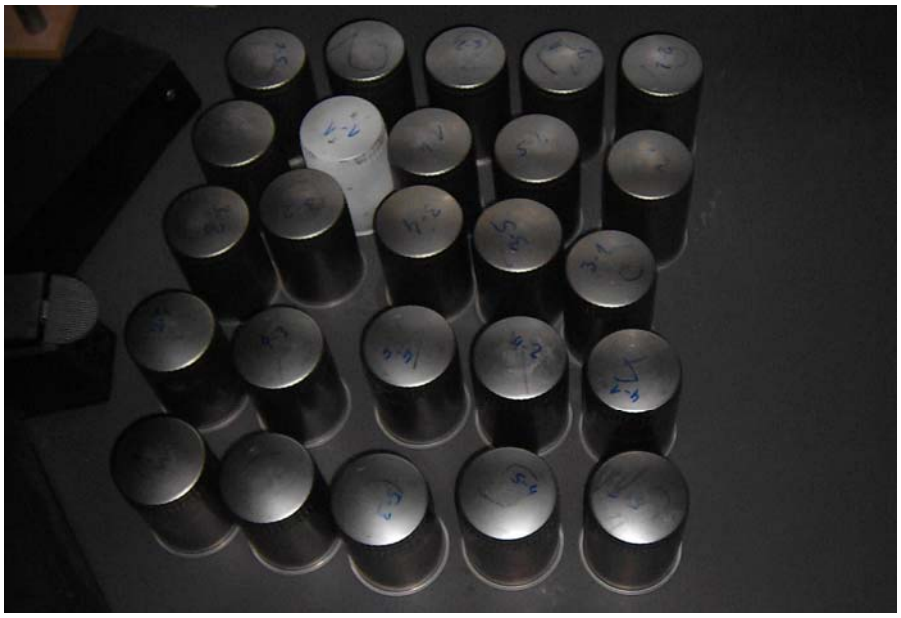

Fig. 5.2. Filter housings prepared for scanning

The dimension used for this analysis is cross-section diameter taken 10 mm measured from the housing top. Consequently, to reduce scanning time, only upper internal part of the housing was scanned. Fig. 5.3 shows the screenshot from 3D scanning software.

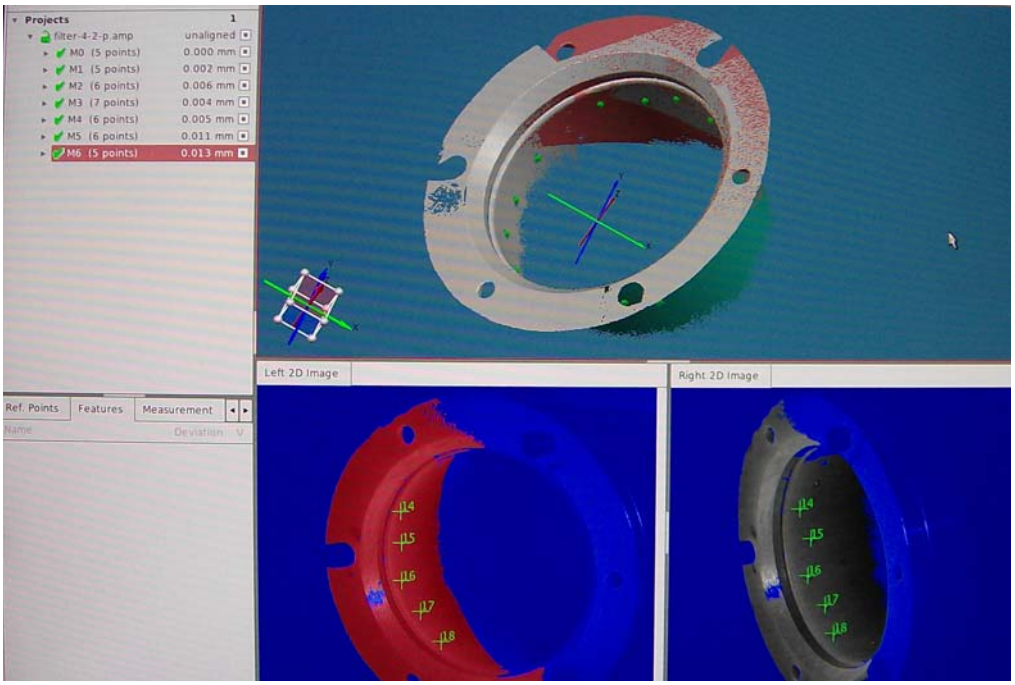

Fig. 5.3. Fitting scans in 3D scanning software GOM

Due to geometry of scanned part, some surfaces are obscured, and the scanning has to be performed in 5 to 8 steps, producing overlapping scans. The fitting of these scans is done within GOM software, by means of reference points applied randomly on scanned part before scanning.

It is important to describe the scanning procedure, because it introduces some deviations which propagate to final measurement results. The typical procedure consists of the following steps:

- scanned object preparation (application of reference points and anti-reflection spraying),
- set of scans taken at different positions (number of scans depends on object complexity),
- joining scans into single point cloud using reference points (Fig. 5.3),
- surface extraction with trimming of unnecessary parts and background objects,
- automatic and manual error corrections (Figs. 5.4, 5.5),
- alignment with chosen coordinate system (Fig. 5.6), and finally
- exporting scanned surface into appropriate format for further processing.

The 3D scanner sensor is positioned freely in front of the object to be measured. For measuring, a fringe pattern is projected onto the object surface which is recorded by two cameras. The software calculates the high-precision 3D coordinates of up to 4 million object points within seconds. Several partial views are joined together using reference points. For each measurement, the calibration of the system, the movements of the object or the sensor and the influence of extraneous light are checked, to ensure secure, precise and quick measurements.

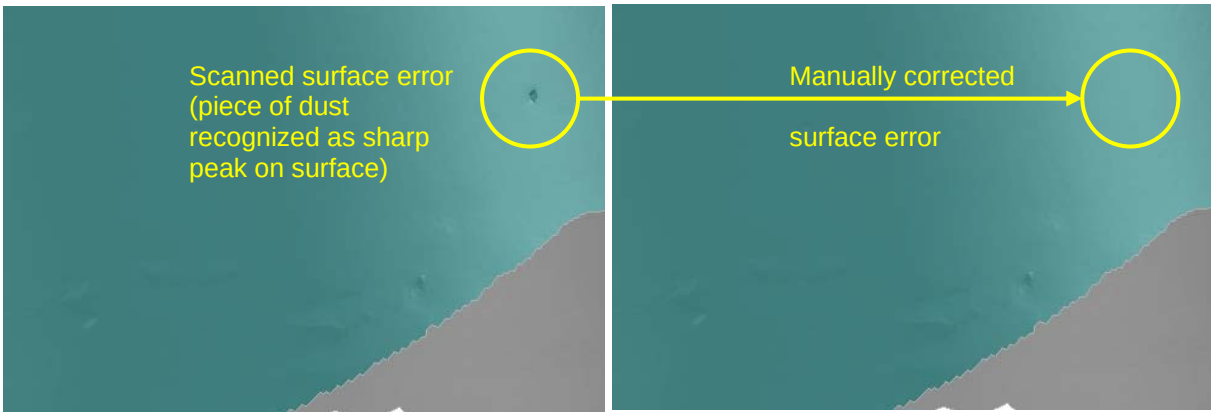

Fig. 5.4. Correction of surface errors in GOM software

Fig. 5.4 shows an example of surface error correction performed after extraction of triangulated surface from scanned point cloud. Some errors are processed and removed automatically, such as elevations that appear due to stickers applied as reference points, and some errors have to be removed manually, using surface interpolation from surrounding triangles.

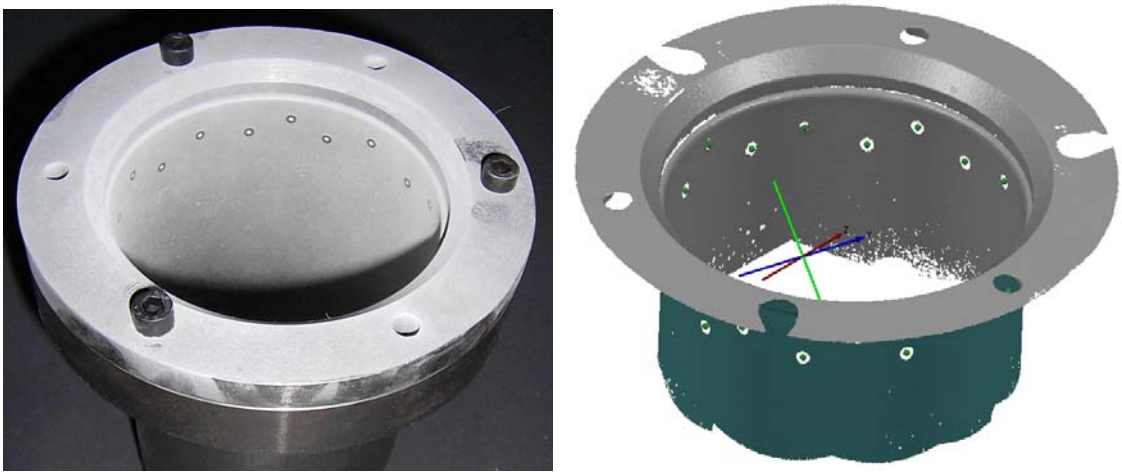

Fig. 5.5. Errors that can be corrected automatically (reference point stickers)

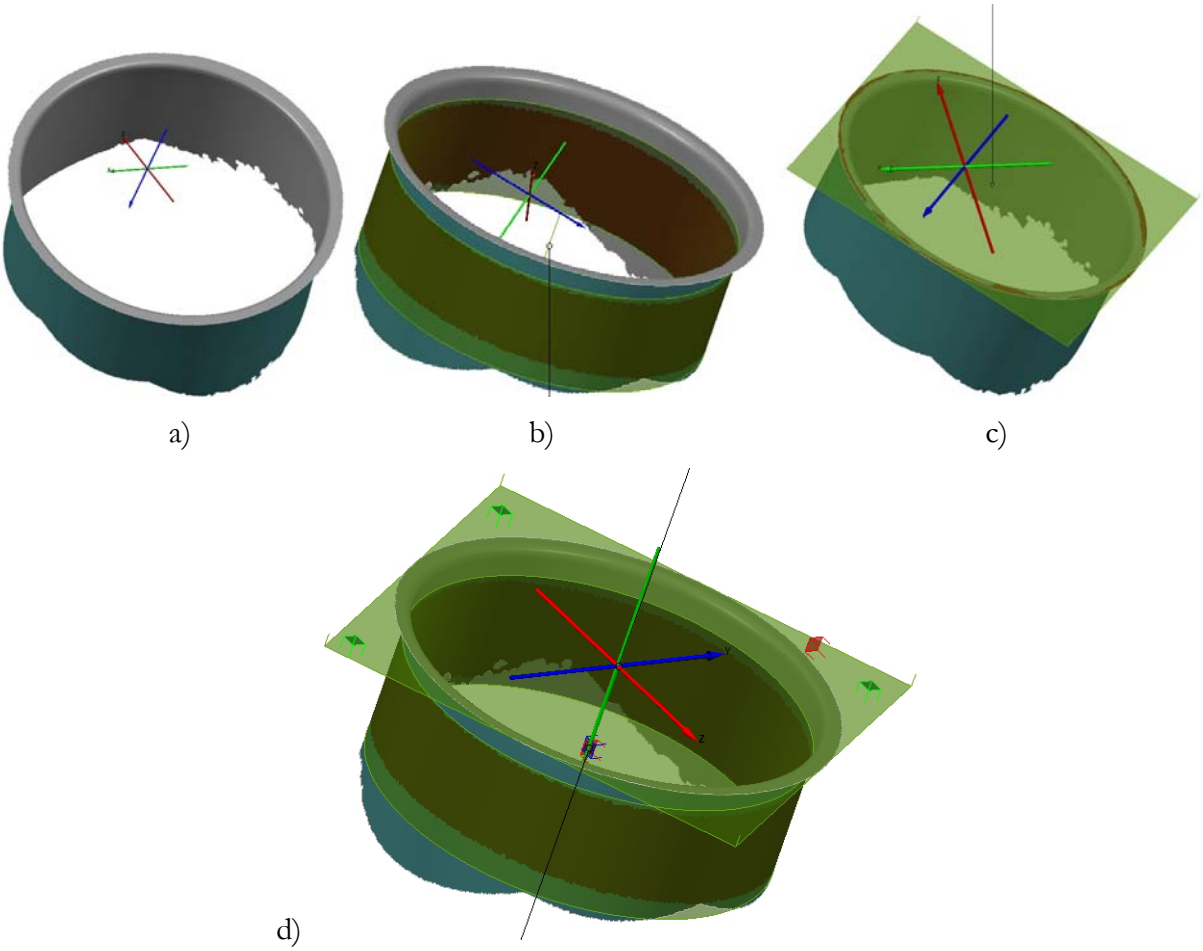

Fig. 5.6. Alignment with reference coordinate system using transformations

The scanned object needs to be aligned with chosen coordinate system in order to be used for further processing. Fig. 5.6 describes the alignment procedure: primitive surfaces are extracted from arbitrarily positioned starting object (a) using best-fit method. In this case, cylinder (b) and planar surface (c) are extracted and aligned with reference coordinate system (d).

For the purpose of simplified initial 2D analysis, another digitizer was used, the NextEngine colour laser 3D scanner at the University of Zenica, Bosnia and Herzegovina (Fig. 5.7). Table 5.1 summarizes the main characteristics of the two scanners used. The major difference between the two scanners is their accuracy. The lower accuracy of the laser scanner is justifiable, since the deformations measured in 3D and 2D cases differ significantly.

Fig. 5.7. Colour laser 3D scanner NextEngine

Table 5.1. Comparison of properties of 3D scanners used

	ATOS II 400	**NextEngine**
Technology	White-light fringe projection	Laser Scanner
Speed	1.400.000 points/sec	50.000 points/sec
Accuracy	±0,010 mm	±0.125 mm
Camera resolution	1,2 Mpixel	3 Mpixel

The saddle brackets used as samples for 2D analysis were made of the same material as the filter housings (sheet metal stripes taken from 5 different rolls). Fig. 5.8 shows the samples used for 2D analysis. It is a manually manufactured saddle bracket, with excessive springback behaviour. It is important to mention that although deformations occurred due to fixturing are large, the stresses show elastic behaviour, and the clip reverses to initial shape after unloading.

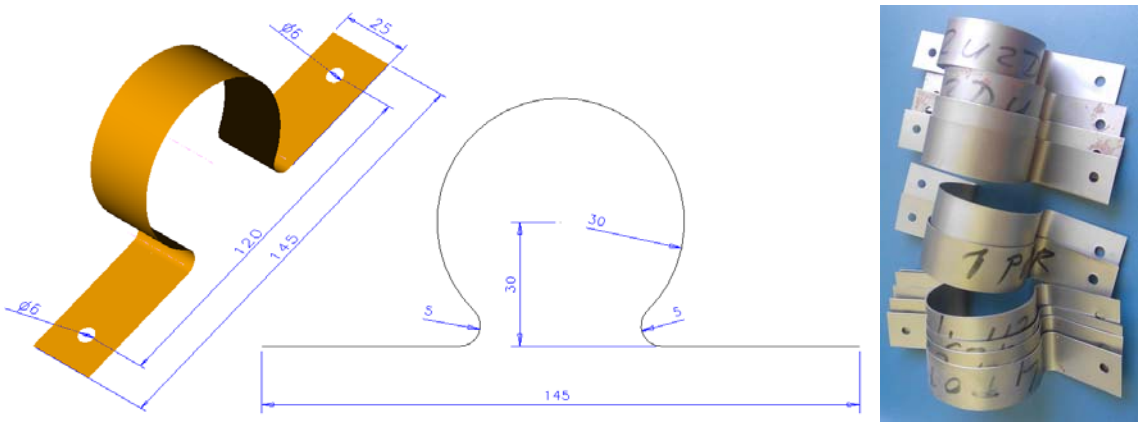

Fig. 5.8. The saddle bracket used for simplified 2D analysis (thickness d = 0,5 mm)

In order to obtain the contour for 2D analysis, each sample was scanned twice, with and without clamping. The samples were clamped to a rigid plate with two bolts, as shown in Fig. 5.9. Both fixed and free samples were positioned under an arbitrary angle with respect to the scanner, in order to avoid obscured regions and to obtain the final scan with as little steps as possible.

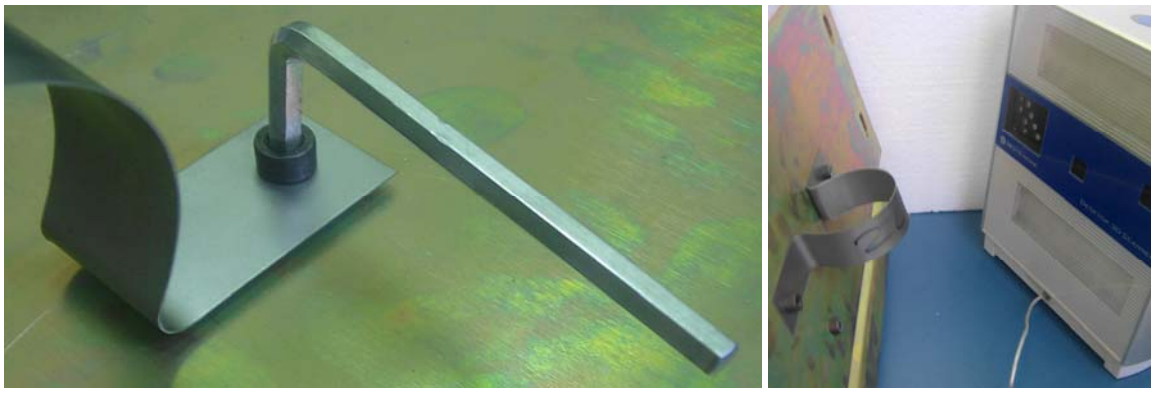

Fig. 5.9. The samples were clamped to a rigid plate with two bolts

The scanning procedure for 2D contour extraction consists of the following steps:

- scanned object preparation (anti-reflection spraying) and positioning,
- set of scans taken at different positions (number of scans depends on object complexity),
- joining scans into single point cloud using reference points (Fig. 5.10),
- creating cross-sections with chosen reference planes (Fig. 5.11), and finally
- exporting scanned contours into appropriate format for further processing.

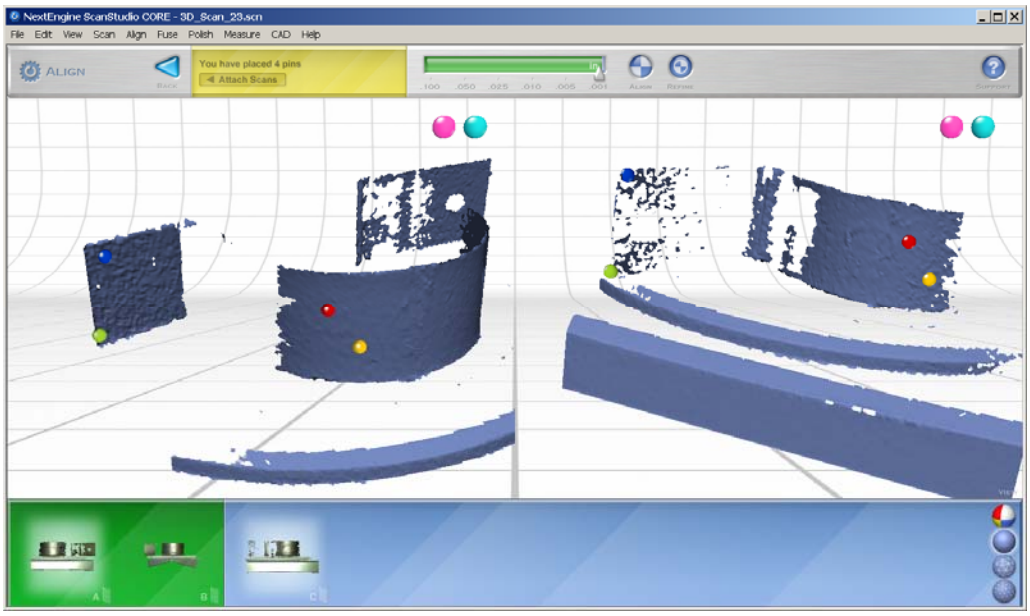

Fig. 5.10. Joining scans into single point cloud using virtual reference points

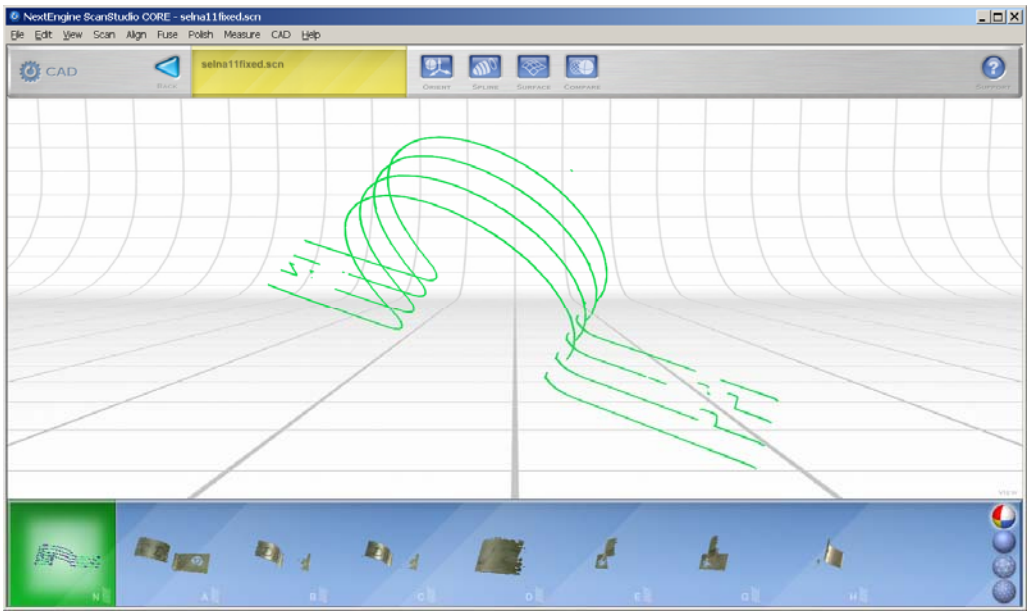

Fig. 5.11. Creating cross-sections with reference planes

For measuring, a set of four parallel laser stripes is projected onto the object surface which is recorded by two cameras. The software calculates the high-precision 3D coordinates which are recorded as point cloud. The partial views are joined together by placing virtual reference points in post processing software (Fig. 5.10). The software enables sectioning of 3D scan by means of reference planes aligned with chosen points (Fig. 5.11). These 2D contours are then exported into appropriate 3D CAD format (IGES in this case).

5.1. 3D file formats

It is common that each scanning software vendor uses its own proprietary data format for storing acquired 3D data. These formats limit user to the functionality of processing software. To be able to perform additional data processing, such as finite element analysis, standard data exchange formats were developed. Each format has its own limitations and advantages, therefore it is important to choose the format which will describe the scanned geometry accurately, preserving as much data as possible, simultaneously enabling desired functionality. The most widely used 3D formats are STL, IGES and STEP.

Surface Tessellation Language (STL) is a simple file format to specify triangle meshes. Every triangle is specified with three points and a unit normal. Each triangle must share two vertices with an adjacent triangle, i.e. two edges cannot coincide unless two vertices coincide. The order of the corners is specified, therefore the unit normal can be considered as redundant information. This file format has a strong position even though its lack of possibilities because of the massive support. Only one mesh can be stored in one STL file. The main problem with STL file is that file size is dependent upon the number of vertices. The STL files have many redundant features which make the file larger unnecessarily. The higher resolution parts with smooth curves require extremely large file sizes. Although this is the most common file format for 3D digitizers, it is very unsuitable for finite element analysis.

Initial Graphics Exchange Specification (IGES) is an independent file format that was initiated 1979 and became an approved ANSI standard Y14.26M in 1981. It enables exchange of object databases among CAD/CAM systems. IGES supports both surface and solid modelling, and NURBS was introduced in the specification in 1983. IGES v4.0 was released 1989 and introduced entities for solid modelling. The IGES 4.0 release also extended the format to describe nodal (e.g. temperature and displacement) and element (e.g. stress and strain) results from FEA methods. The IGES Version 5.3 (1996) is the last published specification, with Version 6.0 currently in the works. IGES is in wide use, especially for transferring 2D drawings. It also supports free-form surfaces, wireframes, annotations, and, most recently, solid models.

STandard for the Exchange of Product Data (STEP), is a collection of standards developed in 1984 that contains a file format for 3D data exchange. STEP can be grouped into five main categories: description methods, implementation and conformance methodology, common resources, abstract test suites, and application protocols. The file format implementation standard

is specified in ISO 10303-21 and is one of the implementation methods for STEP. STEP is divided into several Application Protocols, APs, where each one is subject for an ISO standardization. Each AP is divided into a set of conformance classes that works as subsets to provide a simpler interface for some applications. In addition to the 3D data, STEP also contain Product Data Management (PDM) and Product Life cycle Management (PLM) documents.

Although many CAD/CAE software vendors claim that their software is capable of importing various 3D data exchange formats, the real situation is different. For example, I-deas, NX, FeMAP, Solidworks can import STL triangle mesh and point clouds, but only for visualisation purposes; the 3D data is imported as collection of nodes and connecting lines, and these entities do not have any geometry usable for finite element meshing.

5.2. Converting scanned data into FEA models

In addition to multi-purpose CAD/CAE software packages which have some form of import/export functionality, a variety of specialised software packages was developed for creation of CAD surface out of scanned 3D data.. Unfortunately, most of them are limited or optimised for creation of 3D solid models. Obtaining 3D surface models usable for creation of finite element meshes based on thin-shell elements is not a trivial task, and it requires time-consuming mesh refinement, which introduces deviations from scanned data.

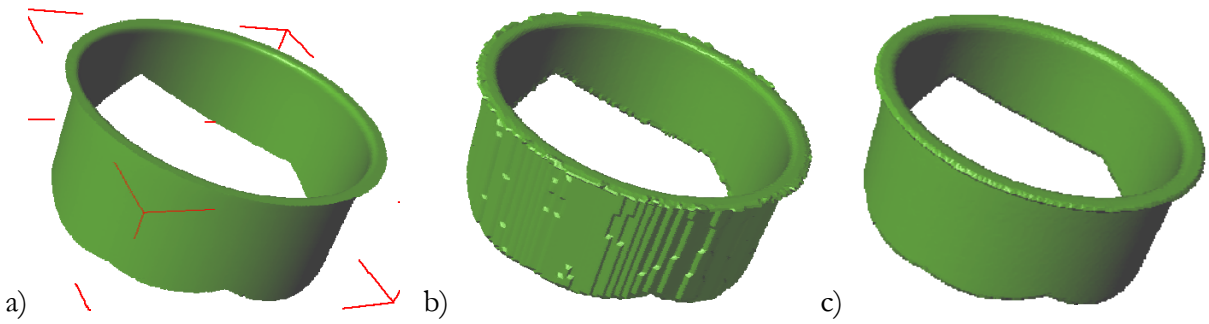

Fig. 5.12. Scanned STL model (a) processed with software ScanCAD (www.simpleware.com) using (b) accurate and (c) robust method

Fig. 5.12 shows an example of software created for the purpose of transforming scanned data set into an usable FEA mesh. The software package, consisting of 3 modules: ScanCAD, ScanIP, ScanFE, is developed mainly for 3D data obtained from medical CT and MRI scans. Although it can use STL data from 3D scanner, the mesh is limited to be solid, and no thin-shell elements are applicable. The software is based on voxelisation, followed by mesh refinement. The mesh obtained is readable by majority of FEA packages: Abaqus, I-deas, Catia, Pro/E, SolidWorks.

Fig. 5.13 shows digitised oil filter housing, converted into FEM model consisting of tetrahedral elements by means of ScanFE software. The mesh accuracy is low, compared with deformation determined by 3D scanning of clamped filter housings.

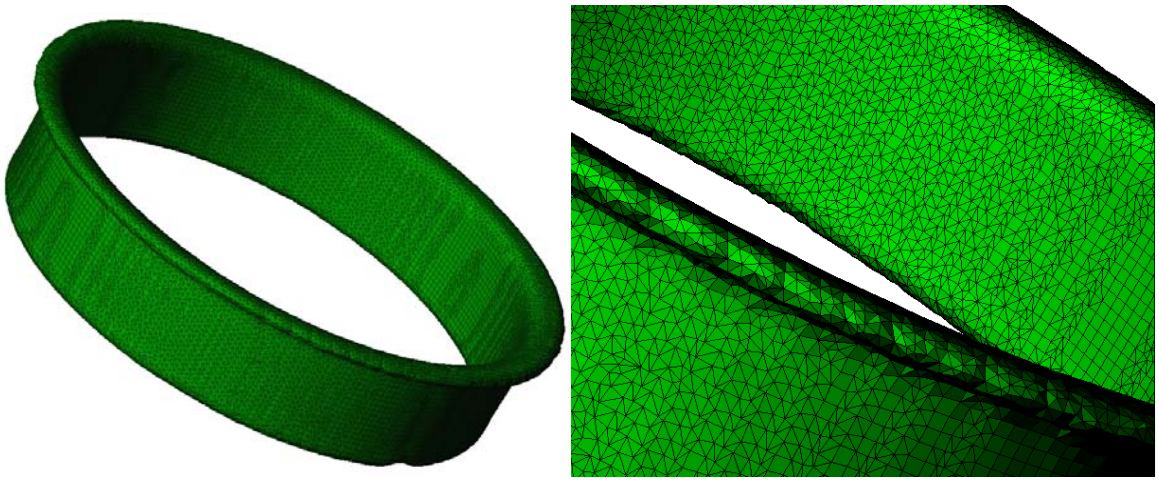

Fig. 5.13. Tetrahedral mesh obtained with of ScanFE software

Another commercial software for pre-processing scanned files towards CAE applications available is 3-matic CAE. It also offers basic CAD-operations (round, hollow, wrapping, offset, move surface, cut) and analyses tools. Via different manual and automatic remesh operations, that control the quality and size of the part's triangulation, the surface mesh is optimized and can be directly exported to Fluent, Ansys, Abaqus, Patran or Nastran file format. Fig. 22 shows an example of scanned surface processed with 3-matic CAE. The quality of automatically generated mesh is low, according to usual quality indicators: element skew, warp, distortion, aspect ratio, stretch (Fig. 5.14), and it requires exhaustive remeshing, which introduces further deviations from originally scanned data.

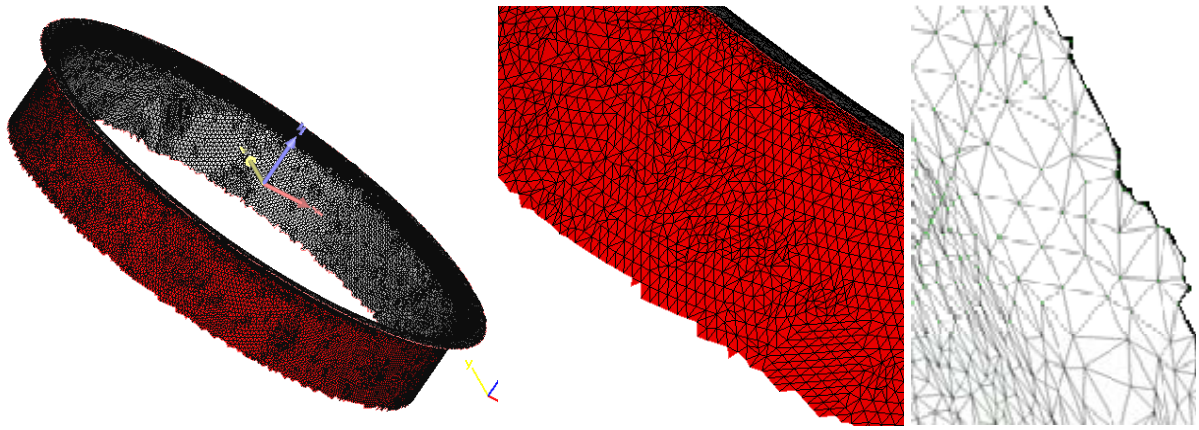

Fig. 5.14. Thin-shell mesh prepared with 3-matic CAE software (www.materialise.com)

Basically, the conversion process of 3D scanned data into usable FEA model consists of the following phases:

- Importing scanned data (usually represented as mesh of points, surface normals and triangles in STL format)
- Fixing erroneous data (self-intersecting triangles, misoriented normals, etc)
- CAD-like manipulation (transformations, scaling, trimming, hole-filling, edge detection)
- Creating interpolated NURBS surfaces from point clouds
- Extracting features (holes, centerpoints, edges, reference points, planes and cylinders)
- Exporting surfaces and features into CAE software readable format (e.g. IGES)
- Importing surfaces and features into CAE software
- Defining material and finite element properties
- Meshing
- Mesh quality control and optional mesh refinement

Having so many data conversion steps, it is reasonable to expect errors which should be quantified and compared with FEA accuracy.

5.3. Estimation of errors induced by data conversion

In order to estimate data conversion errors, a set of scanned data was first transformed from STL file into IGES surface, meshed and then exported back into STL format. These data sets were then compared by means of equivalent diameter determined as shown in Fig. 5.15. The same procedure was performed for 5 different data sets.

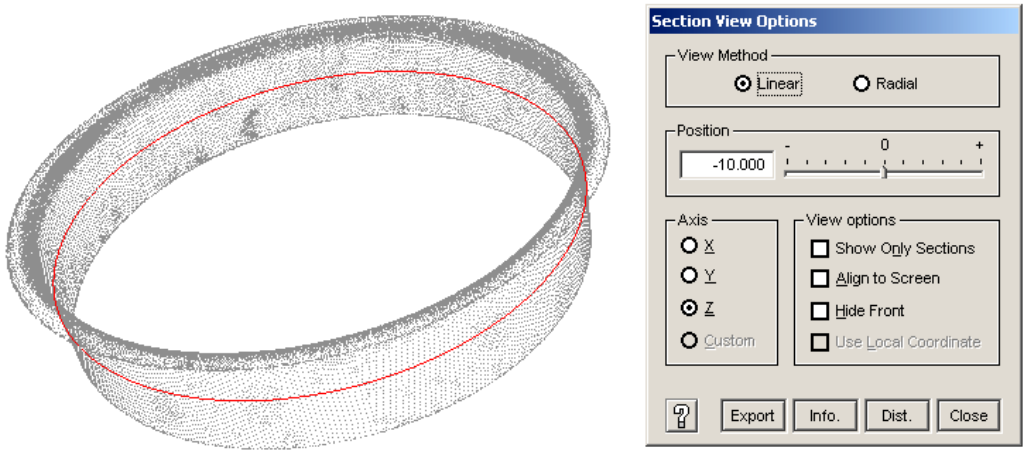

Fig. 5.15. Cross-section used for determination of equivalent diameter

Table 5.2. Equivalent diameters (mm) in different data conversion phases

Sample No.	Scanned STL	Imported to 3-matic, exported to STL	Imported to Femap, exported to STL	Converted to NURBS, exported to Iges, exported to STL	Conversion error STL/NURBS
1	92,07512	92,07512	92,07512	92,09323	-0,018
2	92,12553	92,12553	92,12553	92,13927	-0,014
3	92,12927	92,12927	92,12927	92,12240	0,007
4	92,20939	92,20939	92,20939	92,20488	0,005
5	92,04995	92,04995	92,04995	92,04330	0,007
Average	92,11785	92,11785	92,11785	92,12061	-0,003
St. dev.	0,061247	0,061248	0,061247	0,059537	0,012

Table 5.2 shows that conversion from scanned 3D data from STL format into other formats does not induce any noticeable error. Standard deviation is 0,061 for all conversions, therefore differences between samples have no influence to error. The only error arises from conversion between 3D tessellated data (result of 3D scanning) into NURBS surface. The deviation is between -0,018 and +0,007 mm, far below prescribed tolerances (0,2 mm). However, these results will be used in measurement uncertainty analysis.

Another error that is likely to occur during STL-NURBS conversion is failure to extract NURBS at particular parts of scanned STL mesh, as shown in Figs. 5.16 and 5.17.

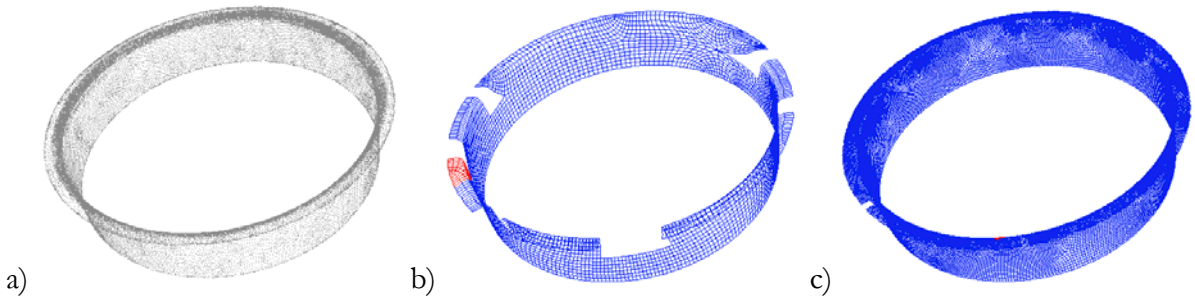

a) b) c)

Fig. 5.16. STL-NURBS conversion: (a) Starting point cloud; (b) Surface model approximated with 100 NURBS; (c) Surface model approximated with 500 NURBS

Fig. 5.16 shows that number of NURBS surfaces generated from tessellated point cloud should be relatively high, if higher fitting accuracy is required. Even for simple geometry, as in example shown, it is common to have hundreds of NURBS surfaces. In that case, data processing is time-consuming and requires higher computing power.

If number of NURBS surfaces is too low, while keeping high demand for fitting accuracy, some areas will not be converted, as shown in Fig. 5.16.b. In that case, the number of surfaces should be increased, or these gaps should be manually meshed (Fig. 5.17). This method is likely to

introduce further deviations from original data, and even surface which is unusable for FEA meshing.

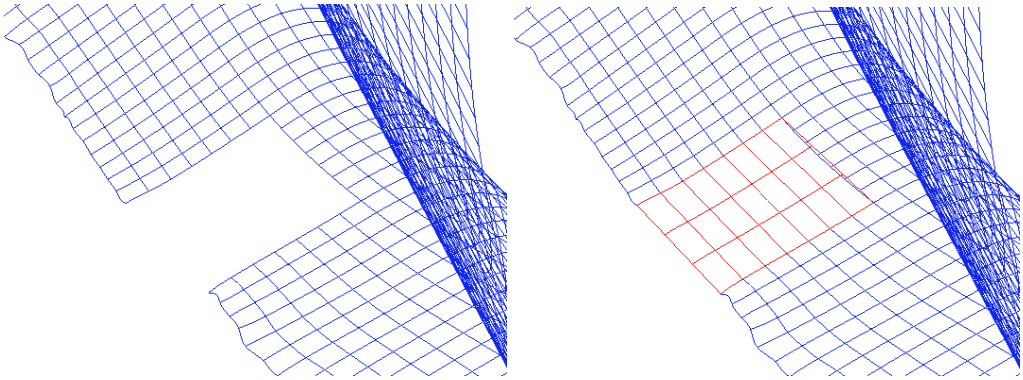

Fig. 5.17. Example of manual meshing after erroneous STL-NURBS conversion

Errors shown in Figs. 5.16 and 5.17 can not be quantized. If these errors occur, the model can not be used for FEA meshing, or special process of model "healing" should be applied within FEA software. Such a method fills the narrow gaps, stitches adjacent edges and smoothens sharp transitions. Another issue to be considered is unwanted smoothing of sharp edges that should remain sharp. Due to all these facts, the data conversion process requires exhaustive user interaction.

6. Deformation analysis

The deformation analysis will be performed for simplified 2D contour derived from saddle bracket samples, and for 3D models of filter housings.

The dimensions used for 2D analysis include horizontal, vertical and rotational components of total deformation of the contour endpoint.

For 3D analysis, the 3D model of oil filter housing is used. Since toleranced dimension of the filter housing, according to technical documentation (Fig. 4.2) is measured 10 mm from the top of filter housing, this cross-section will be analysed in details. The cross-section is nominally circular, the deformations are relatively small, and the analysis will be based on the theory of elasticity of cylindrical shells. The results of 3D scanning will be used to determine the real dimensions and shape of filter housing. The initial dimensions will be derived from unclamped shape, and clamped shape will be used to choose boundary conditions for stress analysis.

6.1. 2D contour deformation analysis

In order to determine stress state of clamped saddle brackets, 2D contours were extracted from scanned data for each sample in free (unclamped) and in clamped state. Fig. 6.1 shows an example of contours used for analysis. The contour (a) in Fig. 6.1 is obtained from 3D scan of a free sample, the contour (b) is obtained from 3D scan of clamped sample, and contour (c) represents an ideal shape. Since samples are manufactured manually, it is normal that clamped shape deviates from ideal shape. Therefore, deformation for further analysis and validation of numerical simulations will be taken from deviations between the free and the clamped sample, as opposed to common practice, when an ideal shape is used to define boundary conditions.

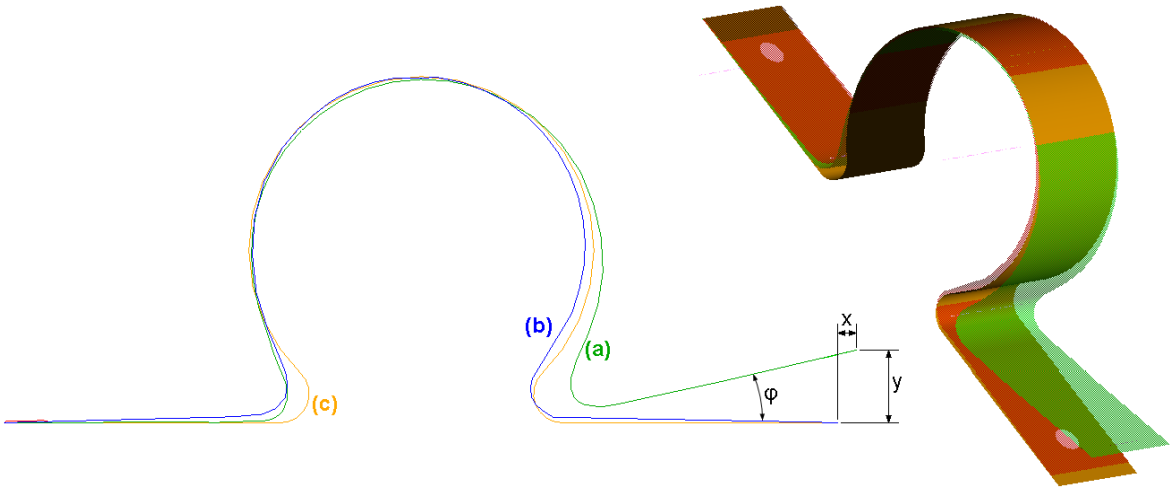

Fig. 6.1. Contours used for 2D analysis: (a) free - unclamped, (b) clamped, (c) ideal contour

Table 6.1 summarizes endpoint deformations and deviations between the free and the clamped contours, which will be used to define boundary conditions for numerical simulations to follow.

Table 6.1. Endpoint deformations between clamped and free contours

Roll No.	Sample No.	Horizontal x (mm)	Vertical y (mm)	Rotational φ (°)
1	1	6,482	12,552	4,104
	2	6,444	12,610	4,108
	3	6,421	12,541	4,095
	4	6,417	12,578	4,096
	5	6,407	12,549	4,098
2	1	6,410	12,531	4,086
	2	6,505	12,542	4,089
	3	6,425	12,542	4,087
	4	6,408	12,532	4,092
	5	6,410	12,530	4,105
3	1	6,408	12,548	4,086
	2	6,490	12,586	4,087
	3	6,499	12,526	4,120
	4	6,460	12,530	4,086
	5	6,440	12,565	4,087
4	1	6,429	12,565	4,095
	2	6,480	12,608	4,090
	3	6,419	12,536	4,090
	4	6,499	12,554	4,088
	5	6,478	12,583	4,104
5	1	6,446	12,634	4,088
	2	6,504	12,605	4,087
	3	6,423	12,541	4,090
	4	6,414	12,532	4,087
	5	6,452	12,599	4,086

The deviations presented in Table 6 were obtained in CAD software I-deas, using the following procedure:

- Importing each scanned contour from IGES files (free and clamped),
- Creating a reference plane that corresponds to imported data,
- Constructing the spline on reference plane, through imported points (Fig. 6.2),
- Extruding the contour to have CAD geometry that can be measured,
- Aligning CAD geometry with respect to each other and to reference plane,
- Dimensioning the endpoints of clamped and unclamped contour (Fig. 6.3).

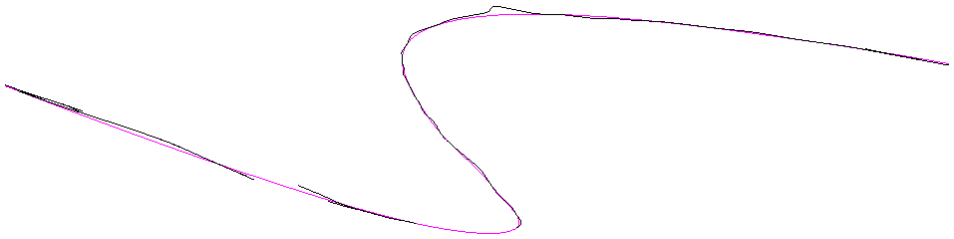

Fig. 6.2. Constructing the spline through imported points from 3D scanned contour

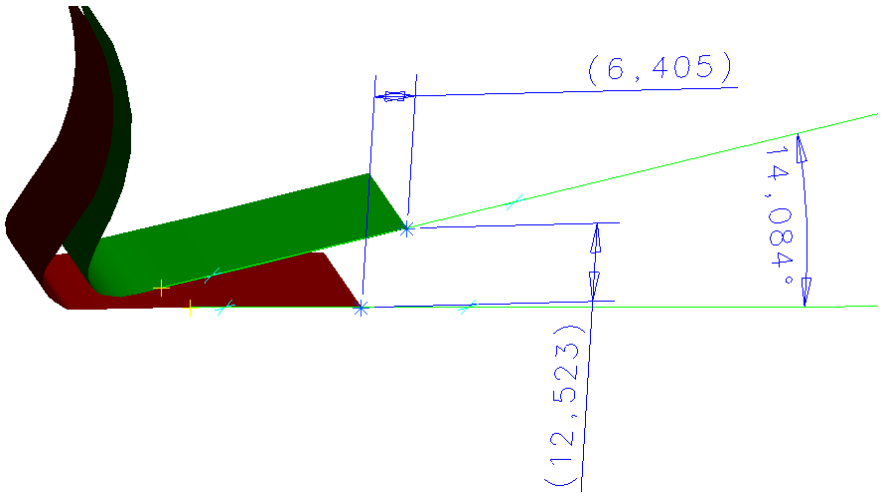

Fig. 6.3. Example of measuring deviations between unclamped and clamped contour

The example shown in Fig. 6.3 illustrates that clamped contour is not necessarily horizontal (there is a slight deviation between ideal horizontal plane and the best-fit plane that corresponds to clamped contour). However, the rotation is measured between two contours obtained from

3D scans, and such an angle represents the real rotation more accurately than the angle between the unclamped contour and the horizontal axis.

6.2. Circular cross-section perimeters

In order to determine stress state of clamped filter housing, cross-section perimeter (Fig. 6.4) is determined from scanned data for each sample in unclamped (P_0) and clamped (P) state.

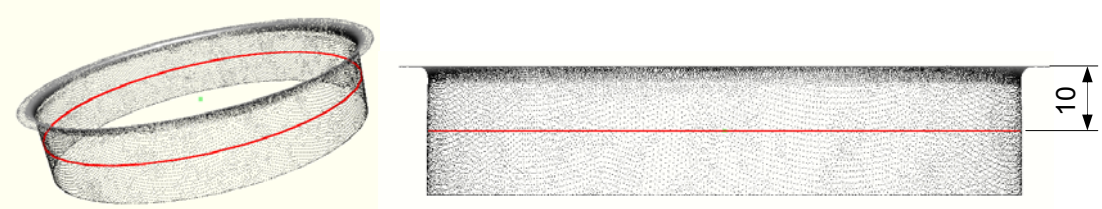

Fig. 6.4. Cross-section used for 3D analysis

Stress state in thin-walled cylindrical object is equivalent to stress state of a thin plate. According to Hooke's law, the uniaxial stress is proportional to strain:

$$\sigma = E \cdot \frac{l - l_0}{l_0} \quad \text{..... (6.1)}$$

where E is Young's modulus, l_0 is initial length and l is current length.

The principal stress in cylindrical objects is the hoop or circumferential stress. When cylinder radius is changed from r_0 to r, the hoop stress equals tension of rectangular plate whose length is changed from $P_0=r_0 \cdot 2\pi$ to $P=r \cdot 2\pi$ (Fig. 6.5).

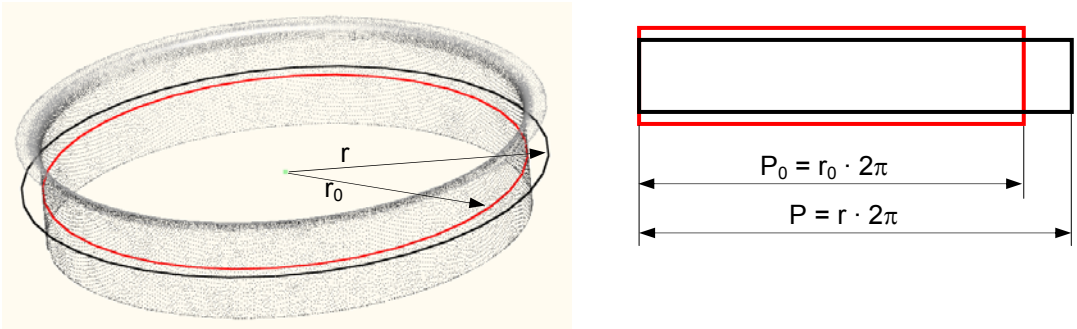

Fig. 6.5. Relation between deformation of a cylinder and a plate

Cross-sections derived from scanned data are almost cylindrical, and they were used to determine perimeters and equivalent stresses in 25 samples of filter housings. Results of calculated hoop stresses are shown in Table 6.2.

Table 6.2. Equivalent hoop stresses in chosen cross-section (E=210000 N/mm^2)

Roll No.	Sample No.	Unclamped perimeter P_0 (mm)	Clamped perimeter P (mm)	Change in perimeter $P-P_0$ (mm)	Strain $100(P-P_0)/P_0$ (%)	Hoop stress (N/mm^2)
1	1	289,165	288,968	-0,197	-0,07	-142,98
	2	289,203	289,003	-0,200	-0,07	-145,18
	3	289,253	289,165	-0,088	-0,03	-63,86
	4	289,473	289,272	-0,201	-0,07	-145,86
	5	289,077	289,037	-0,040	-0,01	-28,91
	Average	289,234	289,089	-0,145	-0,05	-105,357
	St.dev.	0,148	0,127	0,076	0,028	55,245
2	1	289,129	288,876	-0,254	-0,09	-184,20
	2	289,496	289,240	-0,256	-0,09	-185,47
	3	289,290	289,177	-0,113	-0,04	-82,10
	4	289,053	288,964	-0,090	-0,03	-65,05
	5	289,071	288,838	-0,232	-0,08	-168,89
	Average	289,208	289,019	-0,189	-0,07	-137,14
	St.dev.	0,186	0,180	0,081	0,029	58,70
3	1	289,158	288,978	-0,180	-0,06	-130,81
	2	289,323	289,073	-0,251	-0,09	-182,09
	3	289,125	288,993	-0,132	-0,05	-95,84
	4	289,234	289,152	-0,082	-0,03	-59,31
	5	289,420	289,360	-0,061	-0,02	-44,07
	Average	289,252	289,111	- 0,141	-0,06	-102,42
	St.dev.	0,121	0,156	0,077	0,027	55,81
4	1	289,207	288,951	-0,256	-0,09	-185,54
	2	288,999	288,765	-0,234	-0,08	-169,90
	3	289,306	289,066	-0,240	-0,08	-174,28
	4	289,063	288,817	-0,246	-0,08	-178,40
	5	289,039	288,788	-0,251	-0,09	-182,38
	Average	289,123	288,877	-0,245	-0,08	-178,10
	St.dev.	0,129	0,128	0,0087	0,0055	6,24
5	1	289,169	289,047	-0,121	-0,04	-88,09
	2	289,296	289,039	-0,257	-0,09	-186,65
	3	289,542	289,284	-0,258	-0,09	-186,84
	4	289,141	288,918	-0,223	-0,08	-162,25
	5	289,301	289,146	-0,155	-0,05	-112,50
	Average	289,290	289,087	- 0,203	-0,07	-147,27
	St.dev.	0,159	0,137	0,062	0,023	44,87
Total Average		289,221	289,037	-0,185	-0,07	-134,058
Stand. deviation		0,149	0,160	0,072	0,026	52,60

Table 6.2 shows that equivalent hoop stresses calculated over the change in perimeter after clamping process vary significantly. All samples are in compression, because equivalent radii were all reduced by clamping. When these results are analysed per groups of samples, averaged for each roll of material used, it is obvious that dispersion of results is larger within one set of samples (samples made from one roll) than between averaged values from 5 different rolls. Since deviations are very large, it is reasonable to compare these results with other parameters which can be derived from scanned data.

6.3. Deviations between unclamped, clamped and nominal CAD part

To relate 3D scanned data with influence parameters, it is justifiable to extract various parameters showing deviation between unclamped part, clamped part and nominal CAD model. Some analyses can be performed within 3D scanning software, as shown in Fig. 6.6, and other analyses require further calculations.

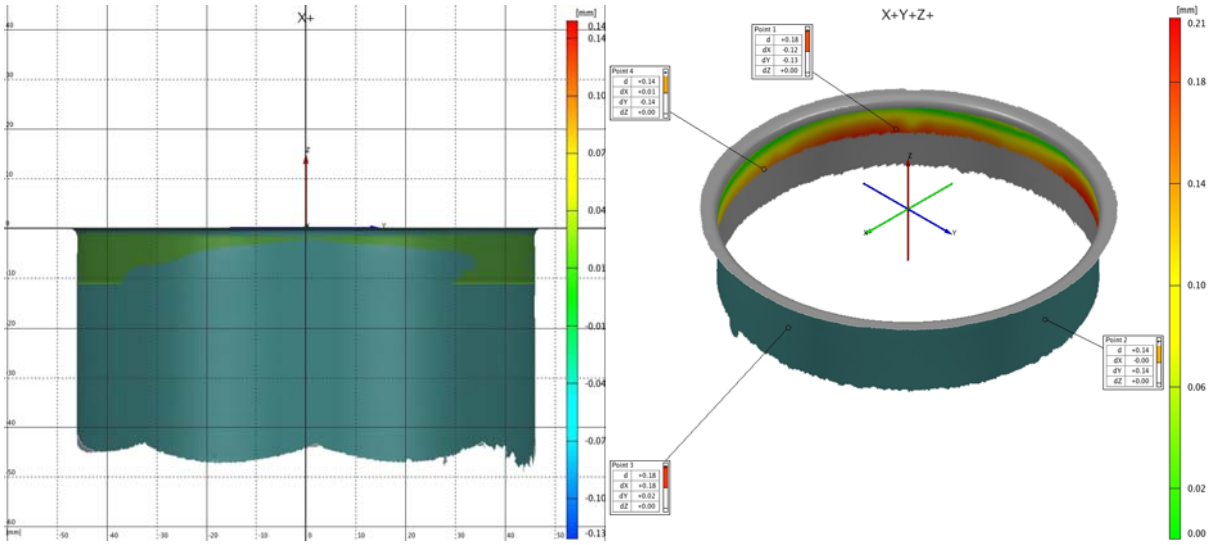

Fig. 6.6. Deviation between unclamped part and nominal CAD data can be calculated and visualised within GOM 3D scanning software

To visualise deviations from nominal cylindrical shape, the cross-section is presented in Cartesian coordinate system, with abscissa showing angles, and ordinate describing radii (Fig. 6.7).

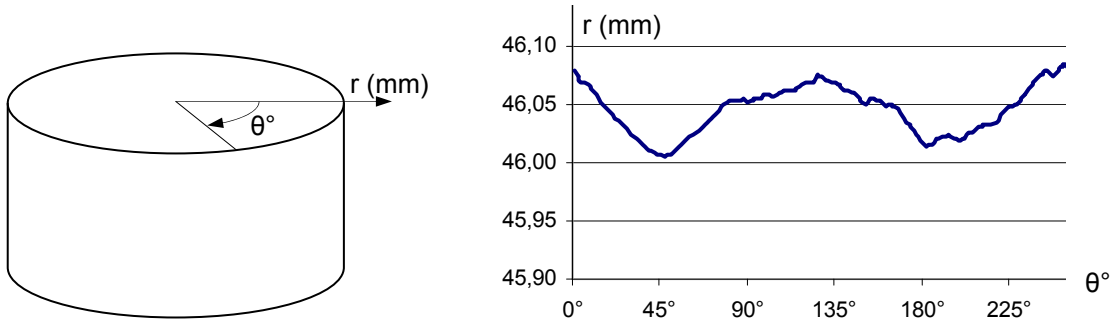

Fig. 6.7. Cartesian coordinate system used to visualise radius deviations

Table 6.3 summarizes radii measured from cross-sections derived from 3D scans. Results show both unclamped and clamped filter housings. Nominal radius for this cross-section is 46,0 mm.

Table 6.3. Radii derived from cross-section of 3D scanned data

Roll No.	Sample No.	Unclamped			Clamped		
		Avg. radius (mm)	Max. radius (mm)	Min. radius (mm)	Avg. radius (mm)	Max. radius (mm)	Min. radius (mm)
1	1	46,022	46,100	45,988	45,991	46,053	45,956
	2	46,028	46,128	46,018	45,996	46,046	45,967
	3	46,036	46,161	45,978	46,022	46,091	45,992
	4	46,071	46,522	45,646	46,039	46,086	46,017
	5	46,008	46,108	45,972	46,002	46,063	45,967
2	1	46,016	46,106	46,012	45,976	46,008	45,960
	2	46,075	46,151	46,062	46,034	46,083	46,014
	3	46,042	46,143	46,014	46,024	46,085	45,992
	4	46,004	46,198	45,873	45,990	46,055	45,962
	5	46,007	46,150	45,982	45,970	46,041	45,934
3	1	46,021	46,145	45,982	45,992	46,079	45,947
	2	46,047	46,176	46,006	46,007	46,069	45,968
	3	46,016	46,117	45,979	45,995	46,078	45,964
	4	46,033	46,138	46,003	46,020	46,007	45,921
	5	46,063	46,164	46,030	46,053	46,103	46,027
4	1	46,029	46,112	46,016	45,988	46,041	45,950
	2	45,996	46,111	46,025	45,958	46,056	45,903
	3	46,045	46,145	46,046	46,006	46,151	45,951
	4	46,006	46,106	46,017	45,967	46,044	45,924
	5	46,002	46,111	46,000	45,962	46,046	45,926
5	1	46,023	46,058	45,979	46,003	46,056	45,974
	2	46,043	46,128	46,033	46,002	46,058	45,980
	3	46,082	46,208	46,104	46,041	46,066	45,991
	4	46,018	46,108	46,024	45,983	46,032	45,954
	5	46,044	46,118	46,018	46,019	46,074	45,997

Fig. 6.8. shows an example of cross-section presented in Cartesian coordinate system. Cross-sections from all 25 samples are given in Annex A.

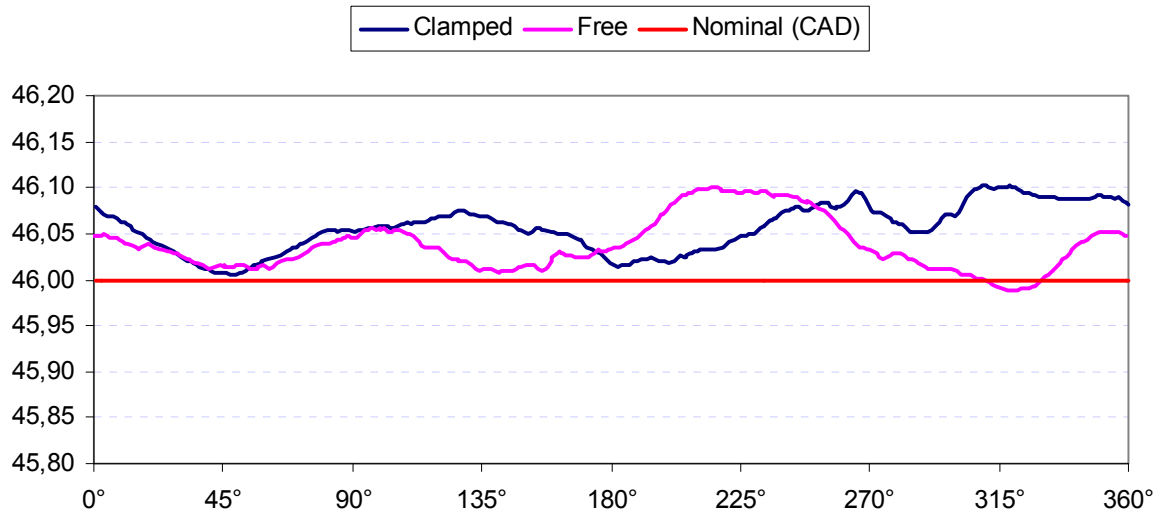

Fig. 6.8. Cross-section radii of unclamped (free) and clamped part

In surface metrology, it is common to describe such profiles with waviness (long wavelength shapes) and roughness (short wavelength features). In this case, the roughness origins from real roughness of scanned part and from scanning errors (dirty surface, consequent calculations, approximate surface representation by triangulation, data format conversions, etc.). On the contrary, the major cause of waviness in this case could be buckling.

After 3D scanning, it is important to orient the scanned part with respect to chosen coordinate system. To relate profiles from clamped and unclamped part (Fig. 6.8), it is important to orient them in terms of angle. Fig. 6.9 shows an example of profile fitting by means of rotation.

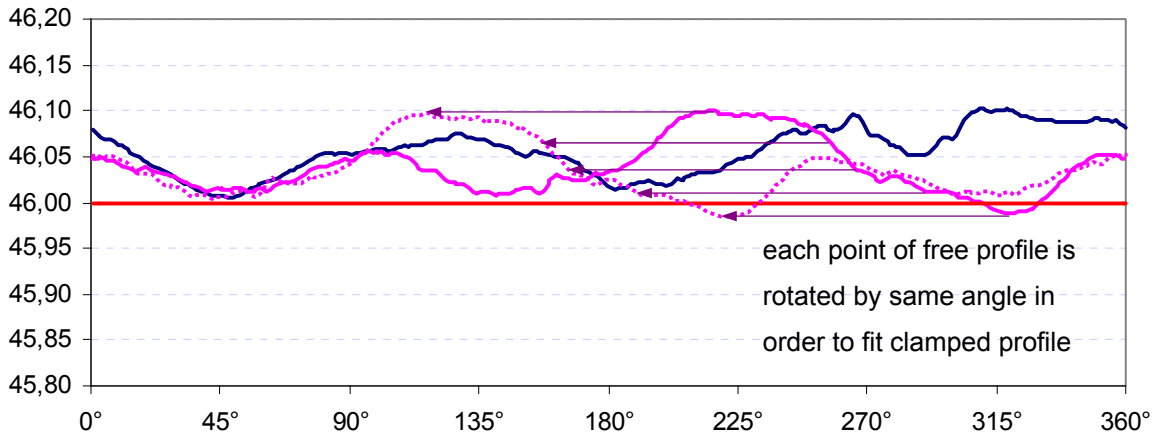

Fig. 6.9. Rotational profile fitting

The two most commonly used error metrics are the L_∞ and L_2 norms [85]. The L_∞ norm, which measures the maximum deviation between the original *g(t)* and the approximation *f(t)* on a given interval [a,b] is defined by

$$\|f-g\|_\infty = \max_{a\le t\le b} |f(t)-g(t)| \quad \text{..... (6.2)}$$

A measure of the average deviation between the two functions *f(t)* and *g(t)* on a given interval [a,b], known as the L_2 norm is defined by

$$\|f-g\|_2 = \sqrt{\int_a^b (f(t)-g(t))^2\,dt} \quad \text{..... (6.3)}$$

The L_∞ norm provides absolute distance bounds, but it can be overly sensitive to any noise that might be present in the original model. In contrast, the L_2 norm better reflects overall fit, but may discount large, but highly localized, deviations. When expression (6.3) is divided by interval

length (b-a), it is called the "root mean square" or RMS error. To determine RMS error between clamped and unclamped scanned data, the models should be oriented properly (Fig. 6.9), and equation (6.3) needs to be adjusted for discrete data sets instead of continual functions.

$$RMS = \frac{1}{2\pi\bar{r}}\sqrt{\sum_{i=0}^{n}\left(r_C - r_U\right)^2} \quad \text{..... (6.4)}$$

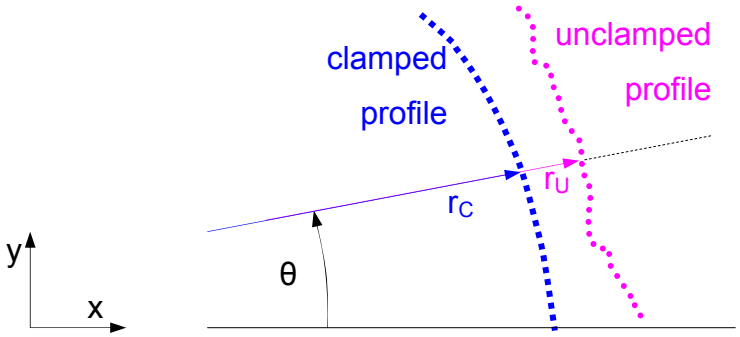

Fig. 6.10. Vectors used to calculate RMS error between clamped and unclamped profiles

Another issue to deal with is the fact that both radii (r_U and r_C) needs to be interpolated, since they are derived from unrelated scanned points, i.e. they do not have common angle θ (Fig. 6.11).

Interpolation and fitting is also useful for FEM analysis, since unrelated points or surfaces cannot be used to define boundary conditions. When interpolation/fitting is performed, pairs of correlated points can be used to define displacement restraints for FEM analysis.

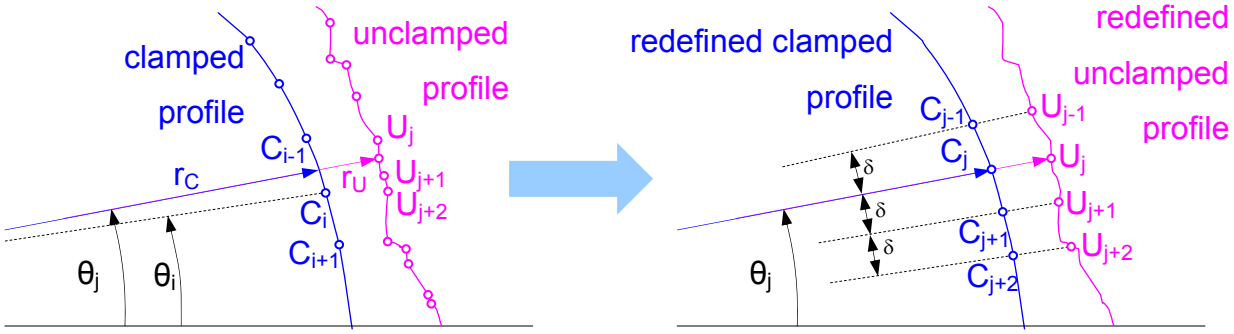

Fig. 6.11. Interpolation of vectors defining clamped and unclamped profiles

As shown in Fig. 6.11, unclamped profile is defined by points U_j, U_{j+1}, U_{j+2},... and each point has its angle θ_j, θ_{j+1}, θ_{j+2},... On the contrary, points defining clamped profile (C_{i-1}, C_i, C_{i+1},...) have their own angles (θ_{i-1}, θ_i, θ_{1+1},...), and these angles are not related to each other. For rotational profile fitting (Fig. 6.9), both point sets should be interpolated to obtain new points, with angles distributed with constant step δ.

In this example, each profile is defined with 300 to 400 points. The computer program was developed to calculate interpolated points, to perform rotational profile fitting and to calculate RMS deviation between profiles. The program algorithm is presented in Fig. 6.12.

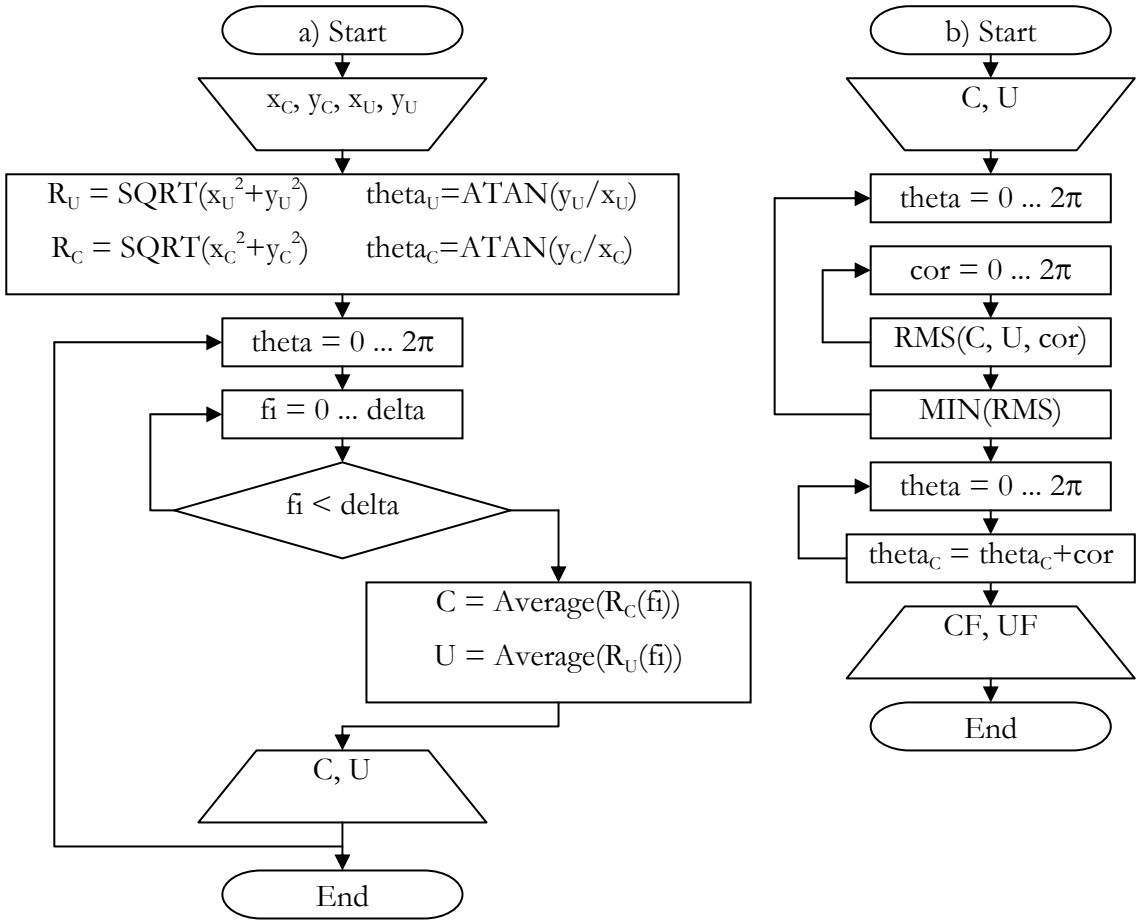

Fig. 6.12. Program for RMS-based profile fitting: (a) Interpolation; (b) Fitting

The program takes Cartesian coordinates from scanned data, and then calculates radii and angles from both clamped (R_C, $theta_C$) and unclamped (R_U, $theta_U$) data set. Angles derived from unclamped profile ($theta_U$) are used for interpolation of clamped points. Both profiles are divided to arcs and average radii C and U are calculated for each value of angle $theta_C$. These data is forwarded to fitting subroutine, which calculates RMS value for a set of correction angles (cor) between 0 and 2π. When minimum RMS is obtained, this angle is used for rotational fitting in such a way that each angle of clamped profile is increased by calculated value "cor".

Fig. 6.13 shows an example of rotational fitting. When profiles are extracted from scanned cross-section in arbitrarily position, RMS between these profiles is 0,00158. After interpolation and fitting, it is calculated that when unclamped profile is rotated by 255°, RMS reduces to its

minimum value: 0,00122. Therefore, unclamped profile (a) needs to be rotated by 255°, as seen in Fig. 6.13.b.

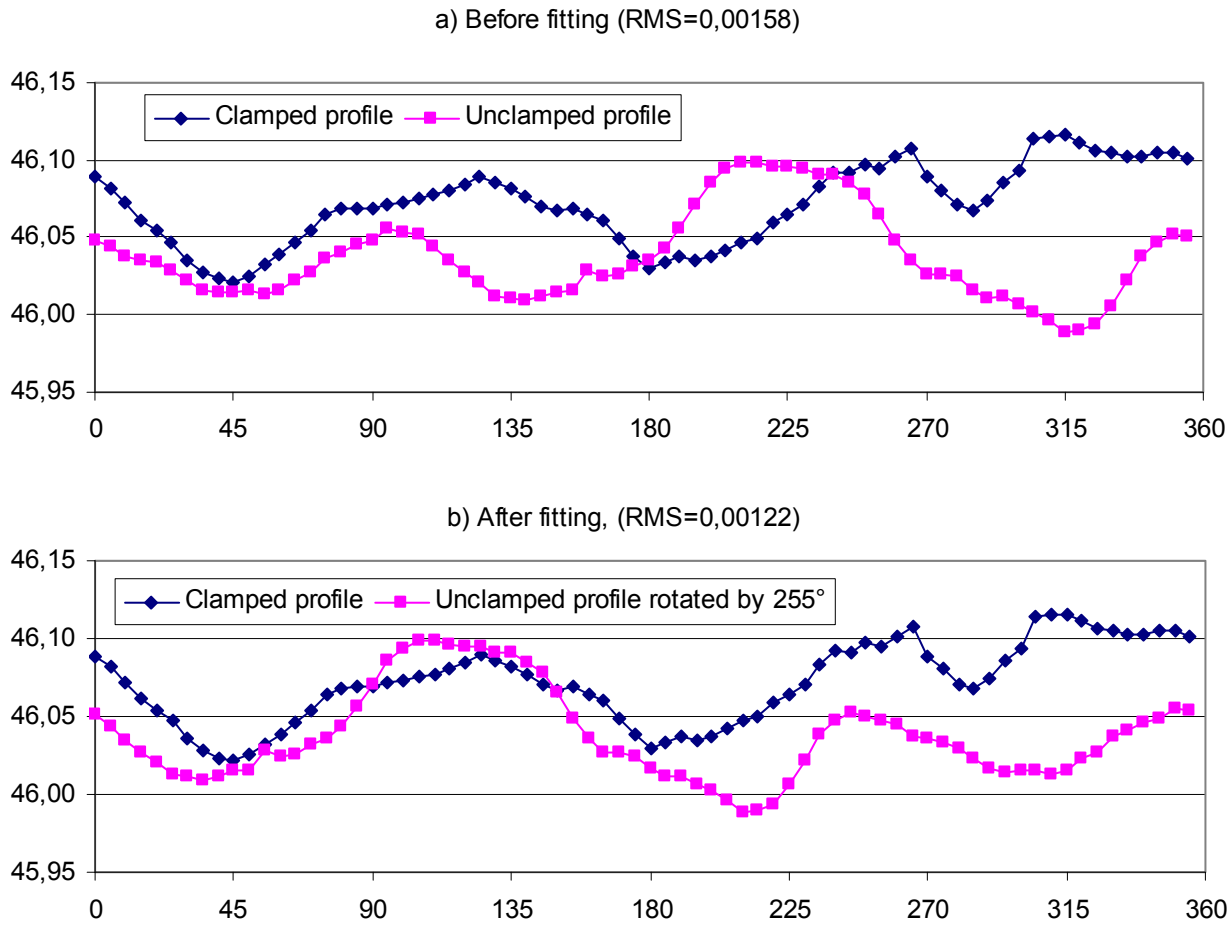

Fig. 6.13. Example of rotational fitting based on RMS

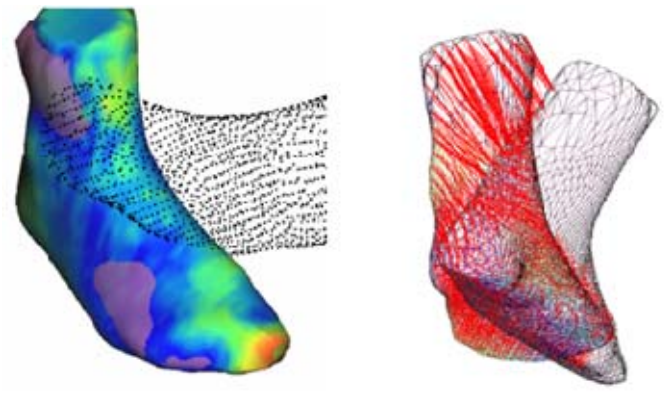

Fig. 6.14. Mapping aligned surface and force vectors [84]

Kos and Duhovnik in [84] used similar technique, the Iterative Closest Point method, to map scanned surface to CAD data. Fig. 6.14 shows an example of 3D fitting procedure used to align

scanned point cloud to CAD data. The purpose of the method used in [84] is to find rotation and translation, which minimises positional error from points on the one surface to the nearest points on the matching surface, by minimising the chosen mean-squares objective function.

Another commonly used geometric error measure is the Hausdorff distance. It is being used in pattern recognition, image matching and 3D surface fitting, especially in approximation of point clouds with CAD surfaces [85, 86]. Hausdorff distance is the "maximum distance of a set to the nearest point in the other set" [87]. Given two point sets A and B, and a parameter k, $1 \leq k \leq |A|$, the directed partial Hausdorff distance from A to B is defined as [88]:

$$H_k(A,B) = K^{th}_{a \in A} \min_{b \in B} dist(a,b) \quad \text{..... (6.5)}$$

where K^{th} returns the k^{th} smallest element of the set, and where dist(a,b) is the Euclidean distance from a to b. An example of practical use of Hausdorff distance is shown in Fig. 6.15, where small image of a airplane is recognised by calculating minimum Hausdorff distance between the contours [89].

Fig. 6.15. Finding best match between two images by minimizing Hausdorff distance [89]

"VCG Metro" is freeware, command-line software designed to evaluate the difference between two triangular meshes by computing the Hausdorff distance between the two surfaces [90]. "VCG Metro" adopts an approximated approach based on surface sampling and point-to-surface distance computation. The setback of this software is limited number of file formats it can read. Although the software is claimed to be able to read STL, GeomView's OFF and PLY 3D file formats, the original STL files obtained by 3D scanning were not readable.

Scanned datasets were exported into PLY 3D format and Hausdorff distance was calculated for pairs of scanned data (clamped and unclamped filter housings) using "VCG Metro" software. The results are summarized in Table 6.4.

Table 6.4. Hausdorff distances between clamped and unclamped 3D scanned data

Roll No.	Sample No.	Hausdorff distance (mm)	Average Hausdorff distance (mm)	Standard deviation
1	1	0,145		
	2	0,171		
	3	0,935	0,477	0,328
	4	0,567		
	5	0,567		
2	1	0,139		
	2	0,177		
	3	0,133	0,179	0,045
	4	0,240		
	5	0,204		
3	1	0,693		
	2	0,337		
	3	0,607	0,377	0,265
	4	0,121		
	5	0,129		
4	1	0,142		
	2	0,296		
	3	0,287	0,380	0,292
	4	0,889		
	5	0,286		
5	1	0,518		
	2	0,191		
	3	0,212	0,274	0,139
	4	0,193		
	5	0,254		
		Total average	0,337	
		Total standard deviation	0,241	

Deviations between sets of data vary significantly (the deviations are almost as large as average distances), and no relation can be established between Hausdorff distance and equivalent stresses (sumxmarized in Table 6.2). Therefore, Hausdorff distance, although common method for geometric error measure, is not related to stress/strain state in deformed sheet metal objects.

7. 3D finite element analysis

The major objective of this research is to validate if numerical simulation can be used to compensate springback-caused deformation of thin-walled products when these products are digitised with 3D scanner. To perform this validation, the same product was scanned in both deformed (clamped) and undeformed (free) state. Clamping was then simulated by means of finite element method. Finite element analysis comprises of several steps, which are described in details in this chapter.

7.1. 2D contour FEM analysis

Due to complexity of the problem, the analysis was initially performed on 2D contour of a simple profile (Fig. 6.1), in order to clarify assumptions and conditions which are essential to obtain the accurate results for the further 3D analysis. The objective of this analysis was to compare the 2D contour of digitized clamped part, and the 2D contour obtained from FEM simulation.

The material properties, the scanning procedure and the geometrical properties were explained in details in Chapters 4.2, 5 and 6.1, respectively. The simulation software used for this analysis is UGS I-deas, Version 11 (Win32), installed on CAD workstation IBM Intellistation M Pro (Intel Core2 6700 CPU, 2.66 GHz, 3 GB RAM). This software was chosen due to its capabilities of exporting analysis results, higher user involvement in meshing and boundary conditions tasks, and low level of automation (contrary to NX, Catia or SolidWorks, which are more user-friendly, but lack customization capabilities of I-deas).

This analysis was performed as 3D geometric nonlinear (due to large displacements) simulation, using thin shell 2D finite elements applied to surface extruded from 2D contour, but taking into

account only two dimensions; the third dimension is used to define model stiffness and for alignment of different meshes (scanned clamped, scanned unclamped and CAD model).

7.1.1. Boundary conditions

The most important aspect in this simulation was to choose the appropriate boundary conditions. It was impossible to define boundary conditions that correspond 100% to the actual model, because the contact between the model and the fixed surface was realised across circular edges. It is not possible to determine pairs of corresponding points between the two positions (free and clamped) before the simulation, and simulation can not be defined without these pairs. Fig. 7.1 illustrates how wrong results arise from faulty boundary conditions. The translation was measured between points that coincide with centres of circular holes on the right side of the model. The angle of rotation was measured between the planes that correspond to the right side of the model in free and in clamped position. These values were applied to all points on the edge of the circular hole (Fig. 7.1.a). Although this concept seems correct at the first sight, the result shows significant discrepancy between simulation results and the real scanned shape (Fig. 7.1.b).

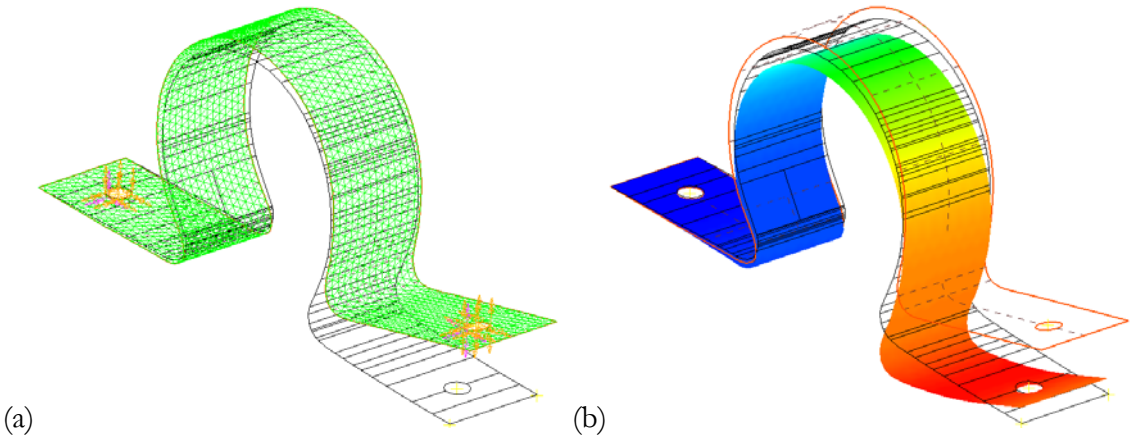

(a) (b)

Fig. 7.1. The erroneous simulation result due to wrong boundary conditions

In order to overcome this problem, the boundary conditions were set on edges (Fig. 7.2). The left edge was clamped, with no translations and no rotations allowed. The right edge was set as forced displacement, defined with two translations and one rotation (determined from measurement between the scanned part in free and clamped position). The model was meshed with parabolic quadrilateral elements, with 0.5 mm thickness as a physical property. The holes were neglected, because in final position (when model is clamped) they are filled with clamping bolts. The simulation results showed that this concept corresponds to the real shape with satisfactory deviation.

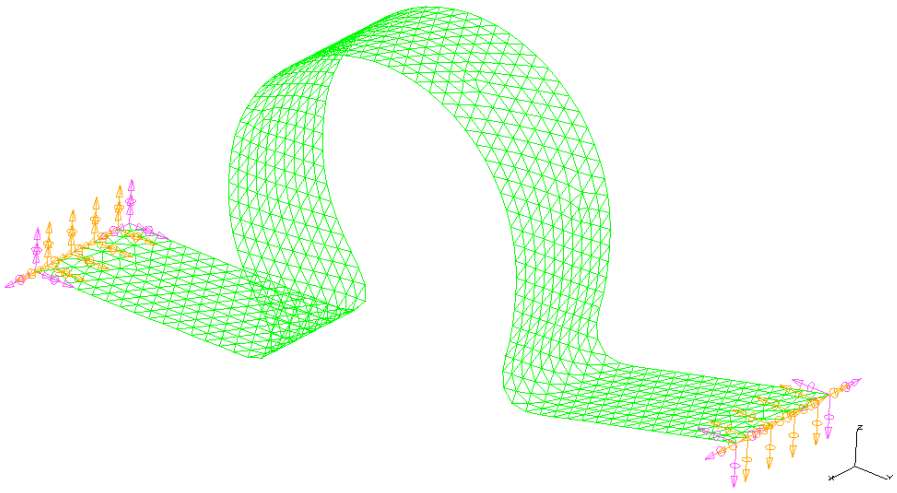

Fig. 7.2. Finite element mesh with boundary conditions

Another example of how important boundary conditions are, is shown in Fig. 7.3. If right edge is defined by two translations and one rotation, the simulation result corresponds very well to the physically clamped part (Fig. 7.3.a). When free rotation of the right edge is enabled, the contour is deformed slightly beyond horizontal plane (Fig. 7.3.b). In that case, it would be necessary to solve the contact problem, which burdens the simulation with more user interaction, a need to define contact surfaces, and much longer solution time.

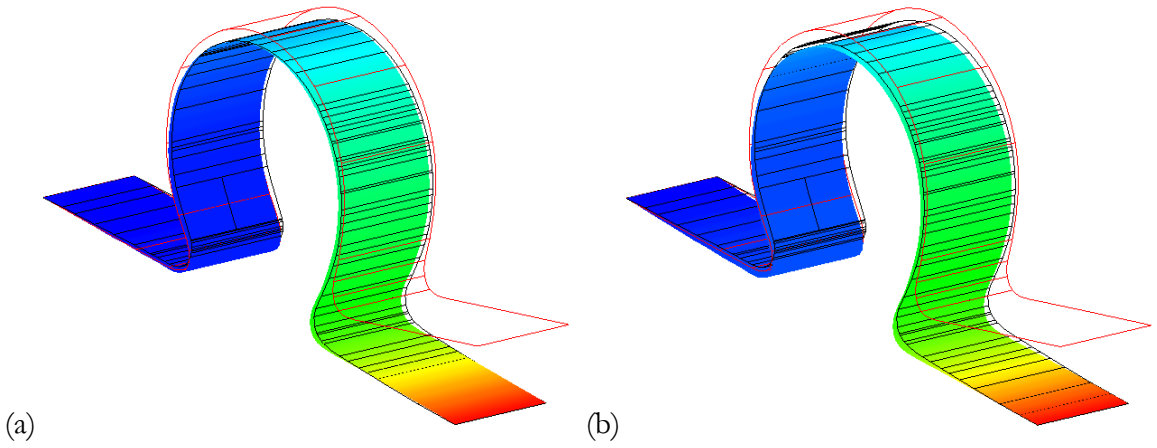

Fig. 7.3. The influence of boundary conditions on simulation results

7.1.2. Analysis results

The simulation results include the maximum stress and the displacement of each node in finite element mesh. The stress values confirmed that deformation is within elastic limits.

The displacements were used to validate the simulation results by scanned contours. To compare the calculated displacements with digitized CAD model of the real clamped part, the FEM model

with simulation results had to be converted to CAD model. That conversion was performed manually, since no currently available CAD/CAE software allows such conversion.

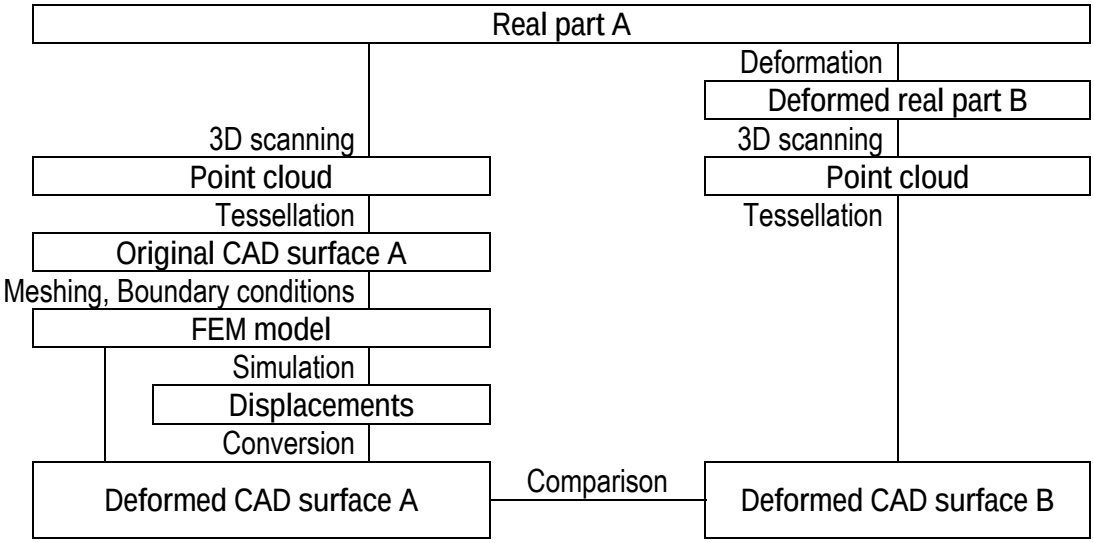

Fig. 7.4. Steps required to validate FEM results by digitized data

Fig. 7.4 shows steps required to validate FEM results by digitized data. The FEM model created from CAD surface A is subjected to simulation, and simulation results (displacements) are applied to each node of the FEM model. Such modified FEM model is then converted to CAD surface, in order to be compared with CAD surface B.

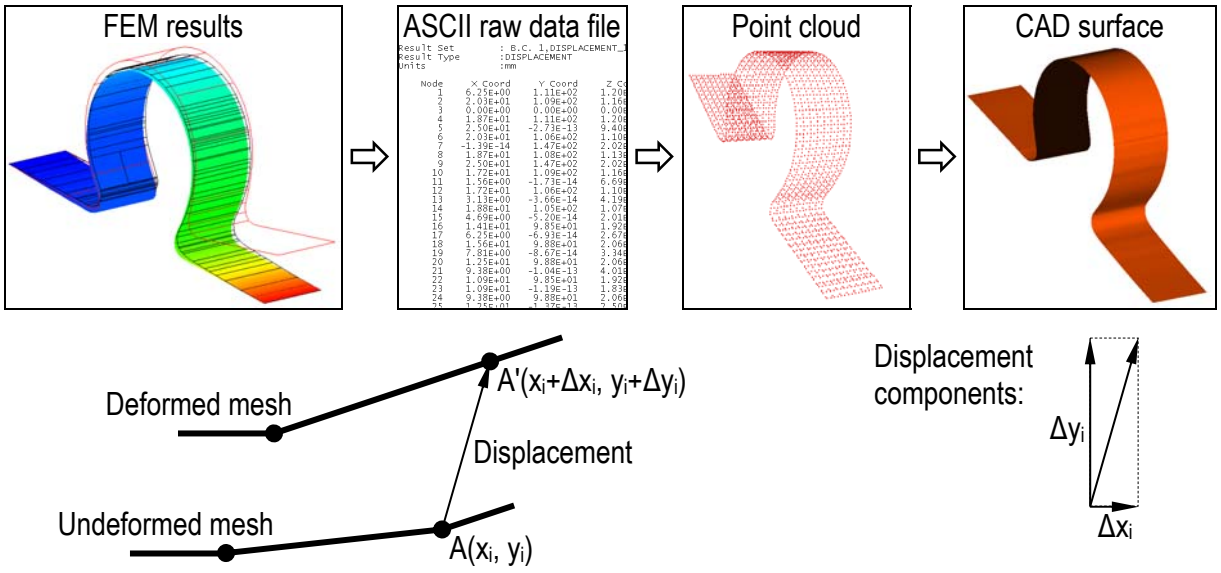

Fig. 7.5. Conversion of FEM results into CAD model

FEM results obtained by simulation (Fig. 7.5) are exported into raw data ASCII text file, as collection of point coordinates and corresponding displacements, defined in chosen reference

coordinate system. The raw data file needs simple calculation in order to be imported into reverse engineering software, as ASCII points file format.

Although this conversion is based on simple mathematical calculations, errors can arise during this conversion, and it is important to take care of the following:

- The reference **coordinate system** should be chosen to allow easy alignment and to minimize need for transformation of coordinates.

- During data conversion, **the decimal separator** should be chosen according to software specifications. American notation uses character dot (.), while European conventions prescribe to use character comma (,) as a decimal separator. In some cases, the decimal separator should be replaced throughout the raw data file. If MS Excel is used for data conversion, decimal number can be misinterpreted as date, resulting with large error.

- **Data representation format** (truncated floating point number notation, number of decimal places) should correspond to desired precision. For example, the result 10.923 can be written in data file as 1.09E+01, if data representation format is not properly set.

Fig. 7.6 shows graphical representation of 2D FEM analysis results, as shown in FEM software. The red line represents the free (unclamped) contour, the black line is digitized contour of physically clamped part, and the multi-coloured line (varying colours represent stress magnitude) is the contour obtained by FEM simulation.

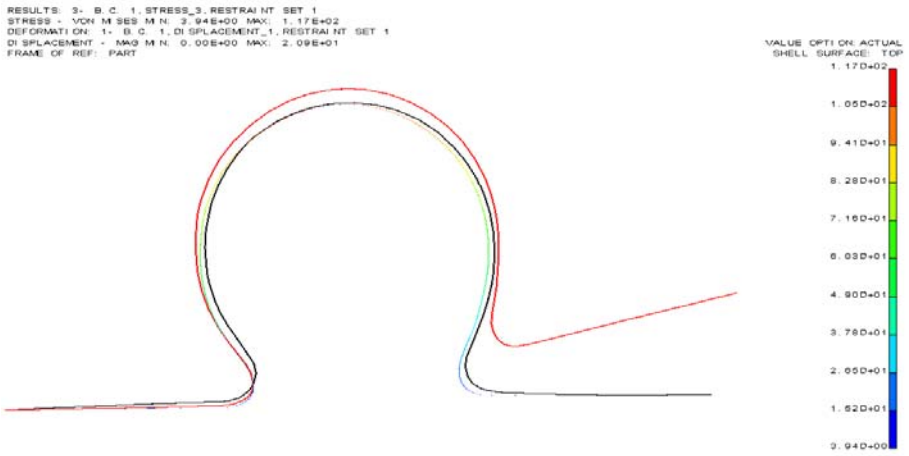

Fig. 7.6. The graphical representation of 2D FEM analysis results

Comparison of two CAD surfaces or 2D contours corresponds to the measurement of form and profile errors of mechanical parts, which involves the fitting of continuous surfaces, curves or lines to a set of coordinate points returned by inspection instrumentation. For example, if contour is circular, both ASME (Y14.5M-1994) and ISO (1101: 2004) prescribe the fitting of a pair of concentric circles with minimum radial separation to a set of discrete coordinate points sampled around the periphery of a surface of revolution at a plane perpendicular to the axis of revolution. This criterion is often referred to as the minimax or minimum zone criterion [91].

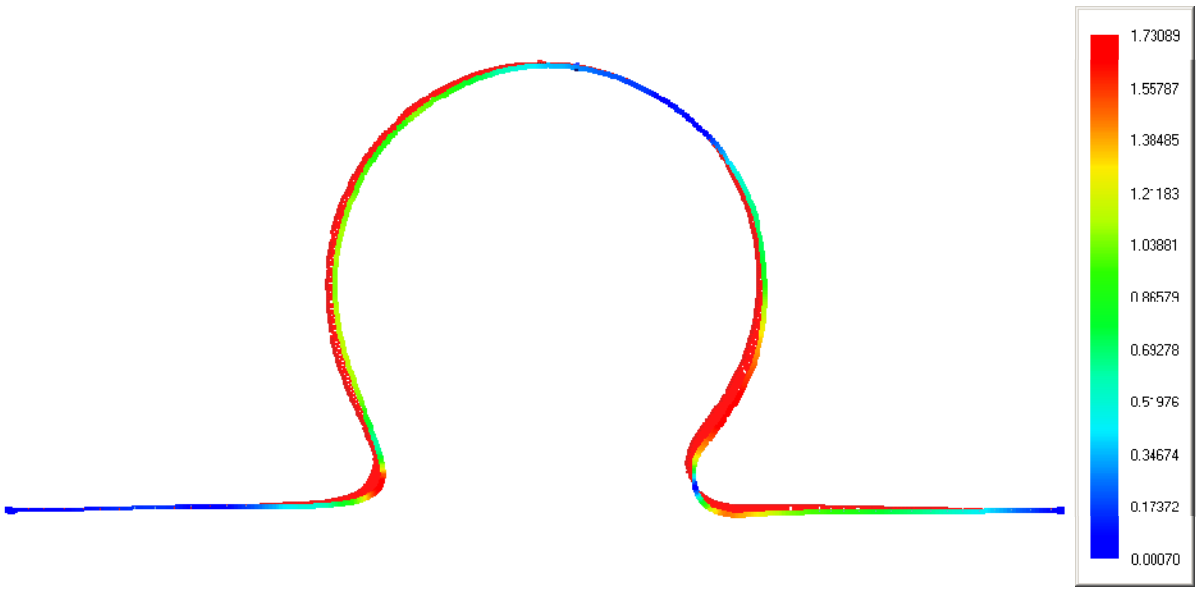

Fig. 7.7. The deviation between 2D contours obtained by real and by simulated clamping

In this case, the simulation results can be validated by comparing the maximum deviations between the 2D contours (ideal, simulated and physically clamped). Fig. 7.7 illustrates how deviation was measured. Table 7.1 summarizes results obtained from simulation:

- Maximum stress (Von-Mises equivalent stress), in MPa,
- Maximum deviation (absolute value) between the ideal CAD contour and the scanned contour of physically clamped part, in mm,
- Maximum deviation (absolute value) between the ideal CAD contour and the contour of part with simulated clamping, in mm, and
- Maximum deviation (absolute value) between the scanned contour of physically clamped part and the contour of part with simulated clamping, in mm.

Table 7.1. 2D FEM simulation results

Roll No.	Sample No.	Maximum stress (MPa)	Maximum deviation (mm)		
			CAD-clamped	CAD-simulated	clamped-simulated
1	1	113	4,34	2,96	1,73
	2	112	4,45	3,03	1,78
	3	114	4,08	2,88	1,65
	4	114	4,11	2,03	1,66
	5	114	4,17	2,26	1,68
	Average	113,40	4,23	2,63	1,70
	St.dev.	0,89	0,16	0,46	0,05
2	1	116	3,82	0,86	1,58
	2	115	3,91	1,21	1,61
	3	116	3,85	0,98	1,59
	4	115	4,00	1,56	1,63
	5	113	4,37	3,08	1,74
	Average	115,00	3,99	1,54	1,63
	St.dev.	1,22	0,22	0,90	0,06
3	1	116	3,83	0,86	1,58
	2	116	3,85	0,98	1,59
	3	111	4,80	3,81	1,87
	4	116	3,82	0,86	1,58
	5	116	3,85	0,98	1,59
	Average	115,00	4,03	1,50	1,64
	St.dev.	2,24	0,43	1,29	0,13
4	1	114	4,08	1,91	1,66
	2	115	3,94	1,33	1,61
	3	115	3,94	1,33	1,61
	4	115	3,88	1,10	1,60
	5	113	4,34	2,96	1,73
	Average	114,40	4,04	1,73	1,64
	St.dev.	0,89	0,19	0,75	0,05
5	1	115	3,88	1,10	1,60
	2	116	3,86	0,98	1,59
	3	115	3,94	1,33	1,61
	4	116	3,85	0,98	1,59
	5	116	3,83	0,86	1,58
	Average	115,60	3,87	1,05	1,59
	St.dev.	0,55	0,04	0,18	0,01
Total average		114,68	4,03	1,69	1,64
Total stand. dev.		1,41	0,25	0,91	0,07

Results presented in Table 7.1 show that deviations between the real part and the nominal CAD contour are more than twice larger than the deviation between the scanned and the simulated contour, i.e. manufacturing errors and deviations are larger than simulation errors. Since samples are manufactured manually, such a result is expected. The more detailed analysis of these results will be performed in the following chapters. To illustrate these results, the data from Table 7.1 is shown graphically in Fig. 7.8.

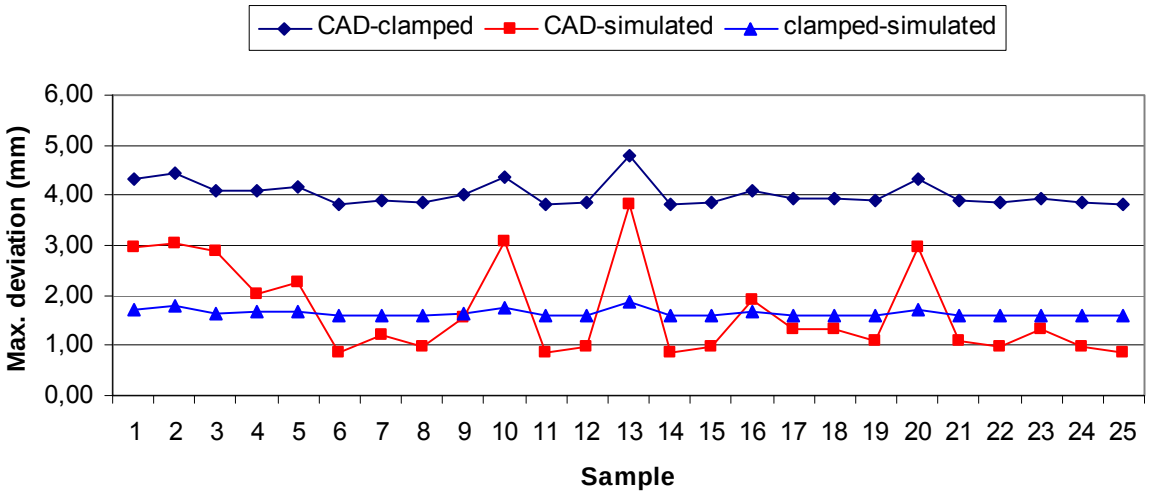

Fig. 7.8. Dimensional deviations derived from 2D FEM simulation results

7.2. 3D model FEM analysis

7.2.1. Meshing

The first step in finite element analysis of thin-walled structures is to discretize the surface with thin-shell finite elements. When surface is created with commonly used 3D CAD modelling methods, it is usually represented with regular surfaces, such as planes, cylinders, cones, revolved or extruded 2D profiles. All FEA software products are capable to mesh such surfaces, either automatically (free mesh) or manually (mapped meshes). The only exception is with spherical surfaces, which usually have to be partitioned, in order to define corners (Fig. 7.9).

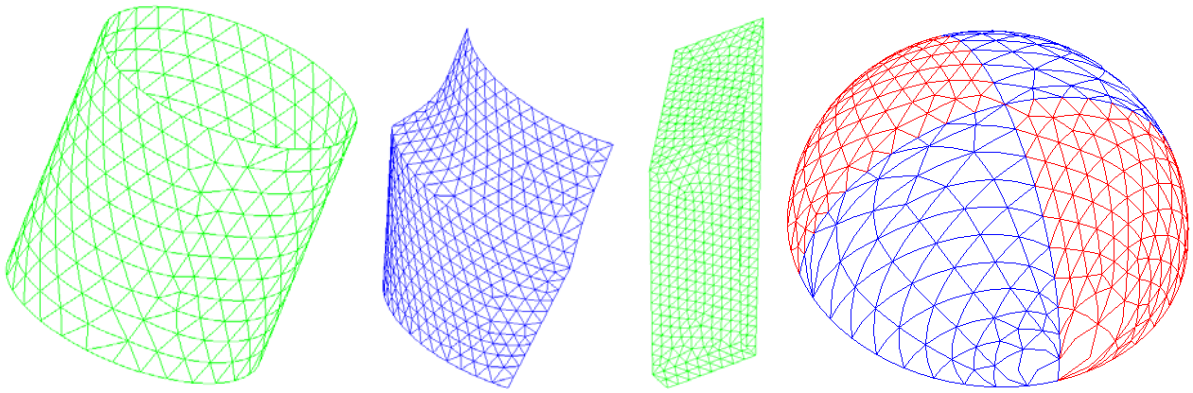

Fig. 7.9. Common regular surfaces discretized with triangular thin-shell finite elements

3D surfaces obtained by 3D scanning or digitising are represented as meshes of triangles, which are usually converted to 3D parametrized NURBS surfaces. NURBS (Non-Uniform Rational B-Splines), are mathematical representations of 3-D geometry that can accurately describe any

shape from a simple 2-D line, circle, arc, or curve to the most complex 3-D organic free-form surface or solid. Because of their flexibility and accuracy, NURBS models can be used in any process from illustration and animation to manufacturing. NURBS can accurately represent both standard geometric objects like lines, circles, ellipses, spheres, and free-form geometry.

There are several types of thin-shell elements, based on the various interpolation inside each element, with reference to the order of the shape functions. The choice of the most appropriate element type and size for particular simulation is a task that require experience and knowledge about phenomena being analyzed. The size and type of finite elements define the total number of degrees of freedom of the model. If mesh is finer, there are more elements and nodes, and this increases the total number of degrees of freedom (DOFs). The important criteria is accuracy, as a function of computational cost, which depends approximately on (number of DOFs)^3. In practice, the optimal relation between the accuracy and the number of DOFs is the main criteria used to select the mesh parameters of a model.

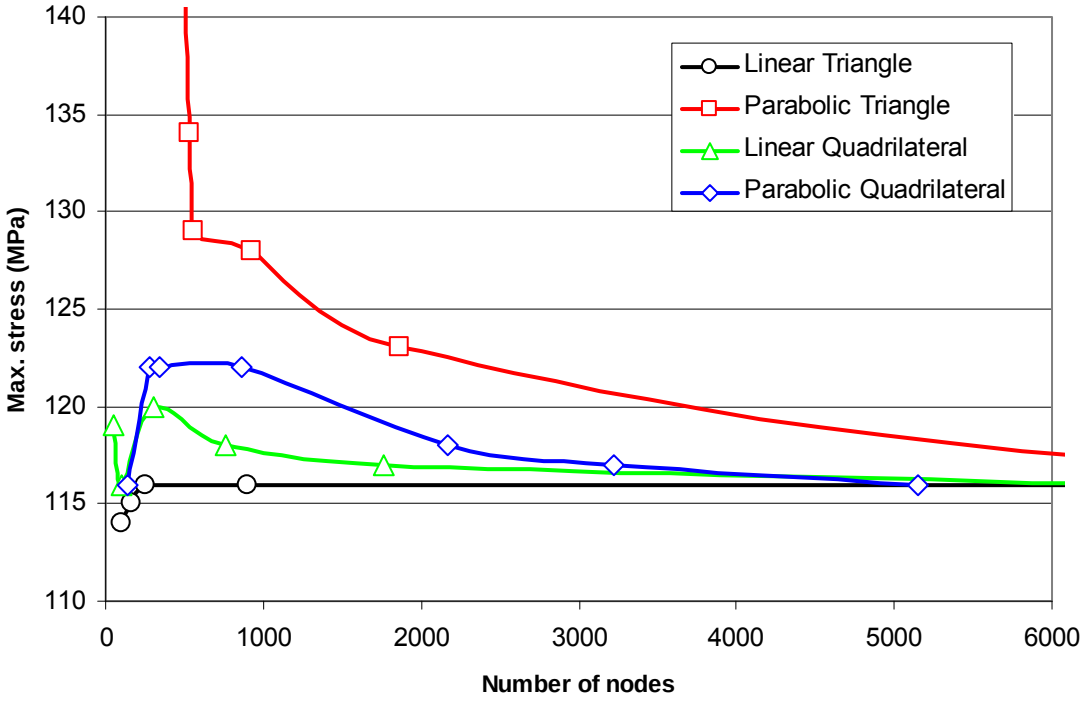

Fig. 7.10. Choosing finite element type and size

Since this research is limited on thin-walled structures, which have the most exceptional occurrence of springback behaviour, the stress and strain distribution across the structure thickness are not of interest, therefore the thin-shell elements are the definite choice. It is only

necessary to choose the element interpolation function and the element size. For that purpose, a preliminary analysis was performed with same boundary conditions, same geometry, and with mesh of various element type and size. Fig. 7.10 shows the results of that analysis.

Parabolic triangular thin shell elements converged to the solution very slowly, and mesh had to be very fine (15000 elements and 29000 nodes) in order to have stable results. These elements are not the right choice for similar problems. The linear triangular elements converged even with coarse mesh, and stable results were obtained with only 400 elements and 250 nodes. Both linear quadrilateral mesh made of 5000 elements and nodes, and parabolic quadrilateral mesh made of 1500 elements and 5000 nodes converged to stable result. According to these results, the further analysis was performed with linear triangular thin shell elements.

7.2.2. Boundary conditions

The development of finite element method during last decade was focused to optimisation of solver algorithms, improving meshing strategies, fluid-structure interaction, and to new finite element formulations for composites, biological tissue and other complex materials. The major trend was to automate the simulation process in order to enable integration to CAD packages. As a consequence, even low-cost CAD packages have some forms of preliminary FE analyses, both static and dynamic, automated as much as possible. However, the boundary conditions available for FE analysis did not change lately. Especially displacement restraints are still node-based. Even when finite element mesh is defined by CAD geometry, boundary conditions can be defined exclusively as six degrees of freedom, three translations and three rotations, because of the limitation in mathematical fundamentals of finite element method.

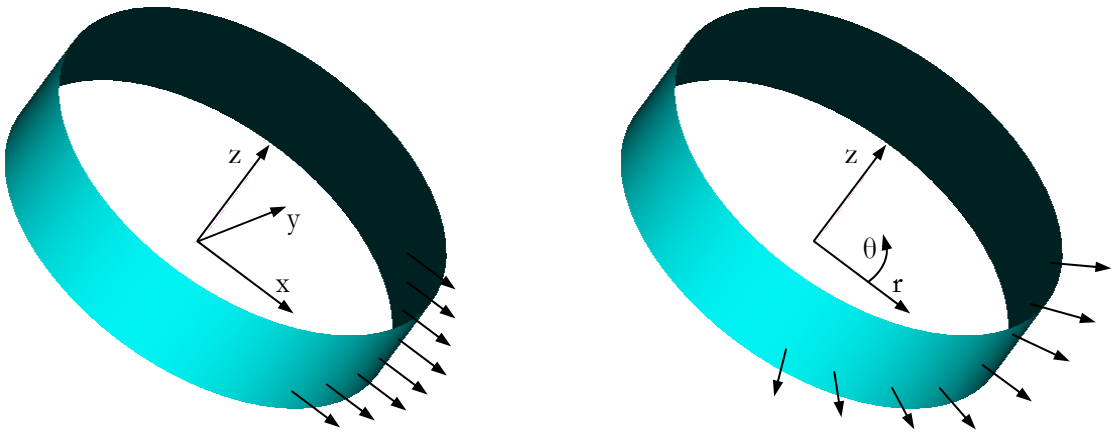

a) Cartesian coordinate system b) Cylindrical coordinate system

Fig. 7.11. Using different coordinate systems to define boundary conditions: single translation

Some boundary condition limitations can be avoided using appropriate local coordinate systems (Fig. 7.11), but the automation is still limited because each node needs to be defined separately.

Some boundary conditions can be simulated with special-purpose finite elements, such as contact gaps, springs, lumped masses etc. Since FE analysis has to have node to node connections, even these boundary conditions are node-based. They have to be defined for each node separately. There is a possibility for automation, for instance, when all nodes are located along one edge, it is easier to select them, but still displacement needs to be defined for each node separately. This is a major disadvantage, and there is a need to overcome this limitation.

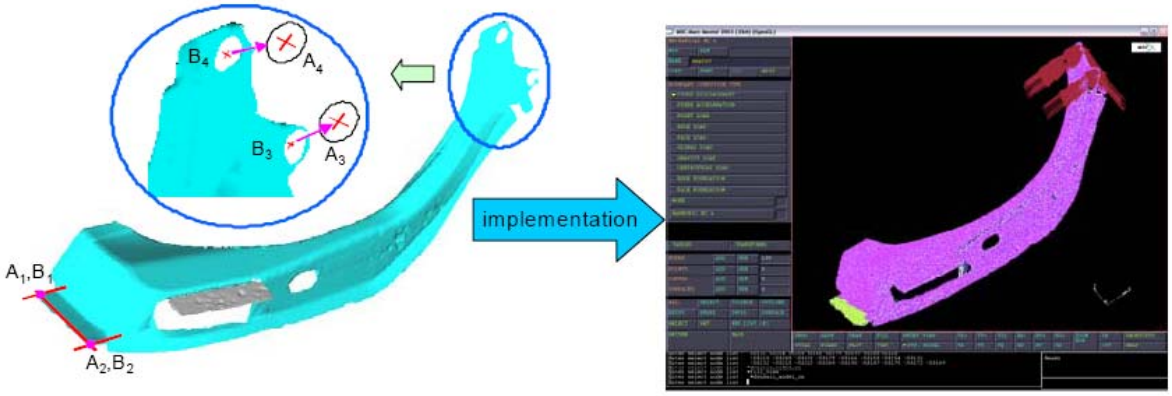

Fig. 7.12. Displacement boundary conditions based on extracted CAD feature [79]

In [79], boundary condition is defined through characteristic points: CAD features extracted from 3D scanned data (Fig. 7.12). Geometry of oil filter housing has no extractable features. Therefore, in order to simulate clamping, there is a need to define surface displacement as a boundary condition, to relate clamped and unclamped shape (Fig. 7.13).

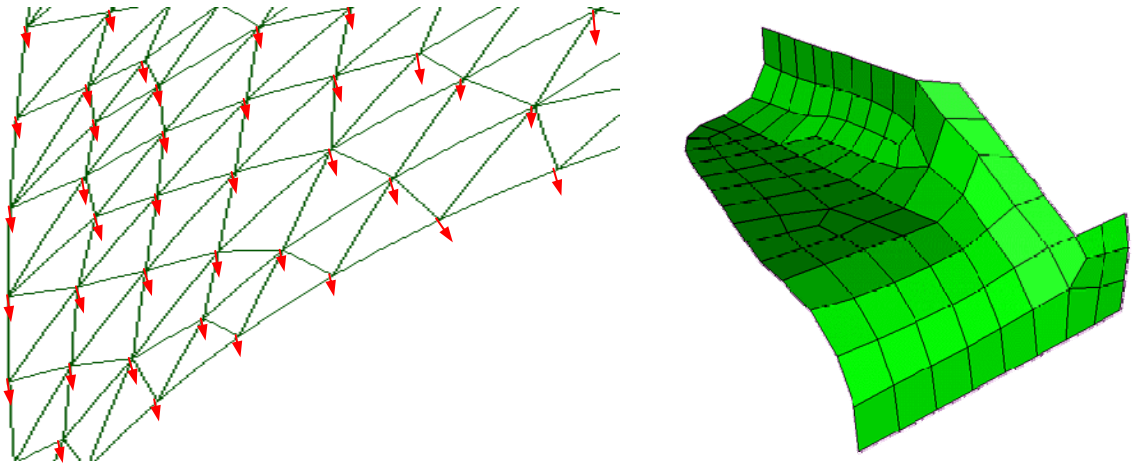

Fig. 7.13. Surface-based boundary conditions, transformed to node-based displacements

It is unjustifiable to set the displacement for each node of the mesh, because it would require too much manual operations (the finite element models are usually meshed with thousands of nodes and elements). The forced displacements can not be applied to lines only, since that leads to incorrect result due to stress concentration. Therefore, surface displacement will be simulated using the equivalent radius of scanned shape (Fig. 7.14), and using a set of interpolated cross-sections (Fig. 7.15). The equivalent radius approximates the displacement averaged across the whole circumference of the part, while interpolated cross-sections enable different radii changes on selected number of cross-sections. The latter method requires more manual interventions, but provides the more accurate deformation image. Both methods will be tested on models.

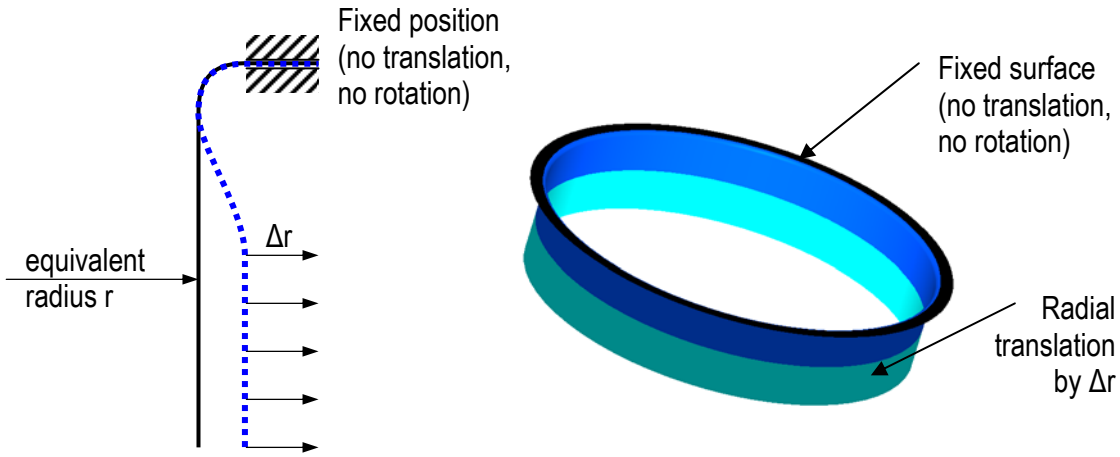

Fig. 7.14. Surface-based boundary conditions with equivalent radius

Equivalent radius r is derived from best-fit cylinder of the scanned free (unclamped) shape. The clamping procedure deforms the part, and changes this radius for value Δr (positive or negative). The equivalent radii which were calculated from scanned parts in Chapter 6.2, are used to define the Δr values. The boundary conditions are then defined as follows:

- The upper surface is completely fixed, with no translations and no rotations allowed (the black circular surface on top of the part shown in Fig. 7.14).

- The radial translation by Δr is applied on the surface of cylindrical section (the bottom surface of the part shown in Fig. 7.14).

Another approximation of the real conditions is shown in Fig. 7.15. The part is sectioned with reference planes which pass through the axis of the best-fit cylinder. Each cross-section has different Δr, which is then applied to each section surface individually. This method requires much more efforts, because average radius has to be calculated for each section, the CAD model

has to be divided into sections, and displacements have to be applied to each section separately. To check if this method is justifiable, its results are compared with results of "equivalent radius" method.

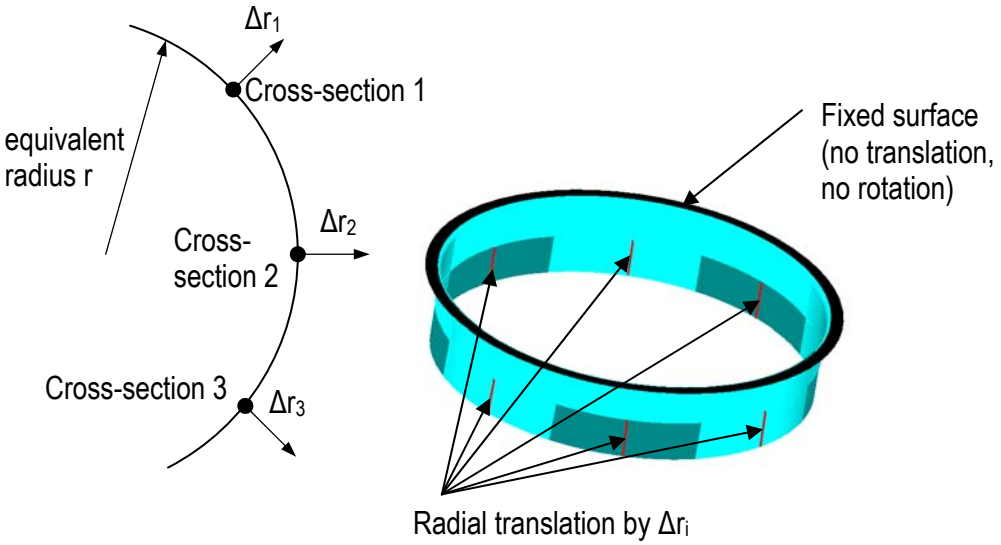

Fig. 7.15. Surface-based boundary conditions with interpolated cross-sections

Fig. 7.16 shows an example how part was sectioned into 8 parts. The boundary conditions were set as forced displacement, measured from deviations of the ideal cylinder radius (46.000 mm). The average displacement was 0.031 mm, and values varied between 0.138 and -0.53 mm. In order to avoid sharp transitions (and therefore stress concentration which really does not exist at the real part), the forced displacements were applied to selected surfaces, excluding sections which are directly connected to neighbouring sections.

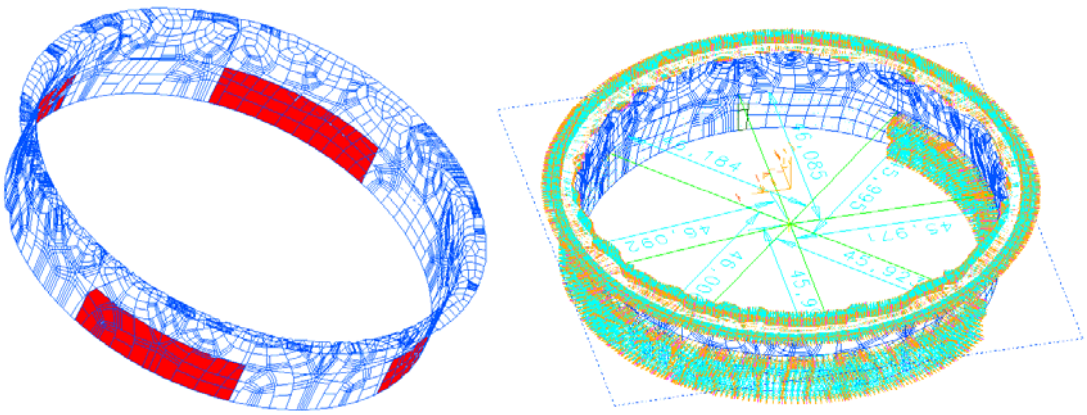

Fig. 7.16. The surface sections of the scanned part with forced displacements

The stress results were not satisfactory, because stress concentration appeared in simulation result (Fig. 7.17). It was not possible to apply forced displacements on segments, without having stress concentration on boundary elements. When displacement results were compared to results obtained when forced displacement was applied as a constant radius change across the whole circumference, the maximum deviation between these surfaces was 0.634 mm. It is unrealistically high value, which does not correspond to the real conditions. This method requires much more user interaction, and anyway expresses significant errors due to false stress concentration.

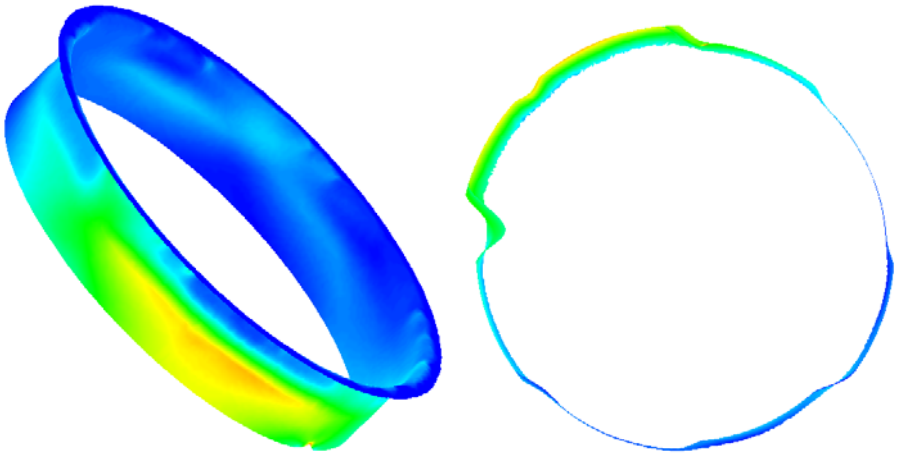

Fig. 7.17. Stress concentration due to different Δr between neighbouring segments

Because of these drawbacks of segmented boundary conditions, the "equivalent radius" method was used in further analysis. All samples were subjected to simulation with forced displacement equal to the difference between equivalent radius of clamped and unclamped part.

7.2.3. Analysis results

Finite element simulation requires proper choice of material and its properties. The most similar replacement material for Euronorm DC04 deep-drawing steel (material used in experiments) is I-deas Standard steel SAE 1010 (Modulus of elasticity E=211669 MPa, Poisson's ratio ν=0.291, Shear modulus G=82047.6 MPa).

Fig. 7.18 shows how boundary conditions were applied to model of 3D scanned oil filter housing. The 3D scanned model was tessellated into set of NURBS surfaces, and oriented with cylindrical coordinate system. The lower, cylindrical portion of the model was defined as forced radial displacement with magnitude calculated from the difference between the equivalent radius of 3D scanned fixed part and 3D scanned free part. All other degrees of freedom are free. The top surfaces (fixed in clamping mechanism) are defined with no translation and no rotation.

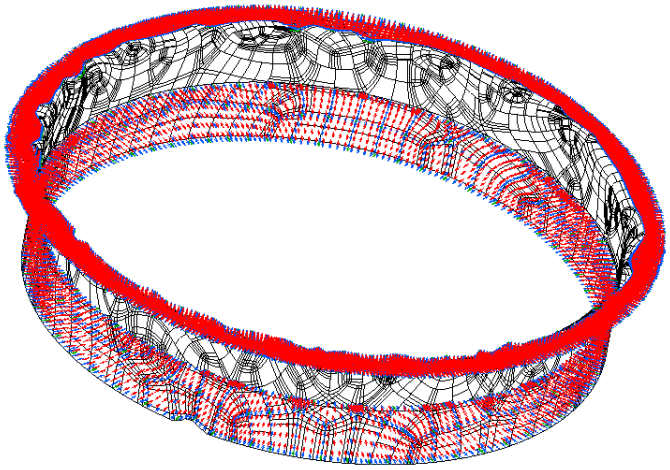

Fig. 7.18. The scanned free part with boundary conditions applied:
forced surface displacement calculated from equivalent radius

The model was discretized with linear triangular thin shell finite elements, using Mindlin formulation (both bending and shear stiffness are taken into account), with 0.5 mm thickness as a physical property. The 25 analyzed models contained approximately 12000 nodes and 23000 elements each. The simulation was performed as linear static analysis, since displacements are small enough and there is no geometric or material nonlinearity. Fig. 7.19 shows the simulation results in FEM software. The stress concentration (208 MPa) appears across the line which separates surface where boundary conditions were applied from the rest of the model.

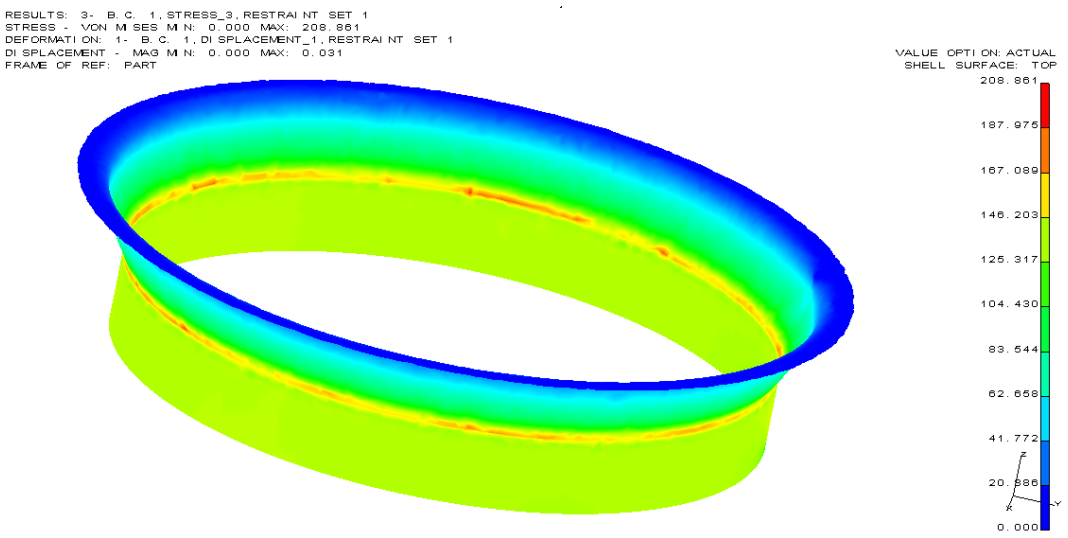

Fig. 7.19. FEM simulation results of the whole model, with faulty stress concentration

To provide more accurate results, this stress concentration must be avoided, therefore results shall be extracted from the lower area, distant enough from the separation line. Fig 7.20 shows such results, and the maximum stress is 149 MPa.

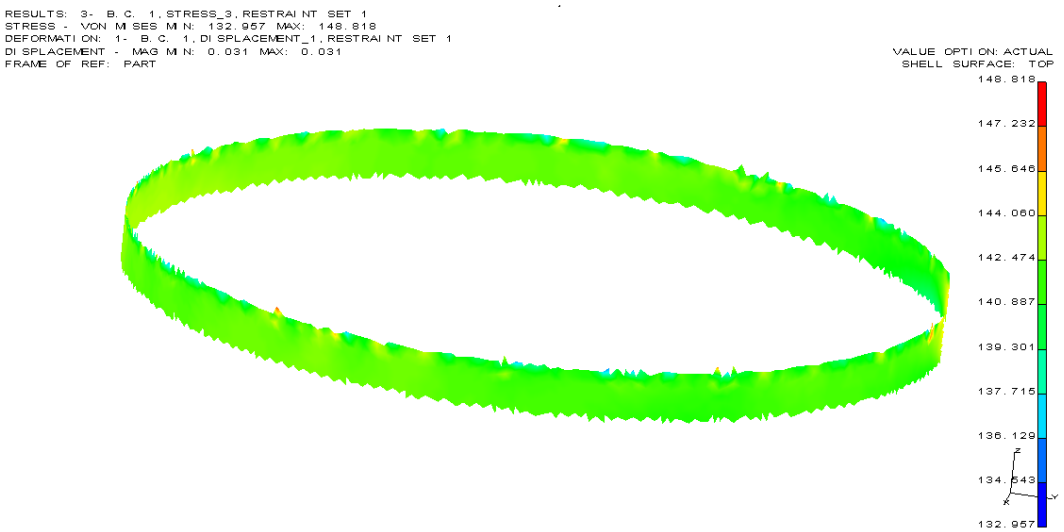

Fig. 7.20. FEM simulation results presented at the lower part of the model

The simulation was performed for each scanned data set, from all 25 samples that were scanned. After the simulation, the data conversion, described in Chapter 7.1.2, was performed on each result, in order to compare the results from physically and virtually clamped part. The deviations were measured at the toleranced cross-section (10 mm from top of the oil housing).

Table 7.2 summarizes the input data (used to define boundary conditions) and the results obtained from simulation and 3D data comparison, with proper and bad boundary conditions:

- Forced displacement used as boundary condition (change of equivalent radii from Table 6.3, derived from cross-section of 3D scanned data), in mm,
- Maximum stress (Von-Mises equivalent stress), in MPa,
- Absolute value of the maximum deviation between the ideal CAD contour and the scanned contour of physically clamped part, in mm,
- Absolute value of the maximum deviation between the ideal CAD contour and the contour of part with simulated clamping, in mm, with proper boundary conditions, and
- Absolute value of the maximum deviation between the ideal CAD contour and the contour of part with simulated clamping, in mm, with poor boundary conditions.

The results of 3D FEM simulation and comparison of simulation and 3D scanning results are graphically presented in Figs. 7.21 and 7.22.

Table 7.2. 3D FEM simulation results

Roll No.	Sample No.	Forced displacement Δr (mm)	Maximum stress (MPa)	Maximum deviation (mm)		
				CAD-clamped	CAD-simulated (good B.C.)	CAD-simulated (poor B.C.)
1	1	-0,031	149	0,053	0,017	0,097
	2	-0,032	159	0,046	0,015	0,113
	3	-0,014	73	0,091	0,029	0,181
	4	-0,032	176	0,086	0,028	0,193
	5	-0,006	30	0,063	0,020	0,130
2	1	-0,040	187	0,040	0,013	0,124
	2	-0,041	186	0,083	0,027	0,152
	3	-0,018	88	0,085	0,027	0,122
	4	-0,014	71	0,055	0,018	0,128
	5	-0,037	174	0,066	0,021	0,132
3	1	-0,029	145	0,079	0,025	0,109
	2	-0,040	186	0,069	0,022	0,170
	3	-0,021	104	0,078	0,025	0,173
	4	-0,013	72	0,079	0,025	0,127
	5	-0,010	45	0,103	0,033	0,167
4	1	-0,041	185	0,050	0,016	0,145
	2	-0,038	186	0,097	0,031	0,185
	3	-0,039	184	0,151	0,049	0,251
	4	-0,039	180	0,076	0,025	0,125
	5	-0,040	182	0,074	0,024	0,161
5	1	-0,020	101	0,056	0,018	0,111
	2	-0,041	185	0,058	0,019	0,125
	3	-0,041	173	0,066	0,021	0,153
	4	-0,035	175	0,046	0,015	0,138
	5	-0,025	130	0,074	0,024	0,110
Total average		**-0,029**	**141**	**0,073**	**0,024**	**0,145**
Standard deviation		**0,012**	**51**	**0,023**	**0,0075**	**0,034**

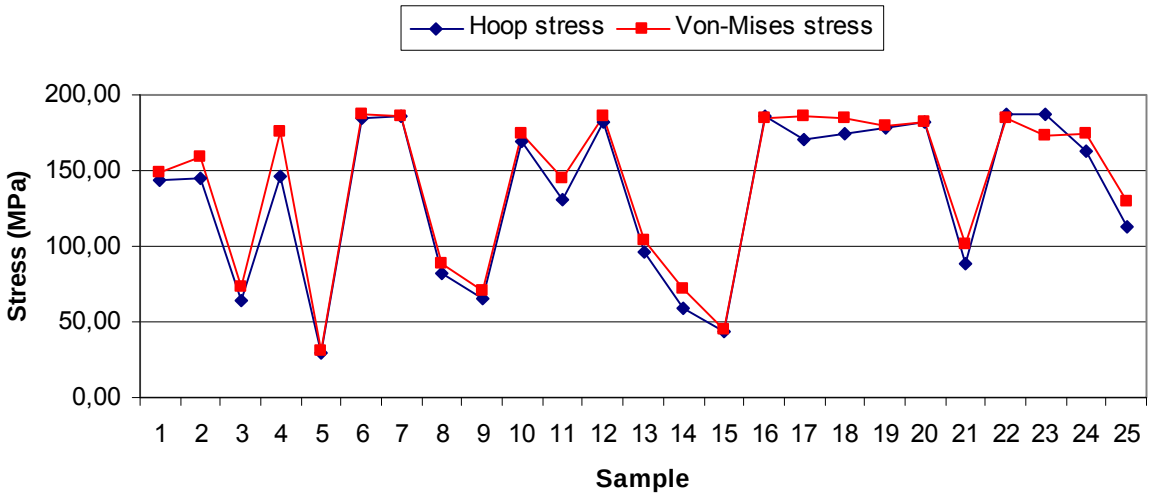

Fig. 7.21. Theoretical hoop stresses (calculated from 3D scanned data) compared with 3D FEM simulation results (Von-Mises equivalent stress)

Results presented in Table 7.2 and Fig. 7.21 show that equivalent Von-Mises stress calculated by 3D FEM simulation corresponds very well to hoop stresses calculated from equivalent radii of 3D scanned samples. Results presented in Table 7.2 and Fig. 7.22 show that deviations between the 3D scanned real part and the nominal CAD contour are larger than the deviation between the scanned and the simulated contour, i.e. manufacturing errors and scanning deviations are larger than simulation errors. When boundary conditions are chosen poorly, the average of equivalent radius maximum deviation is significantly larger, and its dissipation also increases significantly.

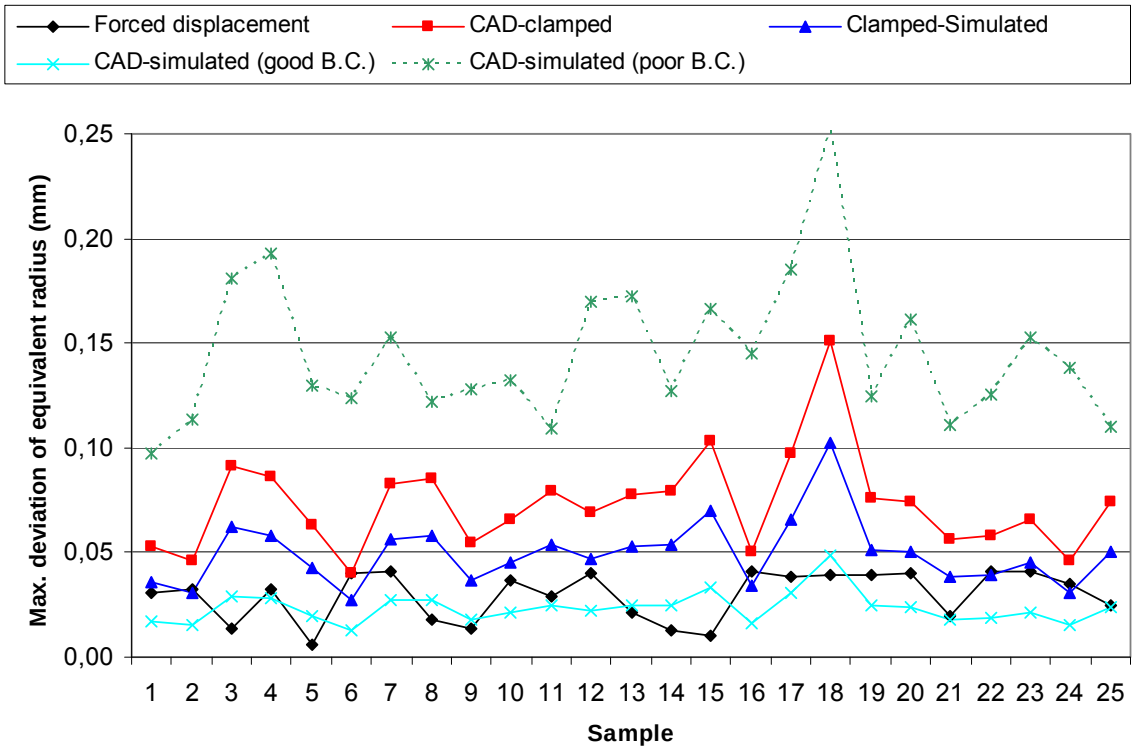

Fig. 7.22. Dimensional deviations between FEM simulation and 3D scanning

Fig. 7.22 also illustrates that the deviations between the ideal and simulated parts are rather constant, and their values are approximately the same as forced displacements used to define boundary conditions.

8. Measurement uncertainty

This Chapter deals with measurement uncertainty, which includes brief description of GUM and basic definitions of terms, detailed analysis of influence factors, creating mathematical model of measurement system, and uncertainty analysis according to procedures described in ISO Guide to the Expression of Uncertainty in Measurement [2].

A measurement result is complete only when accompanied by a quantitative statement of its uncertainty. The uncertainty is required in order to decide if the result is adequate for its intended purpose and to ascertain if it is consistent with other similar results. Over the years, many different approaches to evaluating and expressing this uncertainty have been used. The variation in approaches caused three main problems, especially in international laboratory comparisons: the need for extensive explanations of the measurement uncertainty calculation method used, the separation between random and systematic uncertainties, and deliberate overstating some uncertainties. To overcome these three problems, on the initiative from the CIPM (Comité International des Poids et Measures), the International Organization for Standardization (ISO) developed a detailed guide which provides rules on the expression of measurement uncertainty for use within standardization, calibration, laboratory accreditation, and metrology services. The Guide to the Expression of Uncertainty in Measurement (GUM) was published in 1993 (corrected and reprinted in 1995) by ISO in the name of the seven international organizations that supported its development. The focus of GUM is the establishment of general rules for evaluating and expressing uncertainty in measurement that can be followed at various levels of accuracy and in many fields - from factories to fundamental research. Measurement uncertainty is also used for the verification of the conformity of workpieces (ISO 14253-1:1998) [93].

The Table 8.1 summarizes some of the key definitions given in GUM. Many additional terms relevant to the field of measurement are given in a companion publication to the ISO Guide, entitled the International Vocabulary of Metrology (VIM) [94].

Table 8.1. The definitions given in GUM [2]

Uncertainty (of measurement)	Parameter, associated with the result of a measurement, that characterizes the dispersion of the values that could reasonably be attributed to the measurand • The parameter may be, for example, a standard deviation (or a given multiple of it), or the half-width of an interval having a stated level of confidence. • Uncertainty of measurement comprises, in general, many components. Some of these components may be evaluated from the statistical distribution of the results of a series of measurements and can be characterized by experimental standard deviations. The other components, which also can be characterized by standard deviations, are evaluated from assumed probability distributions based on experience or other information. • It is understood that the result of the measurement is the best estimate of the value of the measurand, and that all components of uncertainty, including those arising from systematic effects, such as components associated with corrections and reference standards, contribute to the dispersion.
Standard uncertainty	Uncertainty of the result of a measurement expressed as a standard deviation
Type A evaluation (of uncertainty)	Method of evaluation of uncertainty by the statistical analysis of series of observations
Type B evaluation (of uncertainty)	Method of evaluation of uncertainty by means other than the statistical analysis of series of observations
Combined standard uncertainty	Standard uncertainty of the result of a measurement when that result is obtained from the values of a number of other quantities, equal to the positive square root of a sum of terms, the terms being the variances or covariances of these other quantities weighed according to how the measurement result varies with changes in these quantities
Expanded uncertainty	Quantity defining an interval about the result of a measurement that may be expected to encompass a large fraction of the distribution of values that could reasonably be attributed to the measurand. The fraction may be viewed as the coverage probability or level of confidence of the interval. To associate a specific level of confidence with the interval defined by the expanded uncertainty requires explicit or implicit assumptions regarding the probability distribution characterized by the measurement result and its combined standard uncertainty. The level of confidence that may be attributed to this interval can be known only to the extent to which such assumptions may be justified.
Coverage factor	Numerical factor used as a multiplier of the combined standard uncertainty in order to obtain an expanded uncertainty
Measurand	Quantity intended to be measured [94]

The standard GUM procedure of determining measurement uncertainty comprises of the following steps [2]:

Step 1: Making a model of the measurement. In most cases, a measurand Y is not measured directly, but is determined from N other quantities (X_1, X_2, ..., X_N) through a functional relationship $Y = f(X_1, X_2, ..., X_N)$.

Step 2: Determining x_i, the estimated value of input quantity X_i, either on the basis of the statistical analysis of series of observations or by other means.

Step 3: Identifying and characterising each uncertainty component u_i (Type A and Type B) of each input estimate x_i.

Step 4: Evaluating the covariances associated with any input estimates that are correlated.

Step 5: Calculating the result of the measurement, from the functional relationship f using for the input quantities X_i the estimates x_i obtained in step 2.

Step 6: Calculating the values of combined standard uncertainty u_{comb} and the effective degree of freedom ν_{eff}. For N uncorrelated uncertainty components, the values of u_{comb} and ν_{eff} are given by equations (8.2) and (8.3), respectively.

Step 7: Calculating the values of the expanded uncertainty U and the coverage factor k.

Step 8: Stating the final result, giving the values of the expanded uncertainty U and the coverage factor k, indicating the confidence interval (CI) used, and ensuring the final result and U are rounded appropriately (rounded up to the next largest figure).

The uncertainty of the final result may be expressed simply as $\pm u_{comb}$, which represents a range of values within which the true value is expected to lie with approximately 68% probability (assuming $\nu_{eff} \geq 20$). This is the traditional one standard deviation or one sigma level. However, the GUM reports the expanded uncertainty U, calculated using equation (8.1).

$$U = u_{comb} \cdot k \quad \text{..... (8.1)}$$

where U is the expanded uncertainty, and k is the coverage factor. Values for U can be calculated such that $\pm U$ has any desired probability of containing the true value, including the increasingly

common 95% probability. The value k is selected from tabulated data, given ν_{eff} and the desired probability (known as confidence interval, CI).

The combined standard uncertainty for N uncorrelated uncertainty components is calculated as:

$$u_{comb} = \sqrt{\sum_{i=1}^{N} (c_i u_i)^2} \quad \text{..... (8.2)}$$

where u_{comb} is the combined standard uncertainty, u_i are the standard uncertainties of components and c_i are the sensitivity coefficients of components. Equation (8.1) is valid if two conditions are met; (a) each uncertainty component is not correlated with any other uncertainty component, and (b) an approximately linear relationship exists between each uncertainty component and the final result for the range of values the uncertainty components are likely to have. For most measurements, if both the above conditions are not met, it is usually possible to alter the way the measurement is made so that both conditions are satisfied.

In order to determine the coverage factor k, it is necessary to calculate the effective degrees of freedom, using Welch-Satterthwaite formula (8.3).

$$\nu_{eff} = \frac{u_{comb}^4}{\sum_{i=1}^{N} \left[\frac{(c_i u_i)^4}{\nu_i} \right]} \quad \text{..... (8.3)}$$

where ν_{eff} is the effective degree of freedom, ν_i are the degrees of freedom of components.

Table 8.2. Determining the coverage factor (k) according to degrees of freedom (ν) [95]

Measurement quality	Degrees of freedom ν	k for 95% confidence interval
Poor	2	4.30
Reasonable	8	2.31
Good	20	2.09
Excellent	1000	1.96

The Table 8.2 shows a relationship between measurement quality (as judged through experience), degrees of freedom (ν) and coverage factor (k) to generate a 95% confidence interval [95].

Regardless of the sources of uncertainties, there are two approaches to estimating them: "Type A" and "Type B" evaluations. In most measurement situations, uncertainty evaluations of both types are needed. Type A evaluations are uncertainty estimates obtained from a number of

observations estimated by statistical analysis expressed by standard deviations. Type B evaluations are non-statistical uncertainty estimates from a pool of information. This could be information from past experience of the measurements, from calibration certificates, manufacturer's specifications, from calculations, from published information, and from common sense.

For a Type A evaluation, when a set of several repeated readings has been taken (for a Type A estimate of uncertainty), the mean ($\overline{x}$), and estimated standard deviation (s), can be calculated for the set. From these, the estimated standard uncertainty (u) of the mean is calculated from:

$$u = \frac{s}{\sqrt{n}} \quad \text{..... (8.4)}$$

where n is the number of measurements in the set, and s is the standard deviation (8.5).

$$s = \sqrt{\frac{\sum_{i=1}^{n}(q_i - \overline{q})^2}{n-1}} \quad \text{..... (8.5)}$$

where q_k is the result of the kth measurement and $\overline{q}$ is the arithmetic mean of the n results.

For a type B evaluation, it is only possible to estimate the upper and lower limits of uncertainty. It is assumed that the value is equally likely to fall anywhere in between a rectangular or uniform distribution. The standard uncertainty for a rectangular distribution is found from:

$$u = \frac{a}{\sqrt{3}} \quad \text{..... (8.6)}$$

where a is the semi-range (or half-width) between the upper and lower limits.

Sensitivity coefficients for each component is determined from the functional relationship between the components $Y = f(X_1, X_2, ..., X_N)$:

$$c_i = \frac{\partial f(X_1, X_2, ...X_N)}{\partial X_i} \quad \text{..... (8.7)}$$

Therefore, the most important step in measurement uncertainty evaluation is to set up a mathematical model of the measurement, on the basis of clearly defined measurement task and the knowledge about the measurement process and the relevant influence factors.

8.1. Influence factors

One of the most important aspects of uncertainty evaluation is the need for a detailed understanding of the measurement task and all potential sources of the measurement uncertainty. The identification of uncertainty sources begins by examining in detail the measurement process.

The measurement task in this research is measurement of internal diameter of circular cross-section measured 10 mm below top of the oil filter housing (nominal diameter 92 mm), when the housing is clamped physically and virtually (numerically simulated). Two different measurement chains with accompanying major influences are presented in Figs. 8.1 and 8.2.

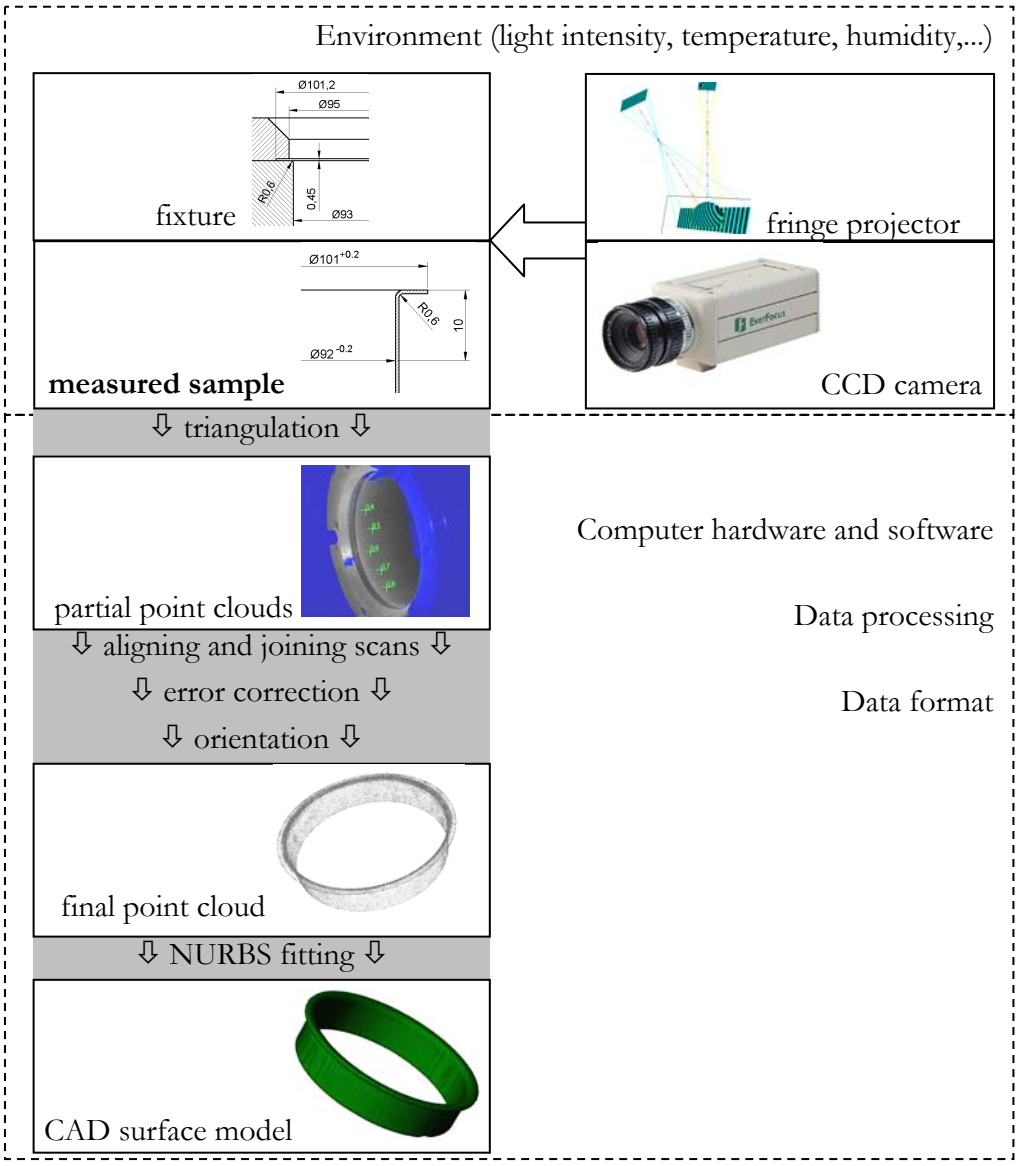

Fig. 8.1. Measurement chain of 3D scanner used to digitize physically clamped part

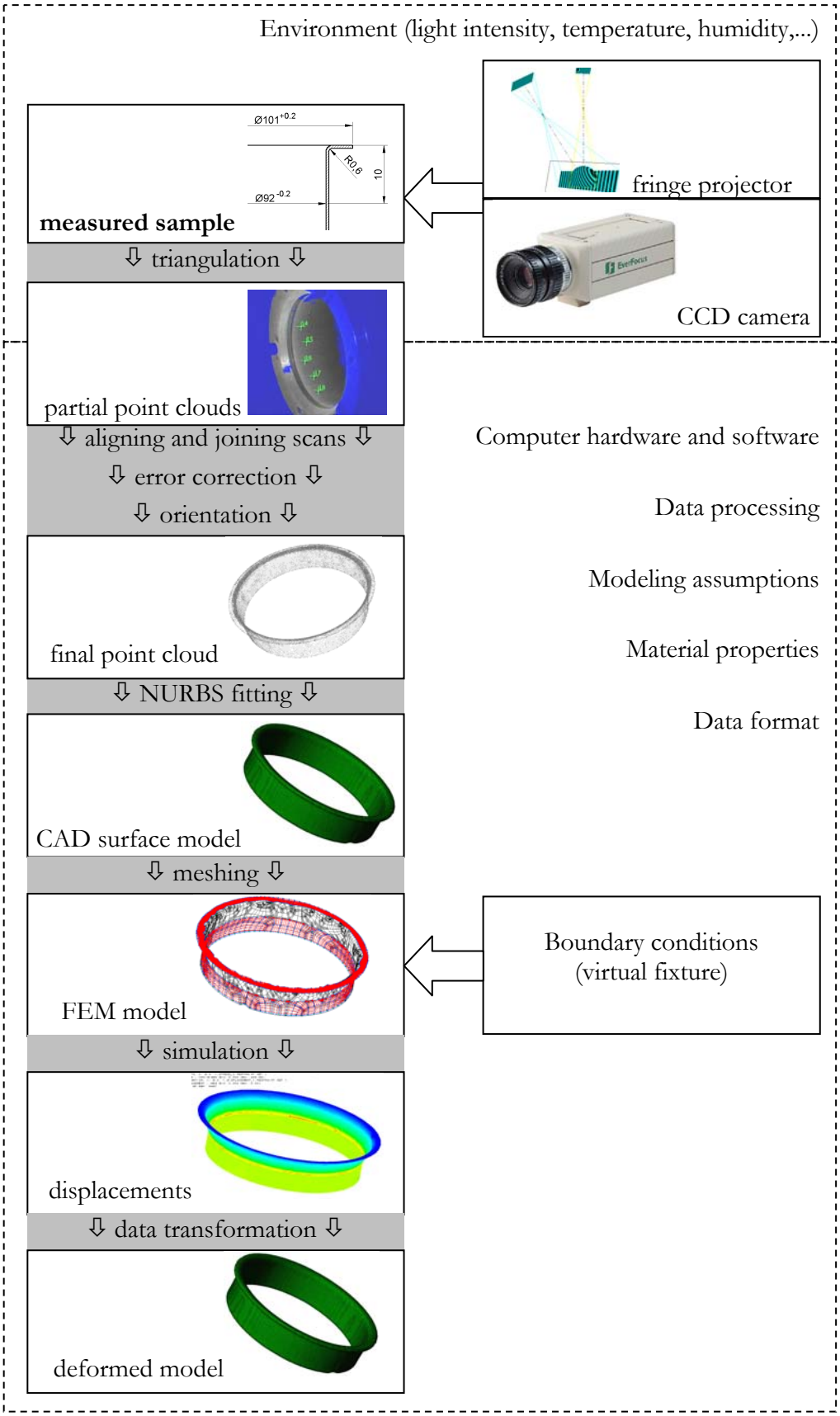

Fig. 8.2. Measurement chain of 3D scanner with numerically simulated clamping of workpiece

Figs. 8.1 and 8.2 show that there are more possible error sources which contribute to uncertainty when simulation is part of the measurement chain. Therefore, the uncertainty influences could be classified into the following categories: environment, measurement object, method, scanning hardware, processing software and simulation software. This classification slightly differs from classifications presented in [1], [96] and [97], and some sources and accompanying elimination methods spread over more than one category. For example, humidity belongs to environmental sources, but careful measurement method can eliminate the influence of humidity.

Environmental sources of uncertainty

The most common concern for environment involves temperature, which is often stated as the largest error source affecting precision of dimensional metrology [1]. The temperature affects both measuring system and measured object. The light sources in optical 3D scanners act as local heat sources, whose temperature compensation and calibration is usually performed within the scanner's hardware. The temperature influence on scanned part dimensions is easily calculated using coefficient of thermal expansion.

Humidity and contamination, can also lead to distortion of parts being measured. In this case, when metallic parts are scanned, humidity influences the reflection of light from measured part. Humidity could also lead to dew condensation on camera and projector lenses, which blurs and distorts the image. The presence of dust and similar contamination in the air can lead to error.

Nonatmospheric concerns include vibration, air pressure, air conditioning systems and power supply. Consideration of the sensitivity of these sources is dependent on the degree of control and the capability required. For example, the environmental control realized within laboratories is generally much greater than that of production areas. Often, a stable environment can shift the sources of error to the machine's and the part's properties within those conditions.

The optical measurements, such as 3D scanning, especially white light fringe projection systems, are very sensitive to lightning conditions. The ambient light can degrade the 3D scanner performance and it is recommended to perform the scanning in dark rooms with minimum external light sources. When light sources cannot be controlled, one should have in mind that different artificial and natural light sources have different colour spectra, which could influence camera performance. For example, fluorescent, incandescent and halogen lights have narrower colour spectra than daylight.

Sources of uncertainty related to measurement object

Many aspects of the parts themselves can be a source of measurement uncertainty. Measurement object's characteristics could be observed as geometrical, material and optical.

Geometrical characteristics include shape (some portions of scanned object can be unavailable due to occlusion, sharp edges can be misinterpreted in point cloud), size (when large parts are scanned, it is necessary to perform more separate scans, whose joining can increase error), microstructure, roughness, type and value of the form deviation. The surface finish and form values greatly affect both the ability to collect scanned points and the number of points required to calculate accurate substitute geometry. Even the conformance to specifications for any given feature can affect the ability of the measurement system to analyze its attributes.

Uncertainties in knowledge of material properties are the dominant factor in the distortion coefficient uncertainties derived from mathematical modelling [99]. The elasticity and coefficient of thermal expansion should be considered a source of error, especially with longer part features, thin-walled structures and with areas lacking stable environmental controls.

The major optical characteristic is the surface reflection. For the purpose of optical 3D scanning, surfaces can be classified into five major groups according to reflection: specular I and II, Lambertian, hybrid I and II [101]. In Lambertian objects, the dominant reflectance component is a diffuse lobe. In specular I objects, the specular spike component dominates the other components. Examples include optical mirrors and shiny metal. In specular II, when the incident angle is large, the dominant reflectance component is a specular spike. However, when the incident angle is small, the specular lobe component becomes dominant. Typical examples are glossy plastic products. Hybrid I and II are composed of a mixture of the specular spike, specular lobe, and diffuse lobe. In hybrid I objects, the specular spike component is larger than the other two, and the angle of the peak in a reflected distribution is equal to the angle of specular reflection. In hybrid II, the specular lobe component is dominant, and the angle of the peak is unequal to the angle of specular reflection owing to the off-specular peak. To overcome the problem of surface reflection, scanned objects are usually sprayed with anti-reflection powder.

It has been observed that surfaces of different reflectivity result in systematic errors in range [102]. For some materials these errors may reach amounts several times larger than the standard deviation of a single range measurement. Some scanners which provide some type of aperture adjustment show errors in the first points after the laser spot has reached an area of a reflectivity

differing considerably from the previous area, and it can be observed that the correct range is achieved only after a few points have been measured. For objects consisting of different materials or differently painted or coated surfaces, one has always to expect serious errors. These can only be avoided if the object is temporarily coated with a unique material which is not applicable in most cases.

Another optical characteristics is nonuniformity. When object contains adjacent surfaces with different reflection characteristics, apparent shift of projected rays in relation to response reflected rays occurs, which can lead to error in 3D point registration.

Sources of uncertainty related to measurement method

This category of influences includes measuring strategy: configuration, number and distribution of measuring points, sampling, filtering, definition of measurement task, measurement process planning, equipment handling, fixturing, as well as operator's influence: training, experience, care, and integrity.

3D scanning strategy should be chosen according to scanned object's characteristics and the measurement objective. This strategy includes appropriate object positioning, in a way that will cause as little shadows as possible. Shadows can lead to holes in the scanned object, and lost details. The light should shine with equal intensity over the object. If some parts are more bright than others, the scanner adjusts its exposure according to the available light, and this will cause the less-illuminated parts of the objects to come out too dark. The number of complementary scans whose results are joined in data processing should be chosen carefully, as an optimum between the scan speed and scan accuracy.

The resolution (meaning number and distribution of measuring points) is usually adjustable, and 3D scanners offer different resolution modes. Uncertainty is directly proportional to scanner resolution. Some authors [103] suggest that uncertainty is 1/12 of the resolution.

Filtering includes standard optical filters for image noise reduction, and manual cleaning of unnecessary points. For example, fixturing assembly is not part of the final scan, but it will be scanned. Manual processing necessarily introduces errors and increases uncertainty, since only operator's skills determine which points will be ignored and which will remain in final scan. The scan refinement is also sensitive part of scanning procedure, and methods such as hole filling, trimming or alignment should be performed carefully and in correct sequence order.

Since only one side of metal is scanned, one must ensure that the measured features are properly offset to account for metal thickness, which is considered to be constant.

The user of the system can greatly influence the performance of any measurement system. Algorithm selection, sampling strategies, and even the location and orientation of the part can affect the uncertainty of measurements. For this reason, scanning personnel must be required to maintain a higher level of competency. Formal, documented procedures should be available for reference.

Part fixturing leads to part distortion within the holding fixture. Other concerns involve the dynamic properties of the fixture's material, but this depends on the application. For example, given a situation where the temperature is unstable and the part is fixtured for a longer period of time, either prior to machine loading or during the inspection, distortion to the fixture translates into distortion of the part. Additional environmental concerns involve the fixture's effect on lighting parameters. Other sources include utility concerns, where air pressure fluctuations can distort parts or affect the ability of the fixture to hold the part securely in place. Other concerns are with regard to the fixtures performance in reproducibility, between machines, and between operators. The sensitivity of fixturing factors is highly dependent on environmental conditions, part and fixturing materials, and the measurement system capability required.

Scanning hardware's influences on uncertainty

Identifying error sources associated with the equipment itself sometimes can be easily accomplished [1]. First, many standards and technical papers discuss the defects of various machine components and methods of evaluation. Second, measurement system manufacturers publish specifications of machine performance capabilities. These two sources provide most of the information required.

The most common influences include: instrument resolution, discrimination threshold, changes in the characteristics or performance of a measuring instrument since its last calibration, incidence of drift, parallax errors, approximations and assumptions incorporated in the measurement method and procedure, cameras, projection system.

The scanning hardware influences could be classified into the following categories: structural elements of the scanner, measurement point and measurement volume forming method, and system calibration [96].

Structural elements encompass image digitizing systems, optical elements, light source and movable components. Image digitizing is performed by means of CCD or CMOS optical sensor arrays. Fringe projection scanner used in this research has monochromatic sensor array, and laser scanner is capable of colour detection. Colour does not contribute to measurement information, it is only used for visualisation of results. On the contrary, the colour of scanned surface has strong influence onto number of points acquired per surface area, regardless of colour capabilities of scanner's sensor.

Optical elements (lenses, prisms, mirrors, aperture) influence detected image quality, due to various phenomena, such as: speckle, depth of field, spherical aberration, chromatic aberration, lateral chromatic aberration, coma, astigmatism, field curvature, curvilinear distortion, decentring distortion. These influences are well investigated and documented and they are usually avoided through scanner calibration.

Light sources can have various intensity. Laser light is very coherent, and it can be focused and controlled more precisely than non-coherent light beam (used in fringe projection scanners). Coherent light scanners are less sensitive to speckle errors, but their light intensity decreases with distance, and they can be used only for short distance scanning.

3D scanners usually have no movable components, with exception of light sources (fringe projectors or lasers). Fringe projector errors are eliminated using Gray binary code for detection of projected stripes. The movable components can include part fixturing mechanisms and rotational tables for automated segmented scanning.

Measurement point and measurement volume forming method influences include influence of sensor geometry to projected position and shape of measurement point on surface of scanned object, as well as the mathematical definition of basic principles, such as optical triangulation. This also includes the reference points used for alignment of partial scans into the final point cloud. The mathematical model is difficult to be determined, due to undocumented correction functions implemented by 3D scanner manufacturers.

System calibration is performed on objects with exactly defined shape and geometry, taking in account the lightning conditions, the light source temperature and intensity, and settings of sensors and other optical elements. Most 3D scanners perform the autocalibration, or alert user when manual calibration is needed.

Sources of uncertainty related to data processing software

Data analysis software has become increasingly important in modern dimensional measurement systems, such as 3D scanners, vision systems, theodolites, photogrammetry, and coordinate measuring machines. Software computations to convert raw data to reported results can be a major source of error in a measurement system. The phrase "computational metrology" is used to describe how data analysis computations affects the performance of measurement systems.

The influences related to data processing software include: algorithms (simplified calculations to improve response time), robustness (ability to recover from invalid input data), reliability (effects of variations in input data), compliance to geometric dimensioning and tolerancing (GDT) standards and correction algorithms (volumetric and temperature) [1]. They also include the errors in values of constants, corrections and other parameters used in data evaluation.

This part of measurement chain is the least documented and mathematical models behind the software are considered intellectual property protected with copyrights, trademarks, patents, industrial design rights and trade secrets. This limitation is overcame with relying on scanning equipment calibration and traceability certificates, and with manufacturer declared uncertainty.

Sources of uncertainty related to simulation software

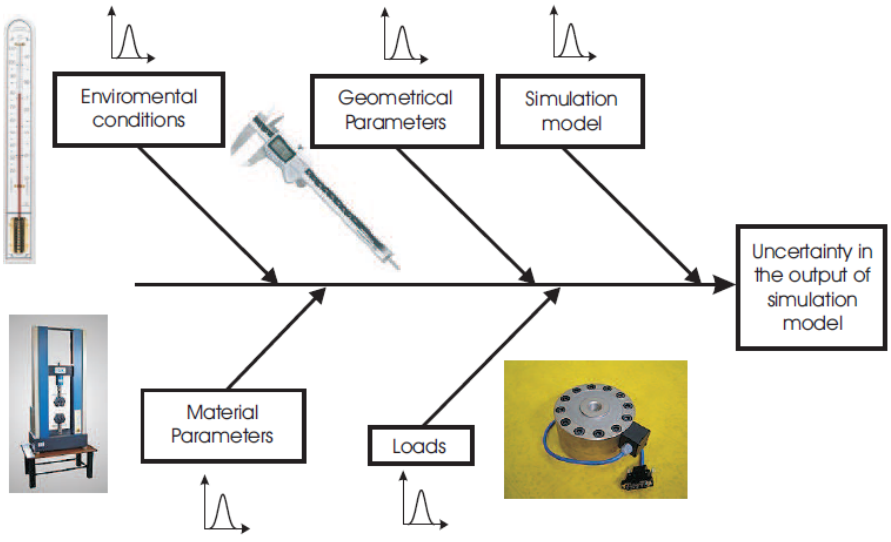

Fig. 8.3. Propagation of measurement uncertainties through simulation model [100]

Fig. 8.3 illustrates the influences of input parameters on uncertainty in the output of simulation model. The simulation is influenced with more parameters than the real experiment, since it

involves more assumptions and approximations, requires more input data and all these parameters have uncertainties that propagate to the final result.

When finite element simulation is performed, the uncertainty influences can be categorised into: mathematical model, domain, boundary conditions, discretization, solving algorithms and post-processing.

The mathematical model defines how well the material formulation in the FE software represents the actual material. This requires knowledge about material properties, such as structural strength, thermal expansion coefficient, Poisson's ratio, anisotropy, etc.

The domain implies geometric simplifications incorporated into the model, such as omission of small details, and the extent of the model surrounding the area of interest. It also includes the approximations by representing a portion of 3D structure with a 2D model, with assumption of uniform sheet metal thickness.

The boundary conditions have the essential influence on the result, since they form the stiffness matrix, along with material properties. This combination defines how the structure will behave under the applied loads and restraints.

Discretization refers to the primitives (finite elements) which represent the model's geometry. Finite elements have limitations on the behaviour that they can represent. This may not just be limited to the accuracy of the approximation of displacement or stress (for example) across an element but can also include an inability to represent some types of behaviour entirely. Examples in structural analysis include shear representation in certain types of shell elements and more obviously, beam elements not representing local stress concentrations for example, where a bracket might be attached or two beams are connected together.

Solver algorithms are usually iterative programming structures, which rely on convergence criteria. These criteria define the accuracy and precision of the result.

Post-processing can lead to misinterpretation of results, since FEM software have very adjustable visualisation settings. For example, the thin-shell models can express results on various layers of the element. Stress results are usually presented as Von-Mises equivalent stresses, and in some cases other stress components are required, such as shear stress or maximum principal stress. The displacement results can be distorted for visualisation purposes.

The Fig. 8.4 summarizes the abovementioned influence factors in an Ishikawa diagram, which is an upgrade to diagram presented in [79]. The blue portion of the diagram (Simulation software) is relevant only when numerical simulations are integrated into the measurement system.

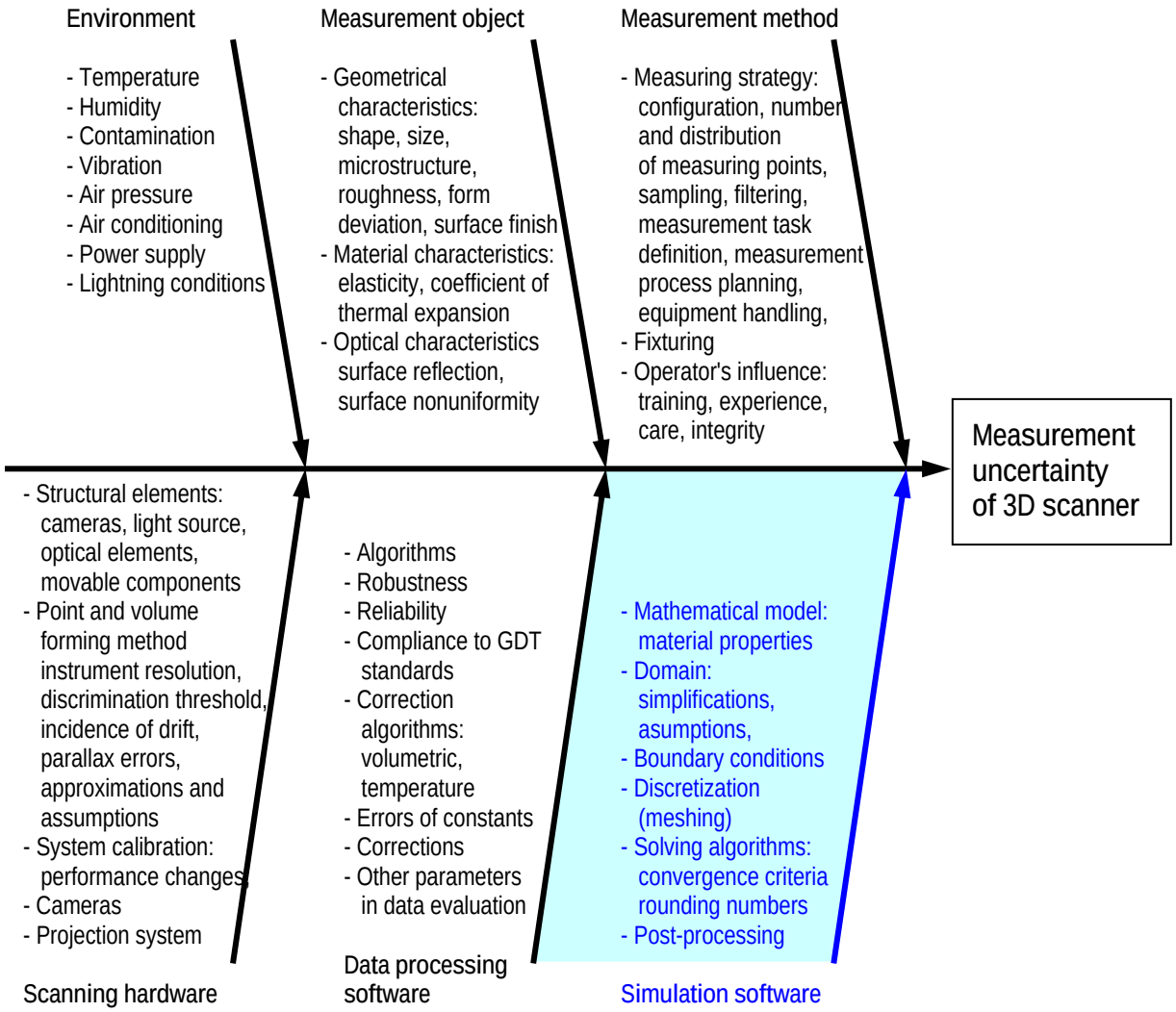

Fig. 8.4. Influences on measurement uncertainty of 3D scanner

This survey indicates the existence of a large number of influential parameters, which by its cause and effect impact on measurement uncertainty of optical 3D scanners. These factors are unique for each particular scanning system because of its specificity caused by construction or by mathematical model used. To fully understand the impact of each influence factor and their interaction, there would be necessary to carefully prepare a series of experiments that would take into account only the specific impact of individual factor. Such an exhaustive analysis is out of the scope of this research. Therefore only the most influencing factors, chosen according to the subjective opinion, will be used in further analysis, especially in forming the mathematical model of the measurement system.

8.2. Mathematical model of measurement system

To develop the uncertainty budget, it is necessary to model the measurement process by a functional relationship. This should identify all measured input quantities that will ultimately be combined to arrive at the value of the output quantity, or measurand, and should indicate the manner in which they are to be combined. In general terms, the functional relationship between the output quantity, y, and the N estimated input quantities, x_i, is in the form $y = f(x_1, x_2, ... x_N)$ but a more specific relationship should be identified where possible.

Some efforts [113, 114] to derive mathematical models of 3D scanners are noticed lately, but they still do not provide enough information to perform the exhaustive measurement uncertainty analysis. Fig. 8.5 shows the model for one component, the coordinate system transformation.

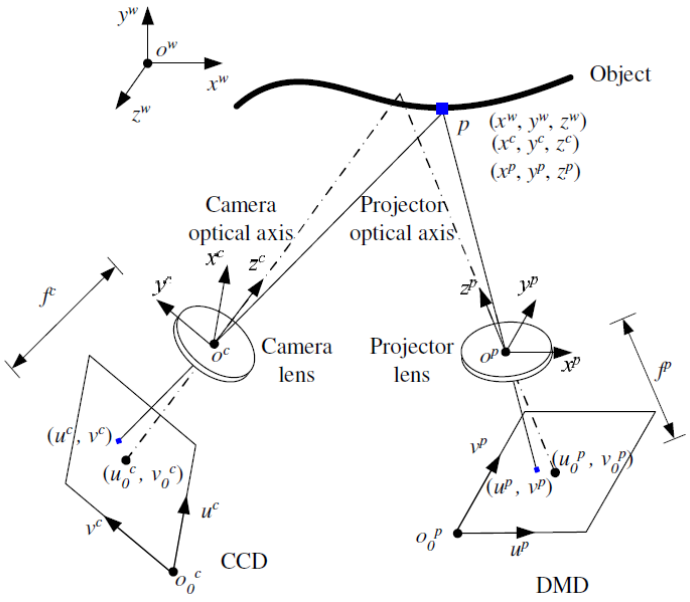

Fig. 8.5. Structured light 3D scanner configuration [113]

Two major types of mathematical models exist for fringe projection systems, optical geometry based and calibration matrix based [104]. The optical geometry based models describe the relationship between the image and the surface shape of the object using a number of equations and parameters that are derived from the optical geometry models of the camera and the projector. Calibration matrix based models use coefficients matrices to describe the measurement volume, which is defined as the intersection of the camera's field-of-view and the projection space of the projector. The calibration matrix based approach is simpler and easier to implement, but has disadvantages, such as truncation errors and the need for repeated calibration procedures.

The major problem in definition of the mathematical model of the whole system is lack of documented relationships and variations of input and intermediate parameters, in terms of both hardware and software. Therefore, some parts of the system will be observed as "black boxes", relying on manufacturer's declarations on uncertainties for these parts.

The output quantity in this case is the diameter (D) or radius (R) of the circular cross-section of the scanned part observed 10 mm below top (nominal value R_0 = 46 mm). The input quantities will be derived from the influence factors. The most important input quantities are:

- Displacements (R_F - R_C) due to physical clamping deformation(u_0). The value is calculated from equivalent average radii presented in Table 6.3. (standard deviation of the difference between equivalent radius of clamped and unclamped part).

- Temperature variation (u_1). Experiment was performed in air-conditioned room at 22±2°C, ΔT=±2°C, thermal expansion coefficient (for steel, $\alpha=1{,}2\cdot10^{-5}$ °C^{-1})

$$\frac{\partial R}{\partial \Delta T} = R_0 \cdot \alpha = 46 \cdot 1{,}2 \cdot 10^{-5} = 0{,}00055 \quad \text{(8.1)}$$

  Although it is common to use the type A and normal, or even U-shaped distribution for temperature influence, temperatures in this experiment were not statistically determined, but taken from declared laboratory conditions. Therefore, it is justifiable to assume type B and rectangular distribution.

- Variations in material properties related to springback (u_2). Springback depends on a complex interaction between material properties, part geometry, die design, and processing parameters. Material yield stress ($R_{p0,2}$) was taken as a property related to springback. Standard deviation of $R_{p0,2}$ from Table 4.2. is used to describe this influence of material elastic properties. The nominal radius R_0 = 46 mm, and Young's modulus E = 210000 MPa are used to determine its influence.

$$R_{p0,2} = E \cdot \frac{R - R_0}{R_0} \quad \Rightarrow \quad R = R_0 + R_0 \cdot \frac{R_{p0,2}}{E} \quad \text{(8.2)}$$

$$\frac{\partial R}{\partial R_{p0,2}} = \frac{R_0}{E} = 0{,}00022 \quad \text{(8.3)}$$

- Other material properties, such as deformation strengthening exponent (n), hardening coefficient (C) and normal anisotropy factor (r) have no influence on springback [106]. On the other hand, it is not possible to express the implicit relationship (8.4) between the radius R and the deformation strengthening exponent (value n from Table 4.2) as an explicit equation. The consequence is lack of sensitivity coefficient. Therefore, this value cannot be used, not even as Type B influence.

$$\sigma = C \cdot (\varphi)^n, \qquad \varphi = \ln \frac{R_0}{R} \quad \text{..... (8.4)}$$

- The difference between the ideal radius and the equivalent scanned radius of the circular cross-section in undeformed position ($R_F - R_0$). This parameter indicates scanning errors related to method and manufacturing errors of a real part (u_3), and its value is determined from Annex D (standard deviation of free part radii).

- Scanned data conversion errors (u_5). Standard deviation of conversion errors is taken from Table 5.2. Sensitivity coefficient is 0,5 (the radius is half of the diameter).

- Displacements ($R_F - R_S$) due to simulated clamping deformation (u_6). This influence is related to method. The value is calculated from maximum deviation between the ideal CAD contour and the contour of part with simulated clamping, from Table 7.2.

The parts of a measurement system which will be observed as "black boxes" include:

- 3D scanner accuracy, as declared by manufacturer (u_4)

- Data processing software deviations evaluated according to possible numerical computation error (u_7). This uncertainty can result from round-off or computer truncation error, the linear interpolation of tabulated values, or using curve fit equations [112]. Computation uncertainty is usually determined heuristically. The uniform distribution is applicable for round-off or computer truncation error. The triangular distribution is appropriate for describing errors resulting from linear interpolation or curve fit equations. The value is calculated from maximum deviation between the scanned contour of physically clamped part and the contour of part with simulated clamping, given in Table 7.2.

The computation uncertainty covers data processing error sources such as rounding, truncation, triangulation, smoothing, and orientation, and it will be discussed in more details.

Commercial FEM software such as NASTRAN uses double-precision arithmetics in calculations. This approach uses 54 binary digits to represent each number in matrices used to describe the mathematical models. Even if single-precision arithmetic is used (with 27 binary digits), the round-off error ratio is around $2^{-27} \approx 7 \cdot 10^{-9}$ (multiplied by calculated values of stress and displacement). Such errors can surely be neglected if one compares them with other error sources.

In order to numerically express the data processing (simulation) software deviations, it is necessary to perform a complex verification and validation (V&V) process [108]. Model verification is a confirmation process that a model can accurately represent the given mathematical model [115]. On the other hand, model validation is a confirmation process that the prediction of a model can adequately predict the underlying physics. In other words, a valid model must well approximate the physical behaviour with a satisfactory level of accuracy. Therefore, experimental results are essential to test the validity of a model. However, experimental results are not assumed to be more accurate than computational results due to uncertainties associated with the experiments. Fig. 8.6 explains the distinction between the verification and validation of a simulation.

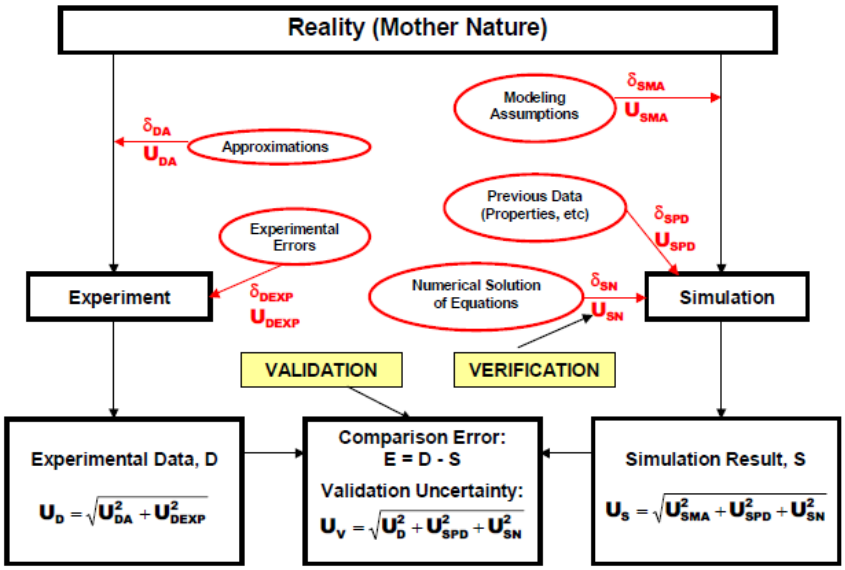

Fig. 8.6. Schematic of Verification and Validation of a Simulation [116]

The accuracy indicates the closeness of agreement between a simulation/experimental value of a quantity and its true value [119]. Error δ is the difference between a simulation value or an experimental value and the truth. As the true values of simulation/experimental quantities are rarely known, errors must be estimated. An uncertainty U is an estimate of an error such that the interval 6U contains the 95% of true value of δ.

Validation is defined as a process for assessing simulation uncertainty U_S by using benchmark experimental data and, when conditions permit, estimating the sign and magnitude of the simulation error δ_S. The comparison error E is defined as the difference of the experimental data D and the simulation result S:

$$E = D - S = \delta_D - \left(\delta_{SMA} + \delta_{SPD} + \delta_{SN}\right) \quad (8.5)$$

where δ_D, δ_{SMA}, δ_{SPD} and δ_{SN} are errors from from experimental data, modelling assumptions, previous data and numerical solution of equations, respectivelly [119]. The model is then validated by comparing the uncertainty U_E in the comparison error with the comparison error E:

$$U_E^2 = U_D^2 + U_{SMA}^2 + U_{SPD}^2 + U_{SN}^2 \quad (8.6)$$

Since there is currently no known method to estimate the uncertainty of modelling assumptions U_{SMA}, the alternative approach is used, by comparing the validation uncertainty U_V with E:

$$U_V^2 = U_E^2 - U_{SMA}^2 = U_D^2 + U_{SPD}^2 + U_{SN}^2 \quad (8.7)$$

The validation is achieved at the U_V level if the absolute value of E is less than the validation uncertainty U_V [119]. The error from the modelling assumptions δ_{SMA} can be determined in special case, when U_V is significantly smaller than E; then δ_{SMA} is equal to the comparison error E.

Significant efforts are put in the past decade in order to standardize the V&V process. The American Society of Mechanical Engineers (ASME) developed two Guides on Verification and Validation; one in Computational Fluid Mechanics (G-077-1998e) and another in Computational Solid Mechanics (PTC 60/V&V 10-2006). In both Guides, the determination of computational uncertainty is quite similar to metrology approach (such as GUM), and it relies on experimental data. It is necessary to identify and quantify the error sources, to model their relationships, perform simulation calculations, and finally to quantify the output uncertainty.

One limitation of existing model validation approaches is that they are restricted to validation at a particular design setting [55]. There is no guarantee that the conclusion can be extended over the entire design space. In addition, model validations are frequently based on comparisons between the output from deterministic simulations and output from single or repeated experiments. Existing statistical approaches, for which the physical experiment has to be repeated a sufficient number of independent times, is not practical for many applications, simply due to the cost and time commitment associated with experiments. Furthermore, deterministic simulations for model validation do not consider uncertainty at all. Although recent model validation approaches propose to shift the effort to propagating the uncertainty in model predictions, which implies that a model validation should include all relevant sources of uncertainties, little work has been accomplished in this area. Because realistic mathematical models should contemplate uncertainties, the assessment of the validity of a modelling approach must be conducted based on stochastic measurements to provide designers with confidence in using a model.

Traditionally, a model has been considered valid if it reproduces the results with adequate accuracy [110]. The two traditional model validation approaches are 1) subjective and 2) quantitative comparisons of model predictions and experimental observations. Subjective comparisons are through visual inspection of x–y plots, scatter plots, and contour plots. Although they show the trend in data over time and space, subjective comparisons depend on graphical details. Quantitative comparisons, including measures of correlation coefficient and other weighted and nonweighted norms, quantify the "distance" but become very subjective when defining what magnitudes of the measures are acceptable. To quantify model validity from a stochastic perspective, researchers have proposed various statistical inference techniques, such as $\chi 2$ test on residuals between model and experimental results. These statistical inferences require multiple evaluations of the model and experiments, as well as many assumptions that are difficult to satisfy. Therefore, there is a need for a model validation approach that uses the least amount of statistical assumptions and requires the minimum number of physical experiments.

The other influence factors shown in Fig 8.4 were neglected, because they did not vary to a significant extent during the experiment.

The influence factors for the two models of measurement system are summarized in Fig. 8.7.

Influence factors			Category of influence factors
Model 1: Physically clamped part	**Symbol**	**Model 2: Simulated clamping**	
Clamping assembly	u_0	-	Method
Temperature	u_1	Temperature	Environment
Material	u_2	Material	Scanned object
Scanning errors	u_3	Scanning errors	Method
Scanner accuracy	u_4	Scanner accuracy	Scanning hardware
Rounding	u_5	Rounding	Data processing software
Truncation		Truncation	Data processing software
Triangulation		Triangulation	Data processing software
Smoothing		Smoothing	Data processing software
Orientation		Orientation	Data processing software
Data conversion		Data conversion	Data processing software
-	u_6	Simulated deformation	Method
-	u_7	Material properties	Simulation software
-		Boundary conditions	Simulation software
-		FE mesh density	Simulation software
-		Post processing (data conversion)	Simulation software

Fig. 8.7. Models of measurement system: (1) Physically clamped part, (2) Simulated clamping

8.3. GUM-based uncertainty analysis

Tables 8.3 and 8.4 show the expanded uncertainty of the two models of measurement system.

Table 8.3. Uncertainty budget associated with the determination of the circular cross-section radius of the physically clamped filter housing:

Symbol	Source of uncertainty x_i	Standard uncertainty $u(x_i)$	Distribution	Divisor	Type	Sensitivity coefficient c_i	Uncertainty contribution u_i
u_0	Physical clamping deformation	± 0,012 mm	Normal	1,0	A	1,0	0,012 mm
u_1	Temperature	± 2 °C	Rectangular	√3	B	0,00055	0,00064 mm
u_2	Material properties	± 13,89 MPa	Normal	1,0	A	0,00022	0,0031 mm
u_3	Scanning errors	± 0,044 mm	Normal	1,0	A	1,0	0,044 mm
u_4	3D scanner accuracy	± 0,010 mm	Rectangular	√3	B	1,0	0,0058 mm
u_5	STL data conversion	± 0,010 mm	Normal	1,0	A	0,5	0,0051 mm
u(R)	Combined standard uncertainty		Normal	$u(R)=\sqrt{\sum_{i=0}^{5} u_i^2}$			0,046 mm
U	Expanded uncertainty		Normal (k=2)	$U = k \cdot u(R)$			0,093 mm

The circular cross-section radius of physically clamped part was **46.00 mm ± 0.09 mm**. The reported expanded uncertainty is based on a standard uncertainty multiplied by a coverage factor k=2, providing a coverage probability of approximately 95%. The uncertainty evaluation has been carried out in accordance with GUM requirements.

Table 8.4. Uncertainty budget associated with the determination of the circular cross-section radius of the filter housing with simulated clamping.

Symbol	Source of uncertainty x_i	Standard uncertainty $u(x_i)$	Distribution	Divisor	Type	Sensitivity coefficient c_i	Uncertainty contribution u_i
u_1	Temperature	± 2 °C	Rectangular	√3	B	0,00055	0,00064 mm
u_2	Material properties	± 13,89 MPa	Normal	1,0	A	0,00022	0,0031 mm
u_3	Scanning errors	± 0,044 mm	Normal	1,0	A	1,0	0,044 mm
u_4	3D scanner accuracy	± 0,010 mm	Rectangular	√3	B	1,0	0,0058 mm
u_5	STL data conversion	± 0,010 mm	Normal	1,0	A	0,5	0,0051 mm
u_6	Simulated deformation	± 0,0075 mm	Normal	1,0	A	1,0	0,0075 mm
u_7	Numerical computation	± 0,024 mm	Triangular	√6	B	1,0	0,010 mm
u(R)	Combined standard uncertainty		Normal	$u(R)=\sqrt{\sum_{i=1}^{7}u_i^2}$			0,046 mm
U	Expanded uncertainty		Normal (k=2)	$U=k\cdot u(R)$			0,093 mm

The circular cross-section radius of the filter housing with numerically simulated clamping was **46.00 mm ± 0.09 mm**. The reported expanded uncertainty is based on a standard uncertainty multiplied by a coverage factor k=2, providing a coverage probability of approximately 95%. The uncertainty evaluation has been carried out in accordance with GUM requirements.

The expanded measurement uncertainties for both models, with physical and with simulated clamping, have identical values, which means that uncertainty contributions, which are not common for both methods (u_0, u_6, u_7) have the same intensity.

Fig. 8.8 illustrates the influence of uncertainty components presented in Tables 8.3 and 8.4. A closer look at uncertainty budget reveals that major contribution to uncertainty comes from scanning errors (u_3) which include method related errors and real part imperfections. Other sources of error are significantly smaller in both methods used.

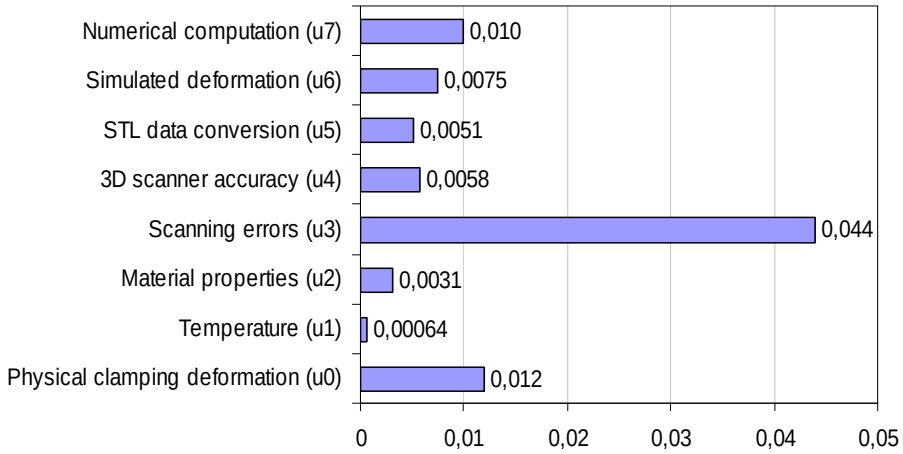

Fig. 8.8. Graphical comparison of uncertainty contributions

To check these results, the expanded uncertainty was also calculated for 5 sets of samples, which were manufactured from 5 different sheet metal rolls. These results are presented in Fig. 8.9 and in Table 8.5.

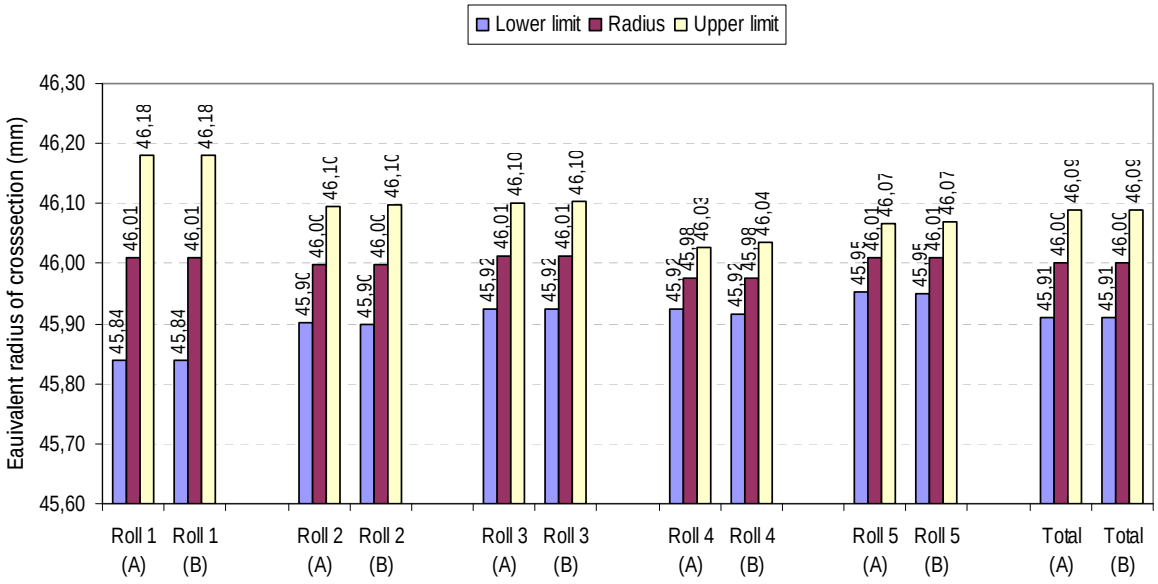

Fig. 8.9. Equivalent radii of cross-section with expanded uncertainties calculated in accordance with GUM requirements: (A) Physically clamped part, (B) Simulated clamping

As shown in Fig.8.9, there is almost no difference in expanded measurement uncertainty of physically clamped samples and samples with numerically simulated clamping. There are some variations between the different rolls of sheet metal, but the uncertainty analysis performed above showed that these variations are not due to different material properties, but they come from the variations of manufacturing quality of individual parts.

Table 8.5. Radii with expanded uncertainties calculated for 5 different sheet-metal rolls.

Roll	Model 1 (physically clamped)	Model 2 (simulated clamping)
1	46.01 mm ± 0.17 mm	46.01 mm ± 0.17 mm
2	46.00 mm ± 0.10 mm	46.00 mm ± 0.10 mm
3	46.01 mm ± 0.09 mm	46.01 mm ± 0.09 mm
4	45.98 mm ± 0.05 mm	45.98 mm ± 0.06 mm
5	46.01 mm ± 0.06 mm	46.01 mm ± 0.06 mm
Total	46.00 mm ± 0.09 mm	46.00 mm ± 0.09 mm

As Fig. 8.8 suggests, the largest contribution to the measurement uncertainty in both cases comes from the scanning errors (u_3). Therefore, it is justifiable to analyse it in more details. These errors include both method related scanning errors and manufacturing errors of a real part. To eliminate the influence of manufacturing errors, the samples were measured on a highly accurate 3D coordinate measuring machine (CMM). The results are presented in Table 8.6.

Table 8.6. Equivalent radii (mm) measured on 3D coordinate measuring machine.

Sample	Roll 1	Roll 2	Roll 3	Roll 4	Roll 5	Total
1	46,073	46,066	46,047	46,014	46,063	
2	46,084	46,079	46,054	45,998	46,063	
3	46,086	46,062	46,059	46,004	46,064	
4	46,068	46,063	46,044	46,014	46,058	
5	46,054	46,064	46,060	46,010	46,060	
Average	46,073	46,067	46,053	46,008	46,061	46,052
St. deviation	0,013	0,007	0,007	0,007	0,002	0,025

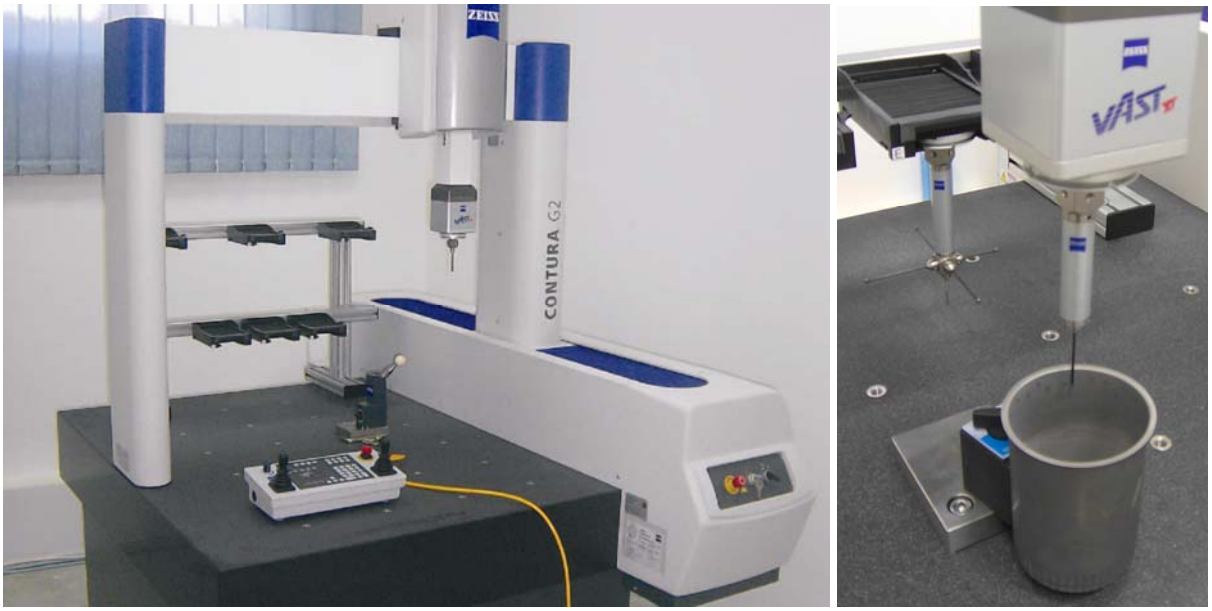

Fig. 8.10. 3D coordinate measuring machine Carl Zeiss Contura G3

The measurements were performed with 3D Coordinate measuring machine Zeiss Contura G2 700 Aktiv, measurement range: 700x1000x600 mm, measurement uncertainty according to ISO 10360-2: MPE_E=(1,8+L/300 μm, MPE_P=1,8 μm), Fig. 8.10.

To eliminate the manufacturing errors from the scanning errors (u_3), it is necessary to create the uncertainty budget, as shown in Table 8.7. The combined standard uncertainty (u_3) consists of manufacturing errors ($u_{3\text{-}1}$), 3D CMM accuracy ($u_{3\text{-}2}$) and 3D scanning ($u_{3\text{-}3}$).

Table 8.7. Uncertainty budget associated with the scanning errors.

Symbol	Source of uncertainty $x_{3\text{-}i}$	Standard uncertainty $u(x_{3\text{-}i})$	Distribution	Divisor	Type	Sensitivity coefficient $c_{3\text{-}i}$	Uncertainty contribution $u_{3\text{-}i}$
$u_{3\text{-}1}$	Manufacturing errors	± 0,025 mm	Normal	1,0	A	1,0	0,025 mm
$u_{3\text{-}2}$	3D CMM accuracy	± 0,0018 mm	Rectangular	√3	B	1,0	0,0010 mm
$u_{3\text{-}3}$	3D scanning method	?	Normal	1,0	A	1,0	?
u_3	Combined standard uncertainty		Normal	$u_3 = \sqrt{\sum_{i=1}^{3} u_{3-i}^2}$			0,044 mm

To determine the measurement uncertainty of 3D scanning method ($u_{3\text{-}3}$), it is necessary to adjust the equation (8.2):

$$u_{3-3} = \sqrt{u_3^2 - u_{3-1}^2 - u_{3-2}^2} \quad \text{..... (8.8)}$$

When values from Table 8.7 are used in equation (8.8), the measurement uncertainty of 3D scanning method $u_{3\text{-}3}$ is calculated as 0,036 mm.

The remaining uncertainty contributions are related to deviations of real parts, referred as manufacturing errors ($u_{3\text{-}1}$) and declared measurement uncertainty of 3D coordinate measuring machine ($u_{3\text{-}2}$). The calculated values show that method-related 3D scanning errors are dominant in digitizing applications.

An exhaustive analysis of these errors, for 3D scanners based on laser triangulation, was performed in [117] and [118]. Most of the optical parameters, which can be adjusted during the laser scanning process were widely analysed by Korošec et al. [117]. They evaluated the influence of sensor-surface distance, surface lean angle and their interaction on the accuracy of scanning results. The results showed that these two parameters have an important influence on the

accuracy of gathered information. Vukašinovič et al. analysed the influence of surface colour in [118]. They proposed that some model uncertainties may be attributed to the lack of some geometrical and topological properties (curvature, slope gradient etc.) of the scanning object.

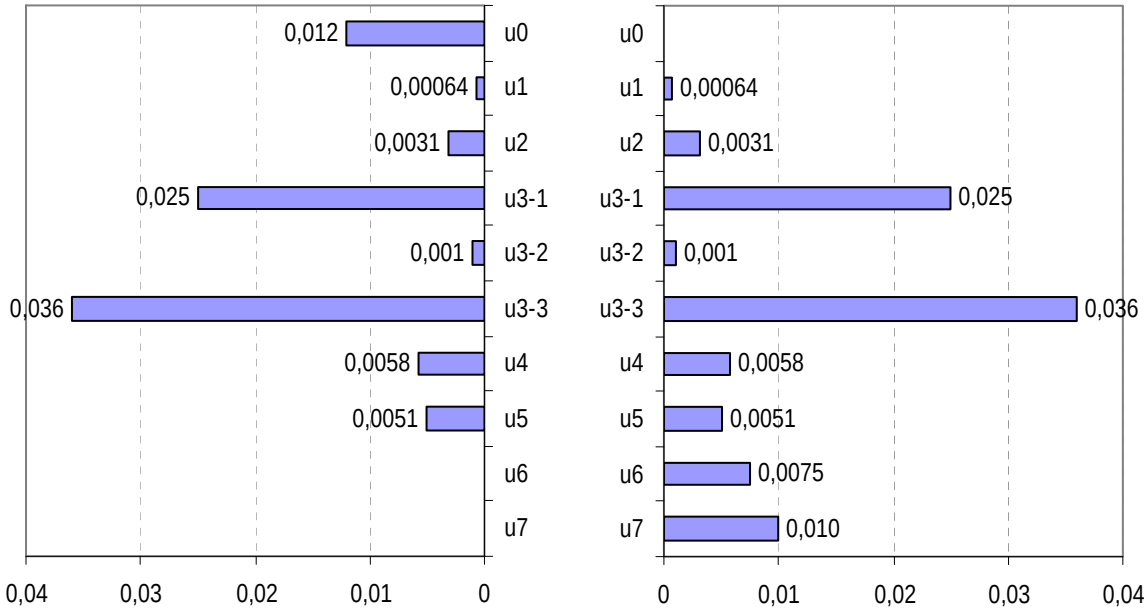

(a) Physical clamping (b) Simulation

Fig. 8.11. Graphical comparison of uncertainty contributions

Fig. 8.11 summarizes uncertainty contributions for physical clamping and simulation (u_0: Physical clamping deformation, u_1: Temperature, u_2: Material properties, $u_{3\text{-}1}$: Manufacturing errors, $u_{3\text{-}2}$: 3D CMM accuracy, $u_{3\text{-}3}$: 3D scanning method, u_4: 3D scanner accuracy, u_5: STL data conversion, u_6: Simulated deformation, u_7: Numerical computation). In both cases, the major contribution comes from the 3D scanning method. The total uncertainty in both cases is the same, since some contributions appear only when part is physically clamped (u_0), while other appear only in simulation (u_6, u_7). These contributions compensate each other.

According to results presented in this research, and the achievements of other researchers, we can suggest that further researches should be performed to analyse the influence factors for fringe-projection 3D scanners in more detail.

9. Statistical analysis

The results of experiments and simulations performed are subjected to statistical analysis, in order to test the hypothesis set in introduction. The results of experiments and simulations are summarized in Table 9.1.

Table 9.1. The results of experiments and simulations averaged per sheet-metal rolls.

	Yield stress $R_{p0,2}$	Anisotropy r_{10}	Deformation strengthening exponent n	Hardening coefficient C	Model 1: Physical clamping		Model 2: Simulated clamping	
					Maximum displacement	Expanded uncertainty	Maximum displacement	Expanded uncertainty
Roll	MPa	-	-	N/mm	mm	mm	mm	mm
1	153,69	2,04	0,223	509,66	0,023	0,17	0,049	0,17
2	147,08	2,05	0,229	501,77	0,030	0,10	0,060	0,10
3	160,01	1,96	0,215	502,92	0,023	0,09	0,048	0,09
4	152,11	1,98	0,222	510,39	0,039	0,05	0,055	0,06
5	148,85	1,95	0,222	509,45	0,032	0,06	0,066	0,06

The first step in statistical analysis is to determine whether observed parameters are correlated. Table 9.2 shows calculated Pearson correlation coefficients between parameters presented in Table 9.1. The strongest correlation exists between the expanded uncertainties of simulated and scanned data. This correlation is significant at the 0,01 level (2-tailed).

Experimental results confirm the statements given in previous chapters, that some material properties have almost no influence on springback and related measurement uncertainty. The weakest correlation exists between the hardening coefficient and calculated uncertainties. The maximum displacements depend to some extent on yield stress, while yield stress has almost no influence onto uncertainty of results in neither of two models.

Table 9.2. Pearson correlation coefficients between observed parameters.

	Yield stress $R_{p0,2}$	Anisotropy r_{10}	Deformation strengthening exponent n	Hardening coefficient C	Maximum physical displacement	Expanded uncertainty of scanned data	Maximum simulated displacement	Expanded uncertainty of simulated data
Yield stress $R_{p0,2}$	1							
Anisotropy r_{10}	-0,364	1						
Deformation strengthening exponent n	-0,895	0,735	1					
Hardening coefficient C	-0,115	-0,243	-0,064	1				
Maximum physical displacement	-0,535	-0,235	0,318	0,403	1			
Expanded uncertainty of scanned data	0,179	0,697	0,156	-0,058	-0,761	1		
Maximum simulated displacement	-0,833	-0,177	0,514	0,111	0,563	-0,540	1	
Expanded uncertainty of simulated data	0,185	0,712	0,161	-0,013	-0,719	0,996	-0,570	1

In order to test the hypothesis: "There is no difference between measurement uncertainty of simulated and physical clamping", a two-sample t-test for equal means was used. The data and the results are shown in Table. 9.3.

Table 9.3. Two-sample t-test for equal means of expanded uncertainties.

	Expanded uncertainty of scanned data (mm)					Expanded uncertainty of simulated data (mm)				
Values	0,17	0,10	0,09	0,05	0,06	0,17	0,10	0,09	0,06	0,06
Mean	0,094					0,096				
Variance	0,00223					0,00203				
Observations	5					5				
Pearson Correlation	0,996404									
Hypothesized Mean Difference	0									
df	4									
t Stat	-1									
P(T<=t) one-tail	0,18695									
t Critical one-tail	2,131847									
P(T<=t) two-tail	0,373901									

Since calculated value of t-test variable (-1) is smaller than the critical value (2,131847), the null hypothesis can be accepted. Therefore, the difference between mean values of extended measurement uncertainty of 3D scanned physically clamped products and 3D scanned products with numerically simulated clamping is not significant.

In order to evaluate the variation of material properties between different rolls of sheet metal used, ANOVA single factor analysis was performed using data presented in Annex A.

The null hypothesis: "The yield stress R_{p02} has the same value for all 5 sheet metal rolls" was tested. The results are given in Table 9.4.

Table 9.4. ANOVA single factor analysis for yield stress R_{p02}.

SUMMARY				
Groups	*Count*	*Sum*	*Average*	*Variance*
Roll 1	15	2305,3	153,6867	125,7127
Roll 2	15	2206,2	147,08	120,2774
Roll 3	15	2400,2	160,0133	88,58838
Roll 4	15	2281,7	152,1133	96,59124
Roll 5	15	2232,8	148,8533	481,3712

ANOVA						
Source of Variation	*SS*	*df*	*MS*	*F*	*P-value*	*F crit*
Between Groups	1508,534	4	377,1335	2,066392	0,094452	2,502656
Within Groups	12775,57	70	182,5082			

Since calculated value of F variable (2,066392) is smaller than the critical value (2,502656), the null hypothesis can be accepted. Therefore, the yield stress R_{p02} does not differ significantly between the 5 rolls of sheet metal used in this experiment.

The null hypothesis: "The deformation strengthening exponent (n) has the same value for all 5 sheet metal rolls" was tested. The results are given in Table 9.5.

Table 9.5. ANOVA single factor analysis for deformation strengthening exponent (n).

SUMMARY				
Groups	*Count*	*Sum*	*Average*	*Variance*
Roll 1	15	3,345	0,223	5,33E-05
Roll 2	15	3,437	0,229133	1,97E-05
Roll 3	15	3,219	0,2146	3,83E-05
Roll 4	15	3,337	0,222467	3,5E-05
Roll 5	15	3,33	0,222	3,97E-05

ANOVA						
Source of Variation	*SS*	*df*	*MS*	*F*	*P-value*	*F crit*
Between Groups	0,001599	4	0,0004	10,74722	7,55E-07	2,502656
Within Groups	0,002603	70	3,72E-05			

Since calculated value of F variable (10,74722) is larger than the critical value (2,502656), the null hypothesis can be rejected. Therefore, the deformation strengthening exponent (n) differs significantly between the 5 rolls of sheet metal used in this experiment.

The null hypothesis: "The hardening coefficient (C) has the same value for all 5 sheet metal rolls" was tested. The results are given in Table 9.6.

Table 9.5. ANOVA single factor analysis for hardening coefficient (C).

SUMMARY				
Groups	*Count*	*Sum*	*Average*	*Variance*
Roll 1	15	7644,9	509,66	165,274
Roll 2	15	7526,5	501,7667	522,4138
Roll 3	15	7543,8	502,92	179,4274
Roll 4	15	7655,8	510,3867	111,9741
Roll 5	15	7641,8	509,4533	270,9184

ANOVA						
Source of Variation	*SS*	*df*	*MS*	*F*	*P-value*	*F crit*
Between Groups	1026,987	4	256,7469	1,026981	0,399514	2,502656
Within Groups	17500,11	70	250,0015			

Since calculated value of F variable (1,026981) is smaller than the critical value (2,502656), the null hypothesis can be accepted. Therefore, the hardening coefficient (C) does not differ significantly between the 5 rolls of sheet metal used in this experiment.

The null hypothesis: "The anisotropy r_{10} has the same value for all 5 sheet metal rolls" was tested. The results are given in Table 9.6.

Table 9.6. ANOVA single factor analysis for anisotropy r_{10}.

SUMMARY				
Groups	*Count*	*Sum*	*Average*	*Variance*
Roll 1	15	31,94	2,129333	0,111521
Roll 2	15	32,63	2,175333	0,195098
Roll 3	15	30,94	2,062667	0,147992
Roll 4	15	30,93	2,062	0,104003
Roll 5	15	31	2,066667	0,20681

ANOVA						
Source of Variation	*SS*	*df*	*MS*	*F*	*P-value*	*F crit*
Between Groups	0,157219	4	0,039305	0,256751	0,904599	2,502656
Within Groups	10,71593	70	0,153085			

Since calculated value of F variable (0,256751) is smaller than the critical value (2,502656), the null hypothesis can be accepted. Therefore, the anisotropy r_{10} does not differ significantly between the 5 rolls of sheet metal used in this experiment.

10. Algorithm for automated measurement process

This chapter describes the novel algorithm for automated measurement process.

The initial algorithm (Fig. 10.1) used as a starting point in this analysis was developed in [5], and further evaluated in [79].

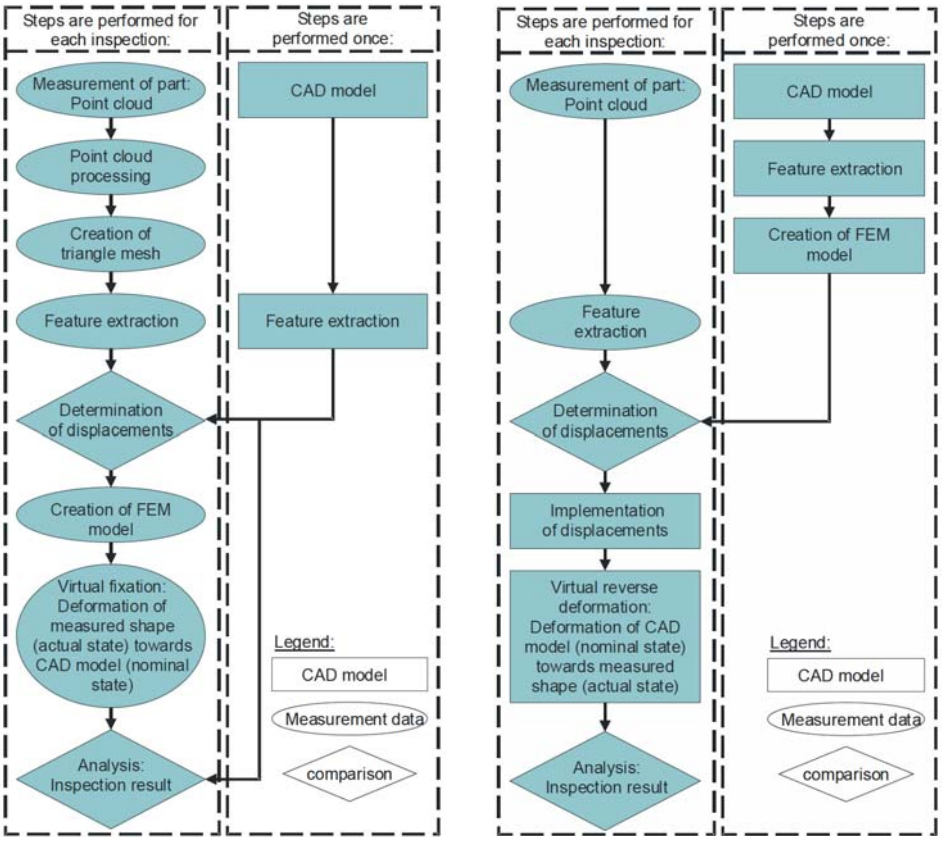

(a) Inspection process (b) Virtual fixation

Fig. 10.1. The initial algorithm for springback compensation in 3D scanning [79]

The algorithm presented in Fig. 10.1 is based on presumption that scanned part has some extractable features (such as holes, grooves, edges, etc.) which can be used to define boundary

conditions. The analysis performed in this dissertation showed that it is not always possible to define such boundary conditions. An illustrative example is edge of a hole: it is necessary to know the exact rotation and translation vectors in order to have realistic simulation of boundary conditions (as it was shown in Fig. 7.1).

However, that algorithm has some deficiencies which led to rather large measurement uncertainty (which was calculated to be ±0.7 mm). This research showed that the most important aspect of numerical simulation is careful definition of boundary conditions. Statistical analysis performed in Chapter 9 proved that virtual fixation of sheet metal components, which are deformed by springback, can have the same measurement uncertainty as the real clamping, but only with careful and proper boundary condition settings.

This analysis showed that, both for simple 2D contours and complex 3D shapes, the difference between the ideal and the scanned contour in undeformed position presents the major contribution to measurement uncertainty. These errors belong to the category of scanning errors related to method. Consequently, another step should be introduced into primary algorithm, which would ensure keeping these errors at their minimum.

Part orientation is also an important issue. When scanned parts have no extractable features, it is very hard and time-consuming to determine their proper position. One example of contour fitting is presented in Chapter 6.3, and computer program was developed (Annex C) to perform the contour fitting which can be used for circular contours.

And finally, to be able to use finite element analysis results for springback compensation in 3D scanning, the data converter software module should be implemented into FEM post-processors, to enable creating deformed CAD models based on FEM analysis results. This feature could also be used for optimization tasks, when CAD model features and parameters are varied in order to obtain the design with maximum performance, reliability and/or minimum weight.

Each step of the numerous data conversions (point cloud - tessellated surface - NURBS surfaces - FEM mesh - calculated displacements - point cloud - NURBS surfaces - toleranced dimensions) gradually contribute to increase in uncertainty. CAD data formats could be improved in order to simplify this process and to enable better exchangeability between these steps.

Fig. 10.2 shows the novel algorithm, with highlighted innovations (steps recognized as essential within this research, which were not defined or which were neglected in previous researches).

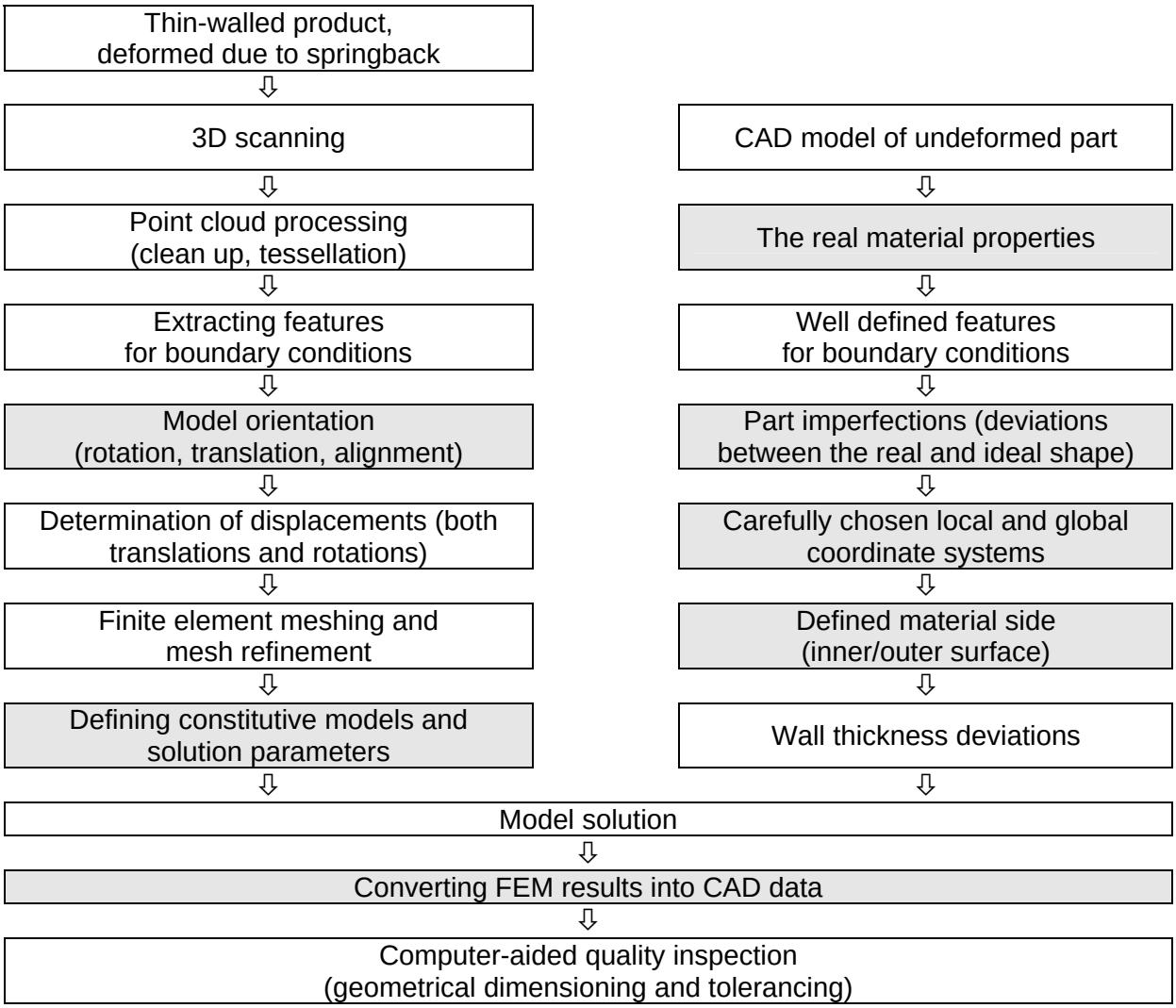

Fig. 10.2. Novel algorithm for springback compensation by numerical simulations

The important steps highlighted in Fig.10.2 will further be discussed, since they represent the improvement of previously used and currently available methods. All these steps should be taken in consideration when the measurement process is planned. Careful planning using this algorithm as a set of guidelines can minimise errors.

a) **The real material properties.** The material of samples used in this research had rather persistent properties, which did not vary significantly. That lead to minor contribution of material properties to total measurement uncertainty of this method. Such a result could mislead to neglecting the importance of material properties. Since this procedure (simulated clamping) is intended to be used in automated measurements in large-scale production, it is justifiable to assume that mechanical properties will have minor variations. However, it is well known that material properties have strong influence onto simulation results, since they are

implemented in constitutive equations for numerical methods. Therefore, it is important to use material properties determined experimentally from real products, in order to have satisfactory results.

b) **Model orientation.** The modern products rarely have extractable features, such as lines, sharp edges or patterns. For aesthetic, ergonomic, manufacturability or other reasons, the modern products usually have curved surfaces. Some features could be inaccessible, due to presence of other parts (bolts, fasteners) or due to optical occlusion. That imposes the need for further model transformations (rotation, translation, alignment). These transformations could contribute to the increase in uncertainty. This problem could be solved by adding extractable, easily accessible and recognizable features in early product development stage. When such a solution is not applicable, best-fit algorithms could be used to achieve the proper part orientation. One example of such algorithm, which uses point interpolation and RMS for circular parts, is presented in this research (Chapter 6.3).

c) **Part imperfections.** This research showed that deviations between the real and ideal shape contribute to measurement uncertainty significantly. In most CAE applications the ideal CAD model is used as a basis for numerical analysis. The real parts, depending on manufacturing technology, can vary in shape and dimensions, and these deviations are usually dominant. Even when CAD model is not created from ideal mathematical shapes, but from optical or tactile digitizing (3D scanner, digitizer, CMM), these deviations will exist, due to numerous data conversions (point cloud - tessellated surface - mesh of finite elements). Especially when optical digitizing methods are used, a number of other influences are present, such as surface quality, surface colour, lighting conditions, etc.

d) **Carefully chosen local and global coordinate systems.** The boundary conditions in numerical simulations are defined as translations, rotations, or applied forces. All these require coordinate systems which correspond to the model. For example, if simulated part is cylindrical, it is almost impossible to define forced displacement with Cartesian coordinates. All modern CAD/CAE software packages support cylindrical, spherical or Cartesian coordinate systems, which could be combined locally and globally. It is very important to choose the proper coordinate systems, and thus avoid further model transformations and unnecessary data processing. The extractable features which were mentioned when model orientation was discussed, are also very useful when coordinate systems are being defined. The measurement strategy relies on well-defined coordinate systems.

e) **Defined material side.** When thin-walled products are used in numerical simulations, it is important to orient the inner and outer surface. Some complex shapes are inaccessible by 3D optical scanners, and the scanning result can have two surfaces. In order to create usable CAD model, these surfaces have to be cleaned and joined into an unique set of surfaces. During this process, it is important to take care of surface orientation. When scanned data consists only of point clouds, it is hard to orient the part surfaces. Therefore, the digitised data should always include the surface orientation. Only the file formats which support surface normals (vectors which define surface orientation) should be chosen for data processing.

f) **Defining constitutive models and solution parameters.** The accuracy of numerical computations relies on properly chosen constitutive models and solution parameters. The behaviour of classical materials such as steel or aluminium is known for decades. The behaviour of new materials, such as biopolymers, ultrahigh performance alloys or complex composites, cannot be simulated using the same constitutive equations as conventional metals. Their properties, such as anisotropy, microstructure, cyclic plasticity, nonlinearity, should be defined prior to numerical simulation, or else the simulation results could be unusable and would not reflect the behaviour of the real structure.

g) **Converting FEM results into CAD data.** Another contribution to increased uncertainty comes from data conversion. In order to validate the proposed use of numerical simulations in dimensional measurements, it is necessary to convert the results of numerical simulations into CAD data which is comparable with digitized model. At the moment, there is no standard file format or procedure for conversion of FEM results into the CAD data. The numerical simulation results are discrete (represented by displacements and rotations of finite element nodes). The digitized models are also discrete (represented by cloud of scanned points), but these two sets of discrete data are not directly comparable. They have to be interpolated or converted to surfaces. For interpolation, it is important to decide on "master" and "slave" dataset, i.e. one set of points is used as a pattern for interpolation of the other set of points.

Although the proposed algorithm for using simulation in dimensional measurement is analysed in details, it is very important to perform the validation of simulation, in order to have confidence into accuracy of these results. The intensity and the criteria of validation must be chosen against the costs of improper decisions made based on computational modelling and simulation.

11. Conclusions

This chapter presents the conclusions, the main research results, scientific contribution and suggestions for future researches.

While 3D scanning and imaging systems are more widely available; standards, best practices and comparative are limited. The causes of uncertainty in 3D imaging systems were discussed in [111] and some of the characteristic that will have to be measured within a metrology framework are pointed out there. Though the optical principles are well known, the specifications stated by manufacturers still generate confusion amongst users. In fact, the definition of standards is critical for the generation of user confidence. These standards will have to address the whole measuring chain from terminology, acquisition, processing, methodology, as well as the user skill level.

Especially when 3D scanning is used in combination with numerical simulations, a number of problems arise. This opens a whole set of unanswered questions which need exhaustive analyses, numerous tests, development of procedures and novel algorithms to overcome limitations arising from immaturity of technology.

The ultimate goal of simulation is to predict physical events or the behaviours of engineered systems [98]. Predictions are the basis of engineering decisions, they are the determining factor in product or system design, they are a basis for scientific discovery, and they are the principal reason that computational science can project itself beyond the realm of physical experiments and observations. It is therefore natural to ask whether specific decisions can rely on the predicted outcomes of an event. How accurate are the predictions of a computer simulation? What level of confidence can one assign a predicted outcome in light of what may be known about the physical system and the model used to describe it? The science, technology, and, in many ways, the philosophy of determining and quantifying the reliability of computer simulations

and their predictions has come to be known as V&V, or verification and validation. Validation is the subjective process that determines the accuracy with which the mathematical model depicts the actual physical event. Verification is the process that determines the accuracy with which the computational model represents the mathematical model. In simple terms, validation asks, "Are the right equations solved?" while verification asks, "Are the equations solved correctly?".

The entire field of V&V is in the early stage of development. Basic definitions and principles have been the subject of much debate in recent years, and many aspects of the V&V remain in the gray area between the philosophy of science, subjective decision theory, and hard mathematics and physics. To some degree, all validation processes rely on prescribed acceptance criteria and metrics. Accordingly, the analyst judges whether the model is invalid in light of physical observations, experiments, and criteria based on experience and judgment.

Verification processes, on the other hand, are mathematical and computational enterprises. They involve software engineering protocols, bug detection and control, scientific programming methods, and, importantly, a posteriori error estimation.

Ultimately, the most confounding aspect of V&V has to do with uncertainty in the data characterizing mathematical models of nature. In some cases, parameters defining models are determined through laboratory tests, field measurements, or observations, but the measured values of those parameters always vary from one sample to another or from one observation to the next. Moreover, the experimental devices used to obtain the data can introduce their own errors because of uncontrollable factors, so-called noise, or errors in calibration. For some phenomena, little quantitative information is known, or our knowledge of the governing physical processes is incomplete or inaccurate. In those cases; we simply do not have the necessary data needed to complete the definition of the model.

Uncertainty may thus be due to variability in data due to immeasurable or unknown factors, such as our incomplete knowledge of the underlying physics or due to the inherent nature of all models as incomplete characterizations of nature. These are called subjective uncertainties. Some argue that since the data itself can never be quantified with absolute certainty, all uncertainties are subjective. Whatever the source of uncertainty, techniques must be developed to quantify it and to incorporate it into the methods and interpretation of simulation predictions.

Although uncertainty-quantification methods have been studied to some degree for half a century, their use in large-scale simulations has barely begun. Because model parameters can

often be treated as random fields, probabilistic formulations provide one approach to quantifying uncertainty when ample statistical information is available. The use of stochastic models, on the other hand, can result in gigantic increases in the complexity of data volume, storage, manipulation, and retrieval requirements. Other approaches that have been proposed for uncertainty quantification include stochastic perturbation methods, fuzzy sets, Bayesian statistics, information-gap theory, and decision theory.

This research gives a modest contribution to automated inspection and quality control of thin-walled, flexible parts, trying to combine the two emerging technologies into a new, hybrid technology. The combination of 3D scanning and computer simulations can be strong support to manufacturing process, but their usage requires strong expertise and extremely careful choice of numerous adjustable parameters.

11.1. Main results

It is shown that numerical simulation of clamping of sheet-metal products with elastic springback has practically the same measurement uncertainty as 3D scanning of physically clamped products, when clamping is simulated with appropriate boundary conditions which describe accurately the behaviour of the physical clamping.

A new computer software was developed for alignment of circular contours obtained by 3D scanning. The iterative algorithm is based on angular division of contours, and calculation of RMS.

It is proved that Hausdorff distance, although common method for geometric error measure, is not related to stress/strain state in deformed sheet metal objects

The influence factors onto 3D scanning and numerical simulation processes are identified and analysed. It is shown that major contribution to measurement uncertainty comes from scanning method. The deviations of parts due to manufacturing technology are the second largest influence factor. The scanning method includes components such as: measuring strategy (configuration, number and distribution of measuring points, sampling, filtering, measurement task definition, measurement process planning, equipment handling), fixturing, operator's influence (training, experience, care, integrity).

A number of important issues are emphasized in detailed procedures of 3D scanning and finite element analysis. The importance of coordinate systems, part orientation, data processing and data conversion are distinguished from other 3D scanning issues.

Material properties are confirmed as less significant factor in numerical simulations, in terms of contribution to numerical errors, when variation in material properties is compared with variations of other influence factors.

The boundary conditions are identified as major source of shape deviation in numerical simulations. The numerical data processing errors, such as round-off or floating-point truncation are proved to be small enough not to influence the final results. Visualised results of FEM analysis are verified with digitized data, and helped to identify boundary conditions as the most important aspect of numerical simulation.

The need for improvements in currently available FEM software solutions is identified and defined. In order to use digitized data in simulations, it is necessary to develop the new boundary conditions, suitable for digitized data. There is also a need to enable automatic data conversion from FEM results to CAD data.

A novel algorithm for automated inspection of springback-deformed components was developed. This algorithm defines and emphasizes the key steps which have to be performed in order to get the correct simulation results. Only when all these steps are followed carefully, the simulated results describes the physical behaviour correctly.

11.2. Scientific contribution

This research showed that numerical methods, such as finite element method, can successfully be used, not only in early product development phase, but also in computer-aided quality control and automated inspection of manufactured parts.

This research proposes a new methodology for springback compensation; instead of costly design interventions on tool and die systems, the imperfect products can automatically be inspected without fixation, and checked whether they are usable as assembly components.

The automated process of dimensional quality inspection is provided with better flexibility, enabling measurement and control of apparently unusable parts.

It is shown that numerical simulation introduces error which is comparably small, or even the same as the error introduced by physical clamping accessories and supplies.

11.3. Suggestions for future researches

Although a lot has been done, a number of issues are still unanswered:

- Detailed analysis of uncertainty sources and contributions in numerical simulation is achievable only as process of verification and validation. Metrology approach could be used to identify and quantify components of numerical simulations, their individual contribution, as well as their correlations

- Currently available software, formulations, constitutive models and algorithms for finite element analysis do not enable automatic feature recognition and alignment of natural features. This limits the boundary conditions needed for automated inspection using hybrid method consisting of 3D scanning and simulated springback compensation.

- Software modules should be developed in order to enable automatic conversion of FEM analysis results into CAD data. That would enable not only possibilities for springback compensation, but also for optimization problems.

11.4. Assessment of the thesis

I claimed in the main hypothesis that numerical simulation of clamping of sheet-metal products with elastic springback has the same measurement uncertainty as 3D scanning of physically clamped products, when clamping is simulated with appropriate boundary conditions which describe accurately the behaviour of the physical clamping.

I also anticipated that it is possible to measure the geometry of thin-walled products, which are deformed as a result of residual stresses, using numerical simulations of clamping process.

The results of research, statistical analysis and the comparison of experimental and simulated data confirmed the hypothesis.

The conditions and assumptions required for the application of the Finite Element Methods to compensate the deformation of measured objects are defined, and an innovative decision-making algorithm was built.

12. References

[1] Drake Jr. P. J. (Editor): "Dimensioning and Tolerancing Handbook", McGraw-Hill, ISBN:0-07-018131-4, 1999

[2] ISO "Guide to the Expression of Uncertainty in Measurement (GUM)", first edition, 1993, corrected and reprinted 1995, International Organization for Standardization (ISO), Geneva, 1995

[3] NIST Technical Note 1297, "Guidelines for Evaluating and Expressing the Uncertainty of NIST Measurement Results", 1994

[4] Hammett, P.C., Baron, J.S.: "Automotive Body Measurement System Capability", Published by Auto-Steel Partnership, 1999

[5] Weckenmann A., Gall P., Ströhla S., Ernst R.: "Shortening of the Inspection Process Chain by using Virtual Distortion Compensation", Proceedings of 8th International Symposium on Measurement and Quality Control in Production, Erlangen, Germany, 2004

[6] Ling Y.E.,Lee H.P., Cheok B.T.: "Performance of Sheet Metal In a Bending Die", International Journal of Engineering Simulation, Vol.1 No.2, ISSN:1468-1137, http://www.wlv.ac.uk/sebe/ijes, 2001

[7] Feng X., Zhongqin L., Shuhui L.: "A Fast Springback Prediction Based on The Deformation Theory Of Plasticity and Implicit Algorithm", Int. J. of Eng. Simulation, Vol.4 No.1, ISSN:1468-1137, http://www.wlv.ac.uk/sebe/ijes, 2000

[8] Carden W.D., Geng L.M., Matlock D.K., Wagoner R.H.: "Measurement of springback", International Journal of Mechanical Sciences 44, pp.79-101, 2002

[9] Zhang Z.T, Hu S.J.: "Stress and residual stress distributions in plane strain bending", Int. J. Mech. Sci. Vol.40, No.6, pp.533-543, 1998

[10] Buranathiti, T., Cao, J.: "An Effective Analytical Model for Springback Prediction in Straight Flanging Processes", International Journal of Materials & Product Technology, Vol. 21 (1/2/3), pp.137-153, 2004

[11] Chun B.K., Jinn J.T., Lee J.K.: "Modeling the Bauschinger effect for sheet metals, part I: theory", International Journal of Plasticity 18, pp.571-595, 2002

[12] Chun B.K., Jinn J.T., Lee J.K.: "Modeling the Bauschinger effect for sheet metals, part II: applications", International Journal of Plasticity 18, pp.597-616, 2002

[13] Crisbon D.J.: "Experimental measurement and finite element simulation of springback in stamping aluminum alloy sheets for auto-body panel application", M.Sc. Thesis, Mississippi State University, Mississippi, 2003

[14] Tekıner Z.: "An experimental study on the examination of springback of sheet metals with several thicknesses and properties in bending dies", Journal of Materials Processing Technology 145, pp-109-117, 2004

[15] Lee S.W.: "A study on the bi-directional springback of sheet metal stamping", Journal of Materials Processing Technology 167, pp.33-40, 2005

[16] Mullan H.B.: "Improved prediction of springback on final formed components", Journal of Materials Processing Technology 153-154, pp.464-471, 2004

[17] Palaniswamy H., Ngaile G., Altan T.: "Optimization of blank dimensions to reduce springback in the flexforming process", Journal of Materials Processing Technology 146, pp.28-34, 2004

[18] Ragai I., Lazim D., Nemes J.A.: "Anisotropy and springback in draw-bending of stainless steel 410: experimental and numerical study", Journal of Materials Processing Technology 166, pp.116-127, 2005

[19] Lingbeek R., Huetink J., Ohnimus S., Petzoldt M., Weiher J.: "The development of a finite elements based springback compensation tool for sheet metal products", Journal of Materials Processing Technology 169, pp.115-125, 2005

[20] Viswanathan V., Kinsey B., Cao J.: "Experimental implementation of neural network springback control for sheet metal forming", ASME Journal of Engineering Materials and Technology. Vol.125, pp.141-147, 2003

[21] Xu W.L., Ma C.H., Li C.H., Feng W.J.: "Sensitive factors in springback simulation for sheet metal forming", Journal of Materials Processing Technology Vol. 151, Issues 1-3, pp 217-222, 2004

[22] Verma R.K., Haldar A.: "Effect of normal anisotropy on springback", Journal of Materials Processing Technology, Vol. 190, Issues 1-3, pp 300-304, 2007

[23] Lee S.W., Kim Y.T.: "A study on the springback in the sheet metal flange drawing", Journal of Materials Processing Technology, Vol. 187-188, pp 89-93, 2007

[24] Merkley K.G.: "Tolerance analysis of compliant assemblies", PhD thesis, Brigham Young University, 1998

[25] Ji S., Li X., Ma Y., Cai H.: "Optimal Tolerance Allocation Based on Fuzzy Comprehensive Evaluation and Genetic Algorithm", Int J Adv Manuf Technol 16: pp.461-468, 2000

[26] Ding, Y., Jin, J., Ceglarek, D., Shi, J.: "Process-oriented Tolerancing for Multi-station Assembly Systems", IIE Transactions, Vol. 37, No.6., pp.493-508., 2005

[27] Chen, Y., Jin, J., Shi, J.: "Integration of Dimensional Quality and Locator Reliability in Design and Evaluation of Multi-station Body-In-White Assembly Processes", IIE Transactions on Quality and Reliability, Vol. 36, No. 9, pp. 826-839, 2004

[28] Shah J.J., Ameta1 G., Shen Z., Davidson J.: "Navigating the Tolerance Analysis Maze", Computer-Aided Design & Applications, Vol. 4, No. 5, pp 705-718, 2007

[29] Khaldi F.E., Lambriks M., Ling D.: "New requirements and recent development in sheet metal stamping simulation", Numisheet 2002: Proceedings of 5th international

conference and workshop on numerical simulation of 3D sheet forming processes, Jeju Island, Korea, Vol.1, 2002

[30] Haepp H.J., Rohleder M., "FE Simulation of Sheet Metal Forming – State of the Art in Automotive Industry", AMR - Advanced Materials Research (Volume 6-8), ISSN:1022-6680, pp.13-18, 2005

[31] Ambrogio G., Costantino I., De Napoli L., Filice L., Fratini L., Muzzupappaa M.: "Influence of some relevant process parameters on the dimensional accuracy in incremental forming: a numerical and experimental investigation", Journal of Materials Processing Technology 153–154, pp.501-507, 2004

[32] Siebenaler S.P., Melkote S.N.: "Prediction of workpiece deformation in a fixture system using the finite element method", International Journal of Machine Tools & Manufacture 46, pp.51-58, 2005

[33] Liu S.C., Hu S.J.: "Variation Simulation For Deformable Sheet Metal Assemblies Using Finite Element Methods", ASME Transactions, Vol 119, pp.368-374, 1997

[34] Cirak F., Scott M.J., Antonsson E.K., Ortiz M., Schröder P.: "Integrated Modeling, Finite-Element Analysis and Engineering Design for Thin-Shell Structures using Subdivision", http://www.multires.caltech.edu/pubs

[35] Majeske, K.D., Hammett, P.C.: "Identifying Sources of Variation in Sheet Metal Stamping", International Journal of Flexible Manufacturing Systems, 2002

[36] Kuzman K.: "Problems of accuracy control in cold forming", Journal of Materials Processing Technology, Vol. 113, No. 1, pp. 10-15(6), 2001

[37] Kuzman K.: "Comments on the cold metal forming processes stability control", J. mater. process. technol.. [Print ed.], Vol. 185, No. 1/3, pp 132-138, 2007

[38] Huang X., Gu P., Zernicke R.: "Localization and comparison of two free-form surfaces", Computer-Aided Design Vol 28, No 12, pp.1017-1022, 1996

[39] Kase K., Makinouchi A., Nakagawa T., Suzuki H., Kimura F.: "Shape error evaluation method of free-form surfaces", Computer-Aided Design 31, pp.495-505, 1999

[40] Sansoni G, Docchio F: "Three-dimensional optical measurements and reverse engineering for automotive applications", Robot. Comput.-Integr. Manuf. 20, pp.359-67, 2004

[41] Huang J., Menq C. H.: "Combinatorial manifold mesh reconstruction and optimization from unorganized points with arbitrary topology", Computer-Aided Design 34, pp.149-165, 2002

[42] Monchalin J.P.: "Optical and laser NDT: A rising star", Proceedings of 16th WCNDT 2004: World Conference on NDT, Montreal, Canada, ISBN:0-9736577-0-7, 2004

[43] Chen F., Brown G.M., Song M.: "Overview of three-dimensional shape measurement using optical methods", Optical Engineering, 39 (1) pp.10-22, 2000

[44] Yang L.X., Du C.Q., Cheng F. L.: "Recent development for surface distortion measurement", Proceedings of 16th WCNDT 2004: World Conference on NDT, Montreal, Canada, ISBN:0-9736577-0-7, 2004

[45] Galanulis K.: "Optical Measuring Technologies in Sheet Metal Processing", AMR - Advanced Materials Research (Volume 6-8), ISSN:1022-6680, pp.19-34, 2005

[46] Jyrkinen, K., Ollikainen, M., Kyrki, V., Varis, J.P., Kälviäinen, H.: "Optical 3D Measurement in the Quality Assurance of Formed Sheet Metal Parts", Proceedings of

17th International Conference on Production Research ICPR-17, Blacksburg, Virginia, USA, 2003.

[47] Gordon S., Lichti D., Stewart M.: "Application of a high-resolution, ground-based laser scanner for deformation measurements", The 10th FIG International Symposium on Deformation Measurements, Orange, California, pp.23-32, 2001

[48] Yan Z., Yang B.D., Menq C.H.: "Uncertainty analysis and variation reduction of three dimensional coordinate metrology. Part 1: geometric error decomposition", International Journal of Machine Tools & Manufacture 39, pp.1199–1217, 1999

[49] Yan Z., Yang B.D., Menq C.H.: "Uncertainty analysis and variation reduction of three dimensional coordinate metrology. Part 2: uncertainty analysis", International Journal of Machine Tools & Manufacture 39, pp.1219-1238, 1999

[50] Huang W., Kong Z., Ceglarek D., Brahmst E.: "The analysis of feature-based measurement error in coordinate metrology", IIE Transactions 36, pp.237-251, 2004

[51] Cordero R.R., Lira I.: "Uncertainty analysis of displacements measured by phase-shifting Moirre interferometry", Optics Communications 237, pp.25–36, 2004

[52] Ceglarek D., Shi J.: "Fixture Failure Diagnosis for Sheet Metal Assembly with Consideration of Measurement Noise", ASME Transactions, Journal of Manufacturing Science and Engineering. Vol. 121, pp.771-777, 1999

[53] Gopalakrishnan K.: "Algorithms, Models and Metrics for the Design of Workholding using Part Concavities", PhD Thesis, University of California, Berkeley, 2004

[54] Gopalakrishnan K., Goldberg K., Bone G.M., Zaluzec M., Koganti R., Pearson R., Deneszczuk P.: "Unilateral Fixtures for Sheet Metal Parts with Holes", IEEE Transactions on Automation Science and Engineering – 1(2), 2004

[55] Chen W., Baghdasaryan L., Buranathiti T., Cao J.: "Model Validation via Uncertainty Propagation and Data Transformations", AIAA JOURNAL Vol. 42, No. 7, 2004

[56] Kreinovich V., Ferson S.A.: "A New Cauchy-Based Black-Box Technique for Uncertainty in Risk Analysis", Reliable Engineering and Systems Safety, Vol. 85, No. 1-3, pp.267-279, 2004

[57] Jing X., Xu B., Wang C., Zhu S., Pu G., Dong S.: "Evaluation of measurement uncertainties of virtual instruments", Int J Adv Manuf Technol DOI 10.1007/s00170-004-2293-2, 2005

[58] Lazzari A., Iuculano G.: "Evaluation of the uncertainty of an optical machine with a vision system for contact-less three-dimensional measurement", Measurement, Volume 36, Issues 3-4, pp.215-231, 2004

[59] Santo M.D., Liguori C., Paolillo A., Pietrosanto A.: "Standard uncertainty evaluation in image-based measurements", Measurement Volume 36, Issues 3-4, pp.347-358, 2004

[60] Locci N., Muscas C., Peretto L., Sasdelli R.: "A Numerical Approach to the Evaluation of Uncertainty in Nonconventional Measurements on Power Systems", IEEE transactions on instrumentation and measurement, Vol.51, No.4, 2002

[61] Locci N., Muscas C., Ghiani E.: "Evaluation of uncertainty in measurements based on digitized data", Measurement, Volume 32, Issue 4, 2002.

[62] Nuccio S., Spataro C.: "Approaches to Evaluate the Virtual Instrumentation Measurement Uncertainties", IEEE transactions on instrumentation and measurement, Vol. 51, No. 6, 2002

[63] Nuccio S., Spataro C.: "Can the effective number of bits be useful to assess the measurement uncertainty?", IEEE Instrumentation and Measurement Technology Conference, Anchorage AK, USA, 2002

[64] Kahan W.: "How Futile are Mindless Assessments of Roundoff in Floating-Point Computation?", http://www.cs.berkeley.edu/~wkahan/, 2005

[65] Kahan W., Darcy J.D.: "How Java's Floating-Point Hurts Everyone Everywhere", ACM 1998 Workshop on Java for High–Performance Network Computing, Stanford University, 1998

[66] Kahan W., Ivory M.Y.: "Roundoff Degrades an Idealized Cantilever", http://http.cs.berkeley.edu/~wkahan/Cantilever.ps, 1997

[67] IEEE 754-1985 "Standard for Floating-Point Arithmetic", 1985

[68] Kalliojärwi K., Astola J.: "Roundoff Errors in Block-Floating-point Systems", IEEE transactions on signal processing, Vol. 44, No. 4, pp.783-790, 1996

[69] Castrup S.: "Why Spreadsheets are Inadequate for Uncertainty Analysis", Eighth Annual Test Instrumentation Symposium, International Test Evaluation Association (ITEA), 2004

[70] Fang C.F., Rutenbar R.A., Chen T.: "Efficient Static Analysis of Fixed-Point Error in DSP Applications via Affine Arithmetic Modeling", SRC-Techcon, 2003

[71] Mitra A.: "On Finite Wordlength Properties of Block-Floating-Point Arithmetic", International journal of signal processing Vol.2 No.2, ISSN:1304-4478, 2005

[72] Pitas I., Strintzis M.G.: "Floating Point Error Analysis of Two-Dimensional Fast Fourier Transform Algorithms", IEEE transactions on circuits and systems, Vol.35, No.1, pp.112-115, 1988

[73] Pitas I., Strintzis M.G.: "On the computation of Two-Dimensional DFTs under memory constraints", Signal processing II: Theories and Applications, pp.739-742, 1983

[74] Shiu, B. W., J. Shi, and K. H. Tse: "The Dimensional Quality of Sheet Metal Assembly with Welding-induced Internal Stress", Proceedings of the Institution of Mechanical Engineers, Part D: Journal of Automobile Engineering, v 214 No. 7. pp. 693-704, 2000

[75] Shiu, B.W., Ceglarek, D., Shi, J.: "Flexible Beam-Based Modeling of Sheet Metal Assembly for Dimensional Control," Trans. of NAMRI, Vol. XXV, pp.49-54, 1997

[76] Lipshitz B., Fischer A.: "Verification of Scanned Engineering Parts with CAD Models Based on Discrete Curvature Estimation", smi, pp.333-336, International Conference on Shape Modeling and Applications 2004 (SMI'04), 2004

[77] Geiger M., Marklein M., Kerausch M., Celeghini M.: "Robust, shortened process sequences for sheet light weight parts", Conference Proceedings - 5th International Conference on Industrial Tools "ICIT 2005", ISBN:961-90401-9-8, Velenje, Celje, Slovenia, pp.3-6, 2005

[78] Zaimović-Uzunović N., Lemeš S.: "Use Of Finite Element Method Simulation To Shorten Measurement Cycle Of Sheet-Metal Parts With Residual Stresses", Conference Proceedings - 5th International Conference on Industrial Tools "ICIT 2005", ISBN:961-90401-9-8, Velenje, Celje, Slovenia, pp.97-100, 2005

[79] Weckenmann A., Weickmann J.: "Optical inspection of formed sheet metal parts applying fringe projection systems and virtual fixation", Metrology and Measurement Systems, Vol. XIII No. 4, 2006

[80] Park E. J. , Mills J.K.: "Three-Dimensional Localization of Thin-Walled Sheet Metal Parts for Robotic Assembly", Journal of Robotic Systems 19(5), pp 207–217, DOI: 10.1002/rob.10035, 2002

[81] Gerth, R.J., Brueckner, S.: "The Digital Body Development System", International Automotive Body Congress, Ann Arbor, Michigan, Sept. 21-23, 2005

[82] Gerth R.J.: "Virtual Functional Build: A Case Study", SAE 2006 World Congress & Exhibition, Detroit, MI, USA, Session: Virtual/Digital Technology and Rapid Prototyping, 2006

[83] Ceglarek D., Huang W., Zhou S., Ding Y., Kumar R., Zhou Y.: "Time-Based Competition in Multistage Manufacturing: Stream-of-Variation Analysis (SOVA) Methodology-Review", The International Journal of Flexible Manufacturing Systems, 16, 11–44, 2004

[84] Kos L., Duhovnik J.: "A system for footwear fitting analysis", Proceedings of the 7th International Design Conference DESIGN 2002, Cavtat, Dubrovnik, Croatia, May 14-17, 2002. Zagreb: Faculty of Mechanical Engineering and Naval Architecture; Glasgow: The Design Society, vol. 2, pp 1187-1192, 2002

[85] Garland M.: "Quadric-Based Polygonal Surface Simplification", PhD Thesis, Carnegie Mellon University Pittsburgh, PA, USA, 1999

[86] Zhu W., Wang H., Lai X., Lin Z., Chen Y.: "A New Method for Fitting Car Doors Allowing for the Thermal Effects of Welding", Proceedings of the Institution of Mechanical Engineers, Part D: Journal of Automobile Engineering, Vol. 220, No. 7, pp 891-900, 2006

[87] Rucklidge W.: "Efficient computation of the minimum Hausdorff distance for visual recognition", Ph.D. thesis, Dept. of computer science, Cornell University, NY, 1995

[88] Mount D. M., Netanyahu N. S., LeMoigne J.: "Efficient Algorithms for Robust Point Pattern Matching and Applications to Image Registration", Pattern Recognition, 32 17-38, 1999

[89] Grégoire N., Bouillot M., "Hausdorff distance between convex polygons", http://cgm.cs.mcgill.ca/~godfried/teaching/cg-projects/98/normand/main.html, McGill University, 1998

[90] Cignoni P.: "VCG Metro", http://vcg.sourceforge.net/tiki-index.php?page=Metro

[91] Huang J., Lehtihet E. A.: Contribution to the minimax evaluation of circularity error, International Journal of Production Research, vol. 39, no. 16, 3813-3826, ISSN 1366-588X, DOI: 10.1080/00207540110064947, 2001

[92] ISO 1101:2004 Geometrical Product Specifications (GPS) - Geometrical tolerancing - Tolerances of form, orientation, location and run-out

[93] ISO 14253-1:1998 Geometrical Product Specifications (GPS) - Inspection by measurement of workpieces and measuring equipment - Part 1: Decision rules for proving conformance or non-conformance with specifications

[94] ISO/IEC Guide 99:2007 International vocabulary of metrology - Basic and general concepts and associated terms (VIM)

[95] Gregory K, Bibbo G, Pattison JE.: A standard approach to measurement uncertainties for scientists and engineers in medicine, Australas Phys Eng Sci Med. 28(2):131-9, 2005

[96] Jecić S., Drvar N., "The assessment of structured light and laser scanning methods in 3D shape measurements", Proceedings of the 4th International Congress of Croatian Society of Mechanics, 237-244, 2003

[97] Beraldin J.A.: Basic theory on surface measurement uncertainty of 3D imaging systems, Proceedings of the SPIE, Volume 7239, pp. 723902-723902-12, doi:10.1117/12.804700, 2009

[98] National Science Foundation Blue Ribbon Panel on Simulation-Based Engineering Science. Simulation-Based Engineering Science. Technical report, National Science Foundation, USA, http://www.nsf.gov/pubs/reports/sbes_final_report.pdf, 2006

[99] Esward T.J., Wright L.: Deriving uncertainties when using simulation in metrology, National Physical Laboratory report DEM-ES-017, March 2007

[100] Neto B., da Rosa E.: Parametric uncertainty analysis considering metrological aspects in the structural simulation in viscoelastic materials, Latin American Journal of Solids and Structures 5, 75–95, 2008

[101] M. Baba, D. Narita, K. Ohtani, "An advanced rangefinder equipped with a new image sensor with the ability to detect the incident angle of a light stripe", Journal of optics A:Pure and applied optics, 10-16, 2004

[102] Boehler W., Vicent M.B., Marbs A.: "Investigating Laser Scanner Accuracy"; CIPA Symposium, Turkey; http://scanning.fh-mainz.de/scannertest/results300305.pdf, 2003

[103] Willink R.: On the uncertainty of the mean of digitized measurements, Metrologia 44 73-81, doi: 10.1088/0026-1394/44/1/011, http://stacks.iop.org/Met/44/73, 2007

[104] Breuckmann B., Halbauer F., Klaas E., Kube M.: 3D-Metrologies for industrial applications. In Proceedings of SPIE 3102, pages 20–29, 1997.

[105] Peng T., Gupta S.K.: Model and algorithms for point cloud construction using digital projection patterns. ASME Journal of Computing and Information Science in Engineering, 7(4): 372-381, 2007

[106] Atzema E.H., Kappert H., Konter A.W.A., Meijers S.E., Meinders T. Sensitivity analysis component 2: Scaled down car roof. Netherlands Institute for Metals Research, 2005.

[107] Brajlih T., Valentan B., Drstvenšek I., Balič J., Pogačar V.: Testing of ATOS 3D optical scanner measuring volumes. Annals of DAAAM for 2007 & proceedings of the 18th International DAAAM symposium "Intelligent manufacturing & Automation: "Focus on creativity, responsibility, and ethics of engineers", 24-27th October 2007, Zadar, Croatia. Vienna: DAAAM International, pp 111-112, 2007.

[108] Castellazzi G.: Verification in computational structural mechanics: recovery-based a posteriori error estimation, PhD Thesis, University of Bologna, 2007

[109] Guide for the Verification and Validation of Computational Fluid Dynamics Simulations, AIAA-G-077-1998, AIAA, Reston, VA, 1998

[110] Gregoire, T. G., and Reynolds, M. R., "Accuracy Testing and Estimation Alternatives," Forest Science, Vol. 34, No. 2, pp. 302–320, 1988.

[111] Beraldin J.A., Blais F., El-Hakim S., Cournoyer L., Picard M.: Traceable 3D Imaging Metrology: Evaluation of 3D Digitizing Techniques in a Dedicated Metrology Laboratory, The 8th Conference on Optical 3-D Measurement Techniques. Zurich, Switzerland. July 9-12, 2007

[112] Castrup, S.: A Comprehensive Comparison of Uncertainty Analysis Tools, Proc. Measurement Science Conference, Anaheim, CA, January 2004.

[113] Zhang S.: "High-resolution, Real-time 3-D Shape Measurement", PhD dissertation, Stony Brook University, 2005.

[114] Häusler G., Ubiquitous coherence - boon and bale of the optical metrologist, Speckle Metrology 2003, Trondheim, Proc. SPIE Vol. 4933, 48–52, 2003

[115] Buranathiti T., Cao J., Chen W., Baghdasaryan L., Xia Z.C.: "Approaches for Model Validation: Methodology and Illustration on a Sheet Metal Flanging Process", Transactions of the ASME, Vol. 128, pp.588-597, 2006

[116] Coleman H.W., Stern H.: "V&V State of the Art", Proceedings of Foundations '02 a Workshop on Model and Simulation Verification and Validation for the 21st Century JHU/APL Kossiakoff Education and Conference Center (Laurel, Maryland USA) October 22-24, 2002

[117] Korošec M., Duhovnik J., Vukašinovič N.: "Process modeling of non-contact reverse engineering process", Proceedings of the 7th WSEAS Int. Conf. on Signal Processing, Computational Geometry & Artificial Vision, Athens, Greece, August 24-26, 2007.

[118] Vukašinovič N., Kolšek T., Duhovnik J.: "Case study - surface reconstruction from point clouds for prosthesis production. Journal of Engineering Design, 18(5):475-488, 2007.

[119] Stern F., Wilson R.V., Coleman H.W., Paterson E.: " Comprehensive Approach to Verification and Validation of CFD Simulations-Part 1: Methodology and Procedures", Journal of Fluids Engineering, Vol. 123, pp 792-802, @DOI: 10.1115/1.1412235, 2001

13. Povzetek v slovenščini

13.1 Uvod

13.1.1 Opis splošnega področja raziskovanja

Značilnost sodobnih izdelovalnih procesov je vse večje povpraševanje po majhnih serijah raznovrstnih izdelkov. Zahtevata se produktivnost ter hitrost, ki morata biti identični kot pri velikoserijski izdelavi. Naslednji pomemben trend, posebno v avtomobilski industriji, je vse pogostejša uporaba lažjih polizdelkov in sklopov s ciljem zmanjšati porabo goriva in s tem emisijo CO_2. Zmanjšanje mase polizdelkov in sklopov se uresničuje z uporabo specialnih lahkih zlitin oziroma z optimizacijo njihove konstrukcije. Tipičen proizvodni proces lažjih izdelkov vključuje tri faze: (i) izdelavo, (ii) montažo in (iii) kontrolo kakovosti. Posledica je nujnost uporabe sodobnih tehnologij v vsaki izmed faz zaradi zmanjšanja stroškov izdelave. V zadnjem času je bilo razvitih veliko tehnik, ki pomagajo pri reševanju problemov in so usmerjene na različne aspekte in faze proizvodnega procesa.

Numerične metode, kot na primer metoda končnih elementov (MKE), imajo široko uporabo pri optimizaciji tehnoloških parametrov procesa izdelave, da zmanjšajo oziroma izključijo napake na izdelkih. Pogosta napaka pri pločevinastih izdelkih je zaostala napetost, ki večinoma povzroča pojav elastične izravnave po preoblikovanju.

Kljub temu da se napakam pri izdelavi ne moremo popolnoma izogniti oziroma to ni rentabilno, ne pomeni, da so izdelki neuporabni. Uporabnost pločevinastih izdelkov je odvisna tudi od posameznih in kompleksnih predpisanih toleranc. Razvite so bile posebne discipline, analiza in sinteza toleranc, kako bi se njihova kontrola s posameznih delov usmerila na celoten sklop.

Zahteve po višji kakovosti pločevinastih izdelkov so pripeljale do potrebe po boljših nedestruktivnih in brezkontaktnih metodah za raziskovanje oblik in dimenzij izdelkov ter polizdelkov. V poglavju o bodoči oceni dimenzij in toleranc [1] Don Day izjavlja: " Vse kapitalne investicije je potrebno realizirati zaradi opreme, ki je kompatibilna z zahtevami dizajna. Oprema in software se pogosto potrjujeta zaradi povračila naložb. Donosnost naložbe je boljša, če se dokaže, da je mogoče kontrolirati več izdelkov v enemu času in ko je oprema za pritrjevanje minimalna oziroma ni potrebna. To pogosto vodi do večje negotovosti". Za dosego takšnega cilja je potrebno razviti nove metode kontrole kakovosti in ta raziskava ponuja eno od rešitev. Glavni del raziskave je usmerjen na ocenitev nenatančnosti pri meritvah, ki nastaja pri uporabi kompleksne kombinacije inženirskih tehnik.

Za potrebe obratnega inženiringa so razvite metode 3D-digitalizacije, ki lahko zelo hitro opravijo transformacijo fizičnega izdelka v digitalni model. Istočasno so numerične metode (kot MKE) omogočile značilne prispevke k dizajnu komponent in sklopov. Numerične metode se načeloma uporabljajo v fazi oblikovanja in konstruiranja in le izjemoma v fazi kontrole končnega izdelka. Ta raziskava predlaga novo področje uporabe numeričnih metod, in sicer v fazi kontrole kakovosti v kombinaciji z metodami obratnega inženiringa.

Poseben problem pri digitaliziranih modelih predstavlja negotovost meritev. Kljub temu da obstaja mednarodni standard za določanje merilne negotovosti [2] skupaj s Smernicam za določanje in izražanje negotovosti [3] je ta standard presplošen za uporabo za vse metode meritev. V zadnjem času so različni avtorji raziskovali meritve digitaliziranih podatkov.

Vpenjalni sistem deformira kontrolirani izdelek [4] in tako pripelje do napake, ki presega predpisane tolerance. Vpenjalni proces je dolgotrajen in zahteva snovanje in izdelavo vpenjalnega sistema za vsak posamezen izdelek. Posledično je upravičeno simulirati vpenjalni proces s pomočjo numeričnih metod kot MKE. Glavni cilj te raziskave je ugotoviti, ali je mogoče uporabiti metodo končnih elementov za simulacijo procesa pritrjevanja v kontroli dimenzij pločevinastih izdelkov, ki so deformirani zaradi elastične izravnave. Za evalvacijo te metode je potrebno poiskati kvantitativne napake in pomanjkljivosti hibridne tehnike.

13.1.2 Opredelitev problema

Ideja za raziskavo je prišla s projektom "Lernfähige Qualitätsmanagementmethoden zur Verkürzung der Prozesskette 'Prüfen'" (Samodoločljive metode upravljanja kakovosti za razvijanje in uporabo skrajšanih procesov) inštituta QFM na Univerzi v Erlangenu v Nemčiji. Ta

projekt predlaga uporabo treh metod za simulacijo procesa: primerjava nominalne/dejanske vrednosti definiranih parametrov iz komponent določenih izmerjenih podatkov in CAD-modela, uporabo nevronskega omrežja za kompenzacijo deformacij iz 3D-posnetkov in metod končnih elementov [5]. Raziskava je pokazala, da je mogoče uporabiti metodo MKE, a sta natančnost in zanesljivost takšne metode neprimerni.

Glavni cilj raziskave je ugotoviti, ali so mogoče meritve geometrije tankostenskih izdelkov, ki so deformirani kot posledica zaostalih naprezanj, z uporabo numeričnih simulacij procesa pritrjevanja.

Naslednji cilj je opredeliti pogoje in predpostavke, zahtevane za uporabo metode končnih elementov, za nadomestitev deformacij merjenih izdelkov; torej zgraditi inovativen odločitveni algoritem.

Cilji disertacije bodo preizkušeni s pomočjo naslednjih hipotez:

- H0: Numerična simulacija pritrjevanja pločevinastih izdelkov z elastičnim izravnanjem ima enako merilno negotovost kot 3D-skeniranje dejansko pritrjenih izdelkov, če se pritrjevanje simulira z ustreznimi robnimi pogoji, ki natančno opisujejo obnašanje pritrjevanja.
- H1: Numerična simulacija pritrjevanja pločevinastih izdelkov z elastičnim izravnanjem ima veliko večjo merilno negotovost od 3D-skeniranja dejansko pritrjenih izdelkov.

13.1.3 Struktura disertacije

V uvodnem poglavju disertacije so opisana splošna raziskovalna področja, cilj raziskave in hipoteze.

Poglavje 2 vsebuje pregled pojavov, povezanih s tem problemom, in pregled literature predhodnih raziskav s tega področja. Pregled literature je razdeljen po področjih kot elastična izravnava, tolerance, proces optimizacije proizvodnje pločevine, obratno inženirstvo, optična 3D-merjenja za kontrolo kakovosti pločevinastih izdelkov, merilna negotovost in uporaba metode končnih elementov v kontroli kakovosti pločevinastih izdelkov.

Poglavje 3 pojasnjuje motivacijo za uporabo numeričnih simulacij v kontroli dimenzij in opisuje faze predlaganega postopka. Raziskava je sestavljena iz naslednjih faz: določanje glavnih značilnosti izbranega izdelka, 3D-skeniranje izdelkov brez pomoči in s pomočjo pritrjevanja,

obdelava rezultatov skeniranja, preverjanje točnosti obratnega inženirstva, simulacija procesa pritrjevanja, statična napetostna analiza, ki temelji na izmerjenih deformacijah, ocena prevladujočih vplivnih dejavnikov, določitev merilne negotovosti, statistična analiza rezultatov testiranja in hipoteze ter finalizacija inovativnega algoritma predlaganega postopka.

Poglavje 4 opisuje izdelke, uporabljene pri poskusih, daje osnovna dejstva o proizvodnem procesu, opremi in rezultatih eksperimentalnih določitev lastnosti materiala ter izgradnji trdnega pritrjevalnega sklopa za 3D-skeniranje. Izdelek, uporabljen za testiranje predlaganega postopka virtualnega pritrjevanja, je ohišje oljnega filtra, ki ga proizvajajo v podjetju Mann+Hummel (Unico Filter) Tešanj, Bosna in Hercegovina. Rezultati merjenja lastnosti materiala ustrezajo mehaničnim lastnostim, deklariranim s strani proizvajalca.

Poglavje 5 obravnava 3D-skeniranje, opisuje opremo, vzorce in postopke, uporabljane pri poskusih, predelavo rezultatov skeniranja, pretvarjanje skeniranih podatkov v FEA-modele in napake, ki jih povzroča konverzija podatkov. Poleg digitalizacije izbranega ohišja filtra je metoda preverjena na manj kompleksnem 2D-obrisu. Poglavje opisuje tudi najbolj uporabljane 3D-datotečne formate s karakteristikami. Opisana so tudi pretvarjanja digitaliziranih podatkov v modele končnih elementov in vse težave in napake, ki se pojavljajo v procesu. Napake so analizirane in predstavljene v tabelah.

V poglavju 6 so rezultati 3D-skeniranja, uporabljeni za določanje dejanskih dimenzij in oblik vzorca izdelka, za izračun odstopanja nevpetih, vpetih in nazivnih CAD-izdelkov. Enake analize so izdelane za 2D-obris in 3D-model ohišja filtra. Računalniški program je bil razvit za izračun interpoliranih točk, za opravljanje rotacijskega prilagajanja profila in za izračun RMS-odstopanj med profili. Rezultati, prikazani tabelarno in grafično, dokazujejo, da so ekvivalentne napetosti, izračunane za spremembo območja po postopku pritrjevanja, zelo različni. Vsi vzorci so v kompresiji. Če te rezultate, analizirane po skupinah vzorcev v povprečju za vsak vzorec materiala, primerjamo, je očitno, da je razpršenost rezultatov večja v enem nizu vzorcev (vzorcev iz enega pločevinastega zavitka) kot povprečje med vrednostmi petih različnih zavitkov. Ker so odstopanja zelo velika, je smiselno, da se rezultati primerjajo z drugimi parametri, ki se lahko pridobijo iz skeniranih podatkov.

Poglavje 7 uporablja digitalizirane posnetke za izvajanje analize z metodo končnih elementov. Zaradi kompleksnosti težave je bila analiza v začetku izvedena na preprostemu profilu, da se pojasnijo predpostavke in pogoji, ki so bistveni za pridobitev natančnih rezultatov. Vsaka faza

numerične simulacije procesa je bila skrbno analizirana, rezultati simulacij pa so bili dokončno pripravljeni za validacijo simulacij. Programska oprema, uporabljena za analizo, je UGS I-deas, v.11 (Win32). Simulacije so pokazale, da so robni pogoji najpomembnejši parameter te analize. Vrednosti napetosti so pokazale, da je deformacija znotraj elastičnega področja. Težave nastajajo zaradi pomanjkanja programske podpore za avtomatsko transformacijo rezultatov simulacij v CAD-model. Rezultati simulacij so dokazali, da so odstopanja med realnim in nominalnim CAD-modelom dvakrat večja kot odstopanja med skeniranim in simuliranim modelom oziroma napake proizvodnje in odstopanja so večje od napak simulacij. Rezultati kažejo ustreznost z Von Mises in ekvivalentnimi napetosti ter večja odstopanja med 3D-skeniranim realnim delom in nominalnim CAD-modelom od odstopanja med skeniranim in simuliranim obrisom oziroma napake proizvodnje in odstopanja skeniranja so večje od napak skozi simulacijo.

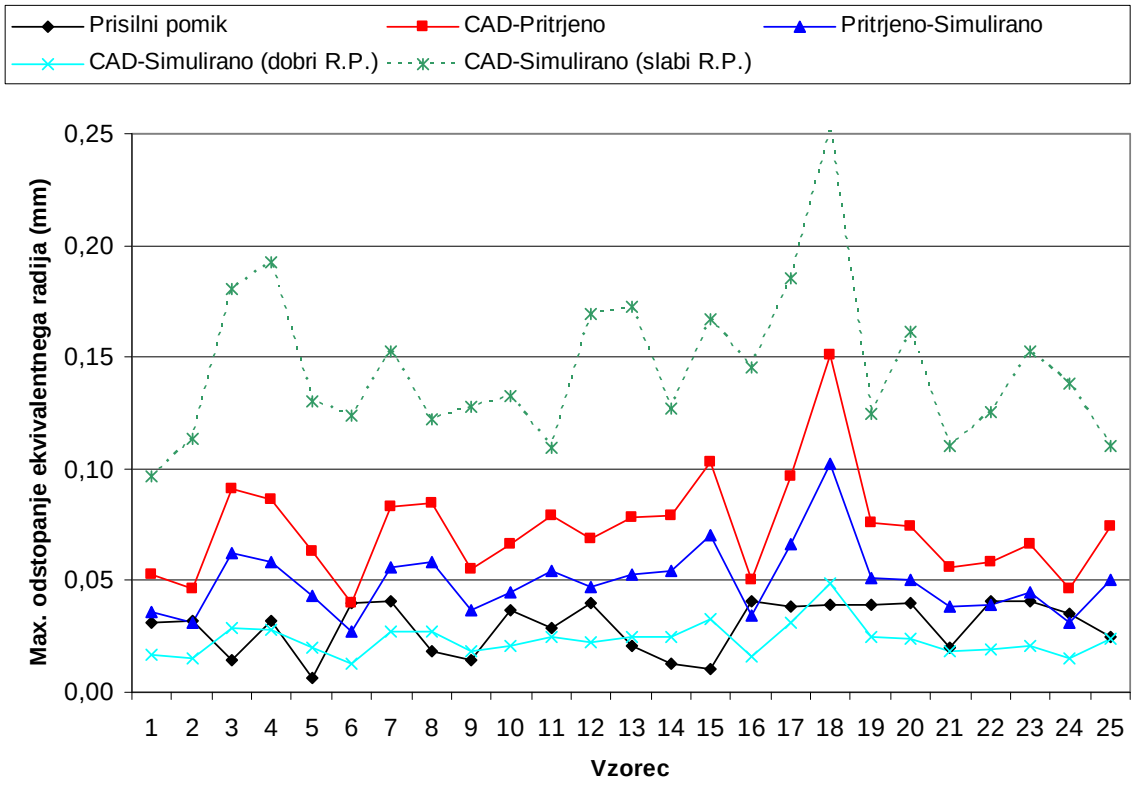

Slika 13.1: Odstopanja dimenzij med MKE-simulacijo in 3D-skeniranjem

Poglavje 8 obravnava merilno negotovost, ki zajema podrobno analizo vplivnih dejavnikov, ustvarjanje matematičnega modela sistema merjenja in analizo negotovosti v skladu s postopki, opisanimi v GUM. Grafični prikaz 13.1 ilustrira rezultate analize merilne negotovosti.

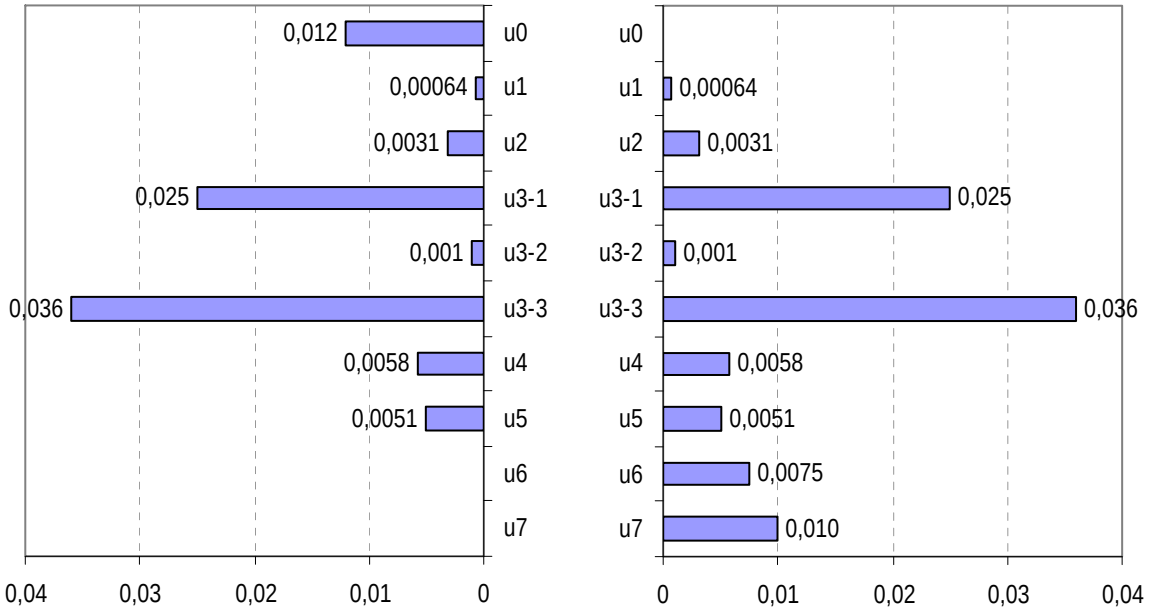

(a) Eksperiment (b) Simulacije

Slika 13.2: Grafična primerjava prispevkov merilne negotovosti

Slika 13.2 prikazuje dejavnike merilne negotovosti za fizično pritrjene objekte in za simulacije (u_0: deformacije dejanskega vpenjanja, u_1: temperatura, u_2: lastnosti materiala, $u_{3\text{-}1}$: napake izdelave, $u_{3\text{-}2}$: natančnost 3D-koordinatnega merilnega stroja, $u_{3\text{-}3}$: metoda 3D-skeniranja, u_4: natančnost 3D-skenerja, u_5: pretvorba STL-podatkov, u_6: simulacija deformacije, u_7: numerično računanje). V obeh primerih je pomembna metoda 3D-skeniranja. Skupna merilna negotovost je v obeh primerih enaka, saj nekateri prispevki se pojavljajo le, kadar je objekt fizično pritrjen (u_0), in drugi se pojavljajo le v simulaciji (u_6, u_7). Ti prispevki nadomestijo drug drugega.

Rezultati poskusov in simulacija so predmet statistične analize v poglavju 9, da bi se preverila hipoteza, določena v uvodu. Analiza je pokazala, da ni razlik med natančnostjo merjenja simulacij in dejansko pritrjenimi izdelki, kar potrjuje postavljeno hipotezo. Analiza je tudi pokazala razlike med vzorci iz petih različnih zvitkov pločevine, iz katerih so izdelani.

Poglavje 10 opisuje novi algoritem za avtomatski proces merjenja. Poglavje 11 predstavlja zaključke, rezultate raziskav, znanstvene prispevke in predloge za nadaljnje raziskave.

13.2 Zaključki

Medtem ko so 3D-skeniranje in sistemi za slikanje dostopnejši, so standardi, najboljše prakse in primerjalniki omejeni. Vzroki za nenatančnost 3D-sistemov za slikanje in nekatere lastnosti, ki jih bo treba meriti v okviru meroslovja, so bili obravnavani v [111]. Čeprav so optična načela znana, specifikacije po navedbah proizvajalcev še vedno povzročajo zmedo med uporabniki. Opredelitev standardov je ključnega pomena za ustvarjanje zaupanja uporabnikov. Ti standardi bodo morali obravnavati celotno verigo merjenja od terminologije, pridobivanja, obdelave, metodologije kot tudi raven spretnosti uporabnika.

Če se 3D-skeniranje uporablja v kombinaciji z numeričnimi simulacijami, nastanejo številne težave. To odpira celo vrsto nerešenih vprašanj, ki potrebujejo popolno analizo, številne teste, razvoj postopkov in novih algoritmov za odpravo omejitev, ki izhajajo iz nezrelosti tehnologije.

Končni cilj simulacije je napovedati fizične dogodke ali obnašanje inženirskih sistemov [98]. Napovedi so podlaga za inženirske odločitve in so odločilni dejavnik pri oblikovanju proizvoda ali sistemskega oblikovanja, so osnova znanstvenih odkritij in so glavni razlog, da lahko računalniška znanost presega področje fizikalnih poskusov in ugotovitev. Normalno je, da se vprašamo, ali se posebne odločitve lahko zanašajo na napovedan rezultat dogodka. Kako točne so napovedi za računalniške simulacije? Kakšna stopnja zaupanja se lahko dodeli predvidenemu izidu glede na to, kar je morda že znano o fizičnem sistemu in modelu, uporabljenem za opis? Znanost, tehnologija ter v mnogih pogledih filozofija določanja in kvantificiranja zanesljivosti računalniške simulacije in njihovih napovedi so postale znane kot preverjanje in potrjevanje. Potrditev je subjektiven proces, ki določa natančnost, s katerim matematični model prikazuje dejanski fizični dogodek. Preverjanje je postopek, ki določa natančnost, s katero računalniški model predstavlja matematični model. Potrditev torej sprašuje: "Ali so prave enačbe rešene?", medtem ko preverjanje sprašuje: "Ali so enačbe rešene pravilno?".

Celotno področje preverjanja in potrjevanja je v zgodnji fazi razvoja. Osnovne definicije in principi so bili predmet mnogih razprav v zadnjih letih in številni vidiki preverjanja in potrjevanja so ostali v sivem območju filozofije znanosti, teorije subjektivnih odločitev ter stroge matematike in fizike. Do neke mere se vsi postopki ovrednotenja sklicujejo na predpisana merila sprejemljivosti in meritve. V skladu s tem analitik presoja, ali je model neveljaven glede fizičnih stališč, poskusov in meril, ki temeljijo na izkušnjah in presoji.

Procesi preverjanja so na drugi strani matematična in računalniška podjetja. Vključujejo protokol programske opreme, odkrivanje napak in nadzor, znanstvene metode načrtovanja in a posteriori oceno napake.

Najosupljivejši vidik preverjanja in potrjevanja ima opraviti z nenatančnostjo podatkov, ki označujejo matematične modele naravnih procesov. V nekaterih primerih se določajo parametri, ki opredeljujejo modele z laboratorijskimi testi, meritvami na terenu ali s pripombami, vendar se izmerjene vrednosti teh parametrov vedno razlikujejo od enega vzorca do drugega ali od ene ugotovitve do druge. Poleg tega lahko uvedejo eksperimentalne naprave, ki se uporabljajo za pridobitev podatkov, svoje napake zaradi neobvladljivih dejavnikov tako imenovanega hrupa ali napake v kalibraciji. Za nekatere pojave je malo znanih kvantitativnih podatkov ali pa je naše znanje o fizikalnih procesih nepopolno oziroma netočno. V teh primerih preprosto nimamo potrebnih podatkov za dokončno opredelitev modela.

Vzrok za nenatančnost je lahko variabilnost podatkov zaradi neizmerjenih ali neznanih dejavnikov, kot so nepopolno poznavanje osnov fizike ali zaradi narave vseh modelov kot nepopolnih karakterizacij naravnih procesov. Imenujejo se subjektivne negotovosti. Nekateri trdijo, da se podatki nikoli ne morejo kvantificirati z absolutno gotovostjo in so vse negotovosti subjektivne. Ne glede na vir negotovosti je treba razviti tehnike za kvantifikacijo in jih vključiti v metode in razlage napovedi simulacije.

Čeprav so metode za določanje natančnosti do neke mere proučevane pol stoletja, se je njihova uporaba v obsežnih simulacijah komaj začela. Ker se model parametrov pogosto obravnava kot naključno polje, verjetnostni pripravki zagotavljajo pristop k veliki nenatančnosti, ko so na voljo statistični podatki. Uporaba stohastičnih modelov pa lahko povzroči povečanje obsega kompleksnosti podatkov, skladiščenja, manipulacije in pridobivanja zahtev. Drugi pristopi, ki so bili predlagani za količinsko natančnost, so stohastične metode motenja, fuzzy logika, statistika Bayesian, informacijska teorija vrzeli, teorija odločanja.

Raziskava daje skromen prispevek za avtomatsko inšpekcijo in nadzor kakovosti tankostenskih, prilagodljivih delov, skuša združiti novi tehnologiji v novo, hibridno tehnologijo. Kombinacija 3D-skeniranja in računalniških simulacij je lahko močna podpora v proizvodnem procesu, vendar zahteva uporaba veliko strokovnega znanja in izjemno skrbno izbiro številnih nastavljivih parametrov.

13.2.1 Glavni rezultati

Prikazano je, da ima numerična simulacija pritrjevanja pločevinastih izdelkov z elastičnim izravnanjem enako merilno negotovost kot 3D-skeniranje dejansko pritrjenih izdelkov, če se pritrjevanje simulira z ustreznimi mejnimi pogoji, ki natančno opisujejo obnašanje pritrjevanja.

Nova računalniška programska oprema je bila razvita za uskladitev krožnih obrisov, pridobljenih s 3D-skeniranjem. Iterativni algoritem temelji na kotni razdelitvi kontur in na izračunu RMS.

Dokazano je že, da razdalja Hausdorff kljub običajni metoda za merjenje geometrijskih napak ni povezana s stanjem napetosti v deformiranih predmetih iz pločevine.

Faktorji vpliva na 3D-skeniranje in procese numerične simulacije so opredeljeni in analizirani. Prikazano je, da nenatančnost velikokrat povzročajo metode skeniranja. Odstopanja delov zaradi proizvodne tehnologije so drugi najpomembnejši dejavnik. Metoda skeniranja vključuje elemente, kot so: strategija merjenja (konfiguracija, število in razporeditev merilnih točk, vzorčenje, filtriranje, opredelitev meritvenega naloga, načrtovanje procesa merjenja, rokovanje z opremo), pritrjevanje, vpliv operaterja (usposabljanje, izkušnje, pozornost, integriteta).

Številna pomembna vprašanja so poudarjena s podrobnimi postopki za 3D-skeniranje in z analizami končnih elementov. Pomen koordinatnih sistemov, usmeritev izdelkov, obdelava podatkov in njihova pretvorba se razlikujejo od drugih vprašanj 3D-skeniranja.

Lastnosti materiala so pri numeričnih napakah pomemben dejavnik, ko se razlike v lastnostih materiala primerjajo z nihanjem drugih vplivnih dejavnikov pri numeričnih simulacijah.

Mejni pogoji so pri numeričnih simulacijah opredeljeni kot glavni vir nepravilnosti oblike. Napake pri numerični obdelavi podatkov, kot so zaokrožanje ali krajšanje številk, so se izkazale za dovolj majhne, da ne vplivajo na končne rezultate. Vidni rezultati analize FEM so preverjeni z digitaliziranimi podatki in so pripomogli k opredelitvi mejnih pogojev kot najpomembnejšemu parametru numeričnih simulacij.

Potreba po izboljšavah dostopnih FEM-programskih rešitev je opredeljena in določena. Za uporabo digitaliziranih podatkov v simulacijah je treba razviti nove mejne pogoje, primerne za digitalizirane podatke. Pojavlja se tudi potreba, da bi omogočili avtomatsko pretvorbo rezultatov FEM v podatke CAD.

Razvit je bil nov algoritem za avtomatski pregled deformiranih komponent zaradi elastičnega izravnanja. Ta algoritem definira in poudarja ključne korake, ki jih je treba opraviti, da bi dobili pravilne rezultate simulacije. Šele ko so vsi ti ukrepi skrbno sprejeti, rezultati simulacij pravilno opisujejo fizično vedenje.

13.2.2 Znanstveni prispevek

Raziskava je pokazala, da se lahko numerične metode, kot so metode končnih elementov, uspešno uporabljajo ne samo v zgodnji fazi razvoja izdelka, temveč tudi v računalniško podprti kontroli kakovosti in avtomatiziranem pregledu izdelanih delov.

Raziskava predlaga nove metodologije za nadomestitev elastične izravnave, namesto dragih oblikovnih posegov na orodje je mogoče nepopolne izdelke samodejno pregledati brez vezave in preveriti, ali so uporabni kot komponente za sestavljanje v sklopih.

Avtomatiziran postopek pregledov kakovosti dimenzij je zagotovljen z boljšo prilagodljivostjo, ki omogoča merjenje in nadzor očitno neuporabnih delov.

Prikazano je, da numerična simulacija uvaja napako, ki je sorazmerno majhna, ali celo ista kot napaka ki je uvajajo pribor in ofizično pritrjevanje.

13.2.3 Predloge za nadaljnje raziskovanje

Čeprav je bilo storjenega veliko, na veliko vprašanj še vedno ni odgovorov:

- Podrobno analizo virov o nenatančnosti in prispevkov za numerično simulacijo je mogoče doseči le kot postopek preverjanja in potrjevanja. Meroslovni pristop bi lahko uporabili za identifikacijo in kvantifikacijo komponent numeričnih simulacij, individualne prispevke kakor tudi korelacije.

- Trenutno dostopna programska oprema, formulacije, konstitutivni modeli in algoritmi za analize metod končnih elementov ne omogočajo avtomatske funkcije prepoznavanja karakteristik in prilagajanja naravnih funkcij. To omejuje mejne pogoje, potrebne za avtomatiziran pregled z uporabo hibridne metode, sestavljene iz 3D-skeniranja in simuliranih kompenzacij elastičnega izravnanja.

- Razviti je potrebno module programske opreme, da bi omogočili samodejno pretvorbo rezultatov FEM-analize v CAD-podatke. To bi omogočilo ne le možnosti za nadomestilo elastične izravnave, ampak tudi optimizacijo težav.

13.2.4 Ocena teze

V tezi, ki smo jo postavili v uvodu disertacije, smo postavili trditev, da ima numerična simulacija pritrjevanja pločevinastih izdelkov z elastičnim izravnanjem enako merilno negotovost kot 3D-skeniranje pritrjenih izdelkov, če se pritrjevanje simulira z ustreznimi robnimi pogoji, ki natančno opisujejo obnašanje pritrjevanja.

Izrazili smo tudi predvidevanje, da so mogoče meritve geometrije tankostenskih izdelkov, ki so deformirani kot posledica dejstva zaostalih naprezanj, z uporabo numeričnih simulacij procesa pritrjevanja.

Rezultati raziskave, statistična analiza in ureditev eksperimentalnih in simuliranih podatkov so potrdili postavljeno tezo.

Opredeljeni so pogoji in predpostavke, zahtevane za uporabo metode končnih elementov za nadomestitev deformacij merjenih izdelkov, in zgrajen je inovativen odločitveni algoritem.

Annex A: Material properties

Roll	Sample	Angle	Starting width	Starting length	Deformation strengthening exponent	Hardening coefficient	Ultimate strength	Yield stress	Yield stress	Strain	Strain	Anisotropy factor	Anisotropy factor
		α	b_0	l_0	n	C	R_m	$R_{p0,2}$	$R_{p0,5}$	A_g	A80	r_{10}	r_{20}
		°	mm	mm	-	N/mm	MPa	MPa	MPa	%	%	-	-
1	1	0	19,90	79,57	0,242	518,6	286,4	162,0	176,6	22,2	40,2	2,68	2,54
1	1	45	19,90	80,58	0,221	519,0	298,4	167,7	181,6	23,5	39,7	1,97	1,75
1	1	90	19,90	79,68	0,231	518,4	293,2	159,9	173,8	23,2	40,3	2,17	2,02
1	2	0	19,90	79,39	0,218	492,9	284,0	156,3	176,1	22,2	36,9	2,63	2,62
1	2	45	19,90	80,38	0,223	522,9	299,2	162,8	178,2	22,1	37,5	1,84	1,75
1	2	90	19,90	79,47	0,229	514,5	292,0	157,3	175,1	24,6	40,5	2,05	1,96
1	3	0	19,93	79,64	0,215	488,3	282,7	163,5	174,8	20,6	31,5	2,33	2,46
1	3	45	20,06	79,89	0,216	517,0	299,0	157,7	182,0	22,3	39,7	1,80	1,72
1	3	90	19,98	79,91	0,222	510,2	292,7	156,9	174,0	24,5	40,5	2,21	2,18
1	4	0	20,00	79,64	0,215	490,0	283,7	136,7	171,7	20,3	35,8	2,41	2,50
1	4	45	20,03	79,48	0,220	521,5	299,4	154,4	176,0	21,9	81,6	1,67	1,66
1	4	90	20,03	79,81	0,225	513,0	293,0	134,4	168,1	23,8	43,4	2,22	2,11
1	5	0	19,97	79,92	0,218	488,2	281,4	138,1	167,5	22,1	35,5	2,29	2,53
1	5	45	19,97	79,57	0,221	518,4	297,3	160,6	182,0	23,7	36,2	1,49	1,59
1	5	90	20,01	79,46	0,229	512,0	290,1	137,0	168,6	24,8	41,2	2,18	2,04
2	1	0	19,90	80,07	0,235	486,8	271,5	141,5	160,2	20,7	30,7	2,63	2,61
2	1	45	19,90	79,41	0,232	540,1	304,2	150,0	175,9	21,8	39,4	1,76	1,67
2	1	90	19,90	80,06	0,221	478,4	275,6	146,0	163,5	25,8	39,9	2,25	2,13
2	2	0	19,90	79,73	0,228	485,5	274,8	148,5	160,7	20,5	30,8	2,73	2,67
2	2	45	19,90	78,83	0,229	534,1	301,6	154,4	174,0	21,1	35,6	1,60	1,59
2	2	90	19,90	79,43	0,233	494,1	279,2	157,0	164,0	24,8	40,4	2,21	2,05
2	3	0	19,99	79,92	0,221	475,7	272,9	143,4	164,0	21,1	31,1	2,52	2,54
2	3	45	20,02	79,01	0,228	530,1	299,9	169,5	177,7	22,9	75,0	1,65	1,62
2	3	90	20,07	80,02	0,234	515,0	289,8	155,6	167,1	24,4	39,0	2,16	2,10
2	4	0	20,01	79,97	0,231	488,0	274,6	126,3	160,6	20,5	29,7	2,34	2,49
2	4	45	20,05	78,90	0,230	534,4	301,1	150,4	170,8	21,6	36,5	1,64	1,60
2	4	90	20,15	79,56	0,224	481,7	276,1	141,7	162,8	24,9	40,6	2,83	2,35
2	5	0	20,00	79,85	0,230	483,1	271,4	126,6	159,1	19,9	27,8	2,67	2,54
2	5	45	20,01	78,95	0,227	495,6	280,5	145,6	165,6	20,4	30,8	1,63	1,77
2	5	90	20,02	79,92	0,234	503,9	284,0	149,7	162,6	24,6	38,4	2,01	2,05

Roll	Sample	Angle	Starting width	Starting length	Deformation strengthening exponent	Hardening coefficient	Ultimate strength	Yield stress	Yield stress	Strain	Strain	Anisotropy factor	Anisotropy factor
		α	b_0	l_0	n	C	R_m	$R_{p0,2}$	$R_{p0,5}$	A_g	A80	r_{10}	r_{20}
		°	mm	mm	-	N/mm	MPa	MPa	MPa	%	%	-	-
3	1	0	19,90	80,25	0,209	486,1	284,4	163,3	186,1	21,5	38,7	2,64	2,59
3	1	45	19,90	79,49	0,213	510,4	297,2	166,6	187,5	22,5	38,3	1,80	1,69
3	1	90	19,90	79,40	0,212	503,5	293,5	169,9	185,6	23,8	42,7	2,24	2,09
3	2	0	19,90	79,19	0,215	491,0	284,4	159,6	178,3	22,2	37,3	2,67	2,58
3	2	45	19,90	79,92	0,216	513,8	297,5	170,2	182,9	22,8	39,7	1,86	1,74
3	2	90	19,90	79,54	0,222	510,1	292,7	156,5	177,3	23,3	40,6	2,25	2,07
3	3	0	20,00	80,03	0,206	482,0	283,5	163,7	182,2	22,1	38,7	2,23	2,41
3	3	45	19,99	78,52	0,213	515,6	299,5	167,4	191,0	21,8	39,7	1,36	1,51
3	3	90	20,04	79,77	0,226	514,4	293,4	149,2	167,5	24,9	40,1	1,91	2,05
3	4	0	20,01	79,67	0,207	485,9	285,4	167,1	182,5	21,1	35,2	2,29	2,44
3	4	45	20,02	78,49	0,216	518,2	299,2	156,4	182,1	21,6	38,6	1,52	1,59
3	4	90	20,04	79,59	0,217	509,7	295,0	165,8	178,4	23,4	41,0	1,99	2,06
3	5	0	20,03	79,94	0,207	481,9	283,0	136,5	177,9	21,4	36,2	2,45	2,56
3	5	45	20,03	78,83	0,215	509,7	295,5	159,7	180,2	22,2	36,6	1,68	1,71
3	5	90	20,02	80,12	0,225	511,5	291,9	148,3	175,3	23,5	40,7	2,05	2,05
4	1	0	19,90	79,36	0,222	501,5	287,0	153,5	179,7	22,1	38,8	2,45	2,45
4	1	45	19,90	79,38	0,236	531,2	296,1	153,4	175,7	22,0	37,0	1,85	1,75
4	1	90	19,90	79,39	0,231	518,8	293,3	155,6	173,4	25,5	42,5	2,13	1,98
4	2	0	19,90	79,24	0,217	498,0	287,5	156,3	178,1	22,4	37,9	2,64	2,57
4	2	45	19,90	79,29	0,222	510,4	292,0	160,6	175,6	24,5	37,5	1,89	1,76
4	2	90	19,90	79,42	0,214	509,3	296,1	164,8	183,9	23,4	40,8	2,19	2,05
4	3	0	20,00	79,77	0,215	491,1	284,6	162,4	174,7	22,4	37,5	2,21	2,34
4	3	45	20,01	79,21	0,223	519,7	296,1	160,5	176,8	22,6	37,3	1,48	1,59
4	3	90	19,89	79,49	0,227	517,2	294,0	143,5	172,8	23,8	40,6	1,85	1,85
4	4	0	20,01	80,12	0,219	499,0	287,1	136,5	175,9	21,5	36,7	2,26	2,32
4	4	45	20,07	79,33	0,219	516,3	296,8	146,4	175,6	21,2	39,6	1,71	1,68
4	4	90	20,04	79,90	0,226	514,5	293,2	146,1	172,8	23,1	41,7	1,84	1,94
4	5	0	20,00	79,77	0,219	499,9	287,1	130,0	166,7	22,7	37,9	2,49	2,40
4	5	45	20,07	79,52	0,222	514,0	294,0	154,8	171,1	22,2	37,5	1,80	1,71
4	5	90	19,91	80,23	0,225	514,9	294,2	157,3	176,6	23,3	42,1	2,14	2,10

Roll	Sample	Angle	Starting width	Starting length	Deformation strengthening exponent	Hardening coefficient	Ultimate strength	Yield stress	Yield stress	Strain	Strain	Anisotropy factor	Anisotropy factor
		α	b_0	l_0	n	C	R_m	$R_{p0,2}$	$R_{p0,5}$	A_g	A80	r_{10}	r_{20}
		°	mm	mm	-	N/mm	MPa	MPa	MPa	%	%	-	-
5	1	0	19,90	79,18	0,220	492,5	282,5	160,3	174,3	21,0	37,9	2,66	2,60
5	1	45	19,90	79,64	0,226	529,0	300,7	163,3	179,8	22,1	39,1	1,60	1,57
5	1	90	19,90	79,39	0,230	516,5	293,0	144,6	170,7	25,9	40,9	2,22	2,06
5	2	0	19,90	79,27	0,217	491,3	283,4	158,5	172,4	21,6	38,4	2,82	2,57
5	2	45	19,90	79,58	0,217	521,5	300,9	176,7	189,8	22,3	37,6	1,69	1,61
5	2	90	19,90	79,46	0,229	515,5	292,3	149,0	173,6	24,1	39,4	2,10	2,06
5	3	0	20,03	79,74	0,214	485,6	281,9	159,7	176,2	22,0	41,1	2,56	2,57
5	3	45	20,08	79,45	0,215	518,5	300,3	171,4	185,6	21,0	38,9	1,61	1,64
5	3	90	19,98	79,44	0,225	514,8	293,6	157,2	172,7	22,4	38,7	2,12	2,04
5	4	0	19,99	79,98	0,220	495,7	284,8	146,4	172,7	20,3	36,8	2,06	2,27
5	4	45	20,07	79,38	0,221	525,7	301,2	158,9	182,5	21,5	37,1	1,54	1,56
5	4	90	19,85	79,69	0,230	523,2	296,1	143,2	168,2	25,0	42,4	1,69	1,84
5	5	0	20,06	79,92	0,213	476,3	276,4	116,7	163,3	22,1	35,4	2,73	2,58
5	5	45	20,04	79,45	0,221	518,5	297,3	89,6	154,2	22,2	37,8	1,54	1,59
5	5	90	19,95	80,18	0,232	517,2	291,6	137,3	167,0	24,4	39,8	2,06	2,00

Annex B: Graphical representation of cross-section deviations

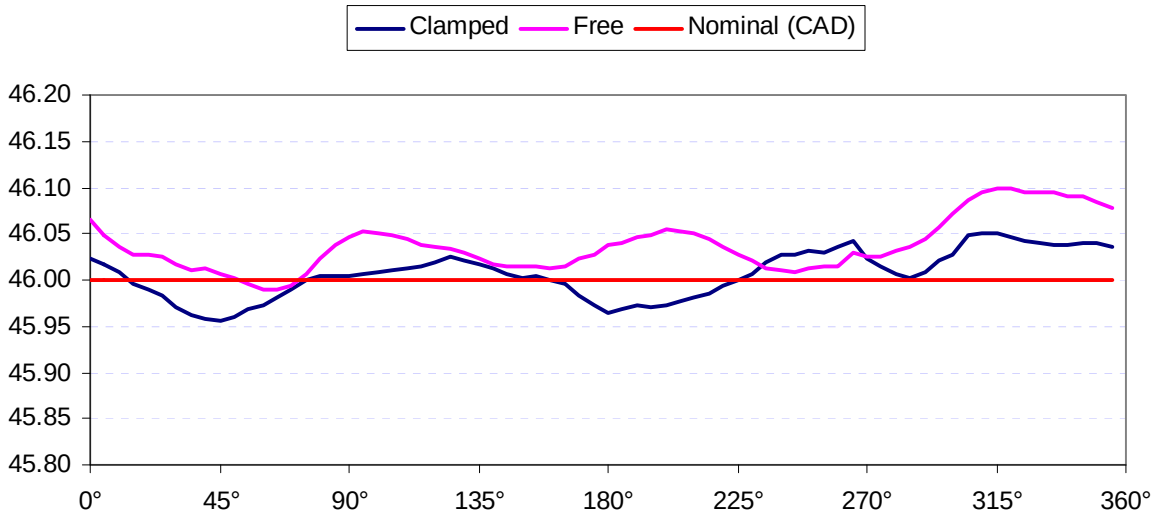

Roll 1 – Sample 1 (cor = 255°, RMS=0,0012)

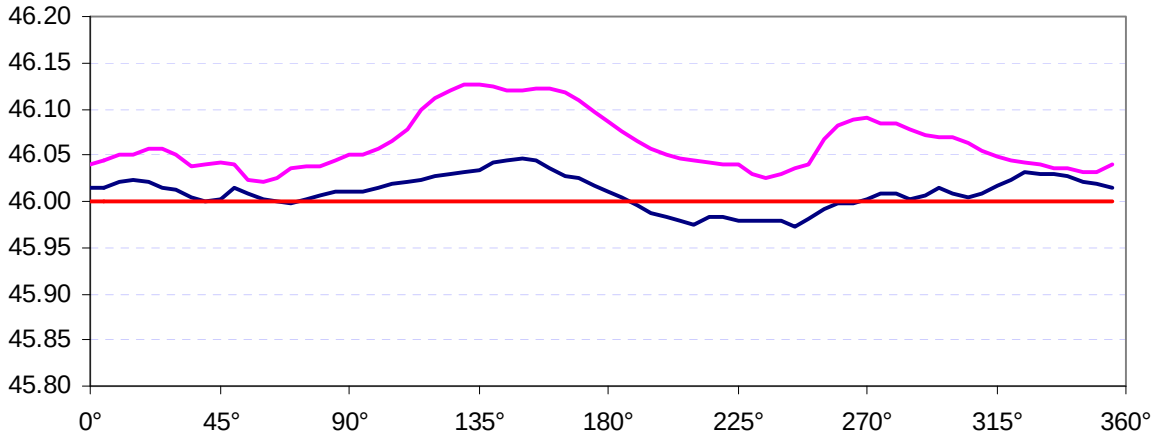

Roll 1 – Sample 2 (cor = 75°, RMS=0,0017)

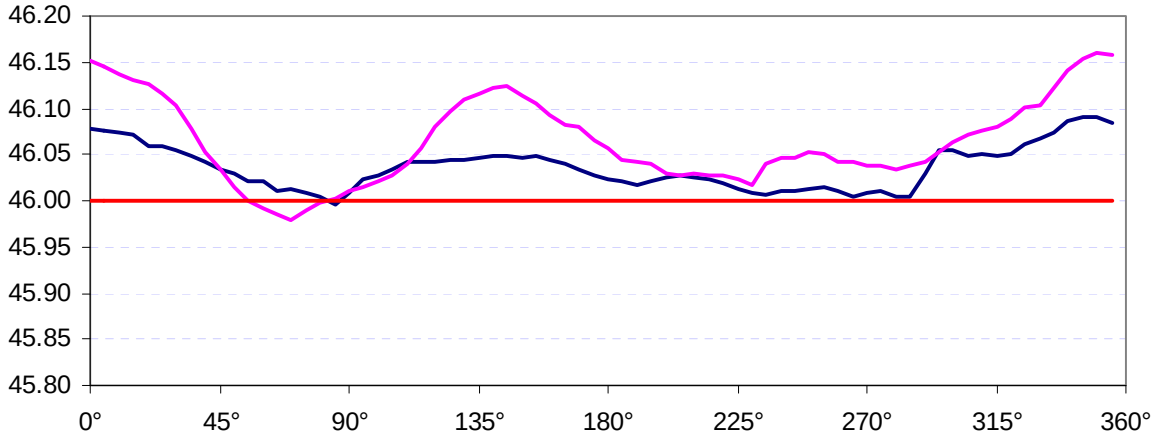

Roll 1 – Sample 3 (cor = 80°, RMS=0,0012)

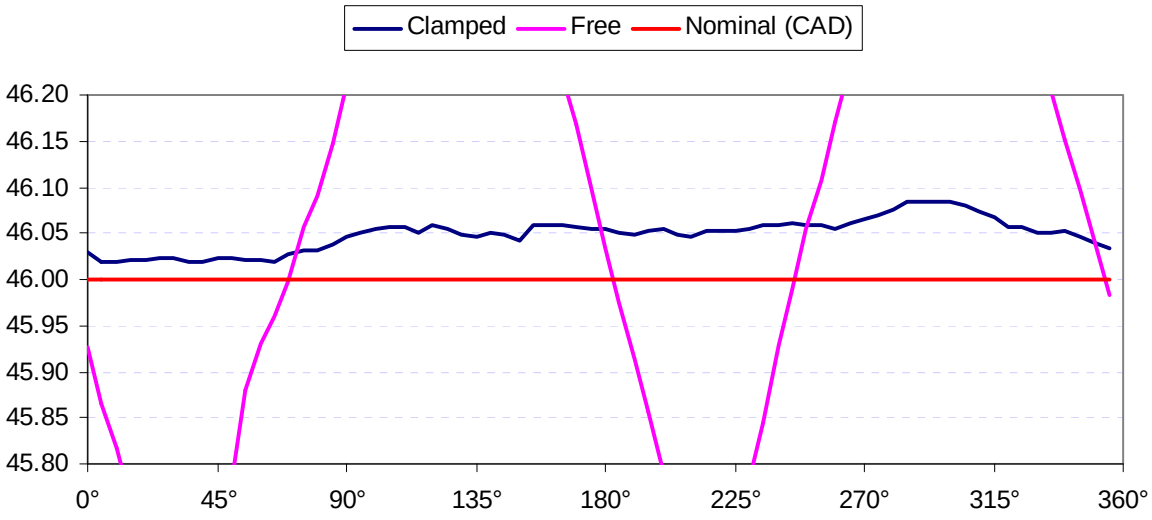

Roll 1 – Sample 4 (cor = 320°, RMS=0,0080)

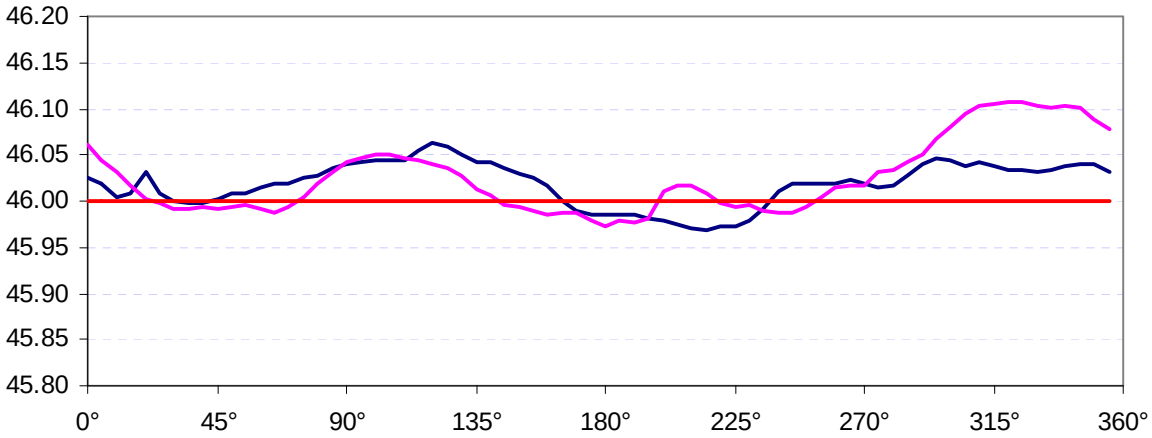

Roll 1 – Sample 5 (cor = 90°, RMS=0,0009)

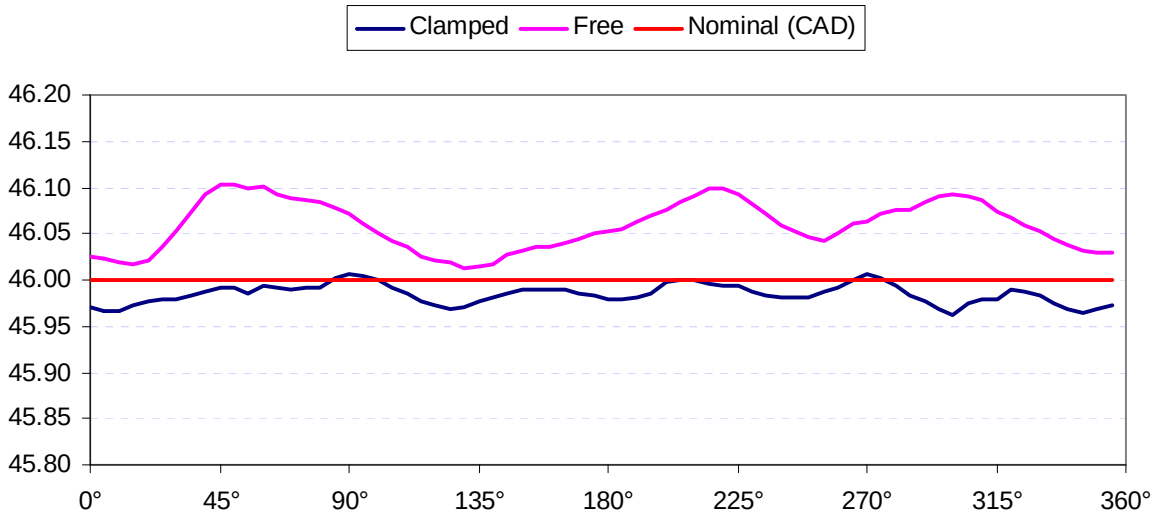

Roll 2 – Sample 1 (cor = 115°, RMS=0,0023)

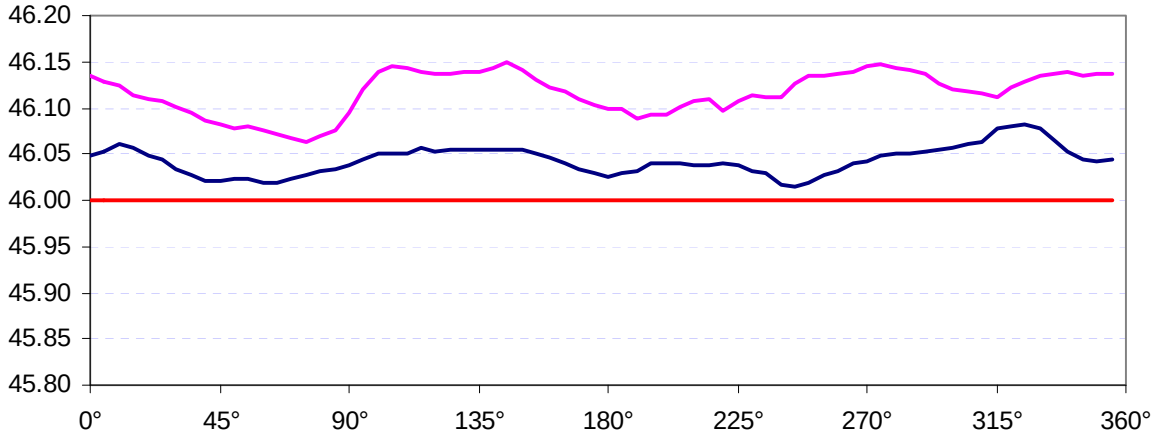

Roll 2 – Sample 2 (cor = 295°, RMS=0,0022)

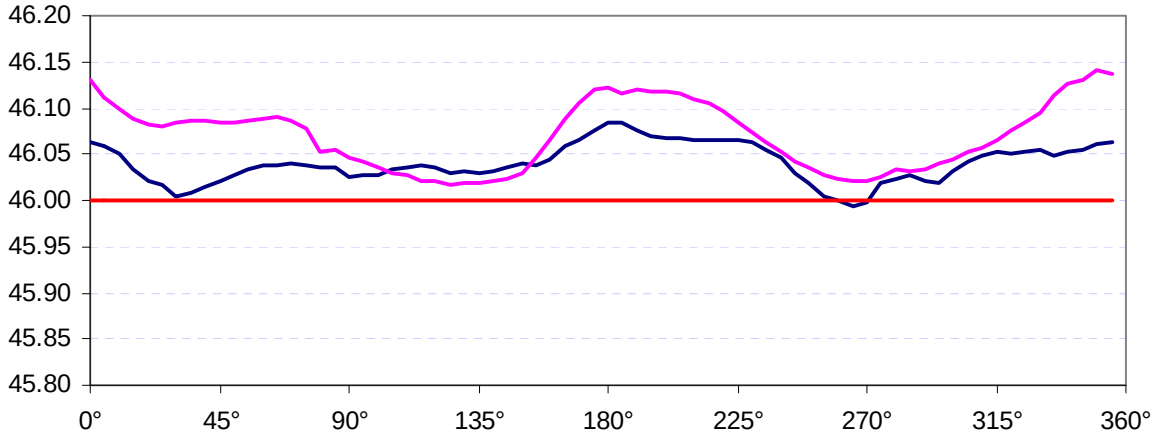

Roll 2 – Sample 3 (cor = 30°, RMS=0,0012)

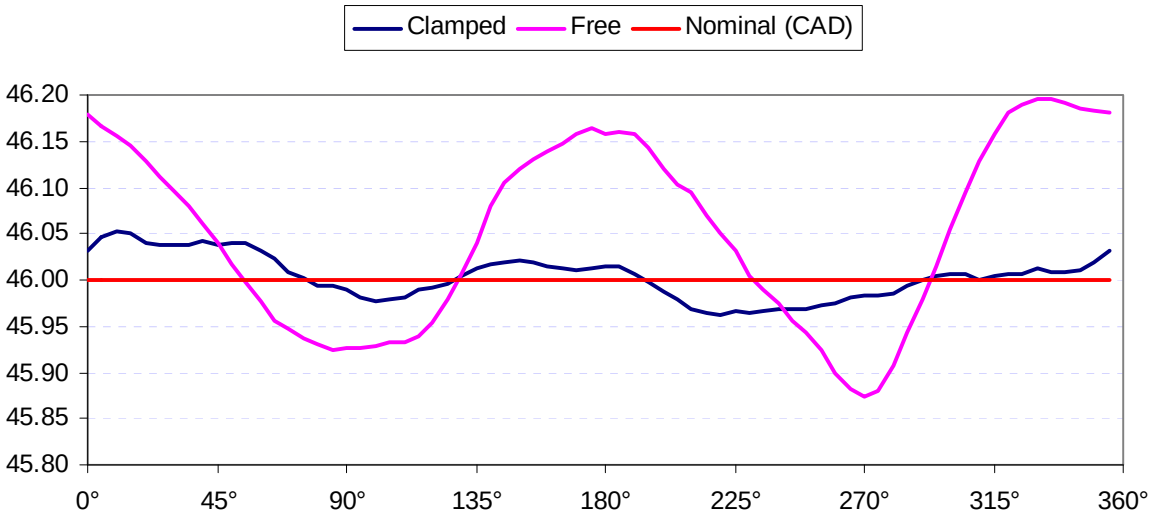

Roll 2 – Sample 4 (cor = 110°, RMS=0,0030)

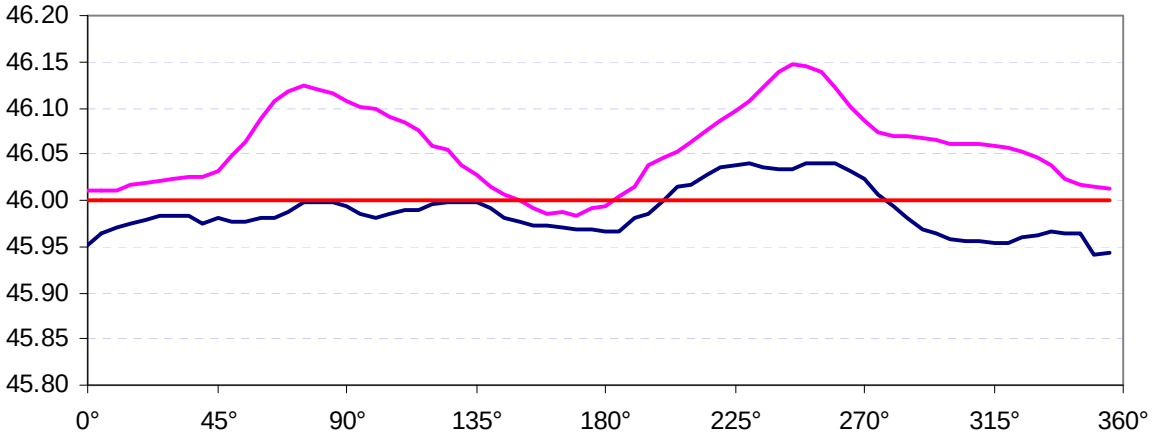

Roll 2 – Sample 5 (cor = 200°, RMS=0,0023)

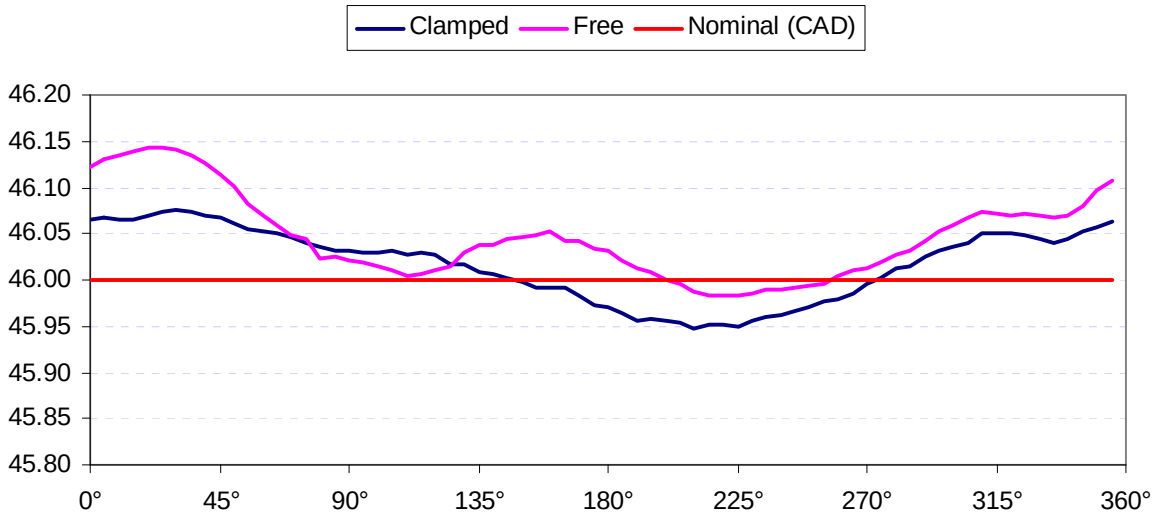

Roll 3 – Sample 1 (cor = 140°, RMS=0,0011)

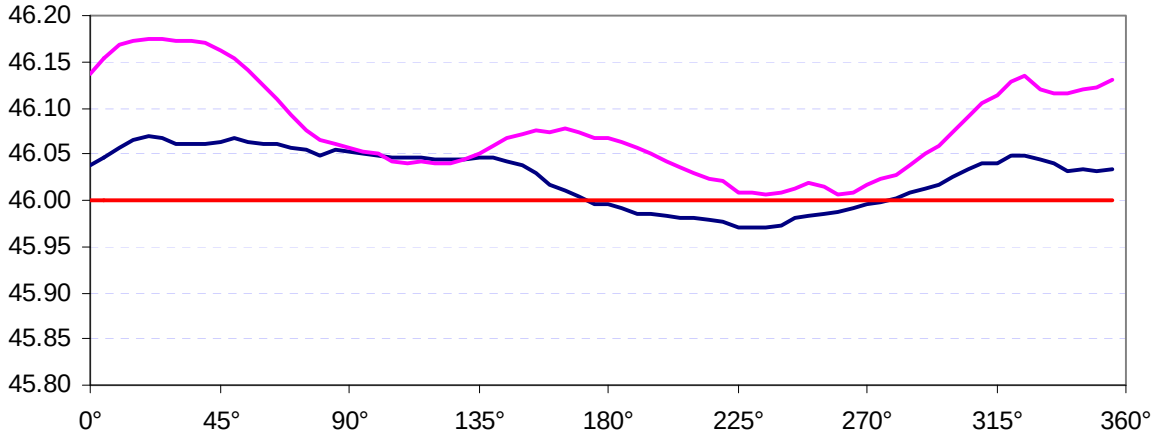

Roll 3 – Sample 2 (cor = 355°, RMS=0,0018)

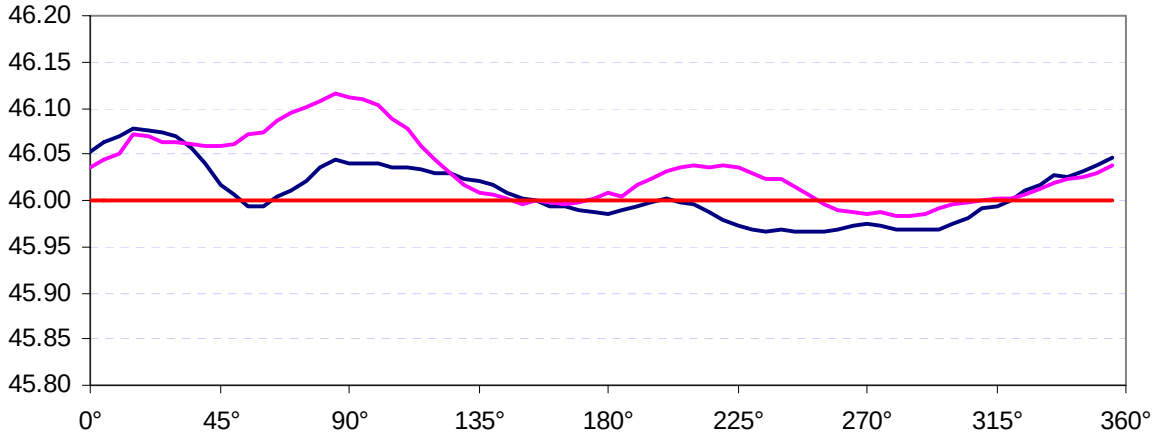

Roll 3 – Sample 3 (cor = 310°, RMS=0,0011)

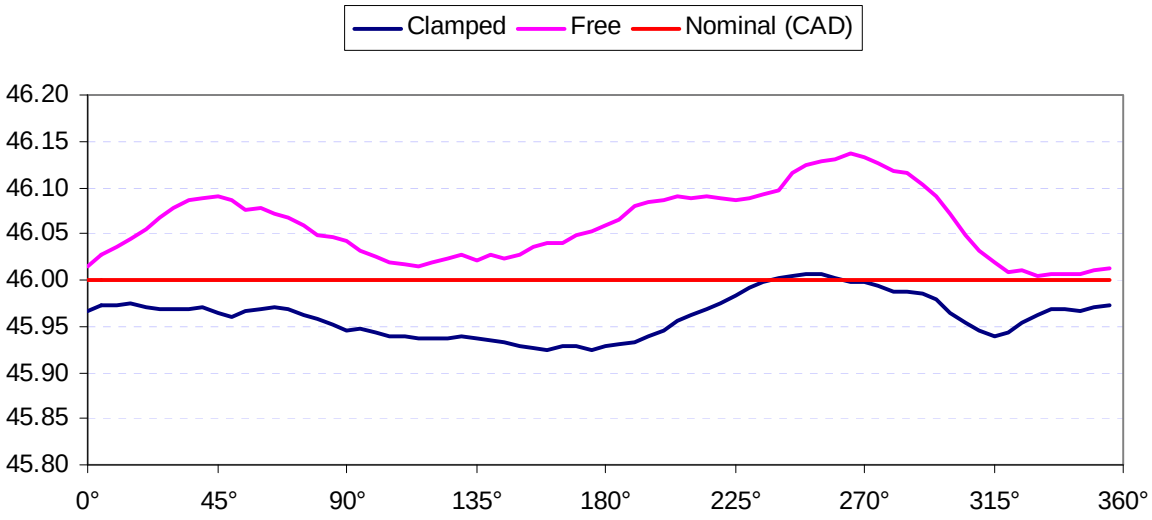

Roll 3 – Sample 4 (cor = 150°, RMS=0,0030)

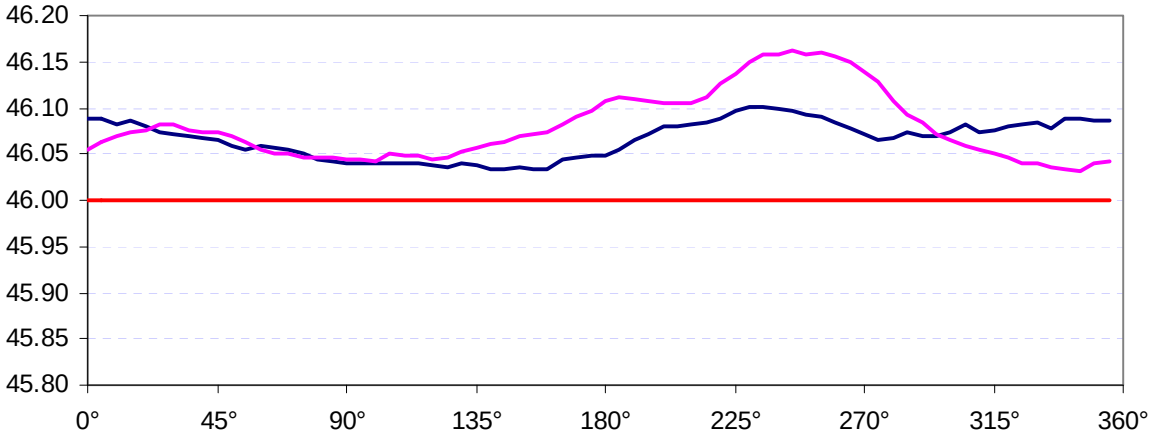

Roll 3 – Sample 5 (cor = 160°, RMS=0,0011)

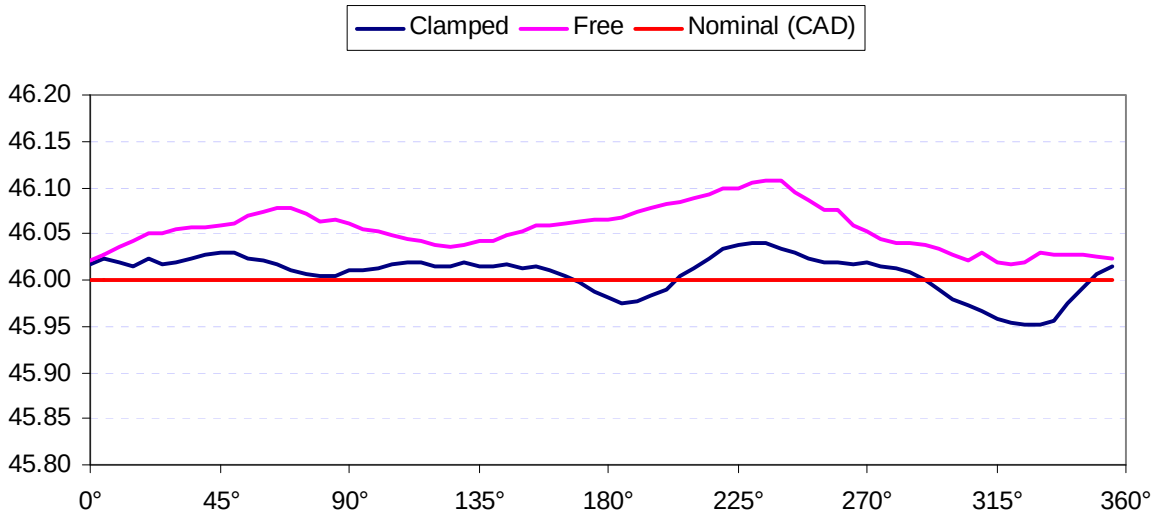

Roll 4 – Sample 1 (cor = 230°, RMS=0,0016)

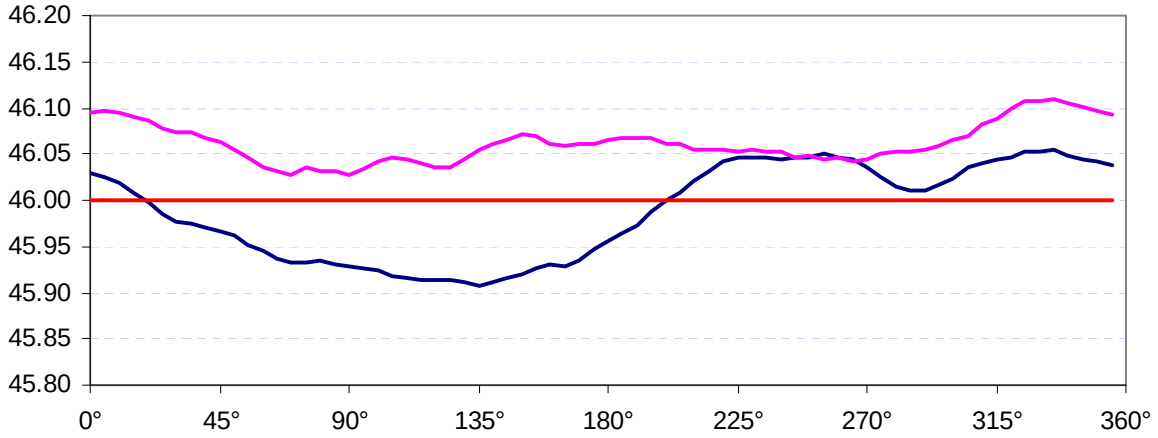

Roll 4 – Sample 2 (cor = 55°, RMS=0,0025)

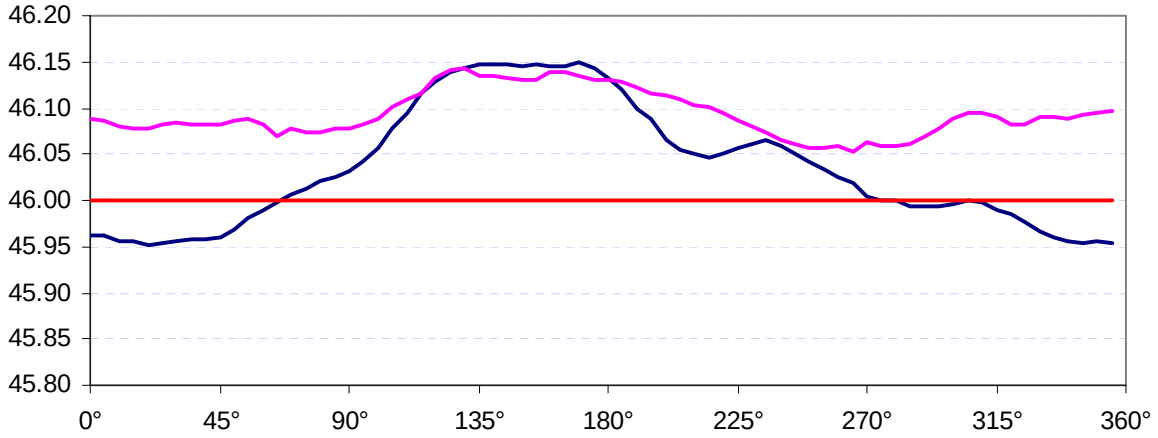

Roll 4 – Sample 3 (cor = 150°, RMS=0,0023)

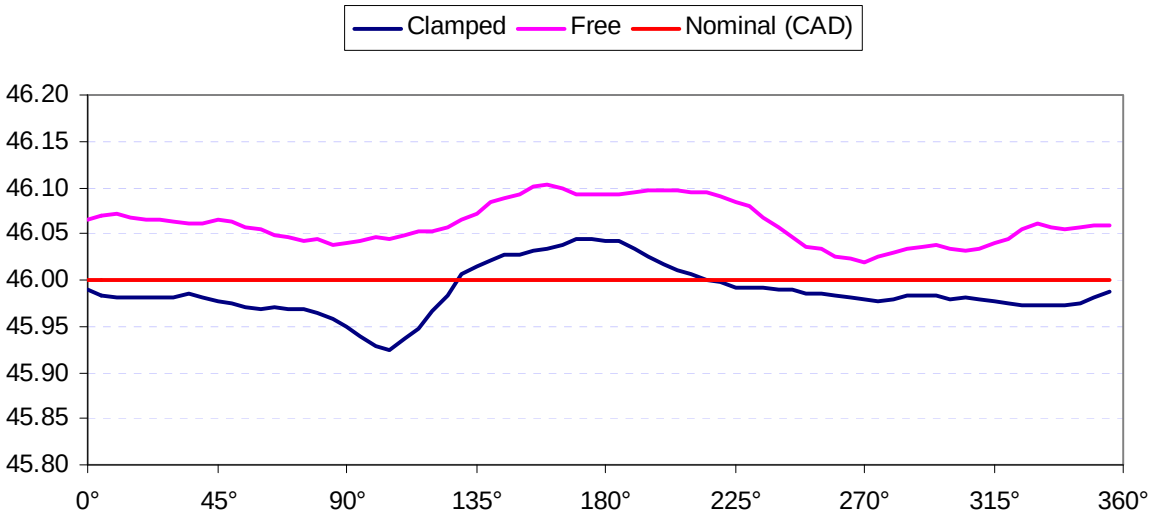

Roll 4 – Sample 4 (cor = 70°, RMS=0,0022)

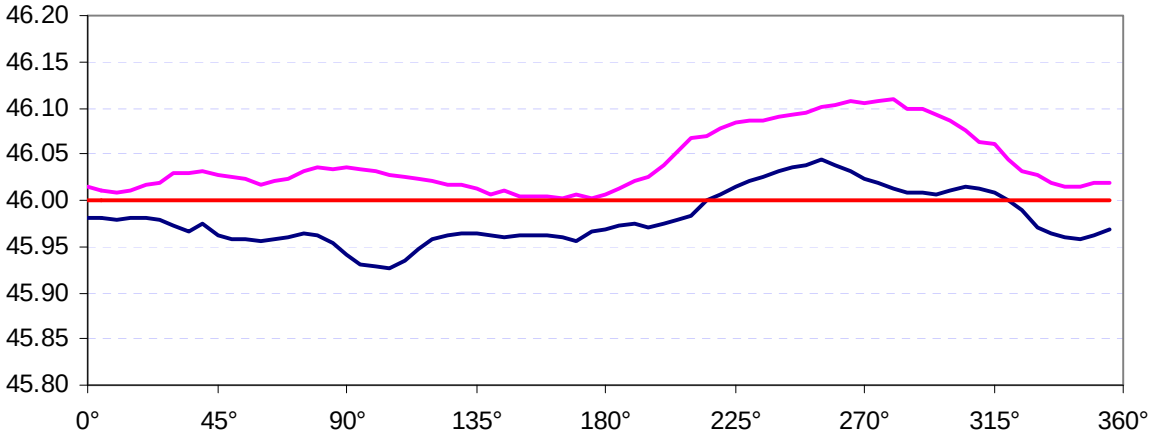

Roll 4 – Sample 5 (cor = 355°, RMS=0,0019)

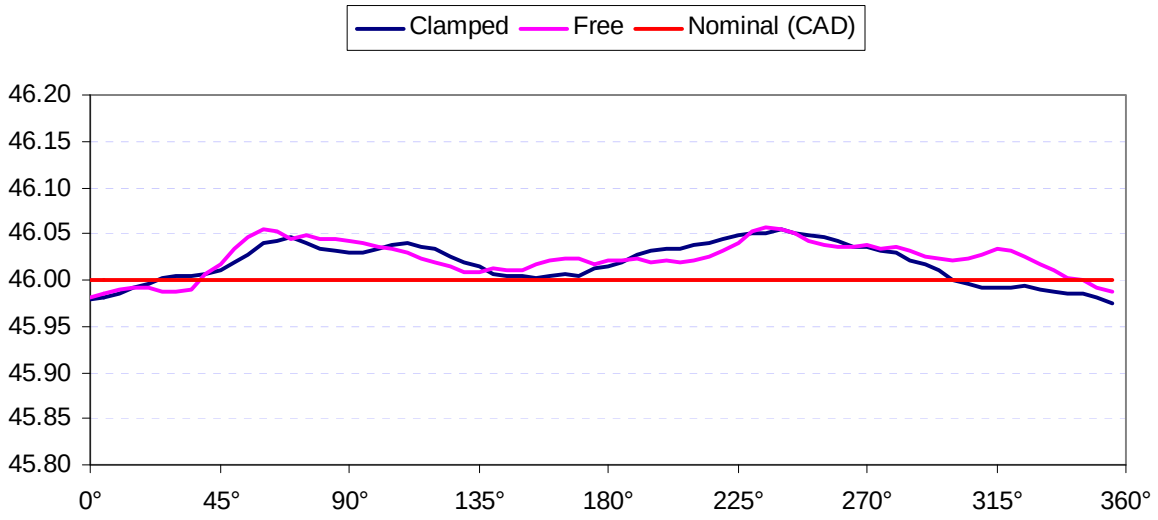

Roll 5 – Sample 1 (cor = 50°, RMS=0,0004)

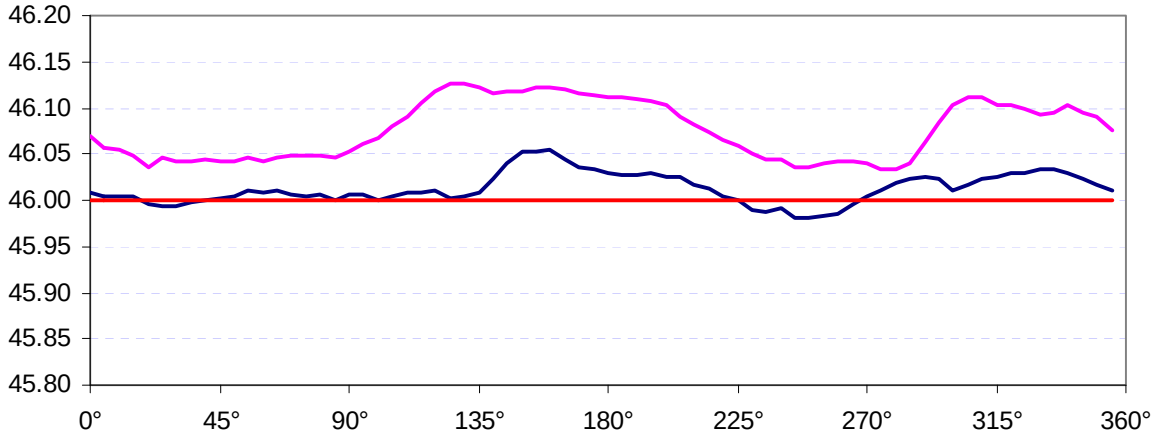

Roll 5 – Sample 2 (cor = 335°, RMS=0,0020)

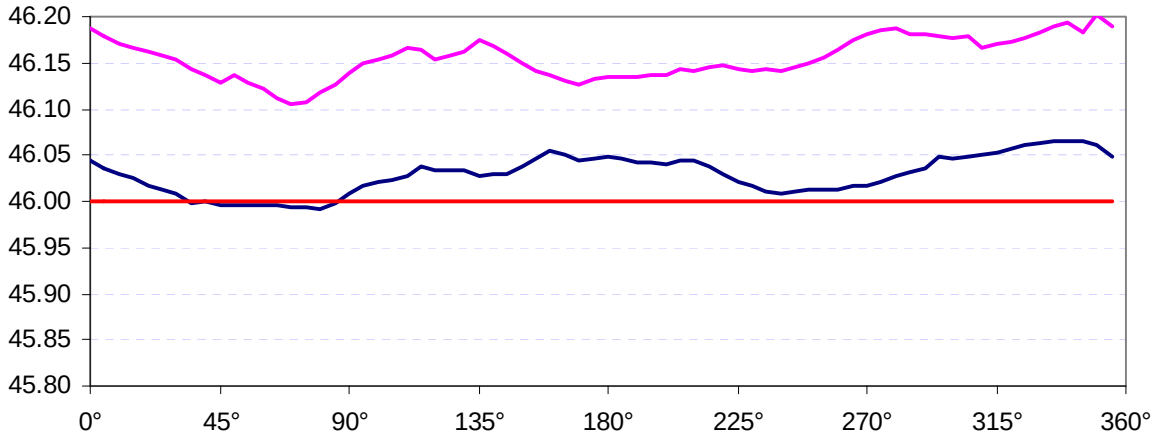

Roll 5 – Sample 3 (cor = 40°, RMS=0,0037)

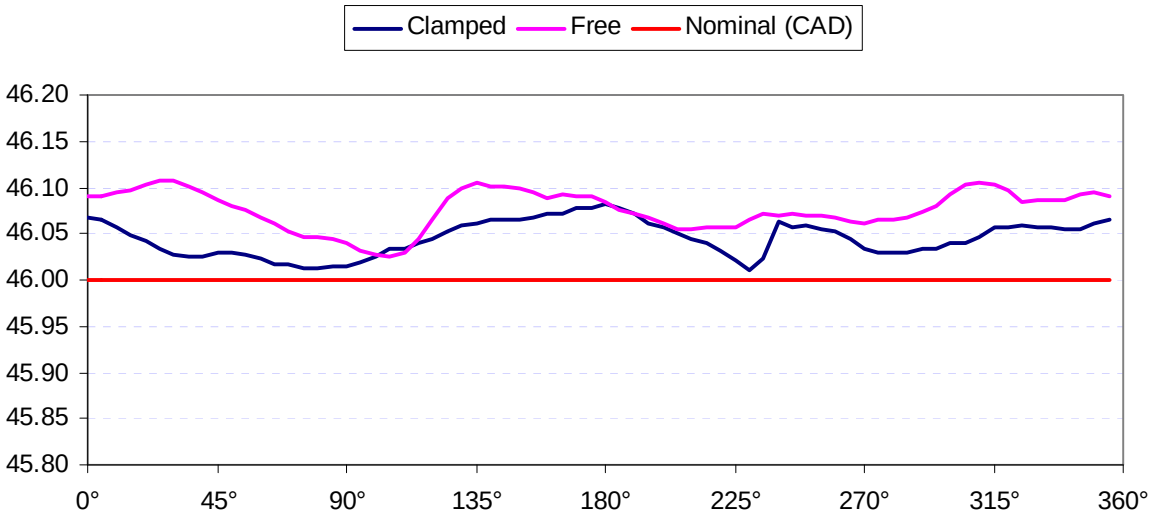

Roll 5 – Sample 4 (cor = 335°, RMS=0,0011)

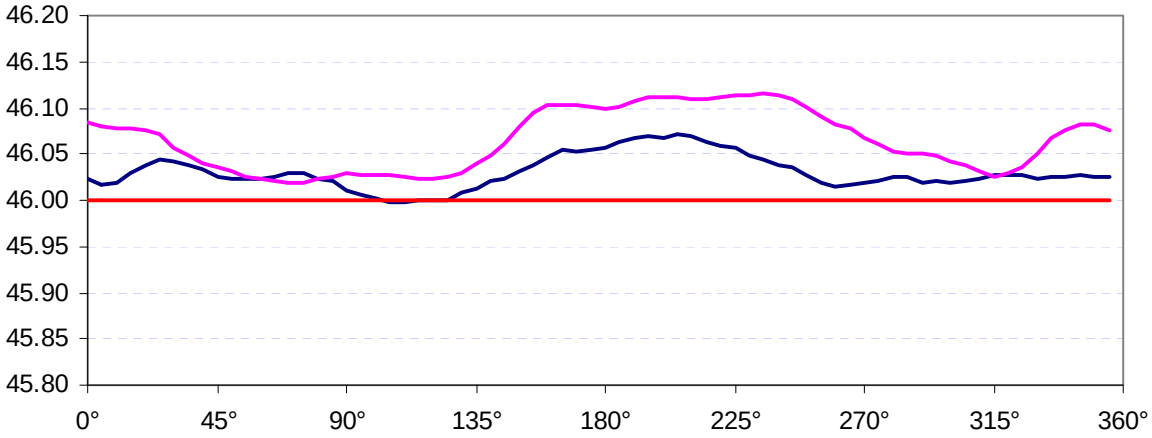

Roll 5 – Sample 5 (cor = 100°, RMS=0,0012)

Annex C: Listings of Fortran programs

Fortran program for calculating equivalent radii of clamped and unclamped data sets:

```
      program Intrpl
      real RC(1000), TC(1000), C(360)
      real RU(1000), TU(1000), U(360)
      integer step, T(360)
      step=5
      open(1,file="c:\\a\\C.txt")
      open(2,file="c:\\a\\U.txt")

C reading clamped point set
      i=0
      do
       i=i+1
       read(1,*,end=100) RC(i),TC(i)
      end do
 100  close(1)
      nC=i-1

C reading unclamped point set
      i=0
      do
       i=i+1
       read(2,*,end=200) RU(i),TU(i)
      end do
 200  close(2)
      nU=i-1

C calculating interpolated clamped points
      do 10 i=1,360/step
  10  T(i)=(i-1)*step
      k=0
      j=1
      do while (j.le.nC)
       k=k+1
       l=0
       suma=0
       do while (TC(j).LT.T(k)+step.and.j.le.nC)
        suma=suma+RC(j)
        l=l+1
        j=j+1
       end do
       if (l.eq.0) then
        C(k)=C(k-1)
       else
        C(k)=suma/l
       end if
      end do
```

```
C calculating interpolated unclamped points
      k=0
      j=1
      do while (j.le.nU)
       k=k+1
       l=0
       suma=0
       do while (TU(j).LT.T(k)+step.and.j.le.nU)
        suma=suma+RU(j)
        l=l+1
        j=j+1
       end do
       if (l.eq.0) then
        U(k)=U(k-1)
       else
        U(k)=suma/l
       end if
      end do

C writing interpolated results in file for fitting
      open(3,file="c:\\a\\TCU.txt")
      do 20 m=1,360/step
  20  write (3,*) T(m),C(m),U(m)
      close(3)
      end
```

Fortran program for RMS-based fitting:

```
      program Fitting
      real C(360), U(360), RMS(360)
      integer T(360)
      PI=3.141592654
      open(1,file="c:\\a\\TCU.txt")

C reading starting point sets
      i=0
      do
       i=i+1
       read(1,*,end=100) T(i), C(i), U(i)
      end do
 100  close(1)
      n=i-1
      step=360/n

C Calculating average C
      AvC=0
      do 5 i=1,n
       AvC=AvC+C(i)
  5   end do
      AvC=AvC/n

C probing set of deltas
      do 10 i=1,n

C shifting array U
       shi=U(1)
       do 25 j=1,(n-1)
        U(j)=U(j+1)
  25   end do
        U(n)=shi

C calculating RMS
       sumCU=0
       do 20 j=1,n
        sumCU=sumCU+(C(j)-U(j))**2
  20   end do
       RMS(i)=1./2./PI/AvC*SQRT(sumCU)
  10  end do

C finding minimum RMS
      RMSmin=RMS(1)
      imin=1
      do 30 i=1,n
       if (RMS(i).LT.RMSmin) then
        RMSmin=RMS(i)
        imin=i
       end if
  30  end do
      print *,'RMS=',RMSmin, '   COR=',imin*step
```

```
C shifting array U for number of steps that will give minimum RMS
      do 40 i=1,imin
       shi=U(1)
       do 35 j=1,(n-1)
        U(j)=U(j+1)
  35    end do
        U(n)=shi
  40  end do

C writing shifted results in files for visualisation: TCUs.txt
C and for FEM: CXY.txt for clamped and UXY.txt for unclamped profile
      open(2,file="c:\\a\\TCUs.txt")
      open(3,file="c:\\a\\CXY.txt")
      open(4,file="c:\\a\\UXY.txt")
      do 50 m=1,n
       write (2,*) T(m),C(m),U(m)
       ang=(T(m)+step/2.)/180.*PI
       write (3,*) C(m)*cos(ang), C(m)*sin(ang)
       write (4,*) U(m)*cos(ang), U(m)*sin(ang)
  50  end do
      close(2)
      close(3)
      close(4)
      end
```

Annex D: Summary data for all scanned points in toleranced cross-section

Roll	Sample	Average radius of free part	Standard deviation of free part radii	Average radius of clamped part	Standard deviation of clamped part radii
		R_0	s_0	R	s
		mm	mm	mm	mm
1	1	46,022	0,029	45,991	0,025
1	2	46,028	0,030	45,996	0,018
1	3	46,036	0,048	46,022	0,025
1	4	46,071	0,274	46,039	0,018
1	5	46,008	0,040	46,002	0,024
	Average	46,033	0,084	46,010	0,022
	St. dev.	0,024	0,106	0,020	0,004
2	1	46,016	0,028	45,976	0,011
2	2	46,075	0,023	46,034	0,016
2	3	46,042	0,036	46,024	0,021
2	4	46,004	0,100	45,99	0,024
2	5	46,007	0,044	45,97	0,027
	Average	46,029	0,046	45,999	0,020
	St. dev.	0,030	0,031	0,029	0,006
3	1	46,021	0,046	45,992	0,041
3	2	46,047	0,052	46,007	0,030
3	3	46,016	0,037	45,995	0,032
3	4	46,033	0,038	46,02	0,023
3	5	46,063	0,037	46,053	0,021
	Average	46,036	0,042	46,013	0,029
	St. dev.	0,019	0,007	0,025	0,008
4	1	46,029	0,023	45,988	0,022
4	2	45,996	0,021	45,958	0,052
4	3	46,045	0,025	46,006	0,066
4	4	46,006	0,023	45,967	0,028
4	5	46,002	0,034	45,962	0,028
	Average	46,016	0,025	45,976	0,039
	St. dev.	0,021	0,005	0,020	0,019
5	1	46,023	0,019	46,003	0,022
5	2	46,043	0,031	46,002	0,017
5	3	46,082	0,023	46,041	0,021
5	4	46,018	0,021	45,983	0,019
5	5	46,044	0,032	46,019	0,018
	Average	46,042	0,025	46,010	0,019
	St. dev.	0,025	0,006	0,022	0,002
	Total Average	46,032	0,044	46,004	0,026
	Total st. dev.	0,023	0,050	0,025	0,012

About the author

Samir Lemeš was born in Zenica, Bosnia and Herzegovina on June, 27th 1968. He attended University of Sarajevo, Mechanical Engineering Faculty in Zenica, where he received both Bachelor's degree (Mechanical Engineering in Metallurgy) in June 1993 and Master's degree (Construction of Machinery) in February 2002. His Master thesis title was "Vibrations of centrifugal pumps used in automotive cooling systems".

He is employed as a senior teaching assistant at the University of Zenica, Chair for Automation and Metrology since October 1996. He published 6 books and more than 30 scientific papers as author or co-author. His main research interests are focused into numerical simulations, computational metrology and reverse engineering.

Izjava

Doktorsko delo predstavlja rezultate lastnega znanstveno raziskovalnega dela na osnovi sodelovanja z mentorjem prof. dr. Karlom Kuzmanom.

Samir Lemeš